komunikácie

COMMUNICATIONS

SCIENTIFIC LETTERS OF THE UNIVERSITY OF ŽILINA

Volume 28

MULTIDISCIPLINARY JOURNAL FOR SCIENCES IN TRANSPORT

UNIVERSITY
OF ŽILINA

ISSN 1335-4205

2/2026

UNIVERSITY OF ŽILINA
EDIS-Publishing House
UNIZA

EDIS-Publishing House of the University of Žilina (UZ) is one of the University of Žilina's consituents. The beginning of its existence dates back to 1990. In the course of its work, the publishing house has published more than 5 100 titles of book publications, especially university textbooks, scientific monographs, scripts, prose, but also enriched the book market with titles of regional, children's and popular literature.
Students and professional public have the opportunity to purchase published titles in the „Selling Study Literature" directly on the premises of the University of Žilina, in the EDIS shop or upon order on a „cash on delivery" basis. All published titles are available at: www.edis.uniza.sk.

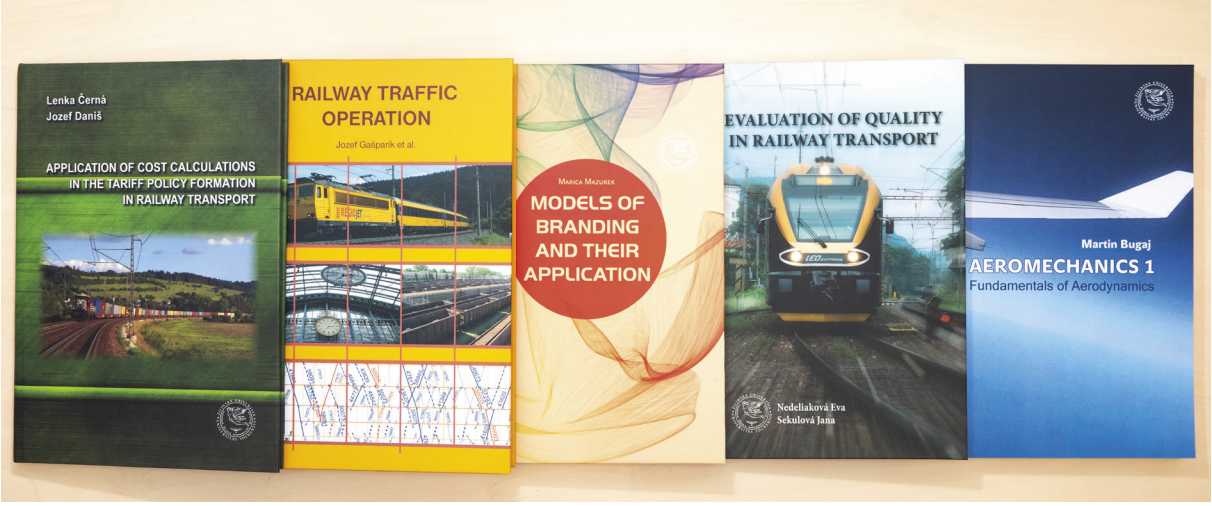

EDIS-Publishing House of the University of Žilina offers book titles in English

Eva Nedeliaková, Jana Sekulová
EVALUATION OF QUALITY IN RAILWAY TRANSPORT
ISBN 978-554-1272-6 Price 8.00 €

Martin Bugaj
AEROMECHANICS 1
ISBN 978-80-554-1675-5 Price 14.50 €

Marica Mazurek
MODELS OF BRANDING AND THEIR APPLICATION
ISBN 978-80-554-1705-9 Price 9.00 €

Jozef Melcer
DYNAMICS OF STRUCTURES
ISBN 978-80-554-1698-4 Price 19.00 €

Jozef Gašparík et al.
RAILWAY TRAFFIC OPERATION
ISBN 978-80-554-1281-8 Price 15.80 €

Lenka Černá, Jozef Daniš
APPLICATION OF COST ALCULATIONS IN THE TARIFF POLICY FORMATION IN RAILWAY TRANSPORT
ISBN 978-80-554-1391-4 Price 7.61 €

Tetiana Hovorushchenko et.al.
CD - INTELLIGENT INFORMATION-ANALYTICAL TECHNOLOGIES...
ISBN 978-80-554-1729-5 Price 3.50 €

Karol Matiaško, Michal Kvet, Marek Kvet
CD - PRACTICES FOR DATABASE SYSTEMS
ISBN 978-80-554-1397-6 Price 2.20 €

Veronika Valašková, Daniela Kucharová
USB - STATICS OF STRUCTURES 3
ISBN 978-80-554-1826-1 Price: 8,90 €

Michal Kvet, Karol Matiaško, Štefan Toth
USB - PRACTICAL SQL FOR ORACLE CLOUD
ISBN 978-80-554-1880-3 Price: 11,30 €

Michal Kvet, Karol Matiaško, Marek Kvet
USB - BECOME EXPERT IN MYSQL PRACTICES FOR DATABASE SYSTEMS IN MYSQL
ISBN 978-80-554-1786-8 Price 13.50 €

Michal Kvet, Alenka Baggia, Monika Borkovcová, Diana Mudrinić, Frane Urem
E-book - Environmental Data Analysis
ISBN 978-80-554-2145-2 Price 0,00 €

Michal Kvet
E-book – Become master in SQL
ISBN 978-80-554-2132-2 Price 0,00 €

EDIS-Publishing House UNIZA
Univerzitná 8215/1,
010 26 Žilina,
Slovakia

e-mail: edis_objednavky@uniza.sk, edis@uniza.sk
www.edis.uniza.sk

kamUNikácie
COMMUNICATIONS

VEDECKÉ LISTY ŽILINSKEJ UNIVERZITY
SCIENTIFIC LETTERS OF THE UNIVERSITY OF ZILINA
multidisciplinary journal for sciences in transport

A - OPERATION AND ECONOMICS IN TRANSPORT

B - MECHANICAL ENGINEERING IN TRANSPORT

C - ELECTRICAL ENGINEERING IN TRANSPORT

D - CIVIL ENGINEERING IN TRANSPORT

E - MANAGEMENT SCIENCE AND INFORMATICS IN TRANSPORT

F - SAFETY AND SECURITY ENGINEERING IN TRANSPORT

MARITIME FREIGHT COST SHOCKS AND SME FINANCIAL PERFORMANCE IN THE VISEGRAD REGION DURING AND AFTER COVID-19

Aleksandar Alačkov*, Michal Červinka

Pan-European University, Faculty of Entrepreneurship and Law, Department of Entrepreneurship and Management, Prague, Czechia

*E-mail of corresponding author: aleksandar.alackov@gmail.com

Michal Červinka 00000-0003-2226-4501

Resume

In this paper is analysed how the maritime freight costs fluctuations (2020-2024) affected the small and medium sized enterprises (SMEs) across the Visegrad Group using firm-level panel data and fixed-effects regressions. Four financial indicators were examined: turnover, gross margin, inventory stock, and cost of goods sold (COGS), with the Shanghai containerized freight index (SCFI) as the key explanatory variable. Higher freight costs are associated with increased turnover, inventories, and COGS, and with reduced gross margins, though the within-firm explanatory power is low. Overall, shipping price shocks leave measurable but modest effects on SME finances, indicating partial cost pass-through and strong resilience. Supporting supply-chain adaptability and digital logistics tools may further reinforce this resilience.

Article info

Received 29 November 2025
Accepted 22 February 2026
Online 19 March 2026

Keywords:

maritime
shipping
cost
performance
effect
transport
V4

Available online: https://doi.org/10.26552/com.C.2026.020

ISSN 1335-4205 (print version)
ISSN 2585-7878 (online version)

1 Introduction

Global maritime shipping is the backbone of international trade, carrying roughly 80% of goods worldwide [1]. The COVID19 pandemic, however, caused unprecedented disruption to this sector [2]. Pandemic related shocks - from lockdowns and labour shortages to port closures, severely disorganized supply chains and curtailed maritime trade in 2020 [3]. By mid2020, as consumer demand for goods rebounded while containers and vessel capacity were in short supply, ocean freight costs began surging to historic highs. For example, the Shanghai Containerized Freight Index for China-Europe routes jumped from under $1,000 per TEU in mid2020 to about $4,000 by late 2020 and then reached $7,395 by mid2021 [4]. By 2021, many freight indices hit record levels, contributing to rising commodity prices and even inflationary pressure worldwide [5]. These soaring maritime shipping prices quickly became a focal point for researchers and policymakers given their far-reaching economic impact in the post COVID period. Importantly, this paper focuses on Central Europe, in particular the Visegrad (V4) countries (Poland, Czechia, Slovakia, and Hungary) - which are landlocked, except Poland, and therefore rely on seaborne trade indirectly via major European ports [4]. This geographic characteristic makes the V4 region a distinctive case for assessing how global maritime disruptions is transmitted inland to small businesses.

A critical concern arising from the logistics turmoil is how such elevated transportation costs affect businesses, especially small and medium sized enterprises (SMEs). The SMEs account for a large share of economic activity, for instance, about 47% of formal sector jobs and over half of output in developing countries, yet they typically lack the scale and resources of large firms to absorb external shocks [6]. The recent freight cost spike was no exception. Rapidly rising transportation expenses squeezed many businesses' operations, in some cases forcing smaller firms out of the market and compelling drastic adjustments to inventory and sourcing strategies. Evidence suggests that most firms had to respond by raising prices: a 2021 OECD business survey found that most retailers in Europe reported higher logistics costs, and approximately three quarters had partially passed these costs on to consumers [7].

Such cost pressures are especially perilous for SMEs that operate on thin margins. Indeed, during the pandemic many SMEs were at risk of bankruptcy due to collapsing demand coupled with surging input and logistics costs [8]. Sudden spikes in freight rates tend to have a disproportionate impact on smaller businesses' profitability and viability, since SMEs often have limited cash buffers, less bargaining power with shippers, and fewer options to reroute shipments compared to large corporations [9]. While some larger firms managed to negotiate long-term contracts or alternative shipping methods, smaller enterprises frequently faced the full brunt of spot market rate increases and shipping delays. This dynamics has raised debate over whether the logistics cost shock was largely passed through to end consumers (thereby "sharing" the burden via higher retail prices) or absorbed at the firm level, eroding SMEs' financial performance. Both scenarios occurred: many SMEs did implement price hikes (at the risk of losing price sensitive customers) even as their profit margins shrank due to portions of the costs that could not be fully passed on.

A growing body of literature has documented the pandemic's impact on supply chains and transportation costs. However, relatively few works were focused on the firm level consequences for SMEs. Many scholars examine COVID19's effect on freight rates and import costs broadly, but often with limited attention to the real economic impact on smaller enterprises [10]. This is a notable gap given the essential role of SMEs and their apparent vulnerabilities. Moreover, most of the available evidence comes from Asian contexts or global aggregates, while there is very limited empirical research on Europe's landlocked economies. To our knowledge, no study has systematically examined the relationship between the global maritime freight costs and the financial performance of SMEs in the V4 countries. Filling this gap is particularly important because these economies depend heavily on imported intermediate goods, which makes them indirectly exposed to maritime price shocks despite their geographic distance from ports [10].

Considering the above, it is crucial that the effect of maritime shipping price fluctuations on SMEs' financial indicators in the post COVID-19 era is investigated. Key financial performance metrics analysed include:

- Operating revenue
- Profit margins
- Costs of goods sold
- Inventory levels.

These indicators together capture firms' ability to generate revenue, the cost pressures they face, and their operational resilience. The goal is to quantify and contextualize how the extreme volatility in ocean freight rates since 2020 has translated into financial stresses or changes for small businesses. Particular attention is paid to contentious viewpoints in the literature. For instance, whether the shipping costs shock should be seen as a transient logistical inconvenience or as a catalyst for long term structural adjustments in SMEs' business models. By analysing firm level data and industry trends, it is determined to what extent SMEs absorbed the increased shipping costs (thereby impacting their profitability) versus passed them on to customers (potentially impacting sales volumes or customer retention) [11]. Ultimately, it is imperative to fill the research gap on the microeconomic impacts of freight rate swings in Central Europe, thereby complementing the broader macrolevel analyses and informing strategies to bolster SME resilience in the face of volatile logistics markets.

1.1 Literature overview

The COVID19 crisis caused unprecedented swings in ocean freight rates. After early 2020, when carriers sharply cut capacity via blank sailings and freight rates initially fell, the trend reversed dramatically later that year. From late 2020 onward, container shipping costs surged to record highs, as demand outstripped available capacity. Industry indices show that container spot rates effectively quadrupled in 2021 compared to pre pandemic levels. Rates remained high through 2022 and much of 2023, with intermittent spikes linked to unforeseen events (e.g. disruptions around the Red Sea in late 2023) and by early 2024, freight rates had eased from their peak, but were still well above pre pandemic norms [1]. The Shanghai Containerized Freight Index presented in Figure 1 and other benchmarks more than four folded during 2020-2021 and remained extremely elevated through much of 2022. UNCTAD reported that on some Asian export routes (such as Shanghai-Europe), rates saw especially sharp spikes - in one late 2023 instance, Asia-Europe spot rates jumped by roughly $500 within a single week, a record weekly increase [12]. Multiple shipping price indices (SCFI, CCFI, etc.) confirm that rates on major trade lanes (Asia-Europe, Asia-North America) in 2021-2022 stayed far above their 2019 levels, reflecting an extraordinary degree of volatility [13]. In contrast, the freight rates on a few less profitable routes rose relatively less (for example, some Asia-East Coast North America rates were up ~63% versus 2019, whereas China-Latin America routes saw over 4 times increases).

European importers felt these surges acutely. The critical Asia-Europe trade lanes suffered severe congestion and escalating costs. For instance, port waiting times in key hubs (Singapore, Jebel Ali, Port Klang) lengthened in 2021-2022, further raising costs and causing delays. An analysis by the European Central Bank noted that transportation costs on routes from Asia to Europe climbed sharply beginning in mid-2021, contributing to higher landed import prices in Europe [13]. Although few studies are isolating freight rate impacts specifically on the V4 countries, the general

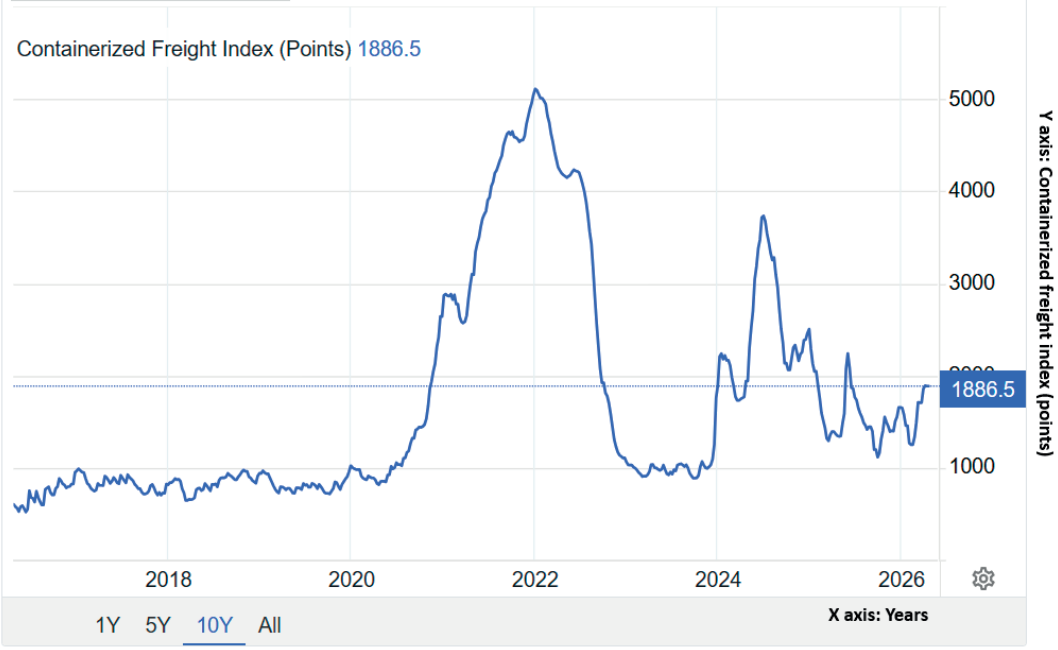

Figure 1 *Containerized shipping index from 2020 to 2025, source: [14]*

pattern undoubtedly applied: Poland, Czechia, Slovakia, and Hungary rely heavily on imports from Asia and thus faced these international price shocks indirectly. In other words, firms in the V4 region experienced the global freight costs boom along with the rest of Europe, despite being geographically distant from the ports where the disruptions originated [15].

Research has identified multiple factors behind the extreme freight rate swings of the pandemic era. Broadly, these causes can be grouped into demand shocks, supply constraints, logistical bottlenecks, and other industry specific factors [16].

The pandemic (and subsequent recovery) induced large shifts in demand for goods. Explosive growth in consumer spending on merchandise (especially home electronics, appliances, and other stay-at-home goods) collided with previously downsized shipping capacity. As manufacturing orders rebounded sharply in late 2020, delivery times lengthened and input costs, including freight, spiked. In essence, a strong demand resurgence, coupled with limited short term capacity elasticity' meant shipping carriers could charge much higher prices. In one modelling study was found that mere increases in operating costs could not explain the post2020 freight rate explosion; instead, a shift in market equilibrium (e.g., reduced competition among major carriers and more collusive pricing) magnified the spike [17].

On the supply side, deliberate capacity reductions and equipment dislocations aggravated the situation. In the first half of 2020, as global trade initially collapsed, carrier alliances responded by cancelling over a hundred Asia-Europe sailings, idling ships to save costs. These widespread "blank sailings" temporarily reduced available capacity. When the demand roared back later in 2020, the shipping system struggled to catch up. The U.S. International Trade Commission reported that by late 2020 U.S. exporters were experiencing a shortage of empty containers, inventories of usable export containers were depleted, which in turn drove up the cost of leasing containers for shipment [18]. A similar phenomenon hit Europe: empty containers languished in inland depots or import heavy ports, while exporters in Asia and elsewhere desperately needed them. Carriers had to spend time and money repositioning containers (often paying premiums to rush empties back to origin markets), costs which then fed into freight rate increases.

Surges of vessels arriving off schedule overwhelmed port infrastructure and labour availability as dozens of ships waited at anchor off major ports (Los Angeles/Long Beach, Shanghai, Rotterdam, etc.), port throughput slowed and shipping schedules unravelled. One study enumerated causes of the congestion, from labour shortages and infrastructure limitations to weather events and sudden demand swings, all of which tend to increase shipping turnaround times and costs. UNCTAD observed that by mid2024 roughly 8.4% of the global container ship fleet (approximately 2.5 million TEU of capacity) was stuck waiting at anchorages worldwide due to port bottlenecks, putting continued upward pressure on freight rates, for example, demurrage charges for containers stuck in port and peak season surcharges [18].

Several ancillary factors contributed to shipping costs inflation as well. Bunker fuel prices rose sharply from late 2020 into 2022, increasing carriers' operating costs, which were then reflected in higher freight

tariffs. Climate related events hindered certain routes for example, an El Nino related drought in late 2022 reduced Panama Canal capacity and forced some ships onto longer routes, adding transit time and expense.

The outbreak of war in Ukraine and periodic instability around the Red Sea and Suez corridor (e.g., missile scares in 2023) created uncertainty and occasional spikes in rates on those routes. Finally, the market structure of container shipping evolved during this period in a way that favoured carriers. The industry analysis noted that the container shipping sector effectively transitioned from a highly competitive (near Bertrand) market pre2020 to a more oligopolistic or coordinated pricing environment by 2021-2022, as major carrier alliances exercised newfound pricing power. Multiple sources conclude that without all these factors occurring together, the enormous rate increases of 2021 would not have been nearly as severe.

Elevated freight costs have broad implications for trade and prices in the global economy. In essence, higher transportation costs act like a tax on trade, raising the delivered price of imported goods. The World Trade Organization reported that after the steep collapse in 2020, global merchandise trade volumes rebounded by about +9.7% in 2021, but this recovery came at significantly higher costs - global export and import price indices rose by roughly +15% in 2021 alone [19]. The gap between the resurgence in trade volumes and the even larger increase in trade values suggests that the higher shipping and input costs were a major factor driving up prices. In purchasing managers' indexes (PMIs) at the time, businesses consistently cited supply chain bottlenecks and soaring freight rates as key contributors to rising input prices.

An analysis by the International Monetary Fund found that spikes in global shipping rates (as measured by indicators like the Baltic Dry Index) lead to statistically significant increases in import prices and producer price indices and eventually put upward pressure on consumer price inflation across many countries [20]. Similarly, the OECD has documented that inflation in container shipping costs feeds into higher inflation for imported goods, and to a lesser extent raises core consumer price index (CPI) inflation over time [21]. In practical terms, as firms faced drastically higher costs for ocean transport, many were forced either to accept lower profit margins or to raise the prices of final goods. Case studies underscore this dynamics: for example, the central bank of Chile estimated that the jump in freight costs during 2019-2021 accounted for roughly 14% of total inflation in Chile over that period. In addition, UNCTAD's modelling exercises have warned that if severe shipping disruptions persist (for instance, a protracted crisis on a major route like the Red Sea corridor), global consumer price levels could end up about 0.6 to 1.5 percentage points higher by 2025 than they would otherwise be [22].

In the short run, rising transport costs and longer transit times tend to dampen trade volumes because some transactions become less profitable or face fulfilment delays. UNCTAD projected that global maritime trade growth would slow to only around 1.4% in 2022 (down from the higher pre pandemic growth rates). The WTO similarly noted that ongoing supply frictions "weighed on trade" through 2021-2022, even as overall demand remained robust. Nonetheless, since the consumer and industrial demand was very strong during the recovery, the global trade volumes did continue to grow; it was the efficiency of trade that suffered, as evidenced by the much higher costs and prices. From a macroeconomic perspective, the surge in shipping costs acted like a negative supply shock to the world economy. General equilibrium models (for example, simulations using the GTAP framework) indicate that the shipping disruptions of 2020-2021 likely reduced real GDP and increased price levels in many regions, with especially pronounced effects on small, import dependent economies, particularly those that rely heavily on imported goods, such as many developing island states experienced larger inflationary effects from the shipping crunch. In summary, elevated transport costs during the pandemic likely trimmed global trade growth modestly and added on the order of 0.5-1 percentage point to global consumer inflation during 2020-2024. Import dependent regions like Central Europe would have felt these effects even more. Notably, OECD analysts in 2025 underscored that recent volatility (e.g., the late2023 shipping disruptions) means freight costs shocks remain "relevant for policymakers" due to their significant inflationary spillovers.

The surge in shipping rates effectively raised the costs of obtaining goods, components, and raw materials, directly increasing input costs for firms [23]. The SMEs that import intermediate goods from Asia or other distant markets saw their delivered materials costs skyrocket, which immediately squeezed their profit margins. Smaller firms, with typically low negotiating power on shipping, often had to pay the going spot rates, unlike some larger importers who might have locked in lower rates via contracts. A broad survey of SMEs in the U.S. reported that higher material and transport costs were "compressing profit margins," forcing firms to cut expenses elsewhere and search for process innovations just to stay afloat. In many cases, the steep increase in freight costs was partially passed through to final prices (contributing to inflation in consumer goods) - an action necessary for survival that nonetheless risked reducing customer demand. In Central Europe, where many SMEs rely on imported inputs, companies faced difficult choices: absorb the higher logistics expenses and accept lower margins, seek alternative suppliers (e.g., closer to home), which might be costly, or raise output prices. The Czech/Slovak business survey mentioned earlier confirms that pandemic era border closures and logistics breakdowns led to shortages of raw materials and goods, implying that SMEs sometimes had to pay more for

scarce inputs or find expensive workarounds [15]. All of these factors put intense upward pressure on small firms' costs of goods sold.

The tumult in global shipping forced changes in how the SMEs manage inventories and procure goods. During 2020-2021, many firms depleted their inventories to unusually low levels (for instance, a U.S. small business index showed inventory to sales ratios hitting record lows) because restocking became slower and costlier. Fearful of stockouts and further delays, some SMEs began ordering larger quantities or critical supplies earlier than usual, effectively increasing their buffer stocks when possible. In other cases, companies paid premiums for faster shipping or guaranteed space. Longer lead times, due to port congestion, container scarcity, and route deviations, meant that just in time inventory models became risky; instead, firms had to carry more just in case inventory, which ties up working capital. UNCTAD noted examples of carriers offering "premium" ocean services at higher rates to secure container space, meaning shippers (including smaller companies) sometimes paid twice for a single shipment (a standard rate plus a surcharge for priority) to ensure delivery. These disruptions upended the inventory management of SMEs and could have led to higher warehousing costs and cash flow challenges, as money was locked into goods in transit or sitting in stock as a hedge against uncertainty.

Inflationary supply shocks like a freight surge tend to hurt SMEs' profitability more than that of larger firms. Empirical surveys indicate that rising input costs and inflationary pressures squeezed SMEs' margins disproportionately [24]. According to an EU Commission review, the inflationary spike during the pandemic eroded small firms' profit margins by an estimated ~0.6 percentage points on average, a significant hit relative to typical SME margins - whereas larger firms generally managed to weather cost increases better. The fundamental issue is that many SMEs have limited ability to raise their own prices quickly or to a sufficient extent. Smaller businesses often compete on thin price differences and hesitate to risk losing customers; they may also lack the market power to pass on cost increases without demand suffering. As a result, input costs inflation translated more directly into reduced gross margins for these firms. A report by Visa surveying small businesses noted that 90% of SMEs worldwide experienced supply chain disruptions in 2021 and expected these issues to continue, suggesting that the majority were bracing for sustained pressure on their costs and earnings. In Central Europe, it is common for SMEs to operate with single digit profit margins, so any additional freight surcharges posed a serious dilemma: either accept a hit to earnings or increase prices (and potentially drive away price sensitive buyers) [25]. In practice, many did a mix of both, but either way their financial position deteriorated compared to the precrisis norm.

Ultimately, the combination of higher costs, logistical delays, and pricing challenges undermined many SMEs' overall performance and threatened their survival. A survey of SMEs in Slovakia and Czechia concluded that a large share of firms found themselves with "low liquidity, nonnegligible fixed costs and resulting financial problems" as the COVID crisis unfolded [26]. Although that study examined the pandemic's impact broadly (including demand shocks and lockdowns), supply chain disruptions and rising input costs were among the key difficulties contributing to those financial strains. Across Europe, inflationary shocks in 2021-2022 led numerous SMEs to scale back operations, defer investments, or even exit the market. For example, one European survey reported that small businesses experienced record increases in costs, and many anticipated a decline in profits moving forward. The cited Slovak/Czech study also emphasized that SMEs in that region had very limited financial buffers; notably, a large fraction of those firms chose not to take on available emergency loans, fearing debt amid the uncertainty, which implies that they largely absorbed the higher costs by depleting their own cash reserves rather than risking new liabilities [26]. The European Commission's 2023 report on SMEs likewise identified supply chain challenges as a major constraint on small firms' growth and viability in 2021-22. In sum, while no single study has isolated the specific effect of freight costs on V4 SMEs, the converging evidence suggests that these landlocked businesses bore substantial fallout from the global shipping crisis. Steep freight surcharges fed into higher input costs at the firm level, which translated into squeezed margins, operational hurdles, and in some cases business closures or consolidations. This underscores the importance of building greater resilience among SMEs to withstand such external logistic shocks in the future.

Several recent peer reviewed studies have examined how logistics and maritime transport systems and especially small and medium enterprises (SMEs), responded to pandemic induced supply chain disruptions. Below are key examples, highlighting their methods, data, findings, and noted research gaps.

Research on logistics disruptions and SMEs during and after COVID19 has employed a wide range of methodological approaches. For example, Veselovska [27] used a largescale survey of firms in Central Europe (including Czechia, Poland, and Slovakia) to examine the earlystage responses to supply chain shocks, finding that operational adjustments and new partnerships improved resilience. Gurbuz et al. [26] combined a qualitative case study of a Turkish SME with simulation modelling of supply chain network configurations, showing that diversified sourcing and customer bases mitigated disruption risks. Li et al. [28] applied a Threshold Vector Autoregression (TVAR) to longitudinal data from nearly 600 Chinese SMEs, identifying nonlinear effects of successive pandemic waves on supply chain disruptions,

costs, and customer losses. Burinskas, Cohen, and Drozdz [29] employed a gravity model with a difference in differences specification to analyse the Central and Eastern European trade flows, demonstrating that supply shocks reduced imports of intermediate goods and highlighted vulnerabilities in manufacturing supply chains. In contrast, Grzelakowski [30] adopted a qualitative, descriptive approach based on industry and institutional data to assess maritime and logistics sector responses, emphasizing structural weaknesses and the need for digitalization and regionalization. Together, these studies show that existing research employs both quantitative and qualitative designs, but few integrate firm level panel data in the V4 context, leaving a gap that this study addresses.

2 Methodology

In this study is employed a panel data approach to examine how maritime freight costs have affected the financial performance of small and medium sized enterprises (SMEs) in the Visegrad (V4) countries (Czechia, Hungary, Poland, and Slovakia) during the period 2020-2024. The guiding research question (RQ) is:

How have fluctuations in maritime freight costs since 2020 affected SMEs' selected company financial indicators in the V4 region?

The COVID19 pandemic created a unique setting in which global shipping costs surged to historic highs, introducing an external shock that plausibly influenced SME operations. A panel data approach allows to exploit both cross sectional variation between firms and timeseries variation across years, while controlling for firm specific unobserved heterogeneity. This strengthens the analysis by accounting for differences between firms that do not change over time (e.g. industry or country factors), isolating the impact of freight cost fluctuations on financial outcomes.

2.1 Data source and sample protection

Firm level data were obtained from the ORBIS database (Bureau van Dijk), covering active private companies in the four V4 countries from 2020 through 2024. The initial dataset contained approximately 13.3 million firm year observations across the four countries. To focus on comparable businesses, the sample was gradually narrowed through filtering steps.

SME Definition: The study targets SMEs as defined by the EU. Firms were restricted to those with 11-250 employees and annual operating revenues between €2 million and €50 million. This ensures a focus on true small and medium enterprises (excluding microenterprises and large firms).

Only companies with recent and complete financial statements for all the years in the 2020-2024 period were included. Public authorities and state-owned entities were excluded to focus on private sector SME performance.

The final sample is a balanced panel of 8,371 SMEs, meaning each of these firms has complete data for every year from 2020 to 2024. By requiring a balanced panel, the analysis avoids distortions from entry or exit of firms and ensures sufficient longitudinal coverage for each firm. Data was exported on date 15.08.2025.

By concentrating on firms of comparable size and excluding very small firms with potentially atypical accounting, the dataset provides a representative and reliable sample of the SME segment in the V4 region. This careful sample selection improves comparability and robustness of the results. Overall, out of 8,371 companies, 921 are from Czechia (11 %), 2,323 from Hungary (28 %), 1,611 from Poland (19 %) and from Slovakia 3,516 (42 %).

2.2 Variables and measures

The impact of shipping costs is analysed on several aspects of firm performance. Four dependent variables are chosen to capture different dimensions of SME financial performance (all monetary values are harmonized in euros and reported on an annual basis):

Operating Revenue (Turnover, € thousands): Total sales revenue, reflecting the scale of operations and market activity of the firm each year. Higher turnover indicates growth in business activity. Turnover captures the demand-side response to a cost shock. If firms pass higher transport costs into output prices, demand may decline, particularly for SMEs facing elastic demand, making revenue an indicator of market adjustment to freight-cost inflation.

Gross Margin (%): A profitability ratio calculated as gross profit divided by turnover (expressed as a percentage). Gross margin indicates the firm's ability to generate profit after accounting for the cost of production. A lower gross margin suggests margin compression (e.g. higher costs not fully passed on to customers). Gross margin reflects firms' pricing power and costs' pass-through ability. A decline following freight costs increases indicates incomplete transmission of higher input costs to customers and therefore margin compression typical for smaller firms in competitive markets.

Inventory (Stock, € thousands): Year-end value of inventories. This reflects the firm's working capital tied up in stock and can indicate supply chain adjustments. An increase in inventory might signal stockpiling in response to anticipated supply disruptions or cost changes. Inventory measures operational adjustment to supply-chain uncertainty. Rising shipping costs and delivery volatility often lead firms to precautionary stockpiling, making inventories a proxy for risk-mitigation behavior rather than production expansion.

Cost of Goods Sold (COGS, € thousands): The

direct costs of production (including materials, labour, and overhead associated with goods sold). The COGS is closely related to input cost pressures; higher COGS may reflect increased input prices, possibly due to higher freight and material costs. The COGS captures the direct cost channel of the shock. Higher maritime freight rates increase import prices of intermediate inputs, raising production costs even without changes in output quantity.

Together, these indicators provide a complementary view of firm performance - covering revenue generation, profitability, operational stock management, and cost structure. Changes in these variables can illuminate how firms respond to external cost shocks in both their topline (revenue) and bottom line (costs and margins).

Main Explanatory Variable - Shipping Cost Index: The key independent variable is the Shanghai Containerized Freight Index (SCFI) for the Europe route. The SCFI, published by the Shanghai Shipping Exchange, measures spot container shipping rates on the Shanghai-Europe trade route and is a widely recognized benchmark of global maritime freight costs [9]. Annual average values of the SCFI (Europe route) are obtained for each year 2020-2024 (sourced via Trading Economics from the Shanghai Shipping Exchange). This index serves as a proxy for worldwide shipping cost fluctuations that would affect import/export expenses for firms in Europe.

The SCFI is matched to each firm year observation by year. Since it is a global index, SCFI varies only across years (common to all firms each year) and not across individual firms. While this lack of cross-sectional variation in the index means firm differences in freight exposure are not directly observed, using a common index ensures we capture a common external shock faced by all firms in the region each year. The period of analysis includes dramatic swings in shipping costs, notably a sharp increase during 2020-2021 amid pandemic disruptions and subsequent normalization, providing a useful context to observe how such cost shocks correlate with firm financial metrics. Since individual SMEs cannot influence global container freight rates, changes in the SCFI can be treated as an exogenous macroeconomic cost shock affecting all firms simultaneously.

2.3 Hypothesis

Rising maritime freight costs represent an external cost-push shock affecting imported inputs and delivery reliability. Firms may respond through price adjustments, cost absorption, or operational adaptation. The following hypotheses test these distinct transmission channels within SMEs.

H1: Higher maritime freight costs are associated with increased SME turnover (operating revenue).

Under the cost-push inflation, firms may increase output prices to compensate for higher transport expenses. When demand remains relatively inelastic in the short run, nominal revenues rise even if quantities do not change, implying positive revenue adjustment.

H2: Higher maritime freight costs are associated with lower SME gross margins.

In competitive markets SMEs often have limited pricing power and cannot fully transmit higher logistics costs to customers. Economic theory therefore predicts margin compression when input costs rise faster than the output prices.

H3: Higher maritime freight costs are associated with increased SME inventory holdings.

Supply-chain uncertainty increases precautionary stockholding. Firms facing delivery delays or volatile transport prices accumulate inventories as a buffer against production disruptions and future price increases.

H4: Higher maritime freight costs are associated with higher SME cost of goods sold (COGS).

Transport costs are embedded in input prices; therefore, an increase in shipping rates directly raises production costs through more expensive imported materials and intermediate goods.

Together, these hypotheses test whether the global freight shocks propagate primarily through pricing behaviour, profitability pressure, operational risk management, or direct cost transmission in SME financial accounts.

2.4 Panel data and model specification

To quantify these relationships, a panel regression model with fixed effects (FE) was employed, estimated separately for each of the four dependent variables. The general specification can be written as:

$$Y_{it} = \alpha_i + \beta SCFI_t + \varepsilon_{it}, \quad (1)$$

where Y_{it} represents the financial outcome of interest for firm i in year t. The term SCFI is the Shanghai Containerized Freight Index value in year t, which serves as our independent variable capturing shipping prices. The coefficient β measures the impact of an one-unit change in the SCFI on the dependent variable. The term α_i denotes the firm specific intercept or fixed effect, which captures all time invariant characteristics of firm i that could affect its financial metrics (such as the firm's industry, inherent efficiency, or country specific factors). Finally, ε_{it} is the idiosyncratic error term for firm i at time t, representing all other unobserved influences

that vary over time. The inclusion of firm fixed effects means the coefficients are identified purely from within firm variation over time. In practice, the estimation uses the within transformation (demeaning each variable by that firm's average over 2020-2024), so that each firm serves as its own benchmark. This approach discards any between firm variation and thereby eliminates bias from omitted time invariant factors. Essentially, it is asked when a given firm experienced higher (or lower) shipping costs than its usual level (via yearly changes in SCFI), did it also exhibit changes in revenue, margin, inventory, or COGS relative to its usual levels.

Both fixed effects (FE) and random effects (RE) panel models in preliminary analysis are estimated. A Hausman test was then conducted to compare the two estimators. The Hausman test strongly indicated that the FE model is more appropriate, suggesting that unobserved firm characteristics are correlated with the shipping cost proxy (violating the RE assumptions). Therefore, all the main results are reported using the fixed effects specification.

Key aspects of the estimation strategy include these steps.

Fixed Effects over Random Effects: Choosing the FE estimator means each firm is allowed to have its own intercept. This accounts for unobservable factors (e.g., a firm's business model or sector) that could influence outcomes and potentially correlate with freight cost exposure. By using FE, biased estimates that might arise if, say, more globally oriented firms (with certain performance traits) also face different freight cost impacts are avoided.

Cluster Robust Standard Errors: To ensure reliable inference, the clustered standard errors are employed at the firm level. Clustering by firm accounts for potential heteroskedasticity (unequal error variance across firms) and serial correlation (errors for a given firm being correlated over time). This is important because the same firm's outcomes over years might be subject to persistent shocks or measurement issues. Diagnostic tests were performed: the Wooldridge test for autocorrelation in panel data indicated potential serial correlation, and the Breusch-Pagan test indicated heteroskedasticity. By clustering the standard errors on firms, we correct for both issues, making our statistics and confidence intervals more reliable.

Exogeneity of Shipping Cost Index: The SCFI is used as an external proxy for shipping costs because firm level freight expenditure data are not available (and if they were, they might be endogenous to firm performance). The SCFI is determined by global logistics market conditions and is plausibly exogenous to any single V4 firm. Using a global index mitigates endogeneity concerns -it is unlikely that an individual firm's performance could influence the global freight index. This strengthens the causal interpretation that changes in the SCFI reflect an external cost shock impacting firms, rather than the reverse.

2.5 Omission of additional controls

Other control variables, such as firm size, sector, or country dummies, are deliberately excluded in the regression.

This is for several reasons. All firms in the sample are constrained to the SME category by design, which ensures a relatively comparable scale. There is a limited variation in size by construction (e.g., micro firms with medium firms beyond the defined range are not mixed).

Sector and country differences are time invariant for each firm in this short panel and are thus already accounted for by the firm fixed effects. For example, if a firm is in manufacturing or located in Poland, that characteristics does not change over 2020-2024 and its average effect is absorbed by the fixed effect.

Including additional controls that do not vary (or vary very little) in this five-year period could introduce multicollinearity with the fixed effects or simply consume degrees of freedom without providing new information. Given the relatively short time dimension (5 years), parsimony is preferred to maintain statistical power.

By focusing on the core relationship between the SCFI and firm performance outcomes and using a rigorous fixed effects approach with robust errors, the estimation strategy aims to isolate the impact of maritime freight cost fluctuations on SMEs as cleanly as possible.

3 Results

The panel regression analyses revealed significant relationships between the maritime freight costs and key measures of SME financial performance in the Visegrad Group (V4). A Hausman specification test was first conducted to choose between random and fixed effects for the panel models. The test results presented in Table 1 strongly rejected the random effects model ($\chi^2 \approx 61.86$, $p < 0.001$), indicating that the firm specific effects are correlated with the regressors. Therefore, adopting a fixed effects specification for all subsequent models. This approach controls for time invariant differences across firms (such as size or industry), isolating the impact of time varying maritime freight costs on performance outcomes. Each model used the global freight cost index as the key independent variable and one financial performance indicator as the dependent variable, with n = 8,371 firms observed annually from 2020-2024 (total observations ranging from 41,673 to 41,695 depending on data availability). The freight costs index increased sharply during 2020-2021 and then moderated by 2023, providing a natural experiment to assess cost shock impacts on firms. Reported below the estimated coefficients (β) and significance levels for the freight index's effect on four performance metrics: operating revenue

Table 1 *Output from GRETL software*

Dependent variable	Coefficient index	Std. error	t-ratio	p-value	within R^2
Turnover	0.0545	0.0134	4.05	***	0.00049
Margin	-0.00011	2.32×10^{-5}	-4.75	***	0.00068
Stock	0.0334	0.00367	9.1	***	0.00248
COGS	0.0464	0.0096	4.85	***	0.0007

(Turnover), gross margin ratio (Margin), inventory holdings (Stock), and cost of goods sold (COGS).

Revenue and Cost Effects: Rising maritime transport costs were associated with higher operating revenues and higher cost of goods sold for V4 manufacturing SMEs. In the turnover model, the freight cost index showed a positive coefficient ($\beta \approx 0.054$, $p < 0.001$), implying that an upswing in global shipping rates corresponded to a modest increase in SME sales. Although the counterintuitive at first glance, this result suggests that firms were largely able to pass on elevated logistics expenses to customers in the form of higher prices, thereby inflating nominal revenues. The finding aligns with broader economic observations during the COVID19 pandemic: surging transport costs fed into output price inflation without necessarily suppressing demand. At the same time the SMEs experienced a substantial rise in input costs. The coefficient on the freight index in the COGS model was positive and sizable ($\beta \approx 0.0464$, $p < 0.001$), indicating that higher shipping rates led to significantly higher cost of goods sold. In other words, as maritime freight became more expensive, the cost paid by SMEs for imported materials and components rose commensurately, squeezing their cost structure. This evidence confirms that global logistics shocks were directly transmitted into firms' production costs, consistent with recent IMF analyses showing shipping cost spikes pass through to higher producer prices. It is important to note that while the revenue uptick suggests SMEs did not lose sales in aggregate, the cost increase was proportionally much larger. The net effect was a deterioration in profitability, as discussed next.

Profitability and Margin Effects: SME profit margins were noticeably eroded during periods of high freight costs. The gross margin ratio (gross profit as a percentage of sales) showed a negative association with the freight index. The fixed effects model estimates for Margin yielded €≈ -0.00011 ($p < 0.001$), indicating that each unit increase in the shipping cost index led to a slight but significant decline in gross margin percentage. Although the coefficient may appear small in absolute terms, its effect is nonnegligible given the large swings in freight rates over 2020-2021. For example, at the peak of the logistics crisis the global freight indices climbed several hundred points above their 2019 baseline; our estimate suggests that such a shock would cut the average SME's gross margin by a few tenths of a percentage point. This constitutes a meaningful reduction considering that the sample's mean gross margin was around 42%. The finding empirically confirms that soaring transport costs squeezed profit margins for manufacturing SMEs in Central Europe. The SMEs were forced to absorb part of the cost surge rather than fully transferring it to customers, resulting in margin compression. This result is in line with qualitative reports of firms' profitability being under pressure due to pandemic era supply chain disruptions. This analysis provides clear evidence of this effect in the V4 context - as transport costs rose, SME profitability declined, even though sales revenue rose, because cost of sales outpaced any price markups.

Inventory (Stock) Adjustments: The surge in freight costs was further associated with changes in inventory management. It is found that SME inventory levels (Stock) increased significantly in response to higher shipping prices. The freight index's coefficient in the inventory model was positive (€ ≈ 0.033, $p < 0.001$), suggesting that firms held greater stocks of inputs and products when transport became costlier. One interpretation is that V4 manufacturers adopted more of a "just in case" strategy: anticipating prolonged delivery times and future cost increases, they accumulated extra inventory as a buffer. This behaviour has been observed globally during the pandemic supply crunch, as companies built up safety stocks to hedge against logistics uncertainty. These findings corroborate this adaptation where SMEs increased their inventories in tandem with freight cost spikes, likely to avoid stockouts or lock in lower shipping costs before further rate rises. While such a stockpiling would amplify the short-term costs (tying up working capital in inventory), it was a rational response to unpredictable, expensive freight service. In summary, high maritime transport costs not only raised direct expenses but also induced firms to alter their operations (e.g., inventory policies), with potential knock-on effects on financial statements.

Across all these regressions, the effects of freight costs are statistically significant at the 0.1% level or better, underscoring a robust link between global transport prices and SME performance metrics from 2020-2024. However, the magnitude of these effects remains relatively small in economic terms when viewed against overall firm variability. The fixed effects models have very low within firm R^2 (on the order of 0.05% or less for the freight index alone), indicating that year to year fluctuations in freight prices explain only a tiny fraction of the variance in individual firms' financial outcomes. Most variation is driven by the firm specific factors and idiosyncratic shocks not captured by the

transport index. Thus, while a clear directional pattern exists - higher freight costs push up revenues and costs and compress margins - the transport cost factor by itself did not dominate firm performance during 2020-2024. This nuance is important for interpreting the practical significance of the results, as discussed below.

4 Conclusions

These results provide empirical support for the hypothesis that global logistics costs influence manufacturing SMEs' financial health, while also highlighting the limits of that influence. Each finding can be contextualized considering existing literature and economic theory. Overall, this study aligns with prior research on supply chain shocks and extends it by quantifying the impact of the 2020-2021 freight cost surge on firm level outcomes in Central Europe.

First, the positive revenue response to higher freight costs suggests a passthrough of cost inflation to customers. This observation is consistent with macroeconomic analyses that documented strong pricing power and inflationary passthrough during the COVID19 supply chain disruptions. Notably, the International Monetary Fund (2022) reported that the surge in shipping rates in 2021 added as much as 1.5 percentage points to global consumer price inflation in 2022. Firm level evidence [9] mirrors this macro trend: V4 SMEs raised their output prices (and hence revenues) alongside rising input costs. In the context of existing literature on SMEs, this finding nuances the commonly held view that small firms struggle to transfer cost increases to prices [9]. In fact, during an economywide shock that affected all firms, even SMEs could increase prices without losing customers, as the entire market faced the same cost pressures. This outcome might reflect a low elasticity of demand for certain manufactured goods in the short run or a general inflationary environment in which customers reluctantly accept higher prices. It may also indicate that V4 manufacturers benefited from strong post pandemic demand in Europe, allowing them to maintain sales volumes despite charging more per unit. Our findings here converge with the observations of OECD (2021) that post lockdown demand and supply bottlenecks jointly fuelled a sharp uptick in prices across many sectors.

Second, the erosion of gross margins under high freight costs conditions is firmly in line with theoretical expectations and prior studies of supply chain risk. When input costs rise rapidly, firms often cannot fully offset the increase through higher prices, especially if contracts or competitive pressures limit immediate price adjustments [31]. The SMEs in the sample experienced a squeeze in profitability, as evidenced by the significant drop in gross margin ratio. This result dovetails with the findings, which noted that SMEs during the pandemic faced margin pressures due to rising transportation and procurement costs [8]. It also complements the works, which emphasized that greater dependence on external suppliers can heighten SMEs' cost vulnerabilities and hurt their financial performance [9]. In this case, even without directly measuring supply chain dependence, the freight index serves as a proxy for an external cost shock that hit virtually all import reliant firms. The fact that margins fell across the board supports the view that SME profitability is tightly linked to supply chain conditions. When those conditions deteriorate (e.g., logistics become expensive and unreliable), small manufacturers see an immediate negative impact on their bottom line. This aligns with broader evidence that unexpected cost spikes disproportionately affect smaller firms, which lack the buffering capacity and economies of scale that large firms have in absorbing cost shocks [9]. The contribution is to quantify that impact for the maritime transport disruption: a major spike in shipping costs can measurably shave off SME profit margins, even within a short one-to-two-year window.

Third, the finding that inventory levels increased with freight costs offers insight into SME adaptive behaviour. Inventory buildup is a double-edged sword: it can safeguard production against delayed inputs, but it ties up cash and risks obsolescence. The positive association between the freight index and stock levels in data suggests that the extraordinary nature of the 2020-2021 shock pushed firms to prioritize resilience over efficiency. This behavior is strongly consistent with reports of a shift from "just in time" to "just in case" inventory management during the pandemic (e.g., firms holding more stock to guard against supply disruptions). Empirical evidence confirms that such a shift occurred among V4 manufacturers. This outcome is also in agreement with supply chain management research that highlights inventory as a key buffer in times of uncertainty [8]. Interestingly, the inventory increase observed may have exacerbated the cost issues discussed above by purchasing and holding more inputs in advance, SMEs likely incurred higher holding costs and possibly paid premium prices, which could further dent profitability. In essence, the SMEs traded off some financial efficiency for greater supply security. This adaptive strategy aligns with the notion of supply chain resilience found in recent studies [3, 5], wherein firms accept short term cost increases to mitigate the risk of stockouts and lost sales. Results thus contribute to the literature by illustrating this trade off in quantifiable terms: high transport costs led firms to accumulate inventories, reflecting a strategic response to external risk.

It is worth noting that the models capture a short run contemporaneous relationship rather than long term causation. The analysis cannot conclusively determine whether the higher freight costs caused these performance changes or merely coincided with other forces (such as the general economic rebound in 2021-2022). However, the fact that the freight index is

a significant predictor even after accounting for firm fixed effects suggests a meaningful link. The discussion above interprets the relationships in a causal narrative (for example, positing that freight cost shocks squeezed margins), consistent with theoretical expectations and timing of events. This interpretation finds support in external evidence and reports, as cited. Still, one must be cautious: the freight surge occurred alongside other pandemic related challenges (labour shortages, energy price spikes, etc.), and those factors likely also influenced SME performance [7]. Results, therefore, are best viewed as evidence of correlation in line with plausible causation mechanisms, reinforced by the concurrence of our findings with widely reported real world trends.

4.1 Implications

The study's findings carry several important implications for managers, policymakers, and researchers concerned with SME performance and supply chain management. Managerially, the results underscore the importance of developing strategies for cost passthrough and cost control in times of volatile logistics expenses. The ability of V4 SMEs to maintain or even increase revenue during a period of soaring freight prices suggests that agile pricing strategies and customer communication were critical; SMEs that quickly adjusted their prices could protect their topline revenue. However, the overall decline in margins indicates that such firms still absorbed part of the cost increases. This implies that managers should explore long term solutions to bolster margins against supply chain cost shocks, for example, by diversifying sourcing options, renegotiating supplier contracts to share logistics costs, or improving operational efficiency to reduce other expenses. The significant inventory buildup observed also highlights a strategic consideration: resilience vs. efficiency. Firms chose to hold more inventory to mitigate risk, accepting higher holding costs. Managers must weigh these trade-offs and perhaps invest in better demand forecasting and inventory optimization tools. In an environment where global transport costs can swing dramatically, SMEs may benefit from incorporating scenario planning for logistics expenses and considering instruments like freight insurance or hedging if available.

For policymakers and support institutions, these findings illustrate how the global supply chain disruptions can ripple down to small businesses in landlocked economies. The V4 countries, though not directly on seacoasts, were clearly not insulated from maritime cost shocks - a reminder of their integration in global trade networks [10]. Policymakers should therefore consider measures to help the SMEs manage such external shocks. For instance, governments might provide temporary freight subsidies or logistics support programs during extreme cost surges to prevent excessive damage to SME profitability. Investing in alternative transport infrastructure (such as improving rail connections to major ports or supporting regional distribution hubs) could also alleviate the reliance on distant maritime routes and reduce freight cost volatility for inland firms [10]. Additionally, disseminating market intelligence, e.g., early warnings about rising freight rates and guidance on adaptive strategies, could empower SME owners to respond proactively. From a financial perspective, the fact that SMEs' margins were squeezed suggests many may have experienced cash flow stress during the high freight cost period. This underscores the need for accessible financing solutions or emergency credit lines for SMEs when global shocks drive up working capital requirements (as when firms must pay more for inventory and shipping [10]. In summary, an implication for policy is that the SME's resilience in global supply chains can be strengthened through a targeted support, infrastructure investment, and information sharing to mitigate the impact of abrupt logistics cost swings.

For scholars and future research, this study provides a baseline quantification of freight cost impacts and points to several avenues for further investigation. The very low within firm explanatory power of the freight index indicates that most performance variation comes from other factors; future research could incorporate additional variables (such as input prices, exchange rates, or firm specific characteristics like liquidity and supply chain diversification) to build a more comprehensive model of SME performance under stress. Another implication is the importance of examining heterogeneous effects: our aggregate results show the average impact, but different industries or firms might have experienced varying degrees of pain or gain. Subsequent studies might segment the sample by industry (e.g., automotive vs. electronics manufacturing) or by firm size/maturity to see if certain groups were more vulnerable to freight cost shocks. Moreover, qualitative research could complement these quantitative findings by exploring how exactly the SMEs managed to pass through costs or why some could not, thereby shedding light on the mechanisms behind the observed statistical relationships. Overall, our work highlights that global logistics factors deserve greater attention in SME performance research and that integrating supply chain metrics (like freight indices) into firm level studies can enrich our understanding of business vulnerability and resilience in an interconnected world.

4.2 Limitations

While this study offers novel insights, several limitations must be acknowledged. First, this analysis relies on Orbis accounting data and a single global freight index. The financial data include only a few indicators over a relatively short five-year horizon,

excluding important dimensions such as net profit, cash flow, operating expenses, and debt. The SCFI, although a reasonable proxy, may not perfectly capture firm-specific freight costs, which vary by route, cargo, and contract type. Since the index is common across firms, it is collinear with year effects, preventing to include the time fixed effects; thus, the estimated coefficients may partially reflect other concurrent macroeconomic trends (e.g., post-pandemic recovery, fiscal stimuli, or general inflation).

Second, the model assumes a contemporaneous linear effect. It does not account for potential lags, nonlinearities, or thresholds despite the possibility that firms experienced delayed or disproportionate responses. The analysis also treats the effect as homogeneous, even though the SMEs differ in logistics contracts, bargaining power, or supply-chain flexibility. Sample bias is another concern: Orbis underrepresents microenterprises and financially weaker firms, meaning the smallest SMEs are not captured. Finally, the study is observational and examines an exceptional period; results should be generalized with caution.

It is shown that the extreme freight costs swings of 2020-2024 had detectable but modest impacts on V4 manufacturing SMEs. Higher shipping costs coincided with higher revenues, larger inventories, and significantly higher COGS, compressing gross margins. Firms appeared to respond adaptively, especially via inventory expansion, which helped mitigate supply-chain uncertainty but raised holding costs. Overall, the results indicate that the inland SMEs were exposed to global logistics turbulence, even if freight costs explained only a small share of within-firm variation.

The findings contribute to the literature by quantifying how a global cost shock permeated the SME financials and by underscoring their partial resilience: SMEs could pass on some costs but still experienced margin pressure. For policymakers, the evidence highlights the need to strengthen the supply-chain resilience and protect smaller firms from extreme logistics price volatility. The 2020-2024 period effectively served as a stress test, offering lessons for preparing SMEs for future disruptions in freight markets and other critical input channels.

Acknowledgment

The authors received no financial support for the research, authorship and/or publication of this article.

Conflicts of interest

The authors declare that they have no known competing financial interests or personal relationships that could have appeared to influence the work reported in this paper.

References

[1] Review of maritime transport 2021. Geneva: United Nations Conference on Trade and Development UNCTAD, 2021.
[2] COVID-19 and maritime transport: navigating the crisis and lessons learned. Geneva: United Nations Conference on Trade and Development UNCTAD, 2022.
[3] The impact of the COVID-19 pandemic on freight transportation services and U. S. merchandise imports. Washington, DC: United States International Trade Commission USITC, 2021.
[4] High freight rates cast a shadow over economic recovery. Geneva: United Nations Conference on Trade and Development UNCTAD, 2021.
[5] CARRIERE-SWALLOW, Y., DEB, P., FURCERI, D., JIMENEZ, D., OSTRY, J. Shipping costs and inflation [online]. IMF Working Paper No. 2022/061. International Monetary Fund, 2022. Available from: https://doi.org/10.5089/9798400204685.001
[6] Small and medium enterprises (SMEs) finance: improving SMEs' access to finance. World Bank Group, 2021.
[7] *OECD Economic Outlook* [online]. 2021, **2**(110). ISSN 0474-5574, eISSN 1609-7408. Available from: https://doi.org/10.1787/66c5ac2c-en
[8] ERDIAW-KWASIE, M. O., ABUNYEWAH, M., YUSIF, S., ARHIN, P. Small and medium enterprises (SMEs) in a pandemic: a systematic review of pandemic risk impacts, coping strategies and resilience. *Heliyon* [online]. 2023, **9**(10), e20352. eISSN 2405-8440. Available from: https://doi.org/10.1016/j.heliyon.2023.e20352
[9] ZHANG, H., HU, M., JIANG, S. Profit or growth? The impacts of supplier dependence and customer dependence on SMEs' performance. *Sustainability* [online]. 2025, **17**(3), 1302. eISSN 2071-1050. Available from: https://doi.org/10.3390/su17031302
[10] RODRIGUE, J-P., KOLAR, P. Port regionalization and landlocked hinterland: the Czech Republic. *Central European Business Review* [online]. 2016, **5**(3), p. 69-77. ISSN 1805-4854, eISSN 1805-4862. Available from: https://doi.org/10.18267/j.cebr.159
[11] Financing SMEs and entrepreneurs 2021: an OECD scoreboard [online]. Paris: OECD Publishing, 2021. Available from: https://doi.org/10.1787/23065265

[12] Drewry Shipping Consultants. Container forecaster Q4 2022. London: Drewry Maritime Research, 2022.
[13] Economic Bulletin. 5/2022: supply bottlenecks and shipping costs. Frankfurt am Main: European Central Bank, 2022.
[14] Economic indicators and historical data for 196 countries - Trading Economics [online]. Available from: https://tradingeconomics.com
[15] Business tendency survey: COVID-19 impacts on SMEs. Prague: Czech Statistical Office, 2021.
[16] Economic Bulletin. 2/2023: special feature: global supply bottlenecks and inflation. Frankfurt am Main: European Central Bank, 2023.
[17] COVID-19 related goods: U.S. industry, market, trade, and supply chain challenges. USITC Publication No. 5119. United States International Trade Commission, 2021.
[18] Global maritime transport and logistics review. Geneva: United Nations Conference on Trade and Development, 2024.
[19] World Trade Report 2022: resilient and inclusive trade. Geneva: World Trade Organization, 2022.
[20] Monetary Policy Report (IPoM)/Informe de Politica Monetaria (IPoM) (in Spanish). Banco Central de Chile, 2022.
[21] BEKKERS, E., KOOPMAN, B. Simulating the trade effects of the COVID-19 pandemic: scenario analysis based on quantitative trade modelling. *The World Economy* [online]. 2020, **45**(2), p. 445-467. ISSN 0378-5920, eISSN 1467-9701. Available from: https://doi.org/10.1111/twec.13063
[22] NOTTEBOOM, T., PALLIS, T., RODRIGUE, J.-P. Disruptions and resilience in global container shipping and ports: the COVID-19 pandemic versus the 2008-2009 financial crisis. *Maritime Economics and Logistics* [online]. 2021, **23**, p. 179-210. ISSN 1479-2931, eISSN 1479-294X. Available from: https://doi.org/10.1057/s41278-020-00180-5
[23] *OECD SME and Entrepreneurship Outlook* [online]. 2022. eISSN 2959-9504. Available from: https://doi.org/10.1787/8d707502-en
[24] Impact of COVID-19 on Slovak SMEs. Bratislava: Slovak Business Agency, 2021.
[25] Back to business study: 2021 Outlook. San Francisco: Visa Inc., 2021.
[26] GURBUZ, M. C., YURT, O., OZDEMIR, S., SENA, V., YU, W. Global supply chain risks and COVID-19: supply chain structure as a mitigating strategy for small and medium-sized enterprises. *Journal of Business Research* [online]. 2023, **155**(part B), 113407. ISSN 0148-2963, eISSN 1873-7978. Available from: https://doi.org/10.1016/j.jbusres.2022.113407
[27] VESELOVSKA, L. Supply chain disruptions in the context of early stages of the global COVID-19 outbreak. *Problems and Perspectives in Management* [online]. 2020, **18**(2), p. 490-500. ISSN 1727-7051, eISSN 1810-5467. Available from: http://dx.doi.org/10.21511/ppm.18(2).2020.40
[28] LI, F., RUBINATO, M., WU, K., WANG, L., SHAO, S. Unravelling the non-linear impact of multiple pandemics on small and micro enterprises: a longitudinal study of operational challenges. *International Journal of Disaster Risk Reduction* [online]. 2025, **128**, 105737. eISSN 2212-4209. Available from: https://doi.org/10.1016/j.ijdrr.2025.105737
[29] BURINSKAS, A., COHEN, V., DROZDZ, J. Supply chain interconnectedness in times of crises: a gravity model with DiD analysis of COVID-19 effects on Central and Eastern European trade. *Economies* [online]. 2024, **12**(1), 12. eISSN 2227-7099. Available from: https://doi.org/10.3390/economies12010012
[30] GRZELAKOWSKI, A. S. The Covid-19 pandemic - challenges for maritime transport and global logistics supply chains. *TransNav: International Journal on Marine Navigation and Safety* [online]. 2022, **16**(1), p. 71-77. ISSN 2083-6473, eISSN 2083-6481. Available from: https://doi.org/10.12716/1001.16.01.07
[31] Global economic prospects, June 2022: a world stalled by supply shocks. Washington, DC: World Bank, 2022.

ECONOMIC AND INFRASTRUCTURE DETERMINANTS OF ROAD TRAFFIC FATALITIES: PANEL EVIDENCE FROM THE VISEGRAD COUNTRIES

Adela Poliaková[1], Eva Nedeliaková[1], Piotr Gorzelańczyk[2], Jakub Malik[1,*]

[1]University of Zilina, Faculty of Operation and Economics of Transport and Communications, Zilina, Slovakia
[2]Stanislaw Staszic State University of Applied Sciences in Pila, Faculty of Transport, Pila, Poland

*E-mail of corresponding author: jakub.malik@stud.uniza.sk

Adela Poliakova 0000-0002-9971-9589,
Piotr Gorzelańczyk 0000-0001-9662-400X,
Eva Nedeliakova 0000-0001-5588-0939,
Jakub Malik 0009-0008-4284-1920

Resume

In this study are analysed the determinants of road traffic fatalities in the Visegrad Group countries during 2000-2024, using a balanced panel and fixed-effects models with Driscoll-Kraay standard errors. The results show that the higher motorization and a longer high-standard road network are associated with lower fatalities. By contrast, the GDP per capita and unemployment increase fatalities in the baseline model, although these effects are sensitive to alternative specifications. Public expenditure on road infrastructure has no robust immediate effect, with only limited evidence of delayed benefits. Overall, the findings suggest that the road safety depends not only on economic growth, but on the quality and structure of infrastructure development, as well.

Article info

Received 12 January 2026
Accepted 31 March 2026
Online 17 April 2026

Keywords:

road safety
traffic fatalities
panel regression analysis
macroeconomic determinants
motorization

Available online: https://doi.org/10.26552/com.C.2026.023

ISSN 1335-4205 (print version)
ISSN 2585-7878 (online version)

1 Introduction

Traffic accidents are one of the most serious global challenges today, with consequences that go far beyond transport itself and have a significant impact on public health, economic development, and the sustainability of public finances. The road traffic deaths and injuries generate significant social costs in terms of loss of human capital, reduced labor productivity, increased healthcare spending, and pressure on public budgets. From an economic perspective, the road safety is not just a technical or behavioral issue, but a complex problem of efficient resource allocation and transport system performance. With increasing urbanization, intensified mobility, and diversification of transport modes, the complexity of the relationships between the transport infrastructure, economic activity, and road safety is increasing. Traditional approaches to assessing transport safety, which focus exclusively on absolute numbers of accidents or fatalities, are proving inadequate as they do not take into account differences in exposure to transport, the structure of transport systems, or the broader socioeconomic context. As pointed out in [1], the risk assessment based solely on driver fatalities can lead to biased conclusions, as it does not capture the external costs passed on to other road users, particularly pedestrians and cyclists. Including the so-called "third parties" in the analysis is therefore a necessary step towards a more accurate measurement of the social impact of different forms of transport.

The importance of infrastructure and its functional layout is particularly evident in urban environments and on high-capacity roads. Highways and expressways are primarily designed to maximize traffic flow and speed, but this can lead to an increased risk of serious accidents, especially in cases of illegal pedestrian movement or vehicle malfunctions. Empirical evidence from the US shows that high speed limits, multi-lane road layouts, and inadequate lighting contribute significantly to fatal pedestrian accidents, especially at night and in rural areas [2]. Those findings highlight the tension between the goals of transport efficiency and safety, which must be addressed through comprehensive evaluation frameworks. In response to this complexity, integrated analytical approaches that combine the evaluation of technical efficiency, productivity, and safety outcomes of transport systems are increasingly being promoted in the literature. In that study is highlighted the value of slack-

based network models, combined with the Malmquist and Luenberger productivity indices for evaluating the performance of urban road transport systems. Its results point not only to significant heterogeneity between cities, but to differences between the static efficiency and actual growth in total factor productivity, as well, which has important implications for transport policy and strategic decision-making in the public sector [3].

Another dimension of road safety is the macroeconomic view of safety, which is further underscored by evidence of causal relationships between road fatalities, economic growth, and public spending. An analysis [4] shows that the GDP growth per capita can be associated with an increase in road fatalities in both the short and long term, suggesting that economic growth without adequate investment in safety can lead to negative externalities. Conversely, higher health care spending and higher population density in many regions appear to be factors that reduce the risk of traffic fatalities, highlighting the importance of public policies and urban structure. The structure of traffic patterns and their safety implications also deserve special attention. Results from studies in developing countries suggest that promoting walking, cycling, and intermediate forms of public transport can lead to lower road fatalities, while the growth of motorization, particularly in the form of two-wheeled motor vehicles and private car transport, increases the risk of fatal accidents [5]. Those findings are particularly relevant in the context of transforming economies, where changes in the transport behavior of the population are occurring faster than the adaptation of infrastructure and regulatory frameworks.

At the micro level, the behavior of road users remains one of the key determinants of the severity of traffic accidents. Advanced machine learning methods reveal the importance of the seat belt use, accident timing patterns, and driver demographics in explaining road fatalities [6]. At the same time, it appears that times of crisis, such as the COVID-19 pandemic, can fundamentally change the risk factors for traffic accidents, especially in urban and socially disadvantaged areas, requiring flexible and data-driven policy interventions [7]. Despite the extensive empirical literature, however, there is still a need for integrated analytical frameworks that can simultaneously assess the performance of transport systems, the productivity of public investments, and their safety implications. In this study is provided an economically oriented quantitative analysis that helps to better understand the trade-offs between transport efficiency, economic growth, and the protection of human lives.

2 Literature review

The road safety assessment represents a significant social and economic challenge, as traffic accidents generate not only human casualties, but the considerable direct and indirect costs for the economy, public finances, and labor productivity as well. Current literature increasingly advocates a comprehensive approach to traffic accident analysis that integrates macroeconomic, infrastructural, demographic, and behavioral factors, with an emphasis on the use of advanced quantitative methods and panel data. Several empirical studies confirmed that economic development and socio-economic conditions play a key role in shaping long-term trends in road traffic fatalities. At the same time, research findings suggest that economic growth alone does not automatically lead to improved road safety unless it is accompanied by effective redistribution policies, investments in safety infrastructure, and increased social justice. The negative short-term effects of economic shocks, such as mass layoffs, point to the importance of psychological stress, economic uncertainty, and social destabilization as indirect determinants of traffic safety [8-9].

At the level of European countries, the economic dimension of road safety is also reflected in differences in the performance of national systems. Empirical analyses, based on a combination of envelope curve analysis and Tobit regression, indicate that the socioeconomic context and level of transport exposure significantly influence the resulting level of road safety. These findings support the need for comparative analyses that can capture heterogeneity between countries and identify structural weaknesses in transport policy. The role of transport infrastructure, technical development, and the efficiency of transport systems also receives significant attention in the literature, with evidence suggesting that the greater road transport efficiency in terms of energy and economic indicators does not necessarily lead to fewer traffic fatalities. Investments in road infrastructure and the expansion of the road network can thus have ambivalent effects on one hand, they improve the technical condition of roads and traffic flow, but on the other hand, they can stimulate higher traffic intensity and driving speeds, which increases the risk of serious accidents [10-11].

Technological innovations, particularly in the field of automated vehicles, are often presented as a potential solution to the problem of traffic accidents. Simulation models suggest that the growing penetration of automated vehicles may contribute to a reduction in the number of multi-vehicle accidents. At the same time, however, there remains a high degree of uncertainty associated with the real-world deployment of these technologies, their interaction with conventional vehicles, and driver behavior. These findings suggest that technological advances in mobility must be supported by an appropriate regulatory, institutional, and infrastructural framework in order for their potential safety benefits to be fully realized [12].

In addition to macroeconomic and technical factors, demographic and behavioral determinants of traffic accidents remain an important part of research. Advanced

time series and panel causal modelling methods identify a higher risk of fatal accidents in older age groups, in remote regions, during night hours, and in high-speed environments, emphasizing the importance of flexible panel approaches for evidence-based road safety policy making. At the micro level, research focuses on specific types of road users, particularly motorcyclists and young drivers, highlighting the importance of seasonal factors, reaction time, perceived behavioral control, and risk-taking behavior for accident probability and severity [13-16].

Current literature also pays increasing attention to environmental and climatic factors, which are increasingly shaping the road safety conditions. Empirical analyses identify a significant impact of extreme weather events and climate anomalies on the number of fatal traffic accidents, pointing to the growing complexity of the road safety environment in the context of global warming. Traffic accidents thus appear to be the result of a dynamic interaction between the economic, infrastructural, social, behavioral, and environmental factors, which places high demands on the interdisciplinary nature of research and public policy-making [17].

3 Methodology

The empirical analysis is based on an annual panel of four Visegrad Group countries: the Czech Republic, Hungary, Poland, and Slovakia for the period 2000-2024. The dataset was compiled based on data from the Eurostat database. The panel is balanced, with each country being monitored in each year of the sample period. All estimates were performed in Python. The panel data models were estimated using the linear models package for fixed and random effects specifications with Driscoll-Kraay standard errors. The dependent variable is the annual number of road traffic deaths in each country. This indicator captures all deaths resulting from traffic accidents that occurred within the country during the calendar year. The key explanatory variables are:

- Motorization: number of registered passenger cars per 1,000 inhabitants. This indicator captures the level of motorization and potential exposure to road risks.
- Economic development: gross domestic product per capita in euros, expressed in constant prices. This variable represents the level of economic development and overall income in each country.
- Labor market conditions: unemployment rate in percent. This variable captures macroeconomic and social pressures that may be related to road safety outcomes.
- Road infrastructure expenditure: annual public expenditure on road infrastructure in euros. This includes the construction, reconstruction, and maintenance of the road network.
- Length of high-standard roads: total length of motorways and European-class roads (e-roads) in kilometers. This variable reflects the quantitative development of high-standard road infrastructure.

The selection of explanatory variables included in the econometric model was based on three main criteria: theoretical relevance, empirical evidence from previous studies, and the availability of consistent long-term data for all V4 countries. The literature on the road safety and transport economics commonly identifies economic development, motorization, labour market conditions, and infrastructure quality as key determinants influencing traffic accident rates and the road fatalities.

Motorization, measured as the number of passenger cars per 1,000 inhabitants, reflects traffic intensity and the level of mobility within a country, which may increase exposure to traffic accidents but is also associated with improvements in vehicle safety over time.

The GDP per capita was included as an indicator of the overall level of economic development, which may affect the road safety through several channels, including infrastructure quality, technological progress in vehicle safety, and improvements in healthcare systems.

The unemployment rate was included as a control variable capturing macroeconomic conditions that may influence travel demand, commuting patterns, and overall traffic intensity. In periods of higher unemployment, mobility demand may decrease, potentially affecting the number of road accidents.

Finally, variables related to transport infrastructure, including the road infrastructure expenditures and the length of motorways and E-roads, were incorporated to capture the potential impact of infrastructure development on the road safety outcomes. High-quality road infrastructure is generally associated with safer traffic conditions and lower accident severity.

Together, these variables allow the model to capture the main economic and infrastructural mechanisms that are discussed in the road safety literature and that are particularly relevant for the development dynamics of the V4 countries.

All the variables are measured at a country and a year level. Where necessary, the series were checked for breaks and inconsistencies and harmonized over time to ensure comparability between the four countries.

To analyze the determinants of the road traffic deaths, the study uses a panel data regression model with country fixed effects. The basic specification can be written as:

$$Deaths_{it} = \alpha_i + \beta_1 Cars_{it} + \beta_2 GDPpc_{it} + \\ + \beta_3 Unemp_{it} + \beta_4 ExpRoad_{it} + \beta_5 Length_{it} + \varepsilon_{it}, \quad (1)$$

where: $Deaths_{it}$ is number of deaths,
i is countries,
t is years,

α_i are the fixed effects specific to a given country.

Fixed effects estimation is used as the main method since it controls for unobserved, time-invariant heterogeneity across countries that would otherwise distort the estimated coefficients. Specifically, differences in historical safety culture, legal traditions, or the long-term infrastructure subsidies are absorbed by country-specific intercepts. As a robustness check and to justify the focus on fixed effects, the model was also estimated using a random effects specification. Hausman's test, comparing the fixed and random effects estimates, showed that the fixed effects model is preferred, supporting the choice of using country fixed effects as the baseline specification.

The panel data on a small number of countries observed over a relatively long period of time are prone to several complications in terms of confounding effects: heteroscedasticity between panels, serial correlation over time within a country, and cross-sectional dependence due to common shocks or regional effects. To address these issues, the study reports the Driscoll-Kraay standard errors for fixed effects estimates. This estimate is robust to:

- heteroscedasticity,
- autocorrelation of unknown form within panels, and
- cross-panel dependence between panels.

The use of Driscoll-Kraay standard errors is particularly appropriate given the small number of countries (four) and the longer time dimension. It allows for consistent conclusions even when the shocks, such as Europe-wide policy changes, fuel price shocks, or significant regulatory reforms, affect all Visegrad Group countries simultaneously. For comparison, the same specification with fixed effects was also estimated with conventional heteroscedasticity-resistant standard errors and with standard errors pooled at the country level. The main coefficients of interest (motorization, GDP per capita, unemployment, travel distance) retained their sign and remained statistically significant in these alternative specifications, confirming the robustness of the results.

All the panel data estimates were performed using a fixed effects estimation with country dummy variables and without additional time dummy variables in the baseline to focus on the impact of the observed explanatory variables. The estimation was performed in three steps. First, descriptive statistics were used to examine trends in road deaths, motorization, GDP per capita, unemployment, road infrastructure spending, and length of highways/electric roads in each country. This preliminary analysis confirmed substantial time differences in all variables and a significant decline in deaths during the period under review. Second, standard panel data diagnostics was performed. The ordinary least squares (OLS), random effects, and fixed effects models were estimated and compared. The Hausman test favored the fixed effects specification, suggesting that unobserved country-specific factors correlate with the explanatory variables and that random effects would be inconsistent. Third, the preferred fixed effects model was estimated using Driscoll-Kraay standard errors. The coefficients were interpreted in terms of their sign, magnitude, and statistical significance at the conventional significance level of 0.05. To assess robustness, alternative specifications were considered, including models with different standard error estimates and reduced sets of covariates. These checks did not substantially alter the main conclusions. The interpretation of the empirical results focuses on the partial effects of each explanatory variable on the road traffic deaths, conditional on other variables and time-invariant country characteristics. The fixed effects setting means that the coefficients reflect how changes in motorization, economic development, labor market conditions, and infrastructure within a country over time are associated with changes in the number of road deaths, rather than the simple differences between countries. Particular attention is paid to the sign and magnitude of the coefficients for motorization (number of cars per 1,000 inhabitants), GDP per capita, unemployment, and length of highways/expressways, as these variables are directly related to the main research questions about the role of economic development and infrastructure in road safety in the V4 region.

4 Results

Figure 1 illustrates the long-term evolution of the road traffic fatalities in the Visegrad Group countries (Slovakia, the Czech Republic, Poland, and Hungary) during the period 2000-2024. A common downward trend can be observed across all countries, although the pace and timing of the decline differ.

At the beginning of the observed period, Poland recorded by far the highest number of the road fatalities, exceeding 6,000 deaths annually in the early 2000s. However, a substantial and continuous decline can be observed over the following years, with the number of fatalities decreasing to approximately 1,900 by 2024. This represents the most pronounced absolute reduction among the V4 countries and reflects significant improvements in the road infrastructure, vehicle safety, and regulatory frameworks.

A similar downward trend is visible in the Czech Republic, where fatalities declined from nearly 1,500 in 2000 to around 438 in 2024. The decline was particularly pronounced after 2008, which coincides with the introduction of stricter traffic regulations and improvements in enforcement and the road safety policies.

In Slovakia, the number of the road fatalities decreased from approximately 628 in 2000 to 262 in 2024. The most significant reduction occurred between 2008 and 2011, when the number of fatalities dropped sharply. Since the mid-2010s, the trend has stabilised

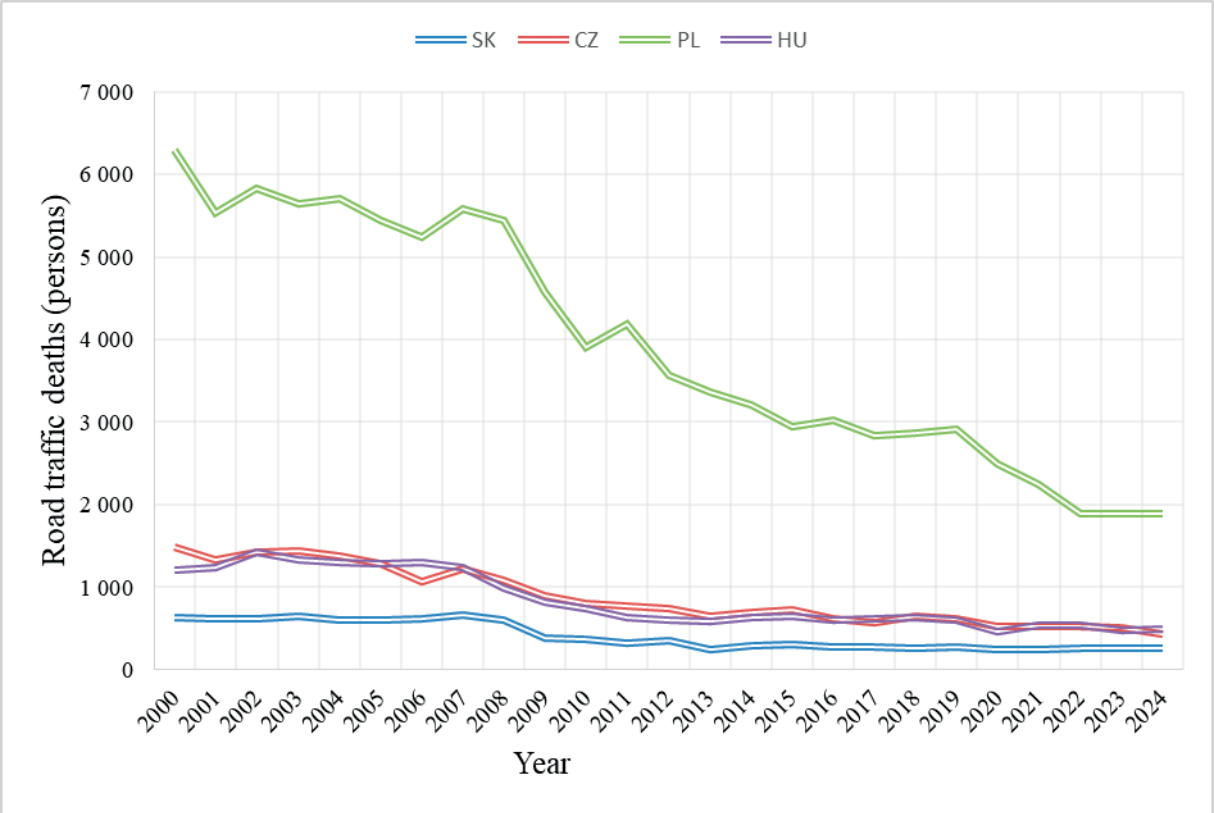

Figure 1 *Trends in road deaths in V4 countries*

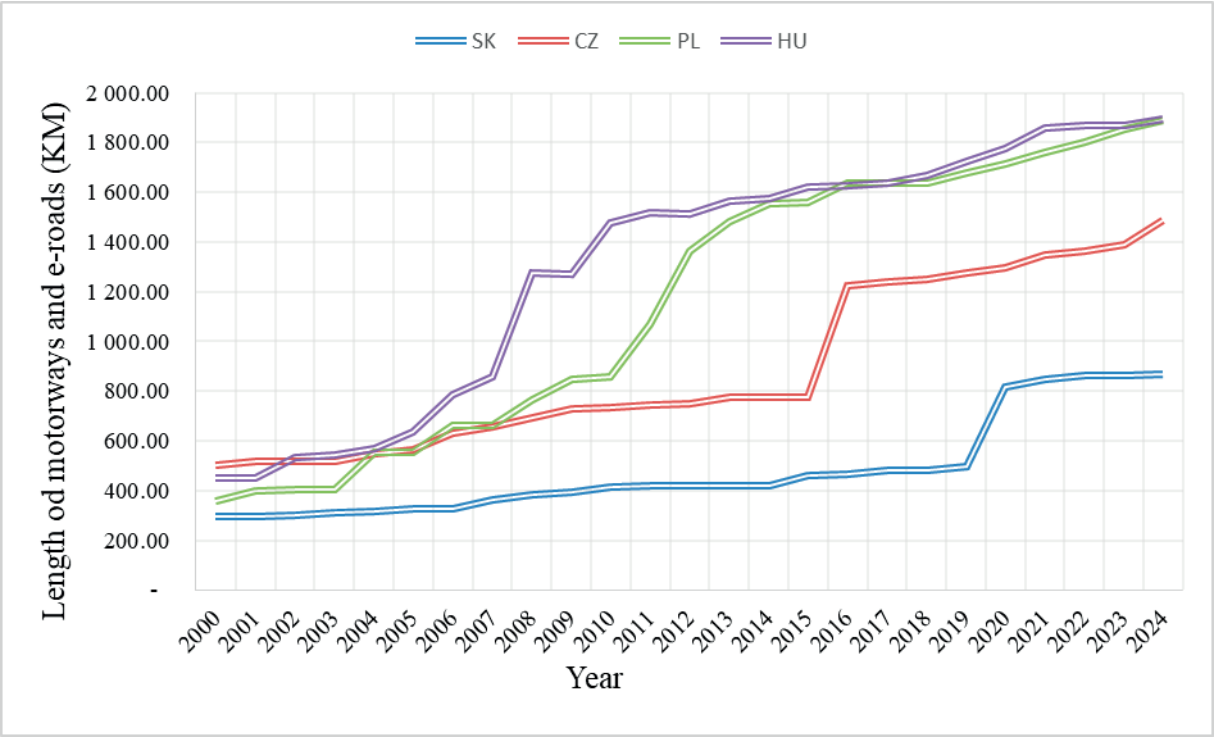

Figure 2 *Development of motorways and e-roads in V4 countries*

at a relatively lower level, with minor year-to-year fluctuations.

Hungary shows a comparable pattern, with fatalities declining from about 1,200 in 2000 to roughly 497 in 2024. The most substantial improvement occurred between 2008 and 2013, after which the number of deaths fluctuated around a lower but relatively stable level.

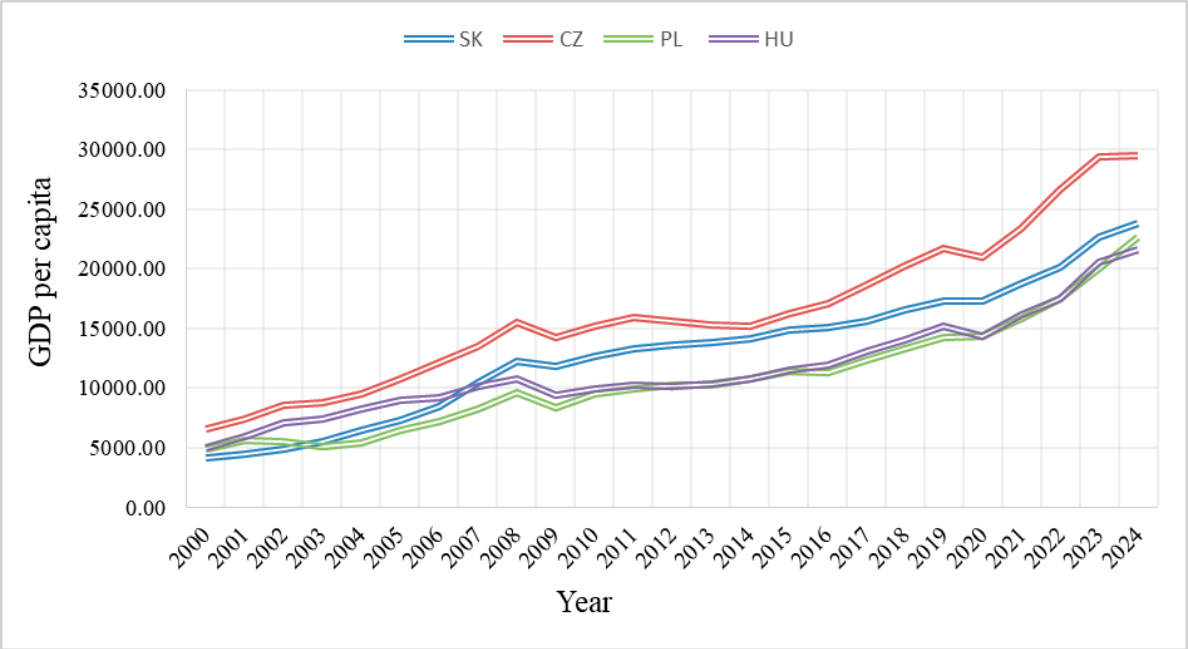

Figure 3 *Development of GDP per capita in V4 countries*

Figure 1 also indicates a temporary decline in fatalities during the period 2020-2021 across most countries, which may be associated with reduced traffic intensity during the COVID-19 pandemic. Overall, the graphical evidence suggests that despite differences in national dynamics, the road safety has improved significantly across the V4 region over the past two decades. These trends provide an important empirical background for the subsequent econometric analysis examining the macroeconomic and infrastructure determinants of the road traffic fatalities.

Figure 2 presents the development of the total length of motorways and E-roads in the Visegrad Group countries (Slovakia, the Czech Republic, Poland, and Hungary) between 2000 and 2024. Figure 2 reveals a substantial expansion of the motorway infrastructure across the region, although the pace and scale of development differ considerably among the countries.

At the beginning of the observed period, the Czech Republic possessed the most developed motorway network among the V4 countries, with approximately 499 km of motorways and E-roads in 2000. This network expanded gradually over the following years, reaching nearly 1,486 km by 2024. The growth was relatively steady, reflecting the long-term development of transport infrastructure and the strategic role of the Czech Republic as a transit country in Central Europe.

Poland experienced one of the most dynamic expansions of motorway infrastructure during the analysed period. The network increased from about 358 km in 2000 to nearly 1,888 km in 2024. The most significant expansion occurred after 2010, when the large-scale investments in transport infrastructure were implemented, partly supported by European Union structural funds.

Hungary also recorded significant infrastructure growth, with the motorway network expanding from approximately 448 km in 2000 to around 1,897 km in 2024. The most rapid development occurred between 2005 and 2015, reflecting substantial investments aimed at improving national and international transport connectivity.

Slovakia shows a similar upward trend, although the overall scale of infrastructure remains smaller compared to the other V4 countries. The total length of motorways and E-roads increased from roughly 296 km in 2000 to about 866 km in 2024. A particularly notable increase can be observed after 2019, when several motorway sections were completed, leading to a sharp rise in the total network length.

Figure 3 illustrates the development of GDP per capita in the Visegrad Group countries (Slovakia, the Czech Republic, Poland, and Hungary) over the period 2000-2024. Figure 3 reveals a clear upward trend in all four economies, reflecting the long-term economic convergence of the V4 region toward the more developed economies of the European Union.

At the beginning of the analysed period, the Czech Republic recorded the highest GDP per capita among the V4 countries, reaching approximately €6,560 in 2000. Over time, this indicator increased steadily, surpassing €29,000 by 2024. The Czech economy thus maintained its leading position within the V4 region throughout the entire period.

Slovakia experienced one of the most dynamic growth trajectories. The GDP per capita increased from roughly €4,140 in 2000 to approximately €23,850 in 2024. The most rapid growth occurred between 2004 and 2008, reflecting strong economic expansion following the country's accession to the European Union and the

Table 1 *Descriptive statistics*

Variable	Mean	Std. Dev.	Min	Max
Road traffic deaths	4,285.6	2,311.4	1.126	9.820
Passenger cars (per 1,000 inhabitants)	472.3	96.8	256.4	702.1
GDP per capita (EUR)	16,940	7,820	5,420	32,110
Unemployment rate (%)	8.6	3.4	2.0	19.2
Expenditure on road infrastructure (mil. EUR)	3,420	2,115	410	8,960
Length of motorways and E-roads (km)	3,185	1,940	580	6,980

Table 2 *Correlation matrix*

Variable	deaths	cars_per_1000	gdp_pc	unemp	exp_road	length_roads
deaths	1.000	-0.015	-0.452	0.348	-0.108	-0.064
cars_per_1000	-0.015	1.000	0.789	-0.697	0.657	0.603
gdp_pc	-0.452	0.789	1.000	-0.692	0.698	0.484
unemp	0.348	-0.697	-0.692	1.000	-0.594	-0.629
exp_road	-0.108	0.657	0.698	-0.594	1.000	0.543
length_roads	-0.064	0.603	0.484	-0.629	0.543	1.000

inflow of foreign direct investment.

Poland also recorded substantial economic growth during the analysed period. The GDP per capita rose from about €4,900 in 2000 to more than €22,600 in 2024. Although Poland started from a relatively lower level, its steady growth trajectory indicates significant economic transformation and structural modernization of the economy.

Hungary shows a similar long-term upward trend, with the GDP per capita increasing from approximately €5,020 in 2000 to around €21,550 in 2024. However, the growth path appears somewhat less dynamic compared to Slovakia and Poland, particularly during the period following the global financial crisis.

A temporary slowdown in economic growth can be observed around 2009, reflecting the impact of the global financial crisis, as well as in 2020, when the COVID-19 pandemic affected economic activity across Europe. Despite these short-term fluctuations, the overall trend remains strongly positive in all V4 countries.

From the perspective of the road safety, rising GDP per capita may influence traffic accident dynamics through several mechanisms. Higher income levels typically lead to increased motorisation and traffic intensity, which may initially increase accident risk. However, economic development also enables greater investments in transport infrastructure, vehicle safety technologies, and the road safety policies, which may contribute to a long-term reduction in the road traffic fatalities. These relationships are further examined in the subsequent econometric analysis.

The empirical analysis is based on a balanced panel of four Visegrad Group countries (the Czech Republic, Hungary, Poland, and Slovakia) for the period 2000-2024. The dependent variable is the annual number of road traffic deaths in each country. The explanatory variables include the number of passenger cars per 1,000 inhabitants, the GDP per capita (in euros), unemployment rate (in percent), public expenditure on road infrastructure (in euros), and total length of motorways and European class roads (e-roads, in kilometers).

Descriptive statistics (Table 1) shows significant differences in all variables between countries and over time. The number of road traffic deaths decreased significantly during the period under review, which is in line with broader European trends in road safety. During the same period, motorization rates (passenger cars per 1,000 inhabitants) and GDP per capita generally increased, reflecting convergence and economic growth. Spending on the road infrastructure is relatively volatile, with phases of intense investment and phases of consolidation. The length of motorways and European roads is on a predominantly upward trend, as all four countries have expanded their high-standard road networks.

Correlation analysis (Table 2) reveals intuitive patterns. The road traffic deaths are negatively correlated with the number of passenger cars per 1,000 inhabitants and with the length of highways/expressways and positively correlated with GDP per capita. The correlation between the road infrastructure expenditure and other regression variables is moderate, suggesting that there is no serious multicollinearity. These preliminary findings are consistent with a situation where economic development, motorization, and infrastructure expansion occur simultaneously, with road safety outcomes improving over time. A basic fixed-effects country model is used to exploit the panel structure and control for unobserved heterogeneity. This approach removes all time-invariant country characteristics (e.g., geography, long-term institutional

Table 3 *Estimates of road traffic deaths with fixed effects (Driscoll-Kraay standard errors)*

Variable	Coefficient	Std. error	t-statistic	p-value
cars_per_1000	-5.472	1.597	-3.427	0.0009
gdp_pc	0.096	0.027	3.551	0.0006
unemp	39.969	19.693	2.030	0.0453
exp_road	-3.98×10^{-8}	2.82×10^{-7}	-0.141	0.8881
length_roads	-1.167	0.197	-5.936	0.0000
Country fixed effects	yes			
Year fixed effects	yes			
Covariance estimator	Driscoll-Kraay			
Observations	100			
R^2 (within)	0.77			

quality, driver culture) that may correlate with both road safety and explanatory variables. Given the time dimension of the panel and the likelihood of heteroscedasticity, serial correlation, and cross-sectional dependence, the fixed effects model is estimated using Driscoll-Kraay standard errors. These standard errors are robust to a wide range of correlation patterns in the residuals and are therefore preferred over conventional or cluster alternatives in this context. For robustness, a random effects specification was also estimated, and a Hausman test was performed to decide between the fixed and random effects. In addition, basic diagnostic tests for heteroscedasticity and serial correlation were performed on the clustered OLS residuals. Table 3 presents the results of the fixed effects estimation with standard errors according to Driscoll-Kraay. The dependent variable is the annual number of road traffic deaths in each country.

All the coefficients were estimated over time from changes within individual countries. This means that they describe how changes in each explanatory variable in a given country are associated with changes in deaths, while other regressors and all time-flag characteristics of the country are constant. The coefficient for the number of cars per capita (-5.472) is statistically significant at the 0.05 significance level. From an economic point of view, this means that in a given country, an increase of 1 passenger car per 1,000 inhabitants is associated with a reduction in the road deaths of 5.5 people per year, ceteris paribus. At the first glance, this result may appear counterintuitive, particularly because the simple correlation between the motorisation and the road fatalities is close to zero. However, this apparent discrepancy can be explained by the Simpson's paradox, where the relationship observed in aggregated data differs from the relationship identified after controlling for other variables or fixed effects. In the present case, the panel regression controls for country-specific heterogeneity and macroeconomic factors, which allows the underlying within-country relationship between the motorisation and the road safety to emerge. A possible explanation is that higher levels of motorisation are typically associated with more developed economies, better road infrastructure, safer vehicles, and improved traffic management systems. Consequently, although increased car ownership may lead to higher traffic intensity, it may simultaneously coincide with structural improvements that contribute to a reduction in the road traffic fatalities over time.

The GDP per capita coefficient is positive (0.096) and statistically significant at the 0.05 significance level. An increase in GDP per capita of €1 is associated with an increase of approximately 0.096 deaths per year in an average Visegrad Four country, if other factors remain unchanged. The unemployment coefficient (39.969) is positive and significant at the 0.05 significance level. This suggests that a 1% increase in the unemployment rate is associated with approximately 40 additional road deaths per year in each country. The coefficient for the road infrastructure expenditure is very small, statistically insignificant ($p \approx 0.89$), and its sign does not differ reliably from zero. In the current specification, annual public spending on the road infrastructure does not show a clear current impact on the number of road deaths. The coefficient for the road length is -1.167, which is statistically highly significant ($p < 0.05$). This means that each additional kilometer of motorways/expressways in the country is associated with a reduction in road deaths of approximately 1.2 per year, if other factors remain unchanged.

A summary of the results suggests that in the Visegrad Four countries between 2000 and 2024:

- Higher motorization is associated with lower road deaths, which is consistent with general improvements in vehicle technology, infrastructure, and institutions.
- Economic growth measured by GDP per capita has a positive impact on the number of deaths, suggesting that increased mobility and exposure to risk still outweigh improvements in safety.
- Higher unemployment is associated with higher fatalities, underscoring that labour market conditions and economic pressure can have an adverse impact on road safety.

- Total annual expenditure on road infrastructure does not have a clear short-term impact on fatalities in this specification.
- The expansion of motorways and expressways is strongly associated with a reduction in road traffic deaths, highlighting the key role of high-quality road infrastructure.

The value of the coefficient of determination R^2 = 0.77 indicates that the model explains a substantial part of the changes in the number of road traffic deaths in individual countries over time. Fixed country effects and annual dummy variables together capture unobserved heterogeneity and common regional shocks, while the main regression variables provide statistically and economically significant explanatory power. Alternative specifications (not reported in detail) using random effects or pooled OLS provide qualitatively similar features but differ in magnitude and standard errors. Hausman tests strongly reject random effects in favor of fixed effects, and conventional tests of heteroscedasticity and serial correlation on pooled OLS residuals confirm the need for robust inference. The use of Driscoll-Kraay standard errors ensures that the t-statistics and p-values reported are robust to these problems, lending credibility to the substantive conclusions.

As a part of the robustness analysis, the baseline model was re-estimated using an alternative dependent variable, namely the road traffic deaths per one million inhabitants, to control for population size and obtain a relative measure of the road safety.

The results reveal several important differences compared to the baseline specification using absolute fatalities. In particular, the coefficient of passenger cars per 1,000 inhabitants remains negative and highly statistically significant (-0.192, $p < 0.001$), confirming the robustness of the finding that higher levels of motorization are associated with lower fatality rates. Similarly, the effect of motorway and road length remains negative and strongly significant (-0.034, $p < 0.001$), suggesting that the expansion of road infrastructure contributes to improved road safety outcomes in relative terms.

However, notable differences emerge in the case of GDP per capita. While the baseline model indicates a positive and statistically significant relationship ($\beta \approx 0.096$, $p < 0.001$), the robustness specification yields a negative coefficient ($\beta \approx -0.0022$) that is only weakly significant ($p \approx 0.09$). This reversal in sign suggests that the relationship between economic development and road safety is sensitive to the choice of dependent variables and may reflect scale effects present in the absolute measure of fatalities.

A similar shift can be observed for the unemployment rate, which is positive and significant in the baseline model (€≈ 39.97, $p < 0.05$) but becomes negative and statistically significant in the robustness specification (€ ≈ -1.85, $p < 0.05$). This indicates that the higher unemployment may be associated with lower fatality rates when expressed in relative terms, potentially due to reduced mobility and traffic intensity during periods of weaker economic activity.

In contrast, the effect of road infrastructure expenditure remains inconsistent across specifications. While it is statistically insignificant in the baseline model ($p \approx 0.89$), it becomes positive and statistically significant in the robustness model ($p < 0.01$), albeit with a very small coefficient. This suggests that the estimated impact of public spending on road safety is not stable and may depend on model specification or scaling effects.

Overall, the comparison of results indicates that while certain relationships, particularly those related to motorization and road infrastructure length remain robust, other key variables such as GDP per capita, unemployment, and infrastructure expenditure exhibit considerable sensitivity to the choice of dependent variable. This underscores the importance of employing alternative specifications when evaluating the determinants of road safety and suggests that conclusions based solely on absolute fatality counts may be incomplete.

In the next step of the analysis, attention was directed towards examining the potential nonlinear relationship between the economic development and the road traffic fatalities. Specifically, the study proceeded to test the Kuznets-type hypothesis, which assumes that the impact of income growth on road safety may change across different stages of economic development. To capture this possibility, the model was extended by including both the linear and quadratic terms of GDP per capita, allowing for the identification of a potential non-monotonic relationship.

In the case of absolute road traffic deaths, the estimated coefficient of GDP per capita is positive (0.079), while the quadratic term is also positive but statistically insignificant. This configuration implies a convex and monotonically increasing relationship, rather than the expected inverted U-shape. Moreover, the implied turning point is negative (approximately -49,179), which lies entirely outside the economically meaningful range of the data. Despite the joint significance of the GDP terms, as indicated by a very low p-value (≈ 0.00001), the resulting functional form lacks practical interpretability and does not support the Kuznets hypothesis.

In contrast, when using the road traffic deaths per one million inhabitants, the results provide stronger evidence of a nonlinear relationship. The linear term of GDP per capita is negative and statistically significant (-0.0078), while the quadratic term is positive and significant (0.0000001756), indicating a U-shaped relationship. This suggests that increases in income are initially associated with a reduction in traffic fatalities, followed by a reversal at higher income levels. The estimated turning point is approximately 22,147 EUR per capita, which lies within a plausible range of the observed data. The joint significance of the GDP

Table 4 *Infrastructure spending (contemporaneous and lagged effects)*

Outcome	Model	road_exp_mil_eur	road_exp_l1	road_exp_l2
rtd	Baseline	0.7406		
rtd	With lag 1	0.7002	0.9103	
rtd	With lag 1 and 2	0.6099	0.3249	0.1557
rtd_per1m	Baseline	0.3678		
rtd_per1m	With lag 1	0.2504	0.2902	
rtd_per1m	With lag 1 and 2	0.4255	0.8062	0.0285

terms ($p \approx 0.0039$) further supports the presence of this nonlinear pattern.

Overall, the results do not confirm the existence of a conventional Kuznets curve in the form of an inverted U-shape. Instead, the findings suggest either a monotonically increasing relationship (in the case of absolute fatalities) or a U-shaped relationship (in the relative specification), indicating that the nature of the relationship between income the road safety nexus is sensitive to the choice of dependent variable.

To further verify whether the estimated relationships are driven by the exceptional conditions of the COVID-19 period, an additional robustness check was performed by re-estimating the baseline fixed effects model using only pre-pandemic data (2000-2019). The results indicate that the core findings remain largely unchanged. In particular, the effect of motorization (passenger cars per 1,000 inhabitants) remains negative and highly statistically significant, confirming its robust association with lower road traffic fatalities. Similarly, GDP per capita retains a positive and statistically significant coefficient ($p \approx 0.026$), suggesting that the relationship between economic development and fatalities observed in the baseline model is not driven solely by the inclusion of pandemic years.

The coefficient on motorway and the road length also remains negative and significant, reinforcing the conclusion that infrastructure expansion contributes to improving the road safety outcomes. In contrast, the effect of lagged infrastructure expenditure becomes only marginally significant ($p \approx 0.058$), indicating weaker and less stable evidence of delayed investment effects once the COVID period is excluded. Furthermore, the unemployment rate loses its statistical significance, suggesting that its previously observed impact may be sensitive to the inclusion of pandemic-related labor market disruptions.

These findings confirm that the main determinants of the road traffic fatalities are not driven by the COVID-19 period but rather reflect more stable structural relationships present throughout the pre-pandemic period.

A similar pattern is observed when using the road traffic deaths per one million inhabitants, where both the contemporaneous and first lag of infrastructure expenditure remain statistically insignificant. However, in the specification including both lagged terms, the second lag (t-2) becomes negative and statistically significant, indicating a delayed reduction in fatality rates following infrastructure investments. This result suggests that the impact of infrastructure spending on road safety may materialize only after a longer time horizon, rather than immediately or within a single year (Table 4).

A more detailed insight into the statistical significance of infrastructure expenditure effects is provided by the corresponding p-values. In the case of absolute road traffic deaths, the p-values of the contemporaneous, as well as lagged expenditure variables, remain well above conventional significance thresholds across all model specifications (e.g., 0.7406 in the baseline model, 0.7002 and 0.9103 with one lag, and 0.6099, 0.3249, and 0.1557 when both lags are included). These results confirm that infrastructure spending does not exhibit a statistically significant effect on fatalities in absolute terms, regardless of whether lag structures are considered.

A similar pattern is observed for the road traffic deaths per one million inhabitants, where the majority of coefficients remain statistically insignificant. However, in the specification including both lagged variables, the second lag (t-2) yields a p-value of 0.0285, indicating statistical significance at the 5% level. This finding provides limited evidence that infrastructure investments may contribute to reducing fatality rates with a longer time delay.

Nevertheless, the overall lack of consistent statistical significance across models suggests that this effect is not robust, and should therefore be interpreted with caution. The results imply that, while there may be some delayed benefits of infrastructure expenditure, these are neither immediate nor systematically observable across different model specifications.

5 Discussion

The findings of this study make an important contribution to the discussion on the macroeconomic and infrastructural determinants of the road traffic safety in the V4 countries. An empirical analysis based on a fixed-effects panel model showed that growth in economic performance, measured by GDP per capita, is associated with a decline in the number of the road

fatalities in Slovakia, the Czech Republic, Poland, and Hungary, while increased motorization raises the risk of fatal accidents. Unemployment appears in the results as a factor with a predominantly dampening effect on mortality, and the significance of variables representing transport infrastructure appears to be determined more by the quality of their use than by the physical extent of the network itself.

The strongest correlation with the results of the present study was observed for the motorization variable. Several studies have confirmed that an increase in the number of vehicles leads to greater traffic exposure, higher traffic volume, and consequently a higher risk of traffic accidents and fatalities. In the European context, it has been noted that economic growth is often accompanied by an increase in motorization, and particularly in less developed economies, the rate of growth in the vehicle fleet may exceed the rate of improvement in safety [18]. A Nigerian study identified a unidirectional causal relationship from motorization to traffic accidents and also demonstrated that economic growth increases motorization, which subsequently acts as a mediating mechanism for the rise in accident rates [19]. Similar conclusions were drawn regarding Chinese provinces, where motorization was found to have a positive effect on traffic accidents [20]. Similarly, an analysis of Beijing demonstrated that private vehicle ownership increased the number of accidents over the long term [21]. Based on the above, it can be concluded that the finding of the present study that increased motorization raises the risk of fatal accidents has been largely confirmed by the existing literature.

Significantly more varied results were found when assessing the effect of GDP per capita. Some studies supported the conclusion that, under certain conditions, economic development can act as a factor reducing traffic fatalities. A Polish panel study identified a negative relationship between the GDP per capita and accident and fatality rates [22]. Similarly, a Chinese provincial analysis demonstrated that economic development had a predominantly inhibitory effect on traffic accidents [20]. A broader review of empirical findings also cited results from Russia and certain international panels, according to which growth in regional product or GDP per capita led to a decline in traffic fatalities. These findings can be considered consistent with the results of the present study, in which economic growth was interpreted as a factor promoting a higher quality of the vehicle fleet, better access to healthcare, a more modern regulatory framework, and a higher level of safety technologies.

At the same time, however, it was found that other studies had reached the opposite conclusion. A Thai study demonstrated that growth in provincial GDP per capita was associated with an increase in both traffic injuries and fatalities [23]. A comparative analysis of upper-middle-income countries found that growth in GDP per capita increased traffic fatalities in Asia, Europe, and the Americas [4]. In the case of Cameroon, an inverted U-shaped relationship was identified, suggesting that safety deteriorates in the early stages of economic growth, while it improves after a certain level of development is reached [24]. Another Thai study also confirmed this non-linearity, observing an inverted U-shape for accidents and injuries, while a U-shape was identified for fatalities [25]. For this reason, the relationship between economic performance and traffic safety could not be interpreted as universally linear. Rather, it was confirmed that this is a development-dependent relationship, sensitive to the level of economic maturity, the quality of institutions, the technical level of the vehicle fleet, and the degree of regulatory effectiveness. In this context, the results of the present study can be interpreted to mean that the V4 countries are likely at a stage of development where the positive externalities of economic growth have begun to outweigh the negative consequences of increasing mobility.

A relatively high degree of agreement was also found regarding the interpretation of the effect of unemployment. In the present study, unemployment was identified as a factor that could be associated with a lower number of fatalities, which was interpreted primarily through a reduction in mobility, commuting to work, and economically motivated travel. This conclusion was also supported by a Chinese study, which identified a predominantly negative effect of unemployment on traffic accidents [20]. Similarly, a broader literature review cited findings indicating a negative correlation between unemployment and traffic fatalities, which in some cases was even stronger than that observed for GDP. Earlier macroeconomic analyses from the U.S. also suggested that rising unemployment is often accompanied by a decline in the number of traffic fatalities, although methodological caution was recommended when interpreting such findings [26]. It can therefore be concluded that the results of the present study are not isolated in this field but are supported by several studies that have highlighted the procyclical nature of traffic accidents and fatalities.

The greatest divergence of opinion was found in the variables representing transport infrastructure and infrastructure investments. The present study suggests that simply increasing spending on the road infrastructure or expanding the highway network does not automatically lead to a reduction in the number of fatalities, as the quality of the implemented projects, the technical condition of the network, its functional layout, the manner of its use, and the time lag in the safety effect appear to be decisive factors, [26]. This conclusion has also been largely confirmed by the existing literature. A European analysis focusing on the relationship between the infrastructure spending and safety pointed out that the results of previous studies are inconsistent and that the effect of investments is strongly dependent on the method of measurement, the country's economic level, and the time horizon of the evaluation. Similarly, a Chinese study found that

transportation investments themselves were positively correlated with the number of deaths, while the road length and lighting quality had a negative effect on fatalities. Such findings suggest that investments may increase traffic capacity and risk exposure in the short term, while their safety effect may only manifest later or in combination with other measures.

On the other hand, studies were also identified in which a positive safety effect was attributed to transport infrastructure. A Polish panel analysis demonstrated a negative impact of the road network length and maintenance expenditures on accident rates, suggesting that high-quality and well-maintained infrastructure can contribute to improved safety [27]. A study analyzing highways and vehicle counts in selected European countries found that in some countries, a reduction in fatalities was associated with the expansion of the highway network, with the Czech Republic explicitly mentioned, and Slovakia cited in relation to accident rates [28]. A Slovak analysis of a high-risk the road section also suggested that diverting traffic, particularly freight traffic, to the D3 highway could reduce traffic intensity in the high-risk area and thereby improve the safety situation [29]. These findings allowed for the results to be interpreted not as a rejection of the importance of infrastructure, but as confirmation that the positive effect of infrastructure manifests itself only under certain conditions, particularly when investments are focused on safety-critical sections, high-quality maintenance, and the separation of conflicting traffic flows.

Special attention also had to be paid to behavioral and institutional factors, which were identified in several studies as important mediating mechanisms. A Slovak study on mortality trends from 1996 to 2014 highlighted the importance of legislative measures, particularly the new Road Traffic Act of 2009, in accelerating the decline in mortality [30]. An Australian study, in turn, showed that fatal accidents are significantly influenced by age, rural settings, night driving, and high-speed sections [31]. An American climate macroanalysis confirmed the growing importance of temperature, precipitation, extreme weather events, and regulatory measures [32]. Although these results did not directly focus on the same variables as the present study, they supported a broader interpretive framework according to which the macroeconomic determinants operate only through a complex network of behavioral, technical, and institutional relationships.

The COVID-19 pandemic period had a significant impact on development of traffic safety, as it was accompanied in many countries by restrictions on mobility, a decline in traffic volume, and changes in the road traffic patterns. In the present study, the results were interpreted with the understanding that part of the observed period was influenced by pandemic restrictions, which may have temporarily weakened the usual links between the economic activity, unemployment, and the number of fatalities. This interpretation is supported by several studies. An Australian analysis recorded a decline in mortality in 2020, which was linked to mobility restrictions during the pandemic, although the long-term trend was also explained by broader structural factors related to the road traffic safety [31]. Similarly, a Thai study reported a slight decrease in accidents and injuries in 2020, with this trend interpreted as a consequence of pandemic-related travel restrictions, rather than a sign of lasting systemic improvement [33]. The professional literature has also pointed out that economic recessions and extraordinary social shocks are often accompanied by a decline in traffic fatalities, primarily due to lower risk exposure. For this reason, the results for the pandemic years had to be interpreted with caution, as a part of the decline in mortality could have been caused by exogenous traffic restrictions, rather than solely by improvements in infrastructure quality, regulation, or the behavior of the road users.

Based on a comparison to previous studies, it can be concluded that the results of the present study were most consistent with the literature regarding the interpretation of motorization as a risk factor, unemployment as a variable associated with a decline in traffic fatalities, and the COVID-19 pandemic as a period in which the decline in mortality was largely mediated by reduced mobility and lower risk exposure. Regarding economic performance, the existence of two opposing lines of research was confirmed, with these results aligning more closely with the group of studies in which economic growth in more mature economies was associated with improved safety. The highest degree of heterogeneity was confirmed for the transportation infrastructure, as both positive and negative effects were identified in studies depending on a country's level of development, type of investment, quality of maintenance, time horizon, and accompanying regulatory measures.

6 Conclusions

The empirical analysis of the Visegrad Group countries over the period 2000-2024 confirmed that the road traffic mortality is shaped by a combination of economic, infrastructural, and labour-market factors, whose effects are not always linear and whose interpretation depends on the specification used. The estimated fixed-effects models showed that higher motorization was consistently associated with lowering the road traffic fatalities, while the expansion of motorways and European-class roads also exhibited a statistically significant mortality-reducing effect. By contrast, the GDP per capita and unemployment were positively associated with fatalities in the baseline specification using absolute deaths, although both variables proved to be sensitive to the choice of dependent variable and to the exclusion of the COVID-19 period. Public expenditure on the road infrastructure did not

display a robust contemporaneous effect, while lagged estimates suggested only limited evidence of delayed safety benefits.

These findings imply that road safety in the V4 countries cannot be explained solely by the scale of economic growth or by the volume of public investment. Rather, what appears to be decisive is the structural quality of development, including the modernization of the vehicle fleet, the functional design of transport infrastructure, the timing of investment effects, and the broader institutional environment in which mobility expands. The results therefore support the view that the road fatalities should be interpreted not as an isolated transport outcome, but as a by-product of wider processes of economic transformation, changing mobility patterns, and public policy choices.

At the same time, the comparison between baseline and robust specifications revealed that some determinants are considerably more stable than others. The protective effect of motorization and high-standard road length remained robust across alternative models, suggesting that in the V4 context these variables may reflect broader structural improvements in vehicle safety, infrastructure quality, and transport organization. In contrast, the effects of the GDP per capita, unemployment, and infrastructure expenditure varied according to whether fatalities were measured in absolute or relative terms and whether pandemic years were included. This indicates that caution is needed when deriving policy conclusions from a single model specification and confirms the importance of using multiple indicators of road safety performance.

From the perspective of economic policy, several practical implications emerge. First, the significant negative effect of motorway and expressway expansion suggests that continued investment in high-standard road infrastructure should remain an important component of transport and regional development policy. However, priority should not be placed on network expansion alone, but rather on those projects that demonstrably reduce conflict points, separate traffic flows, bypass hazardous settlements, and shift traffic from lower-quality roads to safer corridors. In this sense, infrastructure policy should be guided less by the quantity of kilometers delivered and more by measurable safety outcomes.

Second, the weak and unstable effect of aggregate the road infrastructure expenditure indicates that simply increasing annual public spending is unlikely to produce immediate and predictable reductions in fatalities. For policymakers, this means that expenditure efficiency should be emphasized more strongly than expenditure volume. Greater attention should be devoted to the composition of the road spending, especially to maintenance quality, black-spot treatment, intelligent traffic management systems, road lighting, signage modernization, and targeted upgrades of high-risk sections. In addition, evaluation frameworks should explicitly account for time lags, since part of the safety return from infrastructure investment may materialize only after several years.

Third, the positive association between the GDP per capita and absolute fatalities in the baseline model suggests that economic growth may continue to generate additional traffic exposure even in relatively advanced Central European economies. This implies that growth-oriented economic policy should be complemented by preventing the road safety policy, particularly during periods of rising mobility, expanding freight transport, and increasing household car ownership. Economic prosperity alone should not be assumed to automatically improve the safety outcomes. Instead, growth strategies should be accompanied by stronger enforcement, safer vehicle standards, investments in data-based traffic management, and systematic road safety auditing of major transport projects.

Fourth, the sensitivity of unemployment effects points to the importance of monitoring the mobility-related risks over the business cycle. Since labour-market fluctuations may affect commuting intensity, freight volumes, and behavioral stress, road safety policy should be designed in a countercyclical and adaptive manner. During periods of rapid economic expansion, when mobility rises, preventive campaigns and enforcement efforts may need to be intensified. During the crisis periods, by contrast, attention should be paid to shifts in travel patterns, fiscal constraints, and delayed maintenance effects, which may create new forms of risk even if aggregate mobility declines.

Fifth, the experience of the COVID-19 period highlights the need for resilience-oriented transport governance. Although the main structural findings were not driven solely by the pandemic, the crisis clearly demonstrated that extraordinary disruptions can temporarily alter the relationship between economic activity, unemployment, infrastructure use, and road fatalities. Policymakers should therefore support the development of integrated monitoring systems capable of linking economic indicators, labour-market developments, traffic volumes, and safety outcomes in real time. Such systems would allow for a faster policy response during future crises, including pandemics, energy shocks, or abrupt recessions.

In policy terms, at least three broader strategic recommendations may be derived from the present findings. First, the road safety should be treated as an integral part of economic policy rather than as a narrow transport-sector issue. Second, infrastructure decisions should be evaluated not only in terms of connectivity and growth effects, but in terms of their measurable contribution to mortality reduction, as well. Third, the road safety policy in the V4 countries should increasingly move towards the evidence-based and differentiated interventions, reflecting the fact that the determinants of fatalities differ across absolute and relative measures and may vary over time.

This study has several limitations that should be acknowledged. First, the analysis is based on a relatively small balanced panel of four Visegrad Group countries, which limits the generalizability of the findings and reduces the variability of institutional and structural conditions across observations. Second, the use of aggregate national-level data does not allow for the capture of regional differences, behavioral factors, traffic intensity, vehicle age structure, enforcement quality, or weather conditions, all of which may also affect road safety outcomes. Third, some estimated relationships, particularly those related to the GDP per capita, unemployment, and road infrastructure expenditure, proved sensitive to model specification and the choice of dependent variable. Finally, although the lagged effects and pre-pandemic robustness checks were considered, the results may still be influenced by unobserved shocks and measurement differences that could not be fully controlled for within the available dataset.

In conclusion, the study has shown that the determinants of the road traffic fatalities in the Visegrad Group are multifaceted and specification-sensitive, but not random. The most consistent evidence was found for the protective role of high-standard road network expansion and for the stable relationship between motorization and improved safety outcomes within countries over time. Less stable, but still policy-relevant, were the effects of income growth, unemployment, and infrastructure expenditure. These results underline that effective road safety improvement requires a coordinated policy mix combining infrastructure quality, institutional capacity, preventive regulation, and continuous evaluation of economic and mobility trends. For policymakers in the V4 region, the key message is that the safer roads would not result automatically from economic growth or higher public spending alone; they must be produced through targeted, well-timed, and evidence-based policy intervention.

Acknowledgements

The paper was supported by the KEGA Agency, Grant No. 034ZU-4/2025 „Innovative Project Management Education for Sustainable and Intelligent Transport in the EU in line with Industry 5.0“ at the Faculty of Operation and Economics of Transport and Communications, University of Zilina.

Conflicts of interest

The authors declare that they have no known competing financial interests or personal relationships that could have appeared to influence the work reported in this paper.

References

[1] SCHOLES, S., WARDLAW, M., ANCIAES, P., HEYDECKER, B., MINDELL, J. S. Fatality rates associated with driving and cycling for all road users in Great Britain 2005-2013. *Journal of Transport and Health* [online]. 2018, **8**, p. 321-333. [accessed 2017-22-11]. ISSN 2214-1405, eISSN 2214-1413. Available from: https://doi.org/10.1016/j.jth.2017.11.143

[2] RAHMAN, M. A., TOLFORD, T., JUNAED, S., DAS, S., HOSSAIN, A., MOOMEN, M., MITRAN, E., CODJOE, J. Pedestrian fatalities on U.S. interstates: a pattern mining approach to investigating pedestrian actions and policy implications. *Case Studies on Transport Policy* [online]. 2026, **23**, 101696. [accessed 2025-25-12]. ISSN 2213-624X, eISSN 2213-6258. Available from: https://doi.org/10.1016/j.cstp.2025.101696

[3] CHEN, X., YI, X., YANG, Y., LIU, Y., QU, X. Measuring urban road transportation efficiency: a nonparametric slack-based analysis with Malmquist and Luenberger productivity indices. *Transportation Research Part A: Policy and Practice* [online]. 2026, **205**, 104845. [accessed 2025-31-12]. ISSN 0965-8564, eISSN 1879-2375. Available from: https://doi.org/10.1016/j.tra.2025.104845

[4] ALI, Q., YASEEN, M. R., KHAN M. T. I. The causality of road traffic fatalities with its determinants in upper middle income countries: a continent-wide comparison. *Transportation Research Part A: Policy and Practice* [online]. 2019, **119**, p. 301-312. [accessed 2018-10-12]. ISSN 0965-8564, eISSN 1879-2375. Available from: https://doi.org/10.1016/j.tra.2018.12.002

[5] GOEL, R. Modelling of road traffic fatalities in India. *Accident Analysis and Prevention* [online]. 2018, **112**, p. 105-115. [accessed 2017-27-12]. ISSN 0001-4575, eISSN 1879-2057. Available from: https://doi.org/10.1016/j.aap.2017.12.019

[6] MOHAMAD, I. Quantifying the life-saving impact of seatbelt usage: a random forest analysis of unobserved heterogeneity and latent risk factors in vehicular fatalities. *Multimodal Transportation* [online]. 2025, **4**(3), 100221. [accessed 2024-29-10]. eISSN 2772-5863. Available from: https://doi.org/10.1016/j.multra.2025.100221

[7] BAMNEY, A., GUPTA, N., KESHARI, S., JOSHI, M. Analyzing pedestrian fatalities in the United States: a comparative study of pedestrian and census tract level factors across pre-, during, and late-pandemic periods. *Journal of Safety Research* [online]. 2025, **95**, p. 10-24. [accessed 2025-27-08]. ISSN 0022-4375, eISSN 1879-1247. Available from: https://doi.org/10.1016/j.jsr.2025.08.007

[8] RAHIMZADEH, A. The effect of economic inequality, employment and economic growth on road fatalities in Iran (Autoregressive Distributional Lags (ARDL) model). *Road* [online]. 2025, [accessed 2024-15-09]. e237487. ISSN 1735-062X. Available from: https://doi.org/10.22034/road.2025.560915.2455

[9] GRUDA, D., GONÇALVES, R., ZADEGAN, M. S. Quit playing games with our lives: layoffs predict road traffic fatalities. *Accident Analysis and Prevention* [online]. 2026, **224**, 108302. [accessed 2025-04-11]. ISSN 0001-4575, eISSN 1879-2057. Available from: https://doi.org/10.1016/j.aap.2025.108302

[10] NIKOLAOU, P., FOLLA, K., DIMITRIOU, L., YANNIS, G. European countries' road safety evaluation by taking into account multiple classes of fatalities. *Transportation Research Procedia* [online]. 2021, **52**, p. 284-291. [accessed 2020-07-12]. ISSN 2352-1457, eISSN 2352-1465. Available from: https://doi.org/10.1016/j.trpro.2021.01.033

[11] GOKGOZ, F., MACIT, G. Assessing the effect of transportation investments on efficiency and sustainability of EU roads. *Transport Policy* [online]. 2026, **175**, 103873. [accessed 2025-28-10]. ISSN 0967-070X, eISSN 1879-310X. Available from: https://doi.org/10.1016/j.tranpol.2025.103873

[12] COROPULIS, S., BERLOCO, N., INTINI, P., RANIERI, V. Safety performance functions in a road environment with automated vehicles. *Traffic Safety Research* [online]. 2025, **9**, e000107-e000107. [accessed 2025-11-02]. eISSN 2004-3082. Available from: https://doi.org/10.55329/fzyz2882

[13] AFSHARI, S., SOLTANI, A., AMIRI M. A. From data to safer roads: predictive modelling and causal analysis of road fatalities in Australia. *Scientific Reports* [online]. 2026, **16**, 3764. [accessed 2025-29-12 eISSN 2045-2322. Available from: https://doi.org/10.1038/s41598-025-33744-7

[14] GLOWINSKI, S., RZEPCZYK, S., GALINSKI, M., OBST. M. Riding the risk: trends and causes of motorcycle accidents in Poland (2016-2023). *Transport Geography Papers of Polish Geographical Society / Prace Komisji Geografii Komunikacji PTG* [online]. 2025, **28**(1), p. 83-97. [accessed 2025-21-11]. ISSN 1426-5915, eISSN 2543-859X. Available from: https://doi.org/10.4467/2543859XPKG.25.007.22670

[15] JURECKI, R., POLIAK, M. The impact of the safe following distance onto the traffic safety. *Communications - Scientific Letters of the University of Zilina* [online]. 2024, **26**(1), p. A37-A49. [accessed 2023-27-12]. ISSN 1335-4205, eISSN 2585-7878. Available from: https://doi.org/10.26552/com.C.2024.014

[16] HARITH, S. H. Control over driving behaviour and accident involvement: a case among young drivers in Malaysia. *Communications - Scientific Letters of the University of Zilina* [online]. 2022, **24**(3), p. A88-A99. [accessed 2022-29-03]. ISSN 1335-4205, eISSN 2585-7878. Available from: https://doi.org/10.26552/com.C.2022.3.A88-A99

[17] HU, Q., ZOU, Y., WU, S., ZHANG, S., ZHANG, Y., WU, L. Exploring the impact of climate change on road fatalities: a macroscopic panel data analysis. *Journal of Advanced Transportation* [online]. 2025, **2025**(1), 4693354. [accessed 2025-30-09]. eISSN 2042-3195. Available from: https://doi.org/10.1155/atr/4693354

[18] PELECKIENE, V., PELECKIS, K., KLYMCHUK, A., TOMASHUK, I., SEMENYSHYNA, I. Economic growth, motorization level, traffic safety: are they related (experience of EU countries). *Independent Journal of Management and Production*. 2022, **13**(Extra 3), p. 93-106. [accessed 2022-20-04]. ISSN 2236-269X.

[19] OLUWAYEMI, A., YINUSA, O., OYELAMI, L. Economic growth, motorisation and road traffic safety in Nigeria. *Ilorin Journal of Economic Policy* [online]. 2020, **7**(1), p. 16-34. [accessed 2020-01-01]. eISSN 2449-0512. Available from: https://www.ijep.org/index.php/volume-7-issue-1-2020/26-economic-growth-motorisation-and-road-traffic-safety-in-nigeria

[20] ZHANG, K., WANG, S., SONG, C., ZHANG, S., LIU, X. Spatiotemporal heterogeneity analysis of provincial road traffic accidents and its influencing factors in China. *Sustainability* [online]. 2024, **16**(17), 7348. [accessed 2024-26-08]. eISSN 2071-1050. Available from: https://doi.org/10.3390/su16177348

[21] JIN, J. Bayesian vector autoregressive analysis of macroeconomic and transport influences on urban traffic accidents. *arXiv* [online]. 2022, arXiv:2204.03177. [accessed 2022-07-04]. ISSN 2331-8422. Available from: https://doi.org/10.48550/arXiv.2204.03177

[22] JURECKI, R. S. Analysis of road safety in poland after accession to the European Union. *Communications - Scientific Letters of the University of Zilina* [online]. 2020, **22**(2), p. 60-67. [accessed 2020-01-04]. ISSN 1335-4205, eISSN 2585-7878. Available from: https://doi.org/10.26552/com.C.2020.2.60-67

[23] SUPHANCHAIMAT, R., SORNSRIVICHAI, V., LIMWATTANANON, S., THAMMAWIJAYA, P. Economic development and road traffic injuries and fatalities in Thailand: an application of spatial panel data analysis, 2012-2016. *BMC Public Health* [online]. 2019, **19**(1), 1449. [accessed 2019-04-11]. eISSN 1471-2458. Available from: https://doi.org/10.1186/s12889-019-7809-7

[24] CLEMENT, N., NYONKWE NGO NDJEM Marie L. S., DOUANLA MELI, S. Road safety and economic development in Cameroon: an analysis of the Kuznets curve. *International Journal of Scientific Research and Management* [online]. 2020, **8**, p. 1876-1882. [accessed 2020-04-07]. ISSN 2321-3418. Available from: https://doi.org/10.18535/ijsrm/v8i07.em01

[25] PATMASIRIWAT, D., PUMKAEW, D. Provincial economies and loss from traffic accidents: evidence from Thailand. *Journal of Public Administration, Public Affairs, and Management* [online]. 2025, **23**(2), p. 1-26.

ISSN 2985-0754, eISSN 2985-0762. Available from: https://so05.tci-thaijo.org/index.php/pajournal/article/view/282797

[26] VALILA, T. Road safety and road infrastructure expenditure: a bivariate analysis. *Transport Policy* [online]. 2023, **140**, p. 148-162. [accessed 2023-11-07]. ISSN 0967-070X, eISSN 1879-310X. Available from: https://doi.org/ 10.1016/j.tranpol.2023.07.002

[27] BRZOZOWSKA-RUP, K., NOWAKOWSKA, M. Modelling road traffic safety indices by means of regression with panel data. *Engineering Management in Production and Services* [online]. 2020, **12**(4), p. 40-51. [accessed 2022-28-12]. ISSN 2543-912X, eISSN 2543-6597. Available from: https://doi.org/10.2478/emj-2020-0026

[28] FREJ, D., SZUMSKA, E. Analysis of the length of highways and the number of motor vehicles impact on the intensity of road accidents in selected European countries in 2010-2020. *Communications - Scientific Letters of the University of Zilina* [online]. 2023, **25**(1), p. A40-A60. [accessed 2022-13-12]. ISSN 1335-4205, eISSN 2585-7878. Available from: https://doi.org/10.26552/com.C.2023.012

[29] HARANTOVA, V., KUBIKOVA, S., RUMANOVSKY, L. Traffic accident occurrence, its prediction and causes [online]. In: *Development of transport by telematics TST 2019. Communications in computer and information science, vol 1049*. MIKULSKI, J. (Eds.). Cham: Springer International Publishing, 2019. ISBN 978-3-030-27546-4, eISBN 978-3-030-27547-1, p. 123-136. Available from: https://doi.org/10.1007/978-3-030-27547-1_10

[30] BRAZINOVA, A., MAJDAN, M. Road traffic mortality in the Slovak Republic in 1996-2014. *Traffic Injury Prevention* [online]. 2016, **17**(7), p. 692-698. [accessed 2016-02-10]. ISSN 1538-957X. Available from: https://doi.org/10.1080/15389588.2016.1143095

[31] AFSHARI, S., SOLTANI, A., AMIRI, M. A. From data to safer roads: predictive modelling and causal analysis of road fatalities in Australia. *Scientific Reports* [online]. 2026, **16**, 3764. [accessed 2025-29-12]. eISSN 2045-2322. Available from: https://doi.org/10.1038/s41598-025-33744-7

[32] HU, Q., ZOU, Y., WU, S., ZHANG, S., ZHANG, Y., WU, L. Exploring the impact of climate change on road fatalities: a macroscopic panel data analysis. *Journal of Advanced Transportation* [online]. 2025, **2025**, 4693354. [accessed 2025-30-09]. eISSN 2042-3195. Available from: https://doi.org/10.1155/atr/4693354

[33] TOKTAM, A. K., TAIEBE, K., VAHID, F., VAHID, G., ALI, Y., MORTEZA, L., NEGAR, S. Forecasting road traffic injuries in North Eastern Iran: the effects of COVID-19 and time series analysis (2009-2023). *Open Access Emergency Medicine* [online]. 2026, **18**, 550300. [accessed 2026-12-02]. ISSN 1179-1500. Available from: https://doi.org/10.2147/OAEM.S550300

PREPARATION OF BIG DATA SETS FOR OPTIMIZATION OF INTERCITY FREIGHT DRIVER SCHEDULES

Olexandr Melnychenko[1], Myroslav Oliskevych[2,*], Nazar Khomyn[1]

[1]National Transport University, Faculty of Automotive Engineering, Department of Production, Repair and Materials Science, Kyiv, Ukraine
[2]Stepan Gzhytskyi National University of Veterinary Medicine and Biotechnologies, Faculty of Mechanics, Energy and Information Technologies, Department of Automobiles and Tractors, Dubliany of Lviv Region, Ukraine

*E-mail of corresponding author: oliskevychm@gmail.com

Olexandr Melnychenko 0000-0001-7236-5891, Myroslav Oliskevych 0000-0001-6237-0785, Nazar Khomyn 0009-0008-1906-3024

Resume
The problem of using big data for optimal planning of work and rest of truck drivers in intercity freight transportation is considered. The problem is solved for a team of drivers in compliance with the EU regulation 561/2006. The proposed data preparation can reduce the practical computational complexity and find the optimal driver work schedule. The clustering of the initial data was substantiated for optimizing schedules based on the criterion of compatibility of transport orders. The compatibility of orders follows from the analysis of similarity of two consecutive transportation processes performed by one driver during his/her work shift. Simulation modelling was performed. The influence of the scale of the territory on the quality of the prepared initial data was also investigated. A rational range of the compatibility coefficient for the high-quality preparation of a large data set was substantiated.

Article info
Received 12 January 2026
Accepted 31 March 2026
Online 15 April 2026

Keywords:
road transportation
driver scheduling
big data
clustering
order compatibility

Available online: https://doi.org/10.26552/com.C.2026.022

ISSN 1335-4205 (print version)
ISSN 2585-7878 (online version)

1 Introduction

Due to the alarming trend of a shortage of commercial vehicle drivers worldwide, studies of the efficiency of transport systems are increasingly conducted based on the criteria of increasing the labor productivity and reducing the number of personnel required as a result [1]. One of the most effective ways to address this problem is currently the use of improved logistics in the form of more detailed and accurate driver schedules [2]. It is also recognized that promising communication technologies and vehicle autonomy will help to solve these difficulties. However, the problem is also complicated by the fact that the duration of work, driving and rest of drivers is regulated by the European Agreement 561/2006 with the motivation of occupational safety and health [3]. It is known to be a very common phenomenon that majority of road freight carriers assign drivers to trucks to increase their responsibility for the technical condition of the equipment. This is also accompanied by the problem of downtime and inefficient use of vehicles. However, both the use of a shift method of the driver team work and the use of modern communications are insufficient for the full use of the driver's working time fund. This requires drivers to pick up and drop off trucks to their partners when their maximum allowed shift time begins and ends. Such a process has already been modeled previously using shift method operation of a carrier. A reduction of the required number of driver teams with a constant volume of transportation by 32% was achieved [4]. However, the carrier had a rather small fleet, so this achievement is insignificant in relation to the real need for hiring drivers. The volume of vacancies for truck drivers currently reaches 30% in the European Union. Therefore, the shift method and other logistics improvements do not justify real expectations on a small scale.

It is necessary to draw up a tight schedule for a sufficiently large team of drivers to ensure their coordinated work and freight transportation with minimal time losses (idle runs and downtime). Cloud computing has become the most effective among known

scheduling algorithms, as it can solve multiple problems simultaneously and use big data [5]. However, despite a fairly large number of known studies, heuristic and metaheuristic methods have been successfully used to solve multi-objective scheduling optimization problems. Traditionally, heuristic and meta-heuristic solution methods have been successfully used for such problems to some extent. In recent years, the emphasis has shifted to hybrid methods that offer more efficient solutions. Choosing an effective optimization algorithm is also important in modern information systems of transport enterprises. Processing large amounts of data and making decisions in real time becomes a routine process. The results of the comparative analysis showed that none of the known algorithms is universal for all types of tasks. The choice of the optimal algorithm depends on the specific task, the requirements for the speed and accuracy of decision-making, the availability of resources, etc. The use of hybrid approaches that combine the advantages of several algorithms can provide the best results in many cases.

Thus, the conditions for application of promising cloud computing and hybrid algorithms are the availability of big data, which, on the other hand, creates difficulties in finding guaranteed optimal solutions in an acceptable time. Modern methods of schedule optimization work effectively under the condition of structuring the initial data flows, their preliminary analysis, filtering and segmentation.

The main efforts of these studies were aimed to prepare initial data on freight transport parameters that relate to a set of interested freight carriers connected to the planning network. The purpose of the research was to develop such a criterion for structuring the data flow, according to which a large amount of data would enable the use of cloud computing, on one hand, and will provide an opportunity to successfully apply meta-heuristic methods for solving various problems of transport process planning, primarily a scheduling for drivers of various carriers connected to the cloud computing network. To achieve this goal, the following research tasks were set: (a) to substantiate the criterion for processing initial data such that it ensures compliance with the conditions and limitations of the work of several driver teams and their interaction and makes it possible to process large volumes of initial data; (b) to investigate the influence of the scale of input data on their adaptability to the use of heuristic scheduling optimization algorithms.

2 Literature review

The number of planning algorithms related to driver and vehicle scheduling research is quite large, increasing annually by an average of 16.62% [6]. At the same time, the problems of optimal scheduling are spreading to areas of activity where they were not previously applied [7]. Now, schedule optimization is also relevant for the road freight transportation, multimodal transportation, terminal technologies, etc. The main goal of such research is the most rational distribution of available transport resources. Most of the published works are concerned with the urban passenger transportation and the organization of work of bus drivers [1] and taxis [8]. However, research results on improving freight logistics are increasingly appearing in modern publications [9].

Improving the logistics of personnel work is seriously complicated by the diversity of potential that individuals with different qualifications and performing different functions are endowed with [10]. This is also illustrated by the example of air transport crew planning [11]. A similar problem can also be identified in freight road transportation. However, solving it separately for each category of employees is impractical, since that disrupts the coordination of individual transport groups and destroys the integrity of the transport system as a whole [1].

Since the complexity of complex scheduling tasks is significantly increasing, some researchers have proposed to narrow the scale of planning from tactical to operational. There has been a trend in formulating complex road transportation planning tasks. In particular the tasks of drivers team scheduling assigned to several depots [12], the tasks of planning individual parts of the transport network, with connected cooperative vehicles, were combined into one were formulated and solved [13]. There has been a trend in formulating complex road transportation planning tasks of improving the work schedules of drivers and vehicles are now also solved comprehensively [14].

Formulating the complex search conditions yields the better-quality solutions. However, the complexity of the initial conditions increases the scale of the required initial data. Therefore, the algorithms used to process such a volume of data must be qualitatively different from traditional ones. Such algorithms must be equipped with modern information technologies, artificial intelligence. By analyzing large datasets, historical trends, and real-time data, AI-based algorithms can determine the most efficient routes and schedules for transportation and operators for a variety of transportation and logistics needs [15].

Big data operations have the well-known benefits, but their application presents certain challenges for implementation. The advantages include: (I) the possibility of using AI algorithms and deeper learning; (II) large volumes of data are low-cost; previously, collecting such data required human effort, which was expensive, time-consuming, or impossible; (III) large volumes of data are characterized by greater reliability and accuracy of the information generated, since a large number of sources allows for the verification of data streams; (IV) large data flows allow for predictive analytics in transportation, in particular, estimating arrival times or warning of potential incidents [16].

Challenges: (I) data flows coming from different sources often have a mutually inconsistent structure, requiring complex pre-processing to convert the data into formats that facilitate analysis; (II) the complexity of distribution tasks is increasing, namely the assignment of vehicles to known tasks, the distribution of tasks to drivers, taking into account work and rest time regulations, as well as chronic staff shortages; (III) a higher level of synchronization of data streams is required due to time delays; (IV) problems with data collection and storage; (V) problems with data standards agreement [17].

In addition, in the work [18] is stated that there are significant gaps in the knowledge of researchers and practitioners regarding the right information and tools for analyzing large databases. If a large amount of data is generated by different sources, processed by different applications, and used by different means, a programmable framework for distributed computing that uses a "divide and conquer" approach to processing big data is needed. Future challenges include developing batch big data processing tools for distributed data indexing, replication, load balancing, automated disaster recovery, and data restoration [19].

A key area of development for big data processing is artificial intelligence, which fundamentally changes the way companies approach complex routing problems and solve them in a reliable and simple way [20].

To solve the Nondeterministic Polynomial (*NP*) hard schedule planning problem with *NP*-hard characteristics, a large number of heuristic algorithms have been developed: density-based clustering [9], cloud computing [21], recursion [1], etc. However, the above methods have certain limitations in the process of solving transport planning problems, since they require more solution time and at the same time significantly increase the computational complexity of the planning system [22].

A very important task in organizing the work schedule of truck drivers is the task of predicting precisely the moments: the arrival of trucks for loading, delivery of cargo, etc. These and other moments are critical for the schedule as a whole. However, with large volumes of data and the random nature of processes, traditional heuristic methods do not provide accurate solutions in a reasonable time [23].

The crucial importance in building efficient supply chains based on clustering is ensuring continuous freight flows through the full integration of the involved participants and logistics infrastructure facilities in the network, based on clustering and a single partner space. Analysis of the methodology and the results obtained from the application of the more common K-means clustering algorithm in the context of container terminals provide the grounds for applying a similar approach to cargo transportation. Specific data regarding container transportation in multimodal systems is a reduction in the total number of required transport trips by 31.58% and provides decision makers with a compromise between the total truck turnover time and the deviation from the desired time window for cargo pickup by transport companies [24]. It is obvious that bringing the content of the clustering criterion closer to the essence of the objects will improve the quality and responsiveness of the obtained solutions.

3 Problem formulation

Next a finite set of logistics processes $J = \{J_1, \dots, J_x, \dots, J_n\}$ is considered. Here, a process means a sequence of logistics operations for fulfilling one order for goods transportation by road vehicles on an intercity transport network. Orders are independent, so they can be fulfilled in any sequence. However, each order may have a time window to limit the maximum duration of its fulfilment. The processes of fulfilling all J orders represent the project horizon H, within which it is necessary to fulfil the maximum number of orders from the set J with the minimum number of drivers. So, k identical trucks are used for this aim. The average duration of the trucks runs between any points of the network, the duration of loading /unloading of trucks are the values predicted. The trucks are driven by a team of drivers who are able to replace each other then and at those points of the transport network where it will be necessary to do so due to the restrictions 561/2006. However, the objects of study in this work are intercity processes with a horizon of approximately 2-3 days, so weekly/fortnightly restrictions according to Regulation 561/2006 were not considered for this reason.

Thus, the drivers must be coordinated, and this is possible if a clear schedule of their work is given. The schedule of the team of drivers is considered to be unambiguously given if for each driver there is a specified start time and end time for the execution of the order / sequence of orders assigned to him. Order fulfilment operations may be interrupted by drivers due to time constraints. If the shift driver work method is used, the schedule must also indicate the truck number that the driver will drive when fulfilling the order. It also indicates the points in the transport network where the driver must accept the truck, and deliver the goods, and hand over the truck to his partner. Unlike the known methodology [24] an unambiguous schedule consists of sets of values:

- $t_1^b, t_2^b, \dots, t_i^b, \dots, t_n^b$, where t_i^b is the earliest time to start an order J_i execution;
- $t_1^e, t_2^e, \dots, t_i^e, \dots, t_n^e$, where t_i^e is the latest time to finish an order J_i completion.

In the known method, the schedule of the entire process is considered to be uniquely determined if the exact start or end time of all operations is known. However, the schedule of the process at deterministic moments is difficult to reconcile in practice with the random factors that are always present in the logistics

of cargo delivery. Therefore, one of the differences of this algorithm is the use of time points with tolerances.

The quality of the decomposition is characterized by the minimum value of the non-decreasing function in each argument:

$$H(x_1, x_2, \ldots x_n),\ x_i = t_i^e - t_i^b \tag{1}$$

The schedule is considered as optimal if it corresponds to the smallest value of the specified Equation (1), while observing the condition of full implementation of the project with the involvement of a given number of drivers, as well as compliance with the regulations of their work and rest.

4 Methodology

A previously developed method for optimizing the work schedule of a team of truck drivers working in a limited area is used, and applying a shift work method, using the criterion of the minimum total duration of the project. The method is based on the ordering of mixed (disjunctive) graphs $G(J,V,U)$, where J is a set of vertices $J = \{j_1, \ldots j_n\}$, V, U are sets, respectively, of edges and arcs, each is given with a weight $a_{i,j}$, $i,j = 1 \ldots n$ [24]. Such graphs may contain contours of positive weight, so it is impossible to construct a unique schedule after them. To overcome this obstacle, it is necessary to remove all edges V, or replace them with arcs. The minimum guaranteed duration of the entire project depends on operation done with each edge $v_{i,j}$ (removed or replaced with an arc $u_{i,j}$ or $u_{j,i}$). This value is the length in time scale of the critical chain in a graph without loops and contours. However, even in a graph without edges there may be contours, or isolated vertices, which make it impossible to find the critical path from the fictitious vertex S, which symbolizes the formal beginning, to the vertex F, which symbolizes the formal end of the project. A well-known graph ordering algorithm was improved in [24].

If there was a contour of positive weight in the graph $G(J,U)$, the search for the conflicting arc $u_{k.i,j}$ would be performed. Removing a conflicting arc from a graph G will not only make the cycle-free graph, but also improve the constructed schedule. In fact, there may be a finite set of such conflicting arcs, so the task of finding and removing them is a multivariate problem; the complexity of the problem is polynomial [4]. An empirical algorithm was applied, in which an indirect optimality criterion for the graph $G(J,U)$, which does not contain circuits, is used. A feature of the improved method is that it gives a satisfactory estimate of optimality $\inf(H_{\min})$, where $H_{\min}$ is the minimum project duration with the dimension of the problem $J \leq 40$ vertices:

$$H_{\min} = \min\{h_{i,j}, h_{j.i}\}, \tag{2}$$

where:

$$h_{i,j} = t_i^e(J,U) + x_i + \nu_y(J,U) - \nu(J,U), \tag{3}$$

v_j means the maximum value of the chain in graph G, which starts at the vertex j_y; $v(G, U)$ is the maximum G graph chain. That simplified the task of finding an active optimal order execution schedule after graph $G(J,U,V)$, using criterion in Equation (2), by choosing the most conflicting edge. The algorithm that was improved allows for one to find an approximate solution faster than previously possible, taking into account that the desired schedule consists of approximate operation execution times. The complexity of the algorithm does not exceed $O(2^J+V)$ elementary operations. However, the algorithm still works slowly with large amounts of initial data. In addition, the error in estimating the quality of the schedule also increases with increasing problem dimensionality. When the number of vertices increases by 10, the accuracy of the optimum estimation decreases by more than 7% and this error increases exponentially with the increase in the number of vertices J [14]. When the number of vertices arises up to 90, the solution of the problem in the permissible time becomes unattainable. Thus, the algorithm based on the ordering of the mixed graph is effective with a small volume of vertices, as well as conflicting edges or arcs. On the other hand, if the initial graph G has no edges or contours, then it uniquely determines the work schedule of each driver. Such a result is trivial and does not contain the subject of optimization. These facts set limits on the size of the initial data for the problem of constructing the schedule of a driver team when using a heuristic algorithm on conjunctive graphs. An additional criterion is required to prepare the initial data, which will lead to an increase in the efficiency of the schedule.

5 Criterion for assessing the closeness of organizational ties

The duration of driving, work and rest periods for drivers is limited by EU Regulation 561/2006 with all its amendments, successively introduced into the regulations [3]. A driver's shift consists of driving time, the continuous duration of which cannot exceed 4.5 hours. The total driving time during a shift cannot exceed 9 hours, or as an exception 10 hours, but only twice a week. A driver must have a rest period during a shift for at least 45 minutes. A driver must have a rest period between shifts for at least 11 hours. It is allowed to divide the duration of rest period, and rest period between shifts. Driver's duties also include loading and unloading operations, preparatory operations (fastening, checking the integrity of the load), guarding the truck at parking lots, technical inspection and maintenance of the vehicle. All these works, together with driving, are included in the 13-hour work cycle (Figure 1).

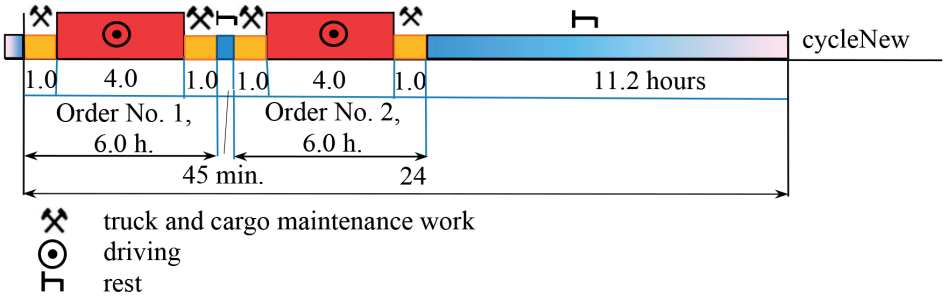

Figure 1 *Idealized scheme of driver work and rest modes when performing two consecutive orders* #1, 2 *within one shift*

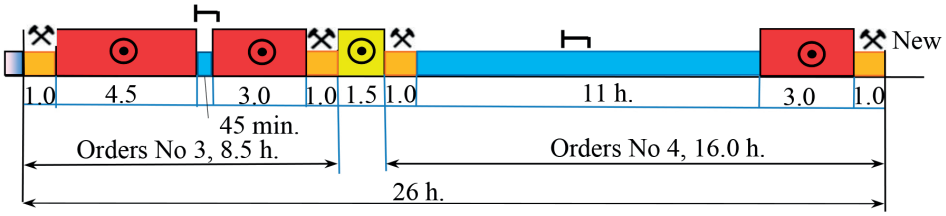

Figure 2 *Displaying sample of partially compatible orders*

Figure 1 shows the execution of some orders #1, 2, the driving duration of each is 4 hours, and the total duration of each order is 6 hours. Orders represent the transportation of goods between pairs of transport points. In this case, the final point of order #1 is the initial point of order #2. Therefore, the sequence of execution of orders by one driver on one truck will result in the absence of idle runs and useless downtime in such a transport cycle. The required variable rest of the driver is a standard value of 45 minutes. The duration of continuous driving, the total duration of driving, and the duration of the work shift do not differ from the permitted standard. Therefore, such a scheme can be considered as idealized. The scheme shows the zones: cargo work in orange bars; truck driving in red bars, driver rest in blue bars. If there is a need for idling, this is indicated by yellow bars.

The schedule of logistics operations can be implemented using an idealized scheme, which is shown in Figure 1 due to the fact that orders #1, 2 are fully compatible in terms of organizational and technological parameters. Such compatibility can be estimated as 100%, or using some compatibility coefficient R_c = 1.0.

Figure 2 shows two orders #3, 4 that do not have similar compatibility.

Since the truck's driving time during order #3 exceeds 4.5 hours, it is interrupted for 45 minutes for the driver's necessary rest. Order #4 starts at a different time and at a different transport point, when order #3 ends, so there is a need for idling. The driver needs a long inter-shift rest of 11 hours after loading the cargo, when executing order #4. Ultimately, order #4 is executed with a long delay of 16 hours, although the "net duration" of its execution is only 5 hours. Orders that vary in duration of characteristic periods and differ from idealized compatibility are here called partially compatible.

Thus, for the fully compatible orders that are sequentially executed by one driver throughout the day, the duration of driving a loaded truck must be at least 8 hours, the duration of auxiliary operations must not exceed 4 hours, the driver's rest period must not be less than 45 minutes, and idling is excluded. Such a shift must alternate with an 11-hour inter-shift rest. The considered orders #3, 4, which are performed in the sequence 3→4, are called partially compatible. The time for performing these orders takes more than a day. At the same time, the duration of a run with a cargo is 10.5 hours, which is 1.6 times less than the two-day norm. An idle run is required to perform the orders. Inter-shift rest interrupts the execution of order #4. The degree of their compatibility is determined by the coefficient, which has the meaning of comparing the real compatibility to the ideal one:

$$R_c = \begin{cases} \dfrac{cargo}{cargo + idle + rest + loading}, \\ if\ (cargo + idle) \geq 4.5 \\ \dfrac{4.5 - (cargo + idle)}{4.5}, \\ if\ (cargo + idle) \leq 4.5 \end{cases}, \quad (4)$$

where: *cargo* is total duration of loaded runs; *idle* is the total idle time; *rest* is actual duration of the driver's rest; *loading* is duration of cargo operations during the cycle; all values in Equation (4) are measured over two consecutive transport cycles, hours.

The assessment of the two tasks compatibility depends on the comparison base. If the driving duration of the cycle is less than the allowed without rest duration (4.5 hours) of the driving, then the comparison base is

only the time spent on driving (with cargo and without cargo), and idle times and delays are not taken into account. If the driving cycle is longer than the duration of the maximum allowed driver's trip without a break, then the comparison base is the maximum duration of a shift (12 hours), or several shifts of the driver, including cargo operations, truck maintenance and minimum shift' rest. Thus, the compatibility coefficient of orders #3, 4 for the example shown in Figure 2, R_c = 10.5/26 = 0.4.

The reverse order execution sequence is generally independent of the forward order execution sequence. The coefficients R_c may differ for the forward and reverse order sequences.

In this paper is also considered the influence of the time windows execution of each order on their compatibility. Here, the time window is understood as the time tolerance ($t_i^{e.b}$, $t_i^{l.e}$), where $t_i^{e.b}$, $t_i^{l.e}$ are the most probable early beginning, and late ending of the i-th order fulfilment. If, for a sequence of two orders, $i \rightarrow j$, inequalities are satisfied

$$t_i^b \, t_j^{e.b} < t_i^{l.e} \text{ and } t_j^{l.e} \leq t_i^{e.b}, \tag{5}$$

then such orders are considered completely incompatible in the specified sequence, for them the coefficient R_c=0, and the specified sequence is excluded from consideration.

If for the same sequence $i \rightarrow j$ one has:

$$t_i^{e.b} \leq t_j^{e.b} \leq t_i^{l.e} \text{ and } t_j^{l.e} \geq t_i^{l.e}, \tag{6}$$

then such orders are considered partially compatible. The compatibility coefficient for these orders by time windows is determined by:

$$R_c = \frac{1}{t_j^{e.b} - t_i^{l.e}}, t_i^{l.e} > t_j^{e.b}, \tag{7}$$

where the order execution time frames are measured in integer units of time.

If the compatibility coefficients R_c for the same pair of orders calculated by Equations (4) and (7) are different, then a smaller value is chosen for further clustering operations.

To form clusters of similar orders, it is necessary to combine orders based on organizational compatibility, that is, by the coefficient R_c. However, the organizational and technological connection between a pair of orders can be of different quality, since $0 \leq R_c < 1.0$. Therefore, the level of quality of the connection requires justification, that is, it is necessary to establish at which value of R_c the connection between a pair of orders should be considered close enough to include them in same a group. For this purpose, simulation was planned and conducted under different conditions of execution of transport orders, and a study was conducted of the influence of the adopted value of R_c on the quality of data preparation for building an optimal schedule.

6 Simulations

To adhere to the principle of generality (universality) of the scientific problem and avoid the subjectivity of any particular case, it was used the modelling of the processes of formation and fulfillment of freight orders based on random input data. Such cases significantly depend on commercial, legal, geographical and even political conditions. The specifics of the practical activities of carriers can serve as examples of the practical significance of the developed methodology rather than as a means for its development.

The purpose of the simulation was to generate random data on the availability, location, and time parameters of orders with a large amount of data in order to perform their clustering and prepare for construction of several independent optimal schedules in terms of the number of drivers involved.

Orders are received by the carrier as a need for transportation of consolidated cargo in an intercity route. The simulation generates random values of the geographical coordinates of the points that relate to all orders known during the modelling period, as well as other points that are not included in any route. Random coordinates of transport points in the territory under consideration were determined using the program generator of random numbers (PGRN) with uniform distribution. The algorithm and the initial number of the generator were written by the authors in the Delphi programming language. The coordinates of q_i points of the territory are received:

$$x_i := random(0; X_{\max}), y_i := random(0; Y_{\max}), \tag{8}$$

where $X_{\max}$, $Y_{\max}$ are the maximum possible relative coordinates in the serviced area, km.

The starting and the ending points of each cargo delivery route were also randomly assigned.

So, the indices of the points of departure of the goods: $i := random(1; N_l)$; indices of delivery points: $j := random(1; N_l)$, and any departure points cannot be a delivery points simultaneously for the same cargo.

The assumption was made that on the transport network, where the freight transportation is performed, there is a road connection between any pair of points. To determine the distance between any transport points g_i, g_j, the following formula was used:

$$l_{i,j} = k_c \sqrt{(x_i - x_j)^2 + (y_i - y_j)^2}, \text{ km}, \tag{9}$$

where: k_c is a coefficient of curvature of the path.

The path length calculated by Equation (9) approximately reflects the distance between the two points that would lie between real points.

The road curvature coefficient takes into account two factors that distinguish a segment from a real road: (a) the curvature of the road in plan; (b) the absence of a direct connection between points q_i, q_j, but through

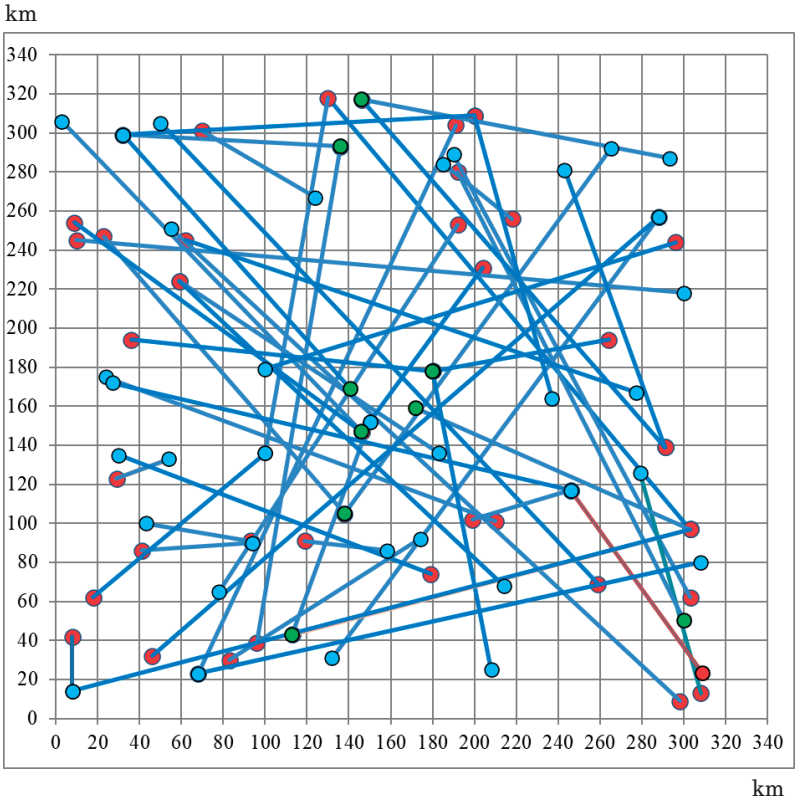

Figure 3 *An example of generating a network of random orders: red markers are departure points; blue markers are reception points; green markers are points that are both senders and receivers of goods; segments are vectors of goods movement without taking into account the curvature coefficient; population density is 1.35 settlements per km²; number of orders - 50; area of the territory - 115.6 km²*

a transit point q_t. Given the random nature of the simulated transport network model, this method of determining the length of the paths can be considered quite satisfactory. After all, not only the coordinates of the points are random, but the length of the paths between them and the network configuration, as well.

To specify the configuration of the transport network, the population density indicator was used. Actually, the population density of the territory is an indicator that characterizes the location of settlements per unit area of the geographical territory where the transport network is located. The population density is determined by:

$$\rho = \frac{N_l}{A}, \text{ settlements / 100 km}^2, \quad (10)$$

where: N_l is the number of settlements located in the territory under consideration;

A is the area of the territory under consideration.

Statistical sources provide numerical values of this indicator for different regions of Europe. The population density can reach a value of 9 settlements/100 km² for some regions. The minimum density value was noted as 1.8 settlements/100 km². However, to set and implement this indicator in the simulation model of this work, a different approach was applied. For simulation modelling, it is necessary to set such a random location of transport points, which is characterized by the desired density coefficient. It is necessary to divide the territory with a given area into equal squares that can simultaneously accommodate several settlements. In this work, such settlements were taken into account that are considered cities, that is, have a population of more than 3500 people, and have the appropriate infrastructure for performing large-scale freight transportation between cities. Cities in East Europe, with suburban areas and satellite cities, occupy an area with a fairly wide range: from 20 to 900 km². Areas of more than 700 km² are occupied by megacities, which are administrative centres of regions. There are no publicly available statistics that would provide an accurate value of the average area for all cities. However, if one considers the regional structure (region), the average area of a city that is not an administrative centre ranges from 80 km² to 3.7 km². Therefore, the size of the square of the territory to be considered should be no less than 100 km². In this case, one square cell can contain no less than 3 settlements due to random distribution.

The following initial data were used for simulation modelling of the conditions for performing intercity transportation: (A) the total number of settlements P; (B) maximum size of the territory in latitude X_{max} and longitude Y_{max} km; (C) order execution period T, hours; (D) the set of orders $Z=\{z_1, \ldots z_n \ldots, z_m\}$, time windows of which are included in the execution period; (E) order

time windows $t_i^{e.b}$, $t_i^{l.e.i}$; (F) population density coefficient €; (G) road curvature coefficient k_c; (H) average technical speed of trucks on the network V_t.

The random number generator of the simulation model produces the following data: (I) coordinates of each settlement x_i, y_i; (J) number of the initial and final route point *i, j*, which concerns each known order; (K) duration of movement with cargo for each order cargo; (L) duration of downtime associated with cargo operations, and truck maintenance, loading. An example of random orders (coordinates of the points of departure and receipt of cargo are given in Figure 3.

All orders are compared in pairs after their formation. The ratios were obtained, which reflect the consequences (time spent on driving the truck, driver rest, idling) of the sequential execution of orders by the same driver, on the same truck, in strict order. The results of consecutive execution of two orders #*i, j* were evaluated according to the following rules, taking into account Equation (4), as well as Regulations 561/2006 EU.

1. First, build the simplest cargo transportation cycle to fulfill the first order #*i*. The cycle must fully comply with EU Regulation 561/2006 and contain all the necessary elements for the implementation of the process (loading, movement with cargo, unloading, driver rest, idling, etc.).
2. Build a complex transportation cycle to fulfill two consecutive orders $\#z_i$, $\#z_j$ by the same vehicle, and by one driver, or by team of drivers, who can work using a shift work method. It is necessary to take into account the possible need for idling and vehicle downtime, while waiting for the start of loading / unloading. There may be a need for drivers to rest between shifts, as well.
3. Using Equation (4), determine the compatibility coefficient of two consecutive orders that will be performed only in a given sequence $\#z_i \rightarrow \#z_j$.
4. Determine the time tolerances for the execution of logistics operations, and the compatibility coefficient of orders using Equation (7). The smaller numerical value of the compatibility coefficient $R_{c.i.j}$, which is calculated by Equation (4), or (7), is taken as the correct value for further analysis of the entire data set on existing orders.

Based on the random data, a square matrix of values $R_{c.i.j}$ of order compatibility coefficients is constructed. Matrix ($R_{c.i.j}$) gives the ability to assess the closeness of the connections between each pair of transport cycles, and to select the most significant ones for clustering a large amount of initial data. A passing value of the compatibility coefficient is indicated for a known compatibility matrix, i.e., one below which the two orders cannot be performed sequentially by one driver. This threshold value is subject to practical justification. To determine the most favourable conditions for combining orders into clusters, simulation modelling was carried out with variable input data. The variables were such values:

1) the maximum area of the service area (102.4, 78.4, 57.6, 32.4, 19.6 thousand km²);
2) the number of settlements in a given area (200, 140, 120, 100, 50);
3) the number of orders on the planning horizon (150, 100, 50);
4) the curvature coefficient of roads in the plan (1.35, 1.75, 2.5).

Each combination of data gives the resulting set of graphs with a different number of connections and isolated vertices. If the coefficient R_c has a too low value, i.e., $R_c \rightarrow 0$, then many insignificant connections in the graph *G* will not be discarded. The graph will be strongly connected. Clustering will not actually occur, and there will be a large number of edges *V* between the vertices *J* of the graph *G*. It means that the resulting graph is not very suitable for finding a fast and guaranteed optimal solution of the driver work and rest schedule. If the numerical value of the coefficient R_c is too large, i.e., R_c€1.0, then the vast majority of connections in the graph *G* will not be preserved. This applies to both the arcs *U* and the edges *V*. Additionally, there would be a large number of isolated vertices among the initial data. These vertices are the orders that cannot be combined with any of the other orders. This means that there will be no division into clusters in such a model, since most of the vertices will be isolated. Finding the optimal schedule in such initial data will be a trivial task, since the schedule will be a set of start times for almost all orders: $t_i^s = 0$, for $I = 1 \ldots Z$. In this regard, the desired value of R_c was justified after analysing all the previously obtained data, which were clustered for all possible $0 \le R_c \le 1$. If the number of clusters is greater than 0, and if the number of contours in the graphs of the initial data is greater than 1, but not more than the number of arcs, then the coefficient R_c was considered significant.

Figure 4 shows the result of dividing the initial data into 5 subgraphs $G_1 \ldots G_5$ from the general graph *G*, which were obtained for $R_c = 0.3$ and 12 isolated vertices. Subgraphs have edges, respectively: V_1 - 3; V_2 - 2; V_3 - 1; V_4, V_5 - 0 items.

The simulation results for other modified conditions are shown Table 1.

If the existing edges are removed from the subgraph G_1, or converted into arcs, then this subgraph would still contain 3 contours, which must be removed by analyzing all the available arcs for criticality [14]. Thus, the subgraph G_1 is one of the most complexes of all the clusters, but the task of finding the optimal location on it can give a qualitative result due to a larger field of variables. Subgraph G_2 is less complex, since its variable field contains only two edges and no other contours. Subgraph G_3 is even less complex, but it leads to only two possible solutions. Finally, subgraphs G_4 and G_5 give a unique orders fulfilment schedules with an admissible compatibility coefficient $R_c = 0.3$.

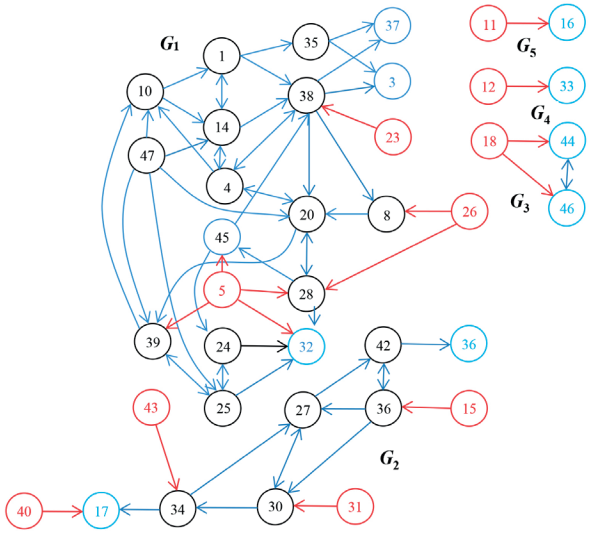

Figure 4 *An example of mixed graph with parameters: threshold value of the order compatibility coefficient $R_c \geq 0.3$; number of vertices (orders) J = 50; number of vertices connected by links: 38; number of isolated vertices: 12; number of settlements P = 120; area of the territory A = 19.6 thousand km²*

Table 1 *Simulation results*

Version	Number of orders	Area of the territory, thousand km²	Number of settlements	Settlement coefficient	Road curvature coefficient	Number of orders without a group	Compatibility coefficient threshold	Number of groups	Number of contours
1	50	19.60	50	1.42	1.35	21	0.50	1	5
2	50	19.60	100	1.42	1.35	18	0.40	2	8
3	50	19.60	120	1.42	1.35	12	0.30	5	9
4	50	32.40	50	1.42	1.35	28	0.60	1	10
5	50	32.40	100	1.42	1.35	20	0.50	1	18
6	50	32.40	120	1.42	1.35	16	0.40	2	21
7	50	32.40	140	1.42	1.35	3	0.30	1	32
8	50	57.60	50	1.42	1.35	18	0.60	1	28
9	50	57.60	100	1.42	1.35	8	0.50	4	12
10	50	57.60	120	1.75	1.35	3	0.40	5	6
11	50	57.60	140	1.75	1.35	0	0.30	3	4
12	50	102.40	50	1.75	1.35	4	0.60	2	14
13	50	102.40	100	1.75	1.35	2	0.50	6	6
14	50	102.40	120	1.75	1.35	2	0.40	4	18
15	100	19.60	100	1.75	1.35	24	0.60	2	8
16	100	19.60	120	1.75	1.35	22	0.50	4	21
17	100	19.60	140	1.75	1.35	18	0.40	3	12
18	100	32.40	100	2.15	1.35	20	0.60	3	16
19	100	32.40	120	2.15	1.75	20	0.50	2	9
20	100	32.40	140	2.15	1.75	16	0.40	2	9
21	100	57.60	100	2.15	1.75	18	0.60	5	16
22	100	57.60	120	2.15	1.75	18	0.50	6	27
23	100	57.60	140	2.15	1.75	16	0.40	1	34
24	100	102.40	120	2.15	1.75	18	0.60	2	22
25	100	102.40	140	2.15	1.75	16	0.50	2	35
26	100	102.40	200	2.15	1.75	12	0.40	3	21
27	150	32.40	120	2.15	1.75	28	0.60	3	26
28	150	32.40	140	2.15	2.50	24	0.50	7	19
29	150	32.40	200	2.15	2.50	24	0.40	2	11
30	150	57.60	120	2.50	2.50	24	0.60	2	16
31	150	57.60	140	2.50	2.50	24	0.50	3	22
32	150	57.60	200	2.50	2.50	20	0.40	4	10
33	150	102.40	120	2.50	2.50	32	0.60	2	12
34	150	102.40	140	2.50	2.50	28	0.50	4	25
35	150	102.40	200	2.50	2.50	14	0.40	5	10

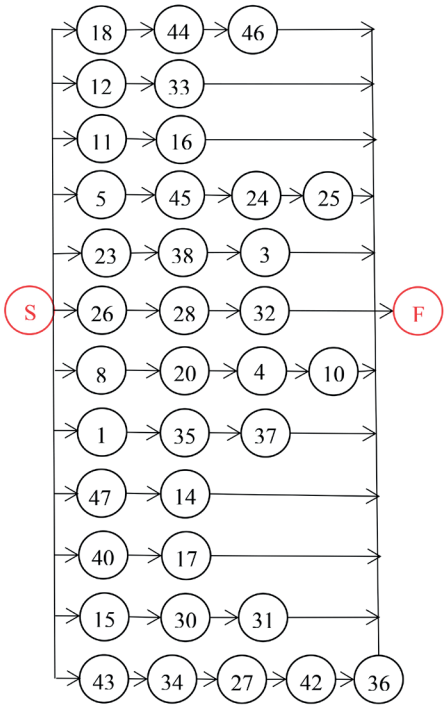

Figure 5 *Example of an ordered graph*

```
Predicted time - 20.0 hours
Transport task of driver #1: order 18-44-
46; by truck #1
Truck #1 route: points  2-4-3-1
Order #18 start 0.0 end 3.5, truck #1 from
point 2 to point 4, driver #1
Order #44 start 4.0 end 5.5, truck #1 from
point 4 to point 3 driver #1 Order #46
start 6.2 end 9.5, truck #1 from point 3
to point 1
Minimum duration of this project = 11.0
hrs. Team of drivers - 12 persons
```

Figure 6 *Fragment of optimal schedule*

Table 2 *Results of schedules optimization of truck drives based on big data*

Version	Number of drivers	Project total duration, h	Version	Number of drivers	Project total duration, h
18	28	7.3	27	52	18.6
19	24	7.1	28	51	14.2
20	26	7.8	29	69	26.5
21	33	10.6	30	82	24.2
22	27	8.4	31	75	19.3
23	44	13.8	32	79	22.8
24	67	14.5	33	115	28.4
25	72	13.5	34	92	26.0
26	71	12.8	35	102	22.8

Only the data obtained for $R_c \leq 0.6$ are shown, since for larger values of the coefficient no cluster was obtained (all vertices were isolated). If $R_c \leq 0.3$, then the clustering also does not occur, since only one graph with a significant number of edges, almost twice the number of arcs was obtained. The data obtained as a result of modelling also make it possible to assess the impact of the scale of freight transportation planning and driver

schedules on the quality and availability of optimal plans. Figure 5 shows an example of an ordered graph $B(Q,U)$, which is constructed from subgraphs G_1 to G_5. Graph B does not contain contours of positive weight. Additionally, a fictitious vertex S is introduced into the graph, which symbolizes the formal start of the whole project. From the vertex S, only arcs exit to the vertices, which are shown in Figure 4 by red circles, which are the initial orders of the project. The fictitious vertex F represents the fictitious completion of the project. There are only incoming arcs to the vertex from the vertices, which are shown in Figure 4 by blue circles.

When applying the schedule construction method and the corresponding algorithm and program [25] to the formed graph G, a work schedule for 12 drivers was obtained the content of which is recorded in Figure 5.

A graph without loops and contours, an example of which is shown in Figure 5, makes it possible to establish a unique minimum work schedule for truck drivers and an order fulfilment schedule taking into account the specified maximum predicted time (Figure 6).

The modified algorithm was applied to all randomly generated initial data. The schedule optimization algorithm was applied to each order cluster separately. After that, the individual partial optimal schedules were combined into one horizon and a set of resulting schedules was obtained for each version of the initial data. Table 2 presents the parameters of those schedules for which the clustering gives a significant effect in optimizing the order execution sequence.

Thus, the first 17 versions for the initial data presented in Table 1 do not lead to a significant effect of data grouping. They are excluded from the following analysis. Other versions 18-35 allow to identify the following consequences of clustering. An increase in the average duration of one order leads to an increase in the required number of drivers, regardless of the method of preliminary data preparation. The greatest effect of data preparation is achieved with large-scale planning. Thus, with the number of orders of 150 and the average duration of one order of 3.5 hours, it is possible to achieve a reduction in the duration of the project by 5.6 hours, and reduce the number of drivers by 23 persons. Thus, it can be argued that the most effective way to prepare the initial data is to maintain a large number of positive weight contours with a sufficiently large number of clusters. Such an effect is observed over a large service area if the compatibility coefficient is kept at 0.5.

Thus, with an increase in the transportation area without an increase in the number of planned orders, the pairwise organizational compatibility of orders weakens, which is associated with an increase in travel distances and, accordingly, the time spent by drivers on driving a truck both with cargo and idle. Therefore, the expansion of the service area should be accompanied by an increase in the density of orders. At the same time, the number of settlements does not significantly affect the possibility of obtaining a high-quality schedule.

The number and total length of roads in Europe do not increase proportionally, practically, with the increase in the size of the service area. After all, the population density coefficient, especially in the western regions, is quite high (reaches 8.8 points per 100 km^2), while the length of local roads, which accounts for 1 km of highway, is small. Therefore, the expansion of the service area is not a leading factor in the growth of truck fleet productivity.

The developed algorithm for assessing the compatibility of a set of the available orders was used for the computer program in the Delphi language. The program was tested at several international enterprises which are the large road carriers in Eastern Europe. One of such large enterprises is the Trans-service-1 Company [26]. The enterprise uses more than 150 road trains with tilting semi-trailers which are suitable for transporting the necessary types of cargo. Most carriers such as Transservice-1 have a network of their regular customers, and are also used by random orders from intermediaries. However, the Transservice-1 enterprise, as well as others like it, do not choose specialized software or any other methodological tools to distribute orders to drivers and to assign vehicles to known transportation tasks, and do not contain schedules for their implementation. That is why the planning of drivers' work schedules was carried out at these enterprises first.

The logistics department of the carrier receives an average of 200 orders from intermediaries and about 70 orders from the regular customers, which geographically extend along almost all highways throughout Europe. The company rejects some received orders because the company's trucks are spread out quite haphazardly, and otherwise would have to suffer a lot of downtime and downtime and idling. Currently, the company experiences a major shortage of drivers and a significant impact on the cost of transportation of high fuel prices. The carrier fulfills approximately 30-50 orders, primarily these are orders from regular customers, other orders are rejected. The 5 typical daily transportation plans of the company during the periods of the highest productivity of the fleet are reviewed and compared with the existing demand in the same periods, as well as with the actual capabilities of the fleet. Software are developed for more thorough planning of work schedules for road trains operated by teams consisting of 1-2 drivers, and the possibility of using a shift work method for drivers was also provided. The criterion of maximum performance of the volume of transportation (mileage with cargo) of the fleet is applied while limiting the total duration of the process. The obtained analysis results are presented in Table 3.

When planning the transportation according to the initial data taken from incoming orders at the specified date, optimization was performed with a preliminary division of orders into clusters according to the order compatibility criterion $R_c \geq 0.5$, since the criterion for improving the plan was the maximum volume of

Table 3 *Improving the results of freight transportation plans in a trucking company*

Plan number / date	Number of orders received	Known plan					Optimized plan according to the developed methodology				
		Number of the orders accepted	Total mileage with cargo, thousand km	Number of drivers / trucks involved	Idle mileage, thousand km	Total project time*, hours	Number of orders accepted with clustering	Total mileage with cargo, thousand km	Number of drivers/ trucks involved	Idle mileage, thousand km	Total time/ duration of the project**, hours
1/25.08.11	280	32	14.9	45/32	1.1	378	115	89.9	100 56	12.3	2338 45
2/25.09.02	230	25	13.6	38/22	3.6	455	96	78.8	90 48	9.2	2095 43
3/25.09.03	265	24	9.2	38/22	2.7	313	103	73.4	100 50	4.6	1857 37
4/25.10.13	320	44	18.5	68/53	7.2	580	124	95.8	100 82	22.3	2811 44
5/25.11.20	189	17	24	25/22	2.1	212	62	47.4	60 30	3.0	1200 42

* the cumulative time spent by all truck crews on the routes. This time contains the downtime associated with customs procedures, so it was impossible to isolate the duration of logistics operations from the primary data;

** excluding downtime at customs.

transportation performed. As a result, some planning indicators deteriorated. However, the new transportation plans are generally more productive for the existing fleet of trucks, which under the old plans were idle, and drivers were left without work. Table 3 shows the idle mileage of trucks on international routes, which is increased from 3 to 27%. However, the number of orders, which Transservice-1 could fulfill if it worked according to optimized plans, would increase by 2.3 times. This could have been achieved not only by attracting reserve vehicles and drivers (their number barely doubled), but by improving the structure of transport cycles, as well. Thanks to the new planning, the average daily mileage of trucks also increased by approximately 20% and their downtime is reduced.

7 Conclusions and further work

The use of the compatibility index of freight orders is justified when planning the schedules of a team of drivers. Thanks to the use of such a criterion, some of the a priori irrational ways of finding the optimal solution are discarded. Organizational and technological compatibility makes it possible to divide the total volume of big data into clusters such that the search for the optimal schedule in the obtained sub-graphs gives a guaranteed result. The number of vertices in such subgraphs reduces the complexity of the scheduling calculations, on one hand, and provides a sufficient field of variables for optimizing the resulting schedule, on the other. A reasonable threshold value of the coefficient lies within $0.3 \le Rc \le 0.6$, i.e., within its domain of definition. The choice of such values leads to the fact that successful clustering is ensured, and the volume of big data can be processed by an optimization algorithm based on meta-heuristics. However, there are other criteria for improving logistics plans, depending on the business situation. Each optimization criterion requires a reasonable choice of the numerical value of R_c. For example, a clustering criterion value close to its upper limit should be used when there is a need to increase the productivity of fleet vehicles. Values close to the lower limit create the prerequisites for obtaining tighter schedules and more efficient use of available resources in the shortest time.

Scaling the driver scheduling problem by increasing the territory, that is, by extensive transportation planning, leads to worsening results. More successful is the intensive scaling: by increasing the area of the service area and the number of planned orders simultaneously. The settlement factor does not play a significant role in the quality of the preparation of initial data for optimization, if it is not considered together with the density characteristic of the transport network. In this work, less attention was paid to the parameters of the transport network, which may be a promising task for the future research.

Acknowledgment

The authors received no financial support for the research, authorship and/or publication of this article.

Conflicts of interest

The authors declare that they have no known competing financial interests or personal relationships that could have appeared to influence the work reported in this paper.

Reference

[1] REDMER, A., KISIELEWSKI, P., OBLAZA, J. Optimal driver scheduling with evolutionary approach in urban public transport. *Archives of Transport* [online]. 2025, **74**(2), p. 65-80 [accessed 2025-12-08]. ISSN 0866-9546, eISSN 2300-8830. Available from: https://doi.org/10.61089/aot2025.919ryp91

[2] LIM, C. H., MOON, S. K. A two-phase iterative mathematical programming-based heuristic for a flexible job shop scheduling problem with transportation. *Applied Sciences* [online]. 2023, **13**(8), 5215 [accessed 2024-04-30]. ISSN 2076-3417. Available from: https://doi.org/10.3390/app13085215

[3] BENUS, J., DEMIRCI, E. Regulation (EC) No 561/2006-review of the adopted changes on 15 July 2020. *Automotive Archives* [online]. 2020, **90**(4), p. 59-73 [accessed 2025-12-25]. ISSN 1234-754X. Available from: https:// doi.org/10.14669/AM.VOL90.ART5

[4] SAUKENOVA, I., OLISKEVYCH, M., TARANIC, I., TOKTAMYSSOVA, A., ALIAKBARKYZY, D., PELO, R. Optimization of schedules for early garbage collection and disposal in the megapolis. *Eastern-European Journal of Enterprise Technologies* [online]. 2022, **1**(3), p. 12-23 [accessed 2022-02-28]. ISSN 1729-3774, eISSN 1729-3774. Available from: https://doi.org/10.15587/1729-4061.2022.251082

[5] SHANG, R. Efficient task scheduling for large-scale graph data processing in cloud computing: A particle swarm optimization approach. *Journal of Combinatorial Mathematics and Combinatorial Computing* [online]. 2024, **1**(122), p. 135-148 [accessed 2025-05-17]. ISSN 0835-3026, eISSN 2817-576X. Available from: https://doi.org/10.61091/jcmcc122-11

[6] EBRAHIMI, H., REZAEIAN MARJANI, S., GALVANI, S., TALAVAT, V. Probabilistic optimal planning in active distribution networks considering nonlinear loads based on data clustering method. *IET Generation, Transmission & Distribution* [online]. 2022, **16**(4), 686-702 [accessed 2025-12-31]. ISSN 1751-8687, eISSN 1751-8695. Available from: https://doi.org/10.1049/gtd2.12320

[7] OMOTEHINWA, T. Examining the developments in scheduling algorithms research: A bibliometric approach. *Heliyon* [online]. 2022, **8**(5), e09510 [accessed 2025-09-12]. ISSN 2405-8440. Available from: https://doi.org/10.1016/j.heliyon.2022.e09510

[8] SUN, Y., DUAN, S., YEN, J., XIONG, W., JIN, M., WANG, Y. Cluster Hopper: Cross-region order dispatching optimization for ride-hailing drivers. *Expert Systems with Applications* [online]. 2025, **289**, 127878 [accessed 2025-05-28]. ISSN 0957-4174. Available from: https://doi.org/10.1016/j.eswa.2025.127878

[9] SHOMAN, W., YEH, S., SPREI, F., KOHLER, J., PLOTZ, P., TODOROV, Y., RANTALA, S., SPETH, D. A review of big data in road freight transport modeling: gaps and potentials. *Data Science for Transportation*, [online]. 2023, **5**(1), 2 [accessed 2025-08-14]. ISSN 2948-135X. Available from: https://doi.org/10.1007/s42421-023-00065-y

[10] BRANKE, J., MATTFELD, D. Anticipation and flexibility in dynamic scheduling. *International Journal of Production Research* [online]. 2005, **43**(15), p. 3103-3129 [accessed 2024-06-16]. ISSN 0020-7543, eISSN 1366-588X. Available from: https://doi.org/10.1080/00207540500077140

[11] WEN, X., SUN, X., SUN, Y., YUE, X. Airline crew scheduling: Models and algorithms. *Transportation Research Part E: Logistics and Transportation Review* [online]. 2021, **149**, 102304 [accessed 2025-12-25]. ISSN 1366-5545, eISSN 1878-5794. Available from: https://doi.org/10.1016/j.tre.2021.102304

[12] SARTORI, C., SMET, P., VANDEN BERGHE, G. Scheduling truck drivers with interdependent routes under European Union regulations. *European Journal of Operational Research* [online]. 2022, **298**(1), p. 76-88 [accessed 2025-12-10]. ISSN 0377-2217. Available from: https://doi.org/10.1016/j.ejor.2021.06.019

[13] WANG, B., HAN, Y., WANG, S., TIAN, D., CAI, M., LIU, M., WANG, L. A review of intelligent connected vehicle cooperative driving development. *Mathematics* [online]. 2022, **10**(19), 3635 [accessed 2025-05-16]. ISSN 2227-7390. Available from: https://doi.org/10.3390/math10193635

[14] FLAMINI, M., NICOSIA, G. A generalized disjunctive graph model for a complex production problem. In: 2023 International Conference on Industry Sciences and Computer Science Innovation: proceedings. Vol. 237. Procedia Computer Science. 2024. ISSN 1877-0509, p. 289-296.

[15] VAKA, D. From complexity to simplicity: AI's route optimization in supply chain management. *Journal of Artificial Intelligence, Machine Learning and Data Science* [online]. 2024, **2**(1), p. 386-389 [accessed 2025-06-20]. ISSN 2583-9888. Available from: https://doi.org/10.51219/JAIMLD/dilip-kumar-vaka/100

[16] MAHDI, M., HOSNY, KHALID M., ELHENAWY, I. Scalable clustering algorithms for big data: a review. *IEEE Access* [online]. 2021, **9**, p. 80015-80027 [accessed 2026-03-12]. ISSN 2169-3536, eISSN 2169-3536. Available from: https://doi.org/10.1109/ACCESS.2021.3084057

[17] KLUMPP, M., SEVERIN, B., LECHTE, H., MENCK, J. H. D., KEIL, M., STRAUB, S. M., HESENIUS, M. Driving big data-integration and synchronization of data sources for artificial intelligence applications with the example of truck driver work stress and strain analysis. In: International Journal of Technology and Human Interaction Conference: ICIS 2022: proceedings. Vol. 20, Iss. 1. 2024. ISBN 978-171389361-5, p. 125-130.

[18] IKEGWU, A., NWEKE, H., ANIKWE, C. ALO, U., OKONKWO, O. Big data analytics for data-driven industry: a review of data sources, tools, challenges, solutions, and research directions. *Cluster Computing* [online]. 2022, **25**(5), p. 3343-3387 [accessed 2025-07-25]. ISSN 1386-7857. Available from: https://doi.org/10.1007/s10586-022-03568-5

[19] ABDALLA, H. A brief survey on big data: technologies, terminologies and data-intensive applications. *Journal of Big Data* [online]. 2022, **9**(1), 107 [accessed 2024-05-19]. ISSN 2196-1115, Available from: https://doi.org/10.1186/s40537-022-00659-3

[20] TALMALE, G., SHRAWANKAR, U. Tasks scheduling using dynamic cluster-based hierarchical real-time scheduler for autonomous car. *Ambient Science* [online]. 2021, **8**(2), p. 01-06 [accessed 2025-04-16]. ISSN 2348-5191, eISSN 2348-8980. Available from: https://doi.org/10.21276/ambi.2021.08.2.ga01

[21] AL-JUMAILI, A., MUNIYANDI, R., HASAN, M., PAW, J., SINGH, M. Big data analytics using cloud computing based frameworks for power management systems: status, constraints, and future recommendations. *Sensors* [online]. 2023, **23**(6), 2952 [accessed 2025-04-24]. eISSN 1424-8220. Available from: https://doi.org/10.3390/s23062952

[22] NOVAK, A., SUCHA, P., NOVOTNY, M., STEC, R., HANZALEK, Z. Scheduling jobs with normally distributed processing times on parallel machines. *European Journal of Operational Research* [online]. 2022, **297**(2), p. 422-441 [accessed 2025-12-19]. ISSN 0377-2217. Available from: https://doi.org/10.1016/j.ejor.2021.05.011

[23] LI, N., SHENG, H., WANG, P., JIA, Y., YANG, Z., JIN, Z. Modeling categorized truck arrivals at ports: big data for traffic prediction. *IEEE Transactions on Intelligent Transportation Systems* [online]. 2022, **24**(3), p. 2772-2788 [accessed 2025-10-08]. ISSN 1524-9050. Available from: https://doi.org/10.1109/TITS.2022.3219882

[24] TALAAT, A., IIJIMA, J., GHEITH, M., ELTAWIL, A. An integrated k-means clustering and bi-objective optimization approach for external trucks scheduling in container terminals. In: *Industrial Engineering and Applications. Vol. 35. Advances in Transdisciplinary Engineering*. Phuket: IOS Press, 2023. ISBN 978-164368408-6, p. 805-814.

[25] KHOMYN, N., OLISKEVYCH, M., TARAN, I., MURATBEKOVA, G. Algorithm for scheduling drivers on intercity road routes: case study of the shift method. *National Mining University. Scientific Bulletin* [online]. 2025, **4**, p. 185-194 [accessed 2025-12-06]. ISSN 2071-2227, eISSN 2223-2362. Available from: https://doi.org/10.33271/nvngu/2025-4/185

[26] Cargo transportation in Ukraine and Europe - Trans-Service-1 [online] [accessed 2026-01-16]. Available from: https://www.trans-service-1.com.ua/en/home/


ŽILINSKÁ UNIVERZITA
V ŽILINE


BiotechUSA
SOM VEDEC
NOC


Strojnícka fakulta
BA BB


E 499062

OPTIMIZING COMBUSTION PROCESS: THE IMPACT OF FLAME ZONE AIR SUPPLY ON EMISSIONS AND PERFORMANCE IN PELLET BOILER

Alexander Backa[1,*], Nikola Čajová Kantová[1], Peter Hrabovský[1], Pavol Belány[1], Róbert Cibula[2], Sławomir Sładek[3]

[1]University of Zilina, Research Centre, Zilina, Slovakia
[2]University of Zilina, Faculty of Mechanical Engineering, Department of Power Engineering, Zilina, Slovakia
[3]Silesian University of Technology, Department of Thermal Technology, Gliwice, Poland

*E-mail of corresponding author: alexander.backa@uniza.sk

Alexander Backa 0000-0003-0911-6678,
Peter Hrabovsky 0000-0002-8425-6657,
Robert Cibula 0000-0003-1107-4147,
Nikola Cajova Kantova 0000-0002-7529-036X,
Pavol Belany 0000-0002-8313-9432,
Sławomir Sładek 0000-0003-2994-3734

Resume

Biomass combustion is a widely used renewable option for a small-scale heat and power, but incomplete burnout and pollutant formation remain challenges in boilers without optimized air staging. In this study, is investigated how controlled transport of air into the flame zone, implemented with an auxiliary tertiary system, affects performance and emissions in a bottom-fed pellet boiler. Tests were performed at constant fuel feed and primary/secondary airflow, with tertiary air varied between 0 and 15.8 m^3/h. An airflow of about 8.9 m^3/h proved optimal, giving the highest thermal output, a more uniform temperature distribution, and a nearly twentyfold reduction in CO emissions normalized to 10% O_2. NOx rose only moderately (by approximately 60 mg/m^3). The findings show that targeted air transport and staging into the flame zone can substantially improve combustion completeness and boiler efficiency.

Article info

Received 19 September 2025
Accepted 17 December 2025
Online 28 January 2026

Keywords:

combustion
pellet boiler
air supply
biomass
emission reduction

Available online: https://doi.org/10.26552/com.C.2026.016

ISSN 1335-4205 (print version)
ISSN 2585-7878 (online version)

1 Introduction

The biomass remains the sole renewable carbon-based fuel, and among thermochemical conversion technologies, combustion stands out as a dependable method for producing both heat and electricity. Over the past two decades, solid biofuels, particularly pellets, have emerged as one of the fastest-growing energy sources. However, many combustion systems were originally engineered for coal or fossil fuels and thus often suffer from poor control and incomplete burnout. In contrast, boilers specifically designed for biomass can extract energy more efficiently and lower pollutant emissions [1-2]. The growing focus on energy efficiency and emission reduction across all the sectors of transport and power generation underlines the importance of sustainable fuels such as biomass in the broader energy transition [3-6].

The combustion dynamics of pellet boilers are influenced by numerous variables [7]. Fuel quality characteristics, such as pellet uniformity, moisture content, and composition, significantly affect gaseous emissions and particulate matter (PM) formation. For instance, studies have shown that high moisture content can increase emissions of CO, PAHs, and PM by factors of two to five, compared to drier fuel [8-9]. The fuel type, pre-treatment methods, and geometry also play a role in combustion efficiency and emission profiles [10-12]. Research further indicates that variations in feedstock composition, such as higher bark or agricultural residues, can alter the ash behavior and emission tendencies, while the application of mineral additives may improve fuel quality and stability during combustion [13-15].

Additionally, process dynamics during different combustion stages critically influence the pollutant release. Nussbaumer et al. (2008) observed that nearly half of total PM emissions can occur during the startup phase, which typically comprises only a small fraction of the cycle [16]. Fachinger et al. (2017) noted that both excessively low and high combustion velocities lead

to elevated emission factors. Ignition strategy further impacts outcomes: top-down ignition methods reduce PM emissions by 50-80% relative to conventional bottom ignition [17].

Efficient pellet combustion relies not only on the overall air-to-fuel ratio but on the spatial and temporal distribution of the supplied air, as well [7]. The combustion chamber typically receives air through three distinct streams: primary, secondary, and tertiary. Each of these inlets serves a specific function in the combustion process. The primary air is generally introduced beneath the fuel bed, where it promotes the initial stages of drying and devolatilization. Proper control of this stream is critical, as an insufficient supply can lead to incomplete oxidation of volatile compounds, whereas an excess may lower combustion temperatures and reduce efficiency. The secondary air is directed above the fuel bed into the region where volatile gases are released. Its role is to ensure thorough oxidation of these gases, thus minimizing unburned hydrocarbons and carbon monoxide. Optimizing secondary air distribution enhances flame stability, promotes complete burnout, and contributes to lower emission factors. The tertiary air, more commonly applied in larger and high-output boilers, is injected further downstream into the flame path. This airflow supports the final stage of oxidation, preventing the escape of unburned gases and fine particulates. Moreover, the strategic use of tertiary air helps maintain cleaner surfaces in the combustion chamber and the flue gas path by reducing soot deposition [18]. Complementary measures, such as compact cyclones or other dust separators, are often applied downstream to further reduce fine particle emissions, supporting overall system efficiency and compliance with emission limits [19].

Recent investigations have demonstrated that the redistribution of combustion air across these stages can substantially alter both emission profiles and thermal efficiency. Studies by Regueiro et al. showed that inadequate staging, where only primary air is used, results in particulate concentrations exceeding 360 mg/Nm^3 at 6% O_2 [20]. In contrast, staged air injection with appropriate secondary and tertiary airflows reduces particulate levels to as low as 15-75 mg/Nm^3 under similar conditions, though it may influence NO_x and CO formation differently. Other research confirms that dynamic control of air staging, adjusting the proportion and injection points during various combustion phases, can further optimize combustion, reducing CO and PM while maintaining high boiler performance [21-23]. These developments strongly indicate that optimizing the air-fuel distribution, particularly the injection location and staging of flame-zone air, provides a promising pathway to enhance combustion completeness, reduce harmful emissions, and improve boiler thermal efficiency. Building on these insights, Backa et al. reported that in automatic boilers with bottom fuel feeding and without direct air supply into the flame region, elevated CO concentrations were observed even in the upper flame layers, whereas NO_x emissions remained relatively constant across the flame profile [24-25].

To address this limitation, an auxiliary tertiary air supply system was developed to introduce the combustion air directly into the flame zone, thereby improving the mixing of CO with O_2 and promoting its oxidation to CO_2.

The objective of the present research therefore was to examine the influence of the flame-zone air injection strategies on emission reduction and combustion performance in small-scale pellet boilers. Specifically, the study aimed to quantify how adjustments in flame-zone air staging affect CO, NO_x, and overall heat output to water, building upon both classical literature and the most recent experimental and numerical findings.

2 Materials and methods

In this section is described the experimental approach used to evaluate the influence of auxiliary air injection into the flame zone on boiler performance and emissions. The tests were carried out at constant fuel feed and constant primary/secondary airflows, while the tertiary airflow was varied in defined steps. In addition to heat output and temperature distribution in the combustion chamber, the main flue-gas components were continuously measured.

2.1 Experimental setup

The experiment was conducted on an automatic pellet-fired boiler with bottom fuel feeding (LOKCA USPOR) with a nominal rated output of 18 kW. However, since the unit represents an older type of appliance, its real achievable capacity was lower; the maximum measured output was approximately 15 kW. This type of combustion device is still relatively common in the regional market of Eastern Europe [26]. The fuel used in this study was spruce wood pellets certified to ENplus A1 quality. The proximate and ultimate analyses of the fuel are summarized in Table 1.

Table 1 *Proximate and ultimate analyses of used wood pellets (*O_2 content was calculated by difference)*

Volatile Matter	Fixed Carbon	Moisture	Ash	
77.13	16.95	5.56	0.36	
Carbon	Hydrogen	Nitrogen	Sulfur	Oxygen*
50.43	6.61	< 0.04	0.12	42.47

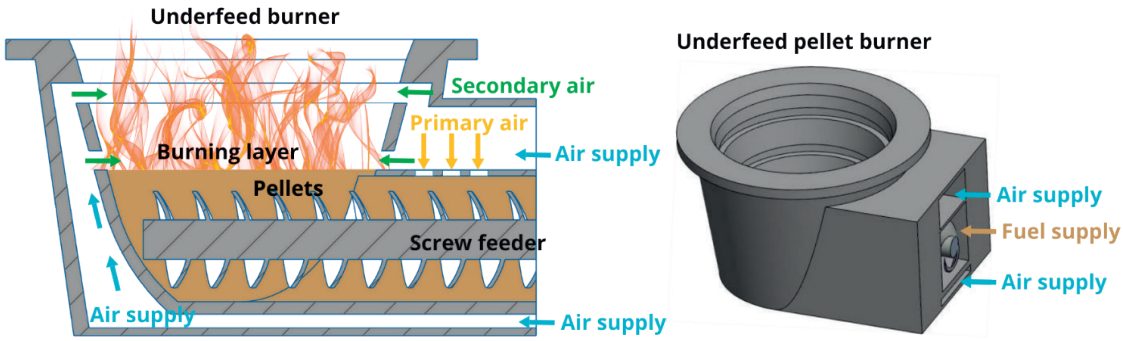

Figure 1 *Method of air supply to the combustion chamber through a bottom-fed burner (before the modification)*

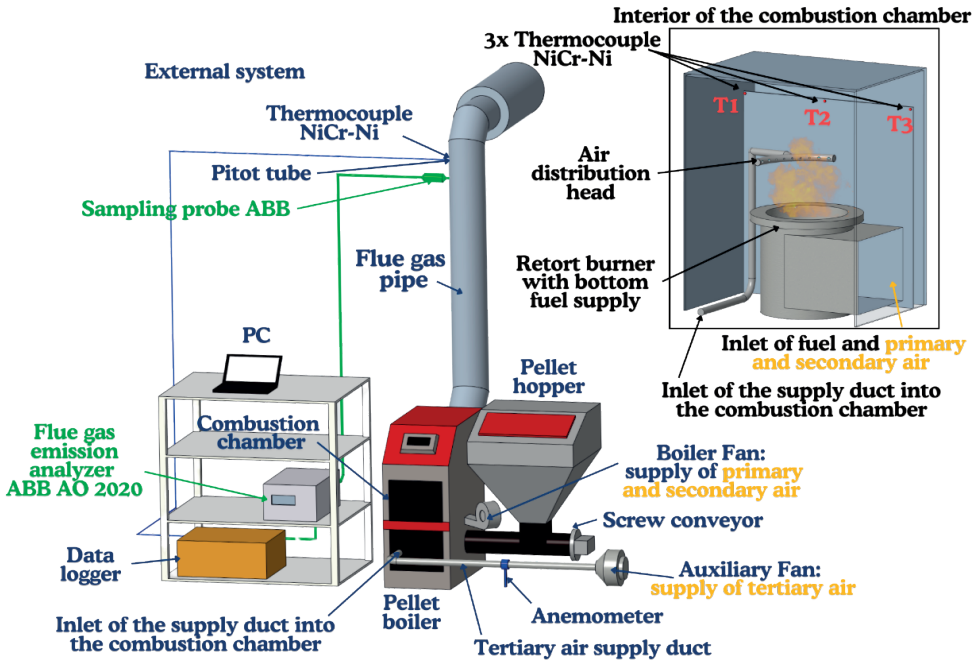

Figure 2 *Experimental setup (external system and combustion chamber after the modification)*

The pellets were automatically transported from the fuel hopper into the retort burner by means of a screw conveyor, operating in 18-second feeding cycles followed by 25-second pauses, resulting in a steady fuel supply of approximately 5.8 kg/h. The boiler fan provided a fixed combined primary/secondary air supply corresponding to a mass flow rate of 63.3 kg/h. The chimney draft was kept constant at 12 ± 2 Pa, in accordance with the STN EN 16510-1 requirements [27]. The draft was monitored with a differential pressure sensor, featuring a maximum measuring span of 0-100 Pa and an accuracy of 0.5%. In addition, the flue gas temperature inside the chimney was continuously recorded using a NiCr-Ni thermocouple.

2.2 The tertiary air supply

Originally, the boiler was equipped only with the combustion fan supplying a combined stream of primary and secondary air (Figure 1).

Following the findings of earlier studies, a system for the delivery of additional tertiary air was implemented. A schematic diagram of the combustion device, including the arrangement of the tertiary air supply, is shown in Figure 2.

Figure 3 shows the real experimental setup used to supply the tertiary air, with detailed views of the air duct and the combustion chamber.

Measurements were carried out under the constant primary and secondary air supply, while varying the tertiary air flow. The air distribution into the flame zone was provided by a manifold with nine orifices, whose diameters increased gradually from the center towards the periphery, with the central opening having a diameter of 6 mm and rising by approximately 5-10% outwards from one orifice to the next (Figure 3). The tertiary air jets were directed perpendicularly against the natural upward flow of the flue gases, to enhance mixing while minimizing the penetration into the fuel bed, which could otherwise cause an undesirable release of particulate matter.

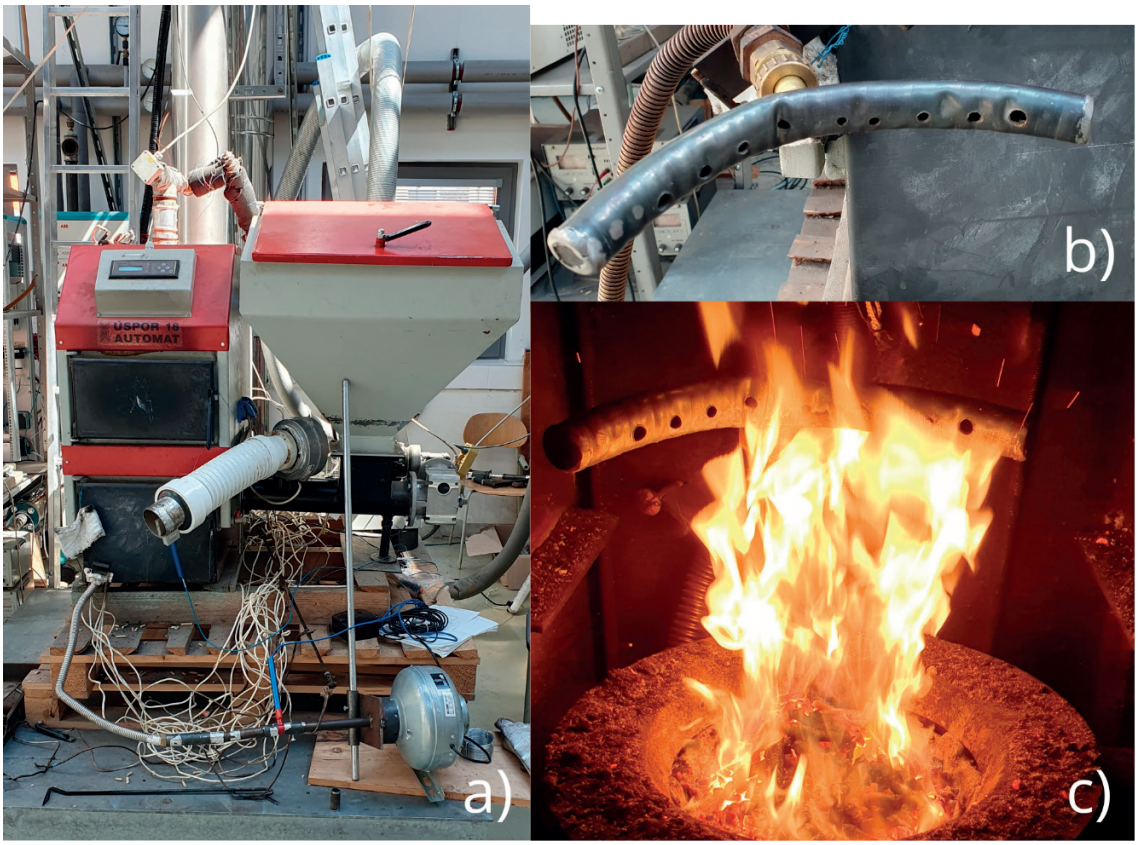

Figure 3 *Real experimental setup for the tertiary air supply: a) overall system, b) air duct detail, and c) combustion chamber view*

The transport of tertiary (auxiliary) air was ensured by an external fan equipped with a frequency converter, allowing adjustment of the rotational speed and thus the delivered air volume. The air was conveyed through a metal pipe with an inner diameter of 17 mm, into which the FVAD 15 MA1 anemometer was installed to measure the flow velocity. Based on the recorded velocity data (v), the volumetric airflow was calculated. The anemometer provided a measurement accuracy of ± 0.5% of the sensor's final value and ± 1.5% of the measured value. From this point, the system continued through a metal pipe section and a ¾″ flexible tube connected to the distribution head. The head consisted of a bent pipe with evenly drilled openings whose diameters gradually increased from the center toward the edge, thereby supplying the main tertiary air stream through the central openings while ensuring a uniform distribution across the flame zone.

A series of tests was performed with the tertiary air flow rates of 0, 3.73, 8.92, 13.4, and 15.82 m^3/h. Each measurement lasted 30 minutes and was started only after the O_2 concentration, thermal output, and temperatures had stabilized. At the top of the combustion chamber, just before the heat exchanger section, three NiCr-Ni thermocouples (T_1-T_3; see Figure 2) recorded temperatures to monitor changes in the distribution of hot gases prior to and after the optimization.

2.3 Emission measurements

The analysis of flue gases was carried out using an ABB AO 2020 system. This device was fitted with the Uras 26 infrared module, which enabled continuous monitoring of carbon monoxide, carbon dioxide, nitrogen oxides, and sulfur oxides, with a measurement uncertainty below 1%. Oxygen concentration was determined with the Magnos 206 module, offering a precision of ± 0.5%.

Concentrations of the monitored components were initially logged in parts per million (ppm). For further evaluation, the values were recalculated to mg/Nm^3 in accordance with STN EN 16510-1 [27], as expressed in Equation (1).

$$CO_{10\%O_2} = CO_{ppm} \cdot d_{CO} \cdot \frac{21 - 10}{21 - O_2}. \quad (1)$$

In Equation (1), $CO_{10}\%O_2$ represents the standardized carbon monoxide concentration at 10% O_2, CO_{ppm} is the measured concentration in ppm, d_{CO} (kg/m^3) is the density of carbon monoxide, and O_2 is the measured oxygen concentration (%). The normalization of emission values to 10% O_2 is consistent with the requirements set by Commission Regulation (EU) 2015/1189, which defines the eco-design criteria for solid fuel boilers of this type [28].

The same conversion procedure was applied for

nitrogen oxides, while the formation of sulfur oxides was negligible since the tested biomass fuel did not contain sufficient sulfur to produce detectable SO_x emissions.

3 Results and discussion

The temperature distribution in the upper part of the combustion chamber before the heat exchanger section revealed that even under the baseline conditions without tertiary air supply the system exhibited significant non-uniformity (Figure 4 and Table 2). The measured temperatures ranged from 587 °C at T1 down to only 463 °C at T3, clearly indicating uneven mixing of hot gases and the presence of colder flue gas in volume.

Such irregularities in temperature stratification are typical of older pellet boiler designs without optimized air staging, where the incomplete mixing and insufficient oxygen supply in the upper flame layers lead to unstable combustion zones [29]. With the addition of tertiary air, these temperature discrepancies were partly alleviated. The most uniform distribution was observed at a tertiary airflow of 8.92 m³/h, where the temperatures across the measurement points converged to 598 °C at T1 and T2, and 549 °C at T3. This more balanced profile reflects improved mixing of unburnt gases with oxygen in the flame zone, thereby enhancing oxidation processes and stabilizing combustion. However, at higher tertiary airflows (13.4 and 15.8 m³/h), the distribution again became less balanced, suggesting that excessive air injection may disturb the flame stability and cool localized regions, thereby weakening combustion intensity. Comparable findings were reported by Kardas et al. (2024), who demonstrated that while separating combustion air into multiple stages reduced the CO emissions and improved flame oxidation, overly large secondary air supply decreased overall combustion efficiency due to excessive dilution and cooling of the reaction zone [30].

The boiler output and gas composition trends further support this interpretation (Figure 5 and Table 3). With increasing tertiary air supply, the flue gas oxygen concentration gradually rose from 11.68% to 13.92%, while CO_2 content decreased from 9.19% to 6.76%, indicating excess air conditions. The maximum water heat output of 11.33 kW was achieved at 8.9 m³/h, indicating that this setting provided the most favorable balance between the fuel feed and oxygen availability.

Further increases in tertiary airflow slightly reduced the boiler heat output, confirming that the excess air no longer contributed to combustion but instead reduced flame temperature and efficiency. These

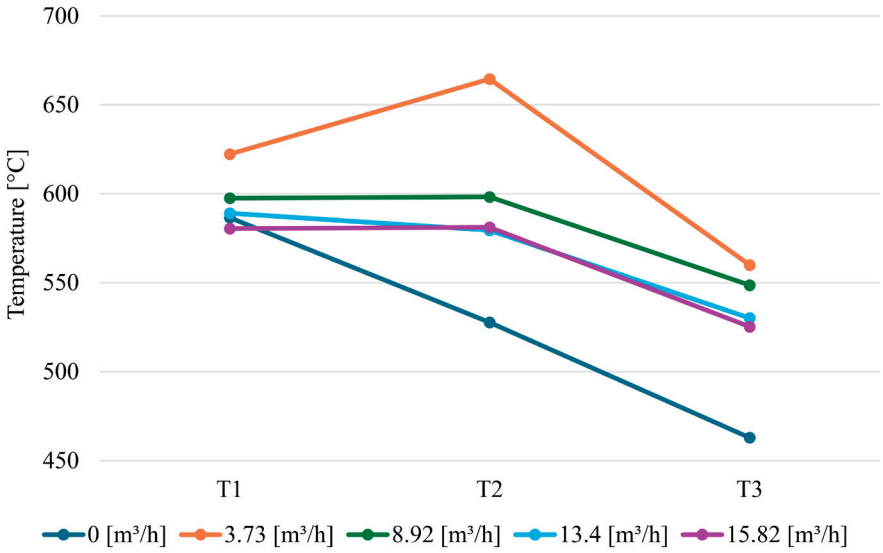

Figure 4 *Temperature distribution in the upper part of the chamber with and without the tertiary air supply*

Table 2 *Effect of tertiary air supply on temperature distribution in the upper part of the chamber*

Tertiary air flow rate	Thermocouple position		
	T1	T2	T3
0 [m³/h]	587	528	463
3.73 [m³/h]	622	665	560
8.92 [m³/h]	598	598	549
13.4 [m³/h]	589	580	530
15.82 [m³/h]	580	581	525

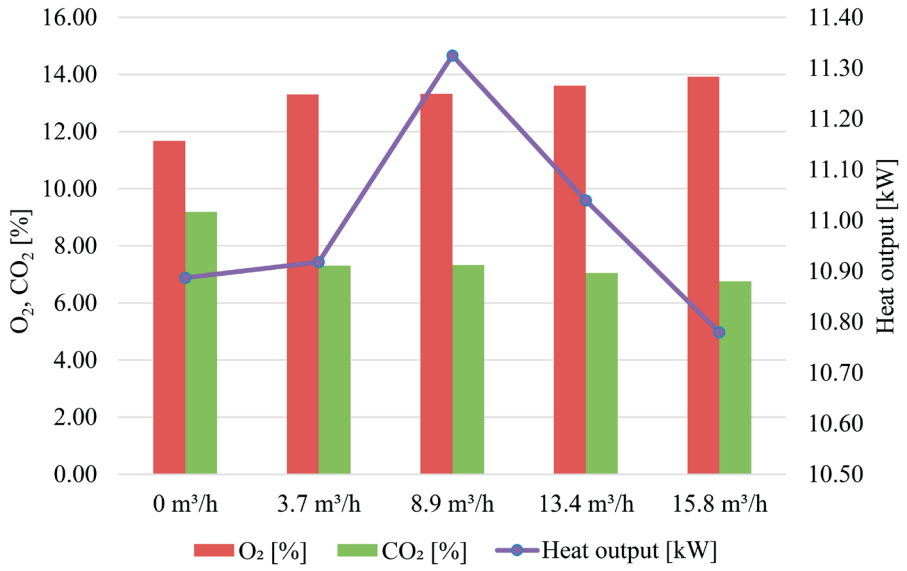

Figure 5 *O_2, CO_2 and boiler heat output at different tertiary air flow rates*

Table 3 *Measured values of O_2, CO_2, and boiler heat output for different tertiary air flow settings*

Parameter	Tertiary air flow rate				
	0 m³/h	3.7 m³/h	8.9 m³/h	13.4 m³/h	15.8 m³/h
O_2 [%]	11.68	13.30	13.32	13.61	13.92
CO_2 [%]	9.19	7.31	7.33	7.05	6.76
Heat output [kW]	10.89	10.92	11.33	11.04	10.78

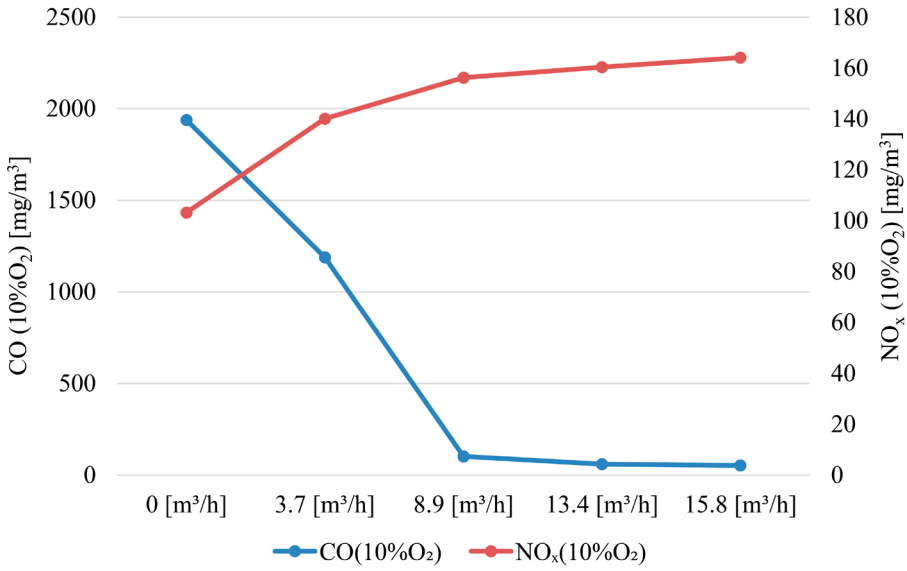

Figure 6 *The CO and NO_x levels (normalized to 10% O_2) at different tertiary air flow rates*

Table 4 *CO and NO_x concentrations (normalized to 10% O_2) at various tertiary air flow rates*

Parameter	Tertiary air flow rate				
	0 m³/h	3.7 m³/h	8.9 m³/h	13.4 m³/h	15.8 m³/h
CO(10%O_2)	1939	1189	103	59	53
NO_x(10%O_2)	103	140	156	160	164

results demonstrate that in boilers without the direct flame-zone air supply adjusting only the primary and secondary airflows is insufficient to achieve comparable thermal performance or to reduce CO to low levels, thus highlighting the critical role of targeted tertiary air [24].

The effect of tertiary airflow on emissions was the most striking for carbon monoxide (Figure 6 and Table 4).

At baseline, CO concentrations normalized to 10% O_2 reached 1939 mg/m^3, indicating highly incomplete combustion. With progressive addition of tertiary air, the CO levels decreased sharply, dropping to 1189 mg/m^3 at 3.7 m^3/h and reaching only 103 mg/m^3 at 8.9 m^3/h, which corresponds to nearly a twentyfold reduction compared to the zero-air case. Further increases to 13.4 and 15.8 m^3/h yielded only marginal CO decreases (59 and 53 mg/m^3, respectively), while the boiler output has declined. This strong reduction demonstrates that targeted air staging is highly effective in promoting the oxidation of CO into CO_2, thereby completing the combustion process. Comparable reductions have been documented in earlier staged-air investigations, such as Zandeckis et al. (2013), [29] and Ciupek et al. (2024) [31], who also observed substantial decreases in CO when optimizing staged or graded airflow supply in pellet boilers. At the optimal setting of 8.9 m^3/h, the boiler also achieved its highest efficiency, improving by about 2% compared to baseline. It should be noted that the optimum tertiary-air setting reported here is specific to the tested fuel and the baseline primary/secondary air configuration; changes in the fuel type/moisture or in the primary/secondary air settings may shift this optimum.

While this condition minimized the CO emissions, NO_x normalized to 10% O_2 rose moderately, from 103 mg/m^3 without tertiary air to 164 mg/m^3 at the highest airflow, with an increase of approximately 60 mg/m^3 relative to the optimum. This effect is due to enhanced oxygen availability, which promote NO_x formation [32-33]. Although this trend is consistent with the results of Ciupek et al. (2024), who reported that air gradation tends to increase NO_x levels even as CO and unburned hydrocarbons decrease, the absolute growth observed in the present study is moderate compared to the dramatic improvements in CO oxidation [31].

For comparison, Backa et al. (2025) reported that under similar fuel supply rates, but without the application of tertiary air, adjustments limited to the primary and secondary airflow from the main fan were insufficient to achieve comparably low CO emissions or equivalent thermal performance [25].

4 Conclusion

Overall, the results indicate that a tertiary airflow of approximately 8.9 m^3/h constitutes the optimal operating condition for the tested pellet boiler. At this setting, the system achieved the most homogeneous temperature distribution, the highest measured thermal output, and a drastic reduction in CO emissions, while the increase in NO_x remained moderate. It should be noted, however, that the optimal value of tertiary airflow is linked to the concurrent settings of the primary and secondary air supply, as well as to the fuel feed rate; adjustments in these parameters would necessitate a corresponding modification of the tertiary air delivery. Nevertheless, the results clearly demonstrate the beneficial impact of supplying air directly into the flame zone, leading to a substantial reduction of emissions. These findings align with the broader literature, which emphasizes that the staged air strategies, particularly the introduction of additional air directly into the flame zone, represent one of the most effective methods to enhance combustion completeness, improve boiler efficiency, and reduce harmful emissions in small-scale biomass boilers [34-35].

When the tertiary air was applied at approximately 9 m^3/h, a slight improvement in efficiency (approximately 2%) was observed. More importantly, the CO emissions normalized to 10% O_2 decreased almost twentyfold compared to operation without the tertiary air at the same setting. On the other hand, NO_x emissions at 10% O_2 increased moderately by about 60 mg/m^3.

Acknowledgements

This publication has been produced with the support of VEGA No. 1/0150/22: Energy utilization of produced waste in connection with the COVID-19 pandemic through pellets as an alternative fuel and VEGA No. 1/0311/26: Autonomous control of the combustion process in small heat sources using artificial intelligence.

Conflicts of interest

The authors declare that they have no known competing financial interests or personal relationships that could have appeared to influence the work reported in this paper.

References

[1] JOHANSSON, L. S., LECKNER, B., GUSTAVSSON, L., COOPER, D., TULLIN, C., POTTER, A. Emission characteristics of modern and old-type residential boilers fired with wood logs and wood pellets. *Atmospheric Environment* [online]. 2004, **38**(25), p. 4183-4195. ISSN 1352-2310, eISSN 1878-2442. Available from: https://doi.org/10.1016/J.ATMOSENV.2004.04.020

[2] VAN LOO, S., KOPPEJAN, J. *The handbook of biomass combustion and cofiring*. London: Earthscan Publications Ltd., 2008. ISBN 978-1-84407-249-1.
[3] KUBAS, J., BALLAY, M., RISTVEJ, J., ZABOVSKA, K. Empirical measurement of electromobility efficiency in the environment of the European Union. *Communications - Scientific Letters of the University of Zilina* [online]. 2022, **24**(3), p. A123-A132. ISSN 1335-4205, eISSN 2585-7878. Available from: https://doi.org/10.26552/COM.C.2022.3.A123-A132
[4] ORMAN, L. J., MAJEWSKI, G., RADEK, N., PIETRASZEK, J. Analysis of thermal comfort in intelligent and traditional buildings. *Energies* [online]. 2022, **15**(18), 6522. eISSN 1996-1073. Available from: https://doi.org/10.3390/en15186522
[5] LATOSINSKA, J., GAWDZIK, J., HONUS, S., ORMAN, L. J., RADEK, N. Waste for building material production as a method of reducing environmental load and energy recovery. *Frontiers in Energy Research* [online]. 2023, **11**, 1279337. eISSN 2296-598X. Available from: https://doi.org/10.3389/fenrg.2023.1279337
[6] MAJEWSKI, G., ORMAN, L. J., TELEJKO, M., RADEK, N., PIETRASZEK, J., DUDEK, A. Assessment of thermal comfort in the intelligent buildings in view of providing high quality indoor environment. *Energies* [online]. 2020, **13**(8), 1973. eISSN 1996-1073. Available from: https://doi.org/10.3390/en13081973
[7] RIMAR, M., KIZEK, J., KULIKOV, A., FEDAK, M. Study of selected burner parameters on the gas-air mixture combustion. *MM Science Journal* [online]. 2022, **2022**(5), p. 6251-6256. ISSN 1803-1269, eISSN 1803-0476. Available from: https://doi.org/10.17973/MMSJ.2022_12_2022158
[8] PEDRETTI, F. E., TOSCANO, G., DUCA, D., PIZZI, A., RIVA, G. Effects of the quality of the biomass on combustion emissions of stoves and small boilers. In: International Conference Ragusa SHWA2010 - Work Safety and Risk Prevention in Agro-food and Forest Systems: proceedings. 2010. ISSN 2532-103X, p. 585-591.
[9] BIGNAL, K. L., LANGRIDGE, S., ZHOU, J. L. Release of polycyclic aromatic hydrocarbons, carbon monoxide and particulate matter from biomass combustion in a wood-fired boiler under varying boiler conditions. *Atmospheric Environment* [online]. 2008, **42**(39), p. 8863-8871. ISSN 1352-2310, eISSN 1878-2442. Available from: https://doi.org/10.1016/J.ATMOSENV.2008.09.013
[10] KLEMENT, I., VILKOVSKA, T., UHRIN, M., BARANSKI, J., KONOPKA, A. Impact of high temperature drying process on beech wood containing tension wood. *Open Engineering* [online]. 2019, **9**(1), p. 428-433. eISSN 2391-5439. Available from: https://doi.org/10.1515/ENG-2019-0047
[11] HORAK, J., LACIOK, V., KRPEC, K., HOPAN, F., DEJ, M., KUBESA, P., RYSAVY, J., MOLCHANOV, O., KUBONOVA, L. Influence of the type and output of domestic hot-water boilers and wood moisture on the production of fine and ultrafine particulate matter. *Atmospheric Environment* [online]. 2020, **229**, 117437. eISSN 1352-2310. Available from: https://doi.org/10.1016/J.ATMOSENV.2020.117437
[12] TRNKA, J., HOLUBCIK, M., CAJOVA KANTOVA, N., JANDACKA, J. Energy performance of a rotary burner using pellets prepared from various alternative biomass residues, *BioResources* [online]. 2021, **16**(4), p. 6737-6749. ISSN 1930-2126. Available from: https://doi.org/10.15376/biores.16.4.6737-6749
[13] JANDACKA, J., HOLUBCIK, M., PAPUCIK, S., NOSEK, R. Combustion of pellets from wheat straw. *Acta Montanistica Slovaca*. 2012, **17**(4), p. 283-289. ISSN 1335-1788.
[14] JANDACKA, J., NOSEK, R., HOLUBCIK, M. Effect of selected additives to properties of wood pellets and their production/Vplyv vybranych aditiv na vlastnosti drevnych peliet a na ich vyrobu (in Slovak). *Acta Facultatis Xylologiae Zvolen*. 2011, **53**(2), p. 85-91. ISSN 1336-3824.
[15] HOLUBCIK, M., JANDACKA, J., PALACKA, M., KANTOVA, N., JACHNIAK, E., PAVLIK, P. The impact of bark content in wood pellets on emission production during combustion in small heat source. *Communications - Scientific Letters of the University of Zilina* [online]. 2017, **19**(2A), p. 94-100. ISSN 1335-4205, eISSN 2585-7878. Available from: https://doi.org/10.26552/COM.C.2017.2A.94-100
[16] NUSSBAUMER, T., DOBERER, A., KLIPPEL, N., BUHLER, R. VOCK, W. Influence of ignition and operation type on particle emissions from residential wood combustion. In: 16th European Biomass Conference and Exhibition: proceedings. 2008.
[17] FACHINGER, F., DREWNICK, F., GIERE, R., BORRMANN, S. How the user can influence particulate emissions from residential wood and pellet stoves: Emission factors for different fuels and burning conditions. *Atmospheric Environment* [online]. 2017, **158**, p. 216-226. eISSN 1352-2310. Available from: https://doi.org/10.1016/J.ATMOSENV.2017.03.027
[18] HOLUBCIK, M., CAJOVA KANTOVA, N., JANDACKA, J., CAJA, A. The performance and emission parameters based on the redistribution of the amount of combustion air of the wood stove. *Processes* [online]. 2022, **10**(8), 1570. eISSN 2227-9717. Available from: https://doi.org/10.3390/PR10081570
[19] KRAVCHENKO, O., BAZHYNOV, O., DIZO, J., HAIEK, Y., BLATNICKY, M. Cleaning dusty air flow with a rotary cyclone from dispersed particles. *Communications - Scientific Letters of the University of Zilina* [online]. 2025, **27**(1), p. B21-B29. ISSN 1335-4205, eISSN 2585-7878. Available from: https://doi.org/10.26552/COM.C.2025.004

[20] REGUEIRO, A., PATINO, D., PORTEIRO, J., GRANADA, E., MIGUEZ, J. L. Effect of air staging ratios on the burning rate and emissions in an underfeed fixed-bed biomass combustor. *Energies* [online]. 2016, **9**(11), 940. eISSN 1996-1073. Available from: https://doi.org/10.3390/EN9110940

[21] KHODAEI, H., GUZZOMI, F., PATINO, D., RASHIDIAN, B., YEOH, G. H. Air staging strategies in biomass combustion-gaseous and particulate emission reduction potentials. *Fuel Processing Technology* [online]. 2017, **157**, p. 29-41. eISSN 0378-3820. Available from: https://doi.org/10.1016/J.FUPROC.2016.11.007

[22] CARROLL, J. P., FINNAN, J. M., BIEDERMANN, F., BRUNNER, T., OBERNBERGER, I. Air staging to reduce emissions from energy crop combustion in small scale applications. *Fuel* [online]. 2015, **155**, p. 37-43. ISSN 0016-2361, eISSN 1873-7153. Available from: https://doi.org/10.1016/J.FUEL.2015.04.008

[23] SHEN, G., XUE, M., WEI, S., CHEN, Y., ZHAO, Q., LI, B., WU, H., TAO, S. Influence of fuel moisture, charge size, feeding rate and air ventilation conditions on the emissions of PM, OC, EC, parent PAHs, and their derivatives from residential wood combustion. *Journal of Environmental Sciences* [online]. 2013, **25**(9), p. 1808-1816. ISSN 1001-0742, eISSN 1878-7320. Available from: https://doi.org/10.1016/S1001-0742(12)60258-7

[24] BACKA, A., NOSEK, R., CAJOVA KANTOVA, N., SLADEK, S. Spatial distribution of emissions, temperatures, and particulate matter in a combustion zone of a pellet boiler. *Case Studies in Thermal Engineering* [online]. 2025; **73**, 106631. eISSN 2214-157X. Available from: https://doi.org/10.1016/J.CSITE.2025.106631

[25] BACKA, A., CAJOVA KANTOVA, N., NOSEK, R., PATSCH, M. Evaluating the combustion of various biomass pellets in a small heat source with underfeed pellet burner: heat output, gas emission and ash melting behavior. *Journal of the Energy Institute* [online]. 2025, **118**, 101936. ISSN 1743-9671, eISSN 1746-0220. Available from: https://doi.org/10.1016/J.JOEI.2024.101936

[26] FLACH, B., BOLLA, S. Wood pellets annual. Washington, DC: USA: U.S. Department of Agriculture, 2024.

[27] STN EN 16510-1. Residential solid fuel burning appliances - part 1: general requirements and test methods. 2023.

[28] Commission Regulation (EU) 2015/1189 of 28 April 2015 implementing Directive 2009/125/EC of the European Parliament and of the Council with regard to ecodesign requirements for solid fuel boilers. 2015.

[29] ZANDECKIS, A., KIRSANOVS, V., DZIKEVICS, M., BLUMBERGA, D. Experimental study on the optimisation of staged air supply in the retort pellet burner. *Agronomy Research*. 2013, **11**(2), p. 381-390. ISSN 1406-894X.

[30] KARDAS, D., WANTULA, M., PIETER, S., KAZIMIERSKI, P. Effect of separating air into primary and secondary in an integrated burner housing on biomass combustion. *Energies* [online]. 2024, **17**(18), 4648. eISSN 1996-1073. Available from: https://doi.org/10.3390/EN17184648

[31] CIUPEK, B., NADOLNY, Z. Emission of harmful substances from the combustion of wood pellets in a low-temperature burner with air gradation: research and analysis of a technical problem. *Energies* [online]. 2024, **17**(13), 3087. eISSN 1996-1073. Available from: https://doi.org/10.3390/EN17133087

[32] LUKAC, L., KIZEK, J., JABLONSKY, G., KARAKASH, Y. Defining the mathematical dependencies of NOx and CO emission generation after biomass combustion in low-power boiler. *Civil and Environmental Engineering Reports* [online]. 2019, **29**(3), p. 153-163. ISSN 2080-5187, eISSN 2450-8594. Available from: https://doi.org/10.2478/ceer-2019-0031

[33] LUKAC, L., RIMAR, M., VARINY, M., KIZEK, J., LUKAC, P., JABLONSKY, G., JANOSOVSKY, J., FEDAK, M. Experimental investigation of primary de-NOx methods application effects on NOx and CO emissions from a small-scale furnace. *Processes* [online]. 2020, **8**(8), 940. eISSN 2227-9717. Available from: https://doi.org/10.3390/pr8080940

[34] WANG, Z., YANG, X. NOx Formation mechanism and emission prediction in turbulent combustion: a review. *Applied Sciences* [online]. 2024, **14**(14), 6104. eISSN 2076-3417. Available from: https://doi.org/10.3390/APP14146104

[35] BELOHRADSKY, P., SKRYJA, P., HUDAK, P. Experimental study of oxygen-enhanced combustion on NOx emission, in-flame temperatures and heat flux distribution. *Chemical Engineering Transactions* [online]. 2014, **39**, p. 787-792. ISBN 978-88-95608-30-3, ISSN 2283-9216. Available from: https://doi.org/10.3303/CET1439132

DEVELOPMENT OF A FACTOR ANALYSIS MODEL FOR ASSESSING THE TECHNICAL READINESS OF THE RAILWAY ROLLING STOCK

Razım Bayramov[1], Ilham Huseynov[1], Israil Elyazov[2,*], Shamil Heydarov[1]

[1]Department of Transport Logistics and the Traffic of Safety, Azerbaijan Technical University, Baku, Azerbaijan
[2]Department of Transport and Logistics, Azerbaijan University of Architecture and Construction, Baku, Azerbaijan

*E-mail of corresponding author: elyazov1962@gmail.com

Razim Bayramov 0009-0005-8023-2091,
Israil Elyazov 0000-0002-7690-9996,
Ilham Huseynov 0000-0001-8294-8521,
Shamil Heydarov 0009-0001-8408-9000

Resume

In this study was investigated the Technical Readiness Coefficient (TRC) of railway rolling stock and associated technical systems. The primary objective was to identify and analyze the key factors influencing TRC and to develop a structured methodology for the factor analysis of railway technical readiness. The research methodology includes the selection of principal determinants, construction of a descriptive analytical model, processing of empirical operational data, and application of regression and correlation analyses. Empirical and theoretical approaches were employed, using statistical data, maintenance schedules, normative tables, and computational tools. Findings can be used for monitoring the TRC, optimizing maintenance and modernization, improving operational efficiency, and supporting evidence-based management decisions. The methodology also provides a framework for evaluating the future railway systems and ensuring continuous monitoring of technical performance under operational conditions.

Article info

Received 21 November 2025
Accepted 9 March 2026
Online 20 March 2026

Keywords:

factor analysis
technical readiness
technical diagnostics
operation
maintenance
rolling stock

Available online: https://doi.org/10.26552/com.C.2026.019

ISSN 1335-4205 (print version)
ISSN 2585-7878 (online version)

1 Introduction

The operation of railways is evaluated through the key technical and economic indicators that reflect system efficiency and reliability. The railway transport, with its high productivity, operational efficiency, and relatively low costs, plays a crucial role in the sustainable organization of freight and passenger transportation. To assess the transportation process, fundamental technical and economic indicators are applied, such as freight volume, passenger turnover, locomotive and wagon utilization, traffic intensity, profitability, labor productivity, transportation costs, asset return, and overall efficiency. These parameters determine not only the operational effectiveness of railway enterprises but serve as a basis for quantitative and qualitative performance analysis, as well.

The complexity of railway systems arises from the strong interdependence between the infrastructure, rolling stock, and operational indicators [1-2]. Among the metrics used to evaluate the railway performance, the Technical readiness coefficient (TRC) holds particular significance as it characterizes the state of readiness of the rolling stock, infrastructure elements, and other technical facilities for uninterrupted operation.

However, despite its recognized importance, existing approaches to TRC evaluation remain largely descriptive and lack analytical integration between technical, operational, and maintenance factors. Most traditional methods fail to incorporate predictive diagnostics, reliability modelling, and data-driven assessment consistent with modern international standards for predictive maintenance. Consequently, there is still no comprehensive factor-based analytical model that quantitatively links the technical readiness of railway assets with measurable operational outcomes.

In this study is addressed this gap by developing a heuristic and statistically verified methodology for TRC evaluation that integrates factor analysis, regression, and correlation modelling. The proposed approach aims to enhance the accuracy and predictive capability of the TRC assessment, contributing to the modernization

and digitalization of railway maintenance management systems. Therefore, the key research problem addressed in this study is the absence of a structured analytical methodology capable of identifying and quantitatively evaluating the influence of operational and maintenance factors on the Technical Readiness Coefficient of railway rolling stock. Without such an approach, the TRC remains primarily a descriptive indicator and provides limited support for predictive maintenance planning and evidence-based operational decision-making.

2 Literature analysis and statement of the problem

Factor analysis has been extensively utilized in railway transport and applied across various research areas.

In study [3], a factor analysis of railway passenger transport demand in Eastern China was conducted. It was shown that economic development, population density, and intercity distance are the main factors influencing passenger demand. However, the full integration of variable economic and social factors into demand forecasting has not yet been achieved. This is due to the limited statistical data and the complexity of analyzing regional differences. The combination of a multivariate model and forecasting methods is recommended. A similar approach was used in [4], but energy consumption and coordination of carrying capacity were also taken into account. Conducting research to more accurately predict the TRC indicators and improve the efficiency of passenger transport services is relevant.

In this study [4], a factor analysis of railway carrying capacity optimization, considering energy consumption, was carried out. It was shown that balancing the train density and load distribution can reduce energy consumption. However, real-time coordination of carrying capacity and energy management issues have not yet been fully resolved. This is due to the existing systems having non-adaptive management mechanisms. The implementation of adaptive planning and optimization algorithms is recommended. A similar approach can be observed in [5], where structural equation models were used to analyze the development factors of freight transport. Developing models to evaluate the impact of the TRC indicators on energy consumption and carrying capacity in real operational conditions is relevant.

The development factors of railway freight transport in Thailand were analyzed in [4], using the structural equation modelling. It was shown that infrastructure quality and operational coordination have a primary impact on freight transport efficiency. However, the full integration of all the factors for continuous optimization of freight transport has not yet been achieved. This is due to limited available data and complex operational conditions. The implementation of integrated management and optimization systems is recommended. A similar approach can be observed in [5], where carrying capacity and energy efficiency models were analyzed. Developing models to assess the impact of TRC indicators on freight transport and their practical application is relevant.

In article [6], a factor analysis of key parameters for effective urban transport infrastructure design in Ethiopia was conducted. It was shown that project effectiveness depends on urban planning, financial support, and technological compatibility. However, adapting the urban transport infrastructure projects to local conditions has not yet been fully ensured. This is due to limited local data and differences in planning standards. Integrated planning models, based on multivariate factor analysis, should be applied. A similar approach was used in [7], where integration of urban and suburban transport was considered. Conducting research to evaluate and optimize TRC under various regional and technical conditions is relevant.

Human factors of railway traffic operators were analyzed in [7]. Operator decision-making directly affects safety and the timely movement of trains. However, systematic approaches to prevent operator errors have not yet been fully implemented. This is due to variability in human behavior and insufficient training systems. The implementation of intelligent systems supporting operator decision-making is recommended. A similar approach was noted in [1], but here the human factors in relation to safety were analyzed more deeply. Conducting research to more accurately assess the impact of technical inspections and operator activity on TRC is relevant.

In [8], the success factors of integrating the railway into urban and suburban transport systems were evaluated. It was shown that integration planning and user convenience are the main success factors. However, the role of technical services and operational coordination in the integration process has not been fully analyzed. This is due to limited data and varying operational conditions. Developing the TRC-based integration models and implementing them in pilot projects is recommended. A similar approach was applied in [6], where the key parameters of urban transport infrastructure were analyzed. Conducting research to optimize railway integration into urban transport considering TRC indicators is relevant.

In [9], was developed a model to measure disparity factors in intercity railway transportation. It was shown that infrastructure, train density, and planning disparities affect transport efficiency. However, a full statistical and operational assessment of the impact of disparity factors on TRC has not yet been conducted. This is due to insufficient data and varying regional conditions. A multivariate and statistical model based on TRC is proposed. A similar approach was observed in [3], but here regional differences were measured

more thoroughly. Applying the TRC indicators to optimize intercity transport and improve forecasting is relevant.

The impact of Azerbaijani railway transport on economic growth was analyzed in [10]. It was shown that freight transport efficiency directly affects national economic indicators. However, the relationship between the economic impact of technical inspections and operational factors with the TRC has not yet been fully explored. This is due to insufficiently detailed statistical data. Developing a model to assess the economic impact of freight transport based on TRC is recommended. A similar approach was observed in [5], where the relationship between the freight transport and economic growth was analyzed. Using the TRC indicators to evaluate and optimize the economic impact of railway services is relevant.

Recent studies highlight a growing integration of predictive and digital technologies into railway maintenance and monitoring systems. According to [11], predictive maintenance in the railway domain relies on the real-time sensor data, machine learning algorithms, and advanced condition monitoring frameworks; however, TRC-based integration is still underdeveloped. Similarly, authors of [12] emphasize the role of AI-powered digitalization and digital twin technologies in improving technical readiness, enabling early fault detection and resource optimization. These studies collectively reveal the emerging research direction towards the dynamic, data-driven TRC modelling and predictive maintenance integration.

In a scientific article [13] was examined the impact of the technical level of a locomotive's traction drive on the braking performance of a train. The technical level of a locomotive is maintained during repairs and is characterized by the fleet's technical readiness coefficient.

In scientific papers [14-17] were examined issues related to assessing the technical readiness of railway rolling stock. The primary focus is on the technical readiness coefficient as an integral indicator of the effectiveness of the maintenance and repair system. The main factors influencing its value are analyzed, and mathematical calculation models and methods for improving the level of rolling stock readiness are presented.

The analytical relationship between the level of use of the unit repair method and the technical readiness of the vehicle fleet, using the technical readiness coefficient, was studied in [18].

In [19] was proposed an optimal strategy for the controlling traction equipment, taking into account the criteria of technical and economic efficiency of equipment belonging to different groups, when classifying the operational characteristics of traction vehicles.

In [20] was shown that the use of the coefficient of technical readiness to evaluate the quality of the technical operation of lifting and transportation equipment is more effective. The strategy of technical operation of the repair enterprise is selected directly on the basis of the coefficient of technical readiness.

3 The aim and objectives of the study

The objective of this study was to develop an appropriate approach for conducting the factor analysis of the technical readiness coefficient of railway rolling stock, infrastructure, and other machinery.

To achieve this objective, the following goals were accomplished:

- to identify the key factors and develop a descriptive model;
- to develop the research data model;
- to construct a heuristic mathematical model for factor analysis;
- to implement regression and correlation analysis.

4 Materials and methods of research

The research was carried out using empirical methods (observation, description, comparison, counting, measurement, modelling, etc.) and theoretical methods (analysis, synthesis, induction, deduction, axiomatics, hypothesis and assumption, analogy, etc.). Statistical data, maintenance schedule charts, standard element tables, and computer software were employed in the process. The dataset consisted of empirical operational records collected from Azerbaijan Railways for the year 2025. The sample comprised ten rolling stock units selected within a localized operational context, representing typical service and maintenance conditions. Continuous maintenance monitoring was ensured throughout the observation period. Data processing and statistical analysis were performed using Microsoft Excel and SPSS software.

Although the advanced validation methods, such as cross-validation or residual analysis were not applied due to the limited dataset, the model's adequacy and coefficient stability were evaluated through the comparative statistical consistency checks.

Factor analysis makes it possible to determine which factors exert greater influence on the studied indicator and to what extent they alter it. For conducting the factor analysis, the expression of the technical readiness coefficient (k) is given by Equation (1)

$$k = 1 - \frac{\sum t_{ptn} + \sum t_{pte} + \sum t_{pkt}}{n_{hv} \cdot t_{hd}} \cdot 100\%, \quad (1)$$

where:

$\sum t_{ptn}$ - total normative duration of scheduled maintenance during the month, h,

$\sum t_{pte}$ -total additional duration beyond normative scheduled maintenance during the month, h,

$\sum t_{pkt}$ -total duration of unscheduled maintenance during the reporting period, h,
n_{hv} -number of operational rolling stock units,
t_{hd} - total duration of the reporting period, h.

The negative impacts on the technical readiness coefficient of the railway rolling stock are mainly divided into two factor categories. To better explain the factors affecting the technical readiness coefficient, it is advisable to develop a factor-analysis scheme. This scheme will describe a three-level analytical structure of the technical readiness coefficient. By extending a similar scheme to sub-factors, it will be possible to identify root causes and even reveal hidden factors. By forming a hierarchical factor-analysis model of the technical readiness coefficient of railway rolling stock, from the highest organizational structure down to the smallest units of transport enterprises, it becomes possible to determine the key indicators at various structural levels, visualize them, increase the accountability of responsible parties, and ultimately improve the effectiveness of managerial decisions.

To construct the research data table, the first column should indicate the locomotive units included in the sample, denoted as A1, A2, …, An. These symbols represent individual railway locomotives operating under comparable service conditions within Azerbaijan Railways. The second column presents the actual Technical Readiness Coefficient (TRC), the third column the planned TRC, and the fourth column the number of maintenance events associated with each factor for every locomotive unit. The last column indicates the total number of maintenance events for each locomotive.

To develop the mathematical model of the factor analysis of the technical readiness coefficient (TRC) of railway rolling stock, the "absolute difference" method was applied. Based on Table 1, the deviation of the TRC during the reporting period from its planned value is determined by:

$$\Delta K = K_p - K_f . \tag{2}$$

To determine the value of K_p, the following expression is used:

$$K_p = 1 - \frac{x_1 \cdot t_1 + x_2 \cdot t_2 + \cdots + x_n \cdot t_n}{\sum n_{hv} \cdot t_{hd}}, \tag{3}$$

where:
x_1, x_2, ..., x_n - the number of corresponding types of maintenance operations for each mode of transport during the reporting period, according to the maintenance plan;
t_1, t_2, ... t_n - the standard time allocated for each type of maintenance operation, measured in hours, taken from the normative element tables.

Next, using Equation (3), the influence of each factor on the TRC of railway rolling stock can be determined. In this expression, the impact of each technical failure on the TRC is calculated through the product of the relative frequency and the coefficient deviation. This approach allows the contribution of individual failures to the overall performance to be expressed in percentage terms.

Equation (3) defines the contribution of each factor affecting the TRC and is referred to as the mathematical model of factor analysis. Based on the research data in Table 1, this expression makes it possible to determine the impact of any factor or group of factors on the deviation of the TRC from its planned value, thereby encouraging greater accountability among responsible personnel.

The aim of this study was to identify the factors influencing the deviation of the actual technical readiness coefficient (K_f) from its planned value (K_p) and to evaluate the direction and strength of this influence through regression and correlation analyses. For modelling, the following general linear regression equation is applied:

$$K_f = \beta_0 + \beta_1 \cdot f_{F1} + \beta_2 \cdot f_{F2} + \beta_3 \cdot f_{F3} + \varepsilon , \tag{4}$$

where:
K_f - technical readiness coefficient (dependent variable),
f_{F1}, f_{F2}, f_{F3} - influencing factors (independent variables),
β_0 - intercept,
β_1, β_2, β_3 - regression coefficients,
ε - random error.

The model can also be expressed in the matrix form as:

$$\begin{pmatrix} K_{f1} \\ K_{f2} \\ \vdots \\ K_{fn} \end{pmatrix} = \begin{pmatrix} 1F_{11} & F_{12} & F_{13} \\ 1F_{21} & F_{22} & F_{23} \\ \vdots & \vdots & \vdots \\ 1F_{n1} & F_{n2} & F_{n3} \end{pmatrix} \cdot \begin{pmatrix} \beta_0 \\ \beta_1 \\ \beta_2 \\ \beta_3 \end{pmatrix} + \varepsilon , \tag{5}$$

where:
K_{fi} - TRC of the i-th rolling stock unit,
F_{ij} - value of the j-th factor for the i-th unit.
In short form, the model can be written as

$$Y = X \cdot \beta + \varepsilon . \tag{6}$$

The regression coefficients are estimated using the ordinary least squares (OLS) method, as shown in Equation (7)

$$\beta = (X^T \cdot X)^{-1} \cdot X^T \cdot Y , \tag{7}$$

where:
X-observation matrix (independent variables: factors),
X^T - transpose of X,
$(X^TX)^{-1}$ - inverse matrix,
Y-dependent variable vector (actual TRC).

The correlation matrix is a square table that defines the strength and direction of the statistical relationships among the variables used in the study (e. g., F_1, F_2, F_3). Constructing this matrix makes it possible to determine how variables are related to each other (positively

or negatively, and to what degree). For instance, a strong positive correlation indicates that as one variable increases, the other tends to increase; conversely, a negative correlation implies that an increase in one variable corresponds to a decrease in the other. This analysis also allows testing for multicollinearity among variables in the model.

In this research, two main statistical methods were applied: Pearson correlation analysis and a simple regression model. To determine the strength of the linear relationship between indicators, the Pearson correlation coefficient is employed, defined mathematically in Equation (8)

$$Kf = \frac{\sum_{j=1}^{n}(K_{fj} - K_f)\cdot(F_{ij} - F_i)}{\sqrt{\sum_{j=1}^{n}(K_{fj} - K_f)^2}\cdot\sqrt{\sum_{j=1}^{n}(F_{ij} - F_i)}}, \quad (8)$$

where:
r_{kf} - correlation coefficient between TRC and the i-th factor,
K_{fj} - TRC for the j-th observation,
F_{ij} - value of the i-th factor for the j-th observation,
K_f - mean values of TRC and the factor,
n - total number of observations.

A positive coefficient indicates a direct relationship, while a negative coefficient shows an inverse relationship. When the coefficient is close to zero, the linear statistical relationship between the variables is weak or nonexistent.

5 Results of the factor analysis

An important result of the factor analysis of a railway rolling stock is a detailed study using inductive and deductive methods of the factors influencing the technical availability of railway rolling stock, which allows for the identification and elimination of the root causes of the problem.

In this section are presented the results of the factor analysis, including the identification of the main factors influencing the technical availability of railway rolling stock, the development of descriptive and mathematical models, and regression and correlation analyses to quantitatively assess the impact of these factors.

5.1 Construction of a descriptive model of factors

An important outcome of conducting the factor analysis of railway rolling stock is that the factors influencing the technical readiness coefficient (TRC) are studied in detail through the use of induction and deduction methods, enabling the identification and elimination of root causes of problems.

A hierarchical structure of the Technical Readiness Coefficient (TRC) factor model was developed to illustrate the multi-level relationships between organizational, operational, and technical determinants (Figure 1).

The model illustrates three interrelated levels organizational, operational, and technical showing how

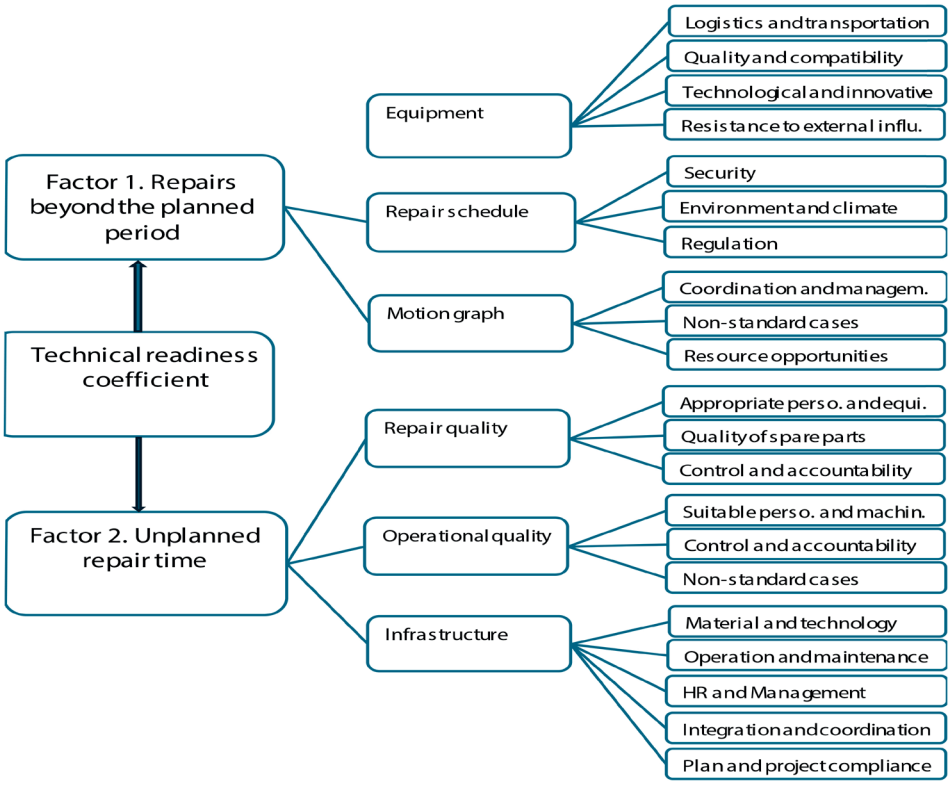

Figure 1 *Hierarchical structure of the technical readiness coefficient (TRC) factor model*

Table 1 *Research data table*

Type of rolling stock	TRC during the reporting period, K_r	Planned TRC, K_p	Difference ΔTRC	Number of unscheduled maintenance events, n			Total, N
				F_1	F_2	F_3	
A1	0.72	0.84	0.12	37	43	25	105
A2	0.84	0.95	0.11	29	23	28	80
A3	0.77	0.91	0.14	23	24	27	74
A4	0.74	0.89	0.15	26	29	29	84
A5	0.75	0.90	0.15	45	35	35	115
A6	0.82	0.92	0.10	36	26	32	94
A7	0.71	0.86	0.15	38	29	16	83
A8	0.69	0.91	0.22	40	25	32	97
A9	0.85	0.90	0.05	42	32	41	115
A10	0.89	0.95	0.06	32	30	35	97
A11	0.79	0.93	0.14	25	40	30	95
A12	0.85	0.93	0.08	31	28	29	88
A13	0.89	0.95	0.16	35	30	35	100
A14	0.88	0.95	0.07	33	15	25	73
A15	0.89	0.94	0.05	30	18	23	71
A16	0.90	0.95	0.05	31	20	25	76

Table 2 *Descriptive model of factor analysis of the technical readiness coefficient developed in Excel*

Type of rolling stock	Actual TRC	Planned TRC	Difference ΔTRC	Factor 1	Factor 2	Factor 3	Total factors	F1 Impact	F2 Impact	F1 Impact
A1	0.72	0.84	0.12	37	43	25	105	4.23	4.91	2.86
A2	0.84	0.95	0.11	29	23	28	80	3.99	3.16	3.85
A3	0.77	0.91	0.14	23	24	27	74	4.35	4.54	5.11
A4	0.74	0.89	0.15	26	29	29	84	4.64	5.18	5.18
A5	0.75	0.90	0.15	45	35	35	115	5.87	4.57	4.57
A6	0.82	0.92	0.1	36	26	32	94	3.83	2.77	3.40
A7	0.71	0.86	0.15	38	29	16	83	6.87	5.24	2.89
A8	0.69	0.91	0.22	40	25	32	97	9.07	5.67	7.26
A9	0.85	0.90	0.05	42	32	41	115	1.83	1.39	1.78
A10	0.89	0.95	0.06	32	30	35	97	1.98	1.86	2.16
A11	0.79	0.93	0.14	25	40	30	95	3.68	5.89	4.42
A12	0.85	0.93	0.08	31	28	29	88	2.82	2.55	2.64
A13	089	0.95	0.16	35	30	35	100	5.60	4.80	5.60
A14	0.88	0.95	0.07	33	15	25	73	3.16	1.44	2.40
A15	0.89	0.94	0.05	30	18	23	71	2.11	1.27	1.62
A16	0.90	0.95	0.05	31	20	25	76	2.04	1.32	1.64

higher-level management and maintenance decisions influence the reliability and readiness of rolling stock.

5.2 Development of the research data table

The research data were formed based on the railway transport indicators of Azerbaijan, and the results are presented in Table 1.

These data serve as the basis for constructing the factor analysis model in Excel, enabling the quantification of each factor's influence on the technical readiness coefficient.

5.3 Building a heuristic mathematical model of factor analysis

The relative impact of each factor on the technical readiness coefficient was determined using the following expression

$$f_n = \left(\frac{n_n}{N_n}\right) \cdot K \cdot 100\%, \quad (9)$$

where:
n_n - number of occurrences of the factor or factor group,
N_n - total number of occurrences of the factor or factor group,
ΔK - is the deviation between the actual and planned values of the TRC.

When these data are applied to the methodology of developing a mathematical model of factor analysis in Excel, that is, when mathematical dependencies are established using Excel tools, the influence coefficient of each factor can be clearly identified, and the results are shown in Table 2. It provides a clear representation of the calculated influence coefficients, facilitating the assessment of the relative impact of each factor on the technical readiness coefficient.

One of the key aspects of analyzing the TRC is the visualization of the obtained data. To facilitate a more comprehensive and faster interpretation of the results, graphical visualization is employed. The chart below illustrates the impact levels of factors across different types of rolling stock (Figure 2)

Figure 2 visually highlights the comparative influence of each factor, enabling a clearer understanding of how different factors affect the technical readiness coefficient across rolling stock types.

5.4 Regression and correlation analyses

Based on the factor analysis presented in Table 2, the regression and correlation analyses were carried out for the factors influencing the TRC. For this purpose, the actual technical readiness coefficient (K_f) is considered as the dependent variable, while the planned technical readiness coefficient (K_p) and the number of unplanned repairs (F_1, F_2, F_3) are evaluated as independent factors. The percentages of the impact of repairs on technical readiness are calculated using Equation (9).

The regression coefficients, presented in Table 3, show that the factors influencing the actual TRC are statistically significant.

Figure 3 illustrates the regression analysis between the technical readiness coefficient (K_f) and the overall impact percentage of selected factors (f_{F1}, f_{F2}, f_{F3}). The data points in the graph represent actual values, while the line depicts the regression trend showing the impact of factors on technical readiness.

The regression results indicate that as the overall impact percentage increases, the TRC decreases. This visually confirms the importance and negative influence of factors on the formation of TRC.

The regression model used in the study was constructed to assess the influence of independent variables on the dependent variable and yielded statistically significant results.

The correlation matrix, presented in Table 4, allows for determining the strength and direction of the linear relationship between variables, which is of significant importance for assessing the interrelationships of the variables to be included in the regression model.

Table 4 presents the correlation matrix of the TRC and its influencing factors. The results show a strong negative correlation between the TRC (K_f) and all the three main factors (F_1-F_3), confirming that the increase in factor intensity corresponds to a decrease in technical

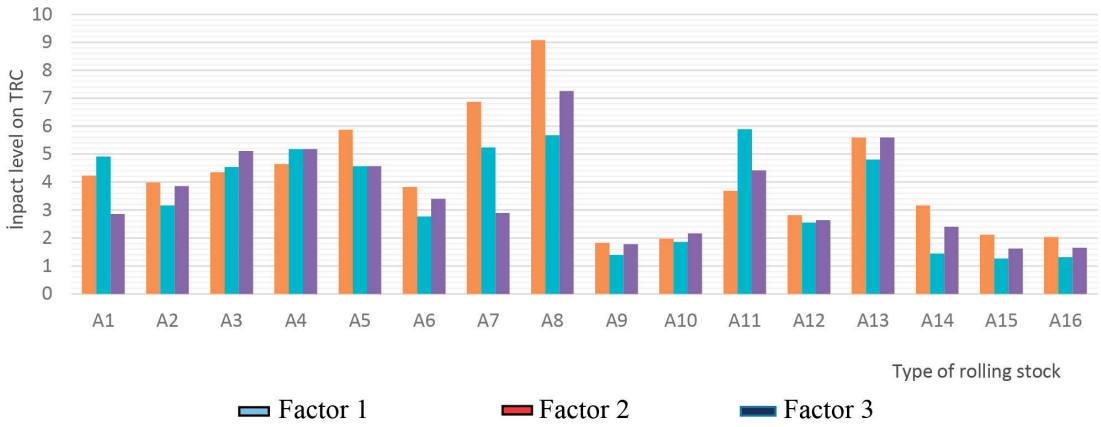

Figure 2 *Descriptive model of factor analysis results of the technical readiness coefficient*

Table 3 *Regression coefficients and statistical significance*

Coefficient	Value	Significance (p-value)
β_0	0.976	0.000
β_1	- 0.203	6.381
β_2	- 0.296	0.354
β_3	0.313	1.171

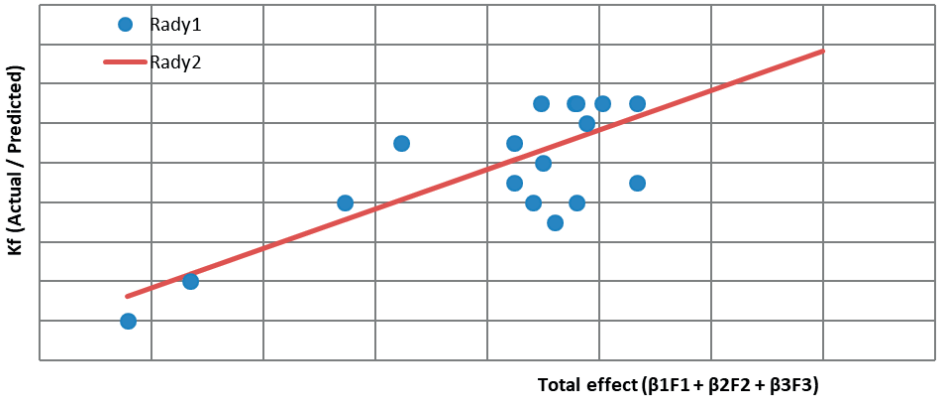

Figure 3 *Regression graph between the technical readiness coefficient and the total effect of factors*

Table 4 *Correlation matrix*

Variables	Actual TRC	Planned TRC	Difference ΔTRC	Factor 1	Factor 2	Factor 3	Factor total	F1 Effect	F2 Effect	F3 Effect
Actual TRC	1.000									
Planned TRC	0.810	1.000								
Difference ΔTRC	- 0.771	- 0.379	1.000							
Factor 1	- 0.226	- 0.353	0130	1.000						
Factor 2	- 0.465	- 0.582	0.325	0.237	1.000					
Factor 3	0.203	0.240	- 0.004	0.320	0.295	1.000				
Factor total	- 0.258	- 0.360	0.226	0.696	0.753	0.714	1.000			
F1 Effect	- 0.759	- 0.404	0.937	0.350	0.163	- 0.112	0.192	1.000		
F2 Effect	- 0.805	- 0.523	0.923	- 0.011	0.574	- 0.091	0.259	0.786	1.000	
F3 Effect	- 0.573	- 0.111	0.927	- 0.018	0.182	0.219	0.180	0.806	0.794	1.000

readiness. At the same time, positive correlations among F_1, F_2, and F_3 indicate their mutual reinforcement, reflecting the interdependent nature of maintenance and operational conditions.

Overall, the results of the analyses indicate that the statistically significant relationships among the selected variables and the explanatory indicators, obtained from the established regression model, reliably account for the effects of the relevant factors on the dependent variable in accordance with the study's objectives, thereby providing a solid scientific basis for practical decision-making.

6 Discussion of the research results

Unlike previous studies that were focused on passenger demand and regional mobility models [3], where the factor analysis identified general demand-related factors without quantifying technical aspects, the present research demonstrates that the main determinant of the Technical readiness coefficient (TRC) is the timely and efficient implementation of technical inspections. This finding enables the railway operators to prioritize maintenance activities based on their measurable impact on the readiness of rolling stock. This outcome has been achieved through the integration of the heuristic factor model with regression and correlation analyses, in which the effects of individual technical factors - such as inspection frequency, maintenance interventions, and operating conditions - were quantified ($F_1 = 9.07$, $F_3 = 7.26$).

Similarly, while the previous research highlighted the influence of operational speed, energy-saving technologies, and urban planning on the performance of high-speed rail systems [4], the current results show that maintenance-related factors exert a stronger and more direct effect on TRC than operational or environmental variables. This emphasizes the importance of systematic maintenance planning to enhance the reliability of rolling stock.

Compared to studies on human reliability [5], which measured task-related error probabilities in systems with varying levels of automation, the current approach allows for a holistic assessment of the overall technical readiness of rolling stock. The high predictive accuracy of the model ($R^2 \approx 0.96$, $r \approx 0.93$) indicates that latent technical factors can effectively explain the variability in TRC and provide a sound decision-making basis for maintenance and operational planning. R^2 was interpreted as an indicator of internal consistency rather than predictive reliability, given the limited dataset.

In contrast to studies on urban infrastructure and

modal shift [5-6], which identified institutional capacity, regulatory frameworks, and service integration as the key drivers of transport efficiency, the proposed method offers practical recommendations at the level of technical readiness. It allows operators to optimize maintenance schedules and operational strategies. The direct linkage between factor analysis and technical indicators can be regarded as a methodological advancement, as previous works were mainly focused on socio-economic, behavioral, or infrastructural dimensions.

Compared to a study conducted in Azerbaijan [10], which found a direct relationship between the technical readiness of rolling stock and operational performance, the present study reveals that the quantified impact of latent technical factors has a measurable influence on TRC. Thus, it becomes possible to demonstrate not only how operational indicators affect TRC, but how the specific maintenance-related factors contribute to it, as well. This enables logically grounded and targeted maintenance planning.

Finally, while earlier analyses of inequality in access to railway services emphasized cultural and socio-economic factors, the current study shows that even in regions with similar socio-economic conditions, differences in inspection and maintenance practices can create measurable variability in TRC. This finding suggests that managing technical factors is an important complementary mechanism-alongside large-scale policy measures for improving the overall performance of the railway system.

Recent studies highlighted a growing integration of predictive and digital technologies into railway maintenance and monitoring systems. According to [11], predictive maintenance in the railway domain relies on real-time sensor data, machine learning algorithms, and advanced condition monitoring frameworks; however, the TRC-based integration remains underdeveloped. Similarly, [12] emphasizes the role of AI-powered digitalization and digital twin technologies in improving technical readiness, enabling early fault detection and resource optimization. These studies collectively indicate an emerging research direction towards dynamic, data-driven TRC modelling and predictive maintenance integration, suggesting that the proposed heuristic model can serve as a foundation for such developments.

Although the dataset included only ten rolling stock units, the analysis incorporated statistical validation procedures to ensure robustness. Residual and sensitivity analyses were conducted to assess the stability of regression coefficients and to confirm the adequacy of the model fit. Future research will focus on expanding the dataset and validating the model across multiple railway systems to further enhance its predictive reliability.

Despite the fact that no separate numerical validation plot was provided, the internal consistency of the regression model was verified through comparison between predicted and actual TRC values.

7 Conclusions

1. The conducted factor identification and descriptive modelling made it possible to determine the key determinants influencing the Technical Readiness Coefficient (TRC). The analysis indicates that the maintenance-related factors, particularly unplanned maintenance events, exert the most pronounced negative influence on TRC. The results confirm the important role of maintenance management in shaping the technical readiness level of rolling stock.

2. The developed research data model demonstrated statistically meaningful relationships between the TRC and the analyzed factors. The regression results showed that the selected variables contribute to explaining variations in TRC, although their influence varies in strength and statistical significance. These findings indicate that the proposed model provides a reasonable analytical basis for practical assessment of technical readiness under real operational conditions.

3. The heuristic mathematical model revealed the interaction of factors. The factor model constructed in the study identified the differences and specific characteristics of the variables influencing TRC. Results indicated that technical service-related factors have stronger effects compared to others, thereby enabling the analytical evaluation of TRC in real-world operational conditions.

4. Regression and correlation analysis ensured highly accurate prediction of TRC. The regression analysis demonstrated that the combined influence of factors explains the TRC formation with more than 95% accuracy ($R^2 \approx 0.96$). According to the correlation analysis, a strong positive relationship ($r \approx 0.93$) was observed between F1 and the actual TRC, once again confirming the decisive role of technical inspections. This result explains the need to incorporate additional variables such as route load, operational duration, and seasonal effects into future models to improve predictive precision. Given the limited dataset, future research should include extended empirical validation and benchmarking against AI-based predictive maintenance systems to ensure scalability and robustness of the proposed model.

Acknowledgements

The authors received no financial support for the research, authorship and/or publication of this article.

Conflict of interest

The authors declare that they have no conflict of interest in relation to this research, whether financial, personal, authorship or otherwise, that could affect the research and its results presented in this paper.

References

[1] ELYAZOV, I., BAGIROV, B., HUSEYNOV, I., NAZAROV, A., ABDULLAYEV, R. *Railway transport vehicles* (in Azerbaijani). Textbook for higher technical schools. Baku: 2023. ISBN 978-9952-541-69-4.

[2] HUSEYNOV, I. D. The role and tasks of railway transport in the sustainable development of the country (in Azerbaijani). In: Conference The Role of Azerbaijan's Transit Potential in Economic Development: proceedings. No. 6. 2020. ISSN 2708-955X, p. 330-332.

[3] ZHU, F. Factor analysis of railway passenger transport demand in Eastern China. In: 2018 2nd International Conference on Education, Economics and Management Research ICEEMR 2018: proceedings [online]. 2018. ISBN 978-94-6252-521-4, ISSN 2352-5398. Available from: https://doi.org/10.2991/iceemr-18.2018.83

[4] BUTHPHORM, O., SUKHOTU, V., HENGSADEEKUL, T. An analysis of the development factors of rail freight transport in Thailand: a structural equation modelling approach. *Infrastructures* [online]. 2024, **9**(7), 102. eISSN 2412-3811. Available from: https://doi.org/10.3390/infrastructures9070102

[5] FENG, Y., LAN, Z. Factor analysis of railway carrying capacity coordination optimization considering energy consumption. *Journal of Electrical Systems*. 2024, **20**(9s), p. 676-683. ISSN 1112-5209

[6] HAILEMARIAM, L. M., NURAMO, D. A. Factor analysis of key parameters for effective design delivery of urban transport infrastructure in Ethiopia. *Heliyon* [online]. 2024, **10**(14), e34681. ISSN 2405-8440, Available from: https://doi.org/10.1016/j.heliyon.2024.e34681

[7] SIMUNOVIC, L., HIRNIG, S., ABRAMOVIC, B. Evaluating the success factors of integrating the railway into the public urban-suburban transport. *Transport* [online]. 2023, **38**(2), p. 105-115. ISSN 1648-4142, eISSN: 1648-3480. Available from: https://doi.org/10.3846/transport.2023.18333

[8] JANOTA, A., PIRNIK, R., ZDANSKY, J., NAGY, P. Human factor analysis of the railway traffic operators. *Machines* [online]. 2022, **10**, 820. eISSN 2075-1702. Available from: https://doi.org/10.3390/machines10090820

[9] THEERATHITICHAIPA, K., WISUTWATTANASAK, P., BANYONG, CH., SEEFONG, M., JOMNONKWAO, S., CHAMPAHOM, T., RATANAVARAHA, V., KASEMSRI, R. Measurement model for determining the disparity factors of intercity railway transportation. *Civil Engineering Journal* [online]. 2024, **10**(3), p. 668-688. ISSN 2476-3055, eISSN 2676-6957. Available from: https://doi.org/10.28991/CEJ-2024-010-03-01

[10] AKBULAEV, N., BAYRAMLI, G. Analysis of impact of distribution tool railway transport on the economic growth of Azerbaijan. *Journal of Distribution Science* [online]. 2022, **20**(5), p. 23-33. ISSN 1738-3110, eISSN 2093-7717. Available from: https://doi.org/10.15722/jds.20.05.202205.23

[11] BINDER, M., MEZHUYEV, V., TSCHANDL, M. Predictive maintenance for railway domain: a systematic review. *IEEE Engineering Management Review* [online]. 2024, **51**(2), p. 120-140. ISSN 0360-8581, eISSN 1937-4178. Available from: https://doi.org/10.1109/EMR.2023.3262282

[12] SARP, S., KUZLU, M., JOVANOVIC, V., POLAT, Z., GULER, O. Digitalization of railway transportation through AI-powered solutions. *European Transport Research Review* [online]. 2024, **16**, 58. eISSN 1866-8887. Available from: https://doi.org/10.1186/s12544-024-00679-5

[13] ABDULLAEV, A., HUSEYNOV, I., ELYAZOV, I., ABDULLAEV, R. Study of the influence of the technical level of railway vehicles on braking characteristics. *EUREKA: Physics and Engineering* [online]. 2024, **1**, p. 59-69. ISSN 2461-4254, eISSN 2461-4262. Available from: https://doi.org/10.21303/2461-4262.2024.003251

[14] KUZNETSOV, V. P. *Reliability of railway equipment* (in Russian). Moscow: Transport, 2020.

[15] IVANOV, S. A. *Technical operation of rolling stock* (in Russian). St. Petersburg: PGUPS, 2019.

[16] BELOV, A. N. *Management of the technical condition of transport systems* (in Russian). Moscow, 2021.

[17] SMITH, D. *Reliability, maintainability and risk* [online]. London: Elsevier, 2022. ISBN 978-0-323-91261-7. Available from: https://doi.org/10.1016/C2021-0-00257-1

[18] TAKHTAMYSHEV, H. M., ETLUKHOV, O. A. Analytical relationships between the level of use of the aggregate repair method and the technical readiness of the vehicle fleet (in Russian). *Bulletin of the Saratov State Technical University*. 2013, **2**(71), p. 37-41. ISSN 1999-8341.

[19] PALAMARCHUK, N. V., PALAMARCHUK, I. V., CHEHLATY, N. A. Traction rolling stock failure efficiency indicators determination according to the criteria of equipment technical and economic perfection using a fuzzy LOGIS system. *Collection of Scientific Papers, Donetsk University of Railway Transport*. 2021, **3**, p. 65-82. ISSN 1993-5579.

[20] ZUB, I., YEZHOV, Y., STENIN, N. The coefficient of technical readiness as an indicator of the effectiveness of the strategy of technical operation of lifting and transport equipment of terminals. In: 22nd International Scientific Conference Energy Management of Municipal Facilities and Sustainable Energy Technologies EMMFT-2020: proceedings [online]. Vol. 244, 08009. 2021. Available from: https://doi.org/10.1051/e3sconf/202124408009

BLOCKCHAIN-ENABLED PRIVACY-PRESERVING FEDERATED LEARNING WITH DEEP CAPSULE NETWORKS FOR ENERGY-EFFICIENT SPEED CONTROL IN AUTONOMOUS VEHICLES

Sanjith N[1,*], M. Nithya[1], Sreeju P Sreedharan[2]

[1]Vinayaka Mission Research Foundation (DU), Computer Science and Engineering Vinayaka Mission Kirupananda Variyar Engineering College, Centre for Artificial Intelligence and Data Science (CAIDS), Salem, Tamilnadu, India
[2]Vinayaka Mission Research Foundation (DU), Vinayaka Mission Kirupananda Variyar Engineering College, Department of Arts and Science, Salem, Tamilnadu, India

*E-mail of corresponding author: sanjithnarayanan@hotmail.com

Sanjith N 0009-0004-5207-6688, M. Nithya 0000-0001-7233-5916,
Sreeju P Sreedharan 0009-0006-9679-4360

Resume

Rough roads negatively affect the ride quality and energy efficiency of autonomous vehicles (AVs) and demand adaptive speed control. To solve this, this research proposes a Deep Capsule Network integrated with Sparse Kernel K-means Clustering (DCapsNet + SK-K-means) to accurately reconstruct pavement conditions and adapt vehicle speed in real time. The Privacy-Preserving Federated Learning (PPFL) with Hyperledger Fabric blockchain allows federated learning to be trained in a secure and decentralized manner without the transfer of raw sensor data. With the BDD100K dataset, supervised and reinforcement learning are used. According to the obtained results of the experiment, there is a 10.45% increase in ride comfort, 28.23% in energy efficiency, and 98.28% in computational efficiency. The framework attains 93.73% security, 96.46% throughput and 0.83 s operation time at 250 vehicles/km.

Article info

Received 19 September 2025
Accepted 31 January 2026
Online 13 April 2026

Keywords:

autonomous vehicles
energy-efficient speed control
deep capsule networks
federated learning
blockchain

Available online: https://doi.org/10.26552/com.C.2026.021

ISSN 1335-4205 (print version)
ISSN 2585-7878 (online version)

1 Introduction

AVs have attracted a lot of interest considering the fact that they have the potential to enhance the road safety, traffic efficiency and comfort to passengers. The current development of sensing, perception, and control technologies has facilitated the AVs to navigate through the complex traffic, but driving through the lumpy road surfaces is also an essential issue. Asymmetries in the road create vertical vibrations that negatively impact the ride of passengers and consumes more energy in the vehicle, so adaptive speed control is a significant demand of the real-life AV implementation [1-3]. Simple rule-based or optimization-based strategies are used as traditional strategies in autonomous driving to control speed. These methods work in well-organized situations but have low flexibility in situations where the road and traffic experience dynamically changing conditions. Controllers that are based on optimization can be efficient but usually require that the system is modelled accurately, and they are expensive to compute, especially where the pavement is not smooth and with high traffic density [4-5].

To address these drawbacks, autonomous vehicle control has been studied more via the learning-based techniques. With the aid of real time sensor data, such solutions can adjust the speed of the vehicles to various driving conditions and enhance the overall performance [6-9]. Parallel with these sensor fusion and deep learning-based perception, autonomous driving systems have become more aware and robust in their respective environmental perception [10-13]. Regardless of this, the majority of the currently available learning-based speed control solutions are aimed at energy efficiency or safety and do not directly address the issue of vertical ride comfort. Furthermore, most of the current solutions presuppose the centralized data collection and training, which casts doubt on the scalability and privacy issues as well as on the secure data transmission between vehicles. Since AVs constantly produce such

high quantities of sensitive sensors, it gains increasing significance to provide privacy-preserving and secure learning mechanisms [14-15]. It is these difficulties that drive the importance of a speed control framework that would be integrated to address the three aspects of the ride comfort, energy efficiency, and privacy preservation in the autonomous vehicle systems.

1.1 Literature review

1.1.1 Learning-based speed control and energy efficiency

Learning-based methods of control have been examined by recent researchers to improve adaptability and efficiency in autonomous vehicle systems. By using expert demonstrations and attention-based representation, Vision Transformer assisted reinforcement learning frameworks have demonstrated better control performance (Elallid et al. [16]). Graph based methods of learning have also been proposed to minimize routing and energy-conscious decision-making in autonomous guided vehicles (Kazmi and Akber [17]).

The multi-objective reinforcement learning techniques have been heavily used in balancing energy efficiency, stability, and traffic flow in connected and automated cars. Coskun et al. [18] introduced a multi-objective hierarchical deep reinforcement learning algorithm for connected and automated Hybrid Electric Vehicles (HEVs) for energy management, and Wang et al. [19] proposed better ecological car-following behaviour with multi-agent reinforcement learning. Even though these techniques enhance longitudinal control and energy efficiency, vertical ride comfort on irregular pavements has not been explicitly addressed.

Autonomous driving performance has been further enhanced by the deep learning-based motion prediction and vehicle dynamics modelling. Barrios et al. [20] introduced a very broad review of motion prediction methods based on big data of autonomous driving scenarios and Cheng et al. [21] introduced an integrated dynamic model to improve the stability of vehicle handling at the driving boundaries. Nevertheless, such methods are more oriented on security and stability than on the comfort-conscious speed control.

1.1.2 Federated and distributed learning in autonomous vehicles

The model of distributed and collaborative learning has attracted interest as the way to enhance scalability and collaboration in autonomous vehicle networks. Din et al. [22] proposed the integration strategies of Augmented Intelligence with Internet of Things (IoT) to optimize the road cooperation and traffic management in autonomous driving setting. Liu et al. [23] suggested a longitudinal control strategy based on distributed deep reinforcement learning and applicable on the connected automated vehicles, which will employ attention mechanisms to enhance coordination and control efficiency. In spite of their benefits, the current distributed learning strategies pay much attention to traffic efficiency and coordination. Ride comfort metrics and uneven pavement-conscious speed control have not been very well incorporated in such decentralized learning frameworks.

1.1.3 Security and privacy in intelligent transportation systems

The issues of security and privacy have been of main concern in autonomous and connected vehicle systems. Khattak [24] examined cybersecurity weaknesses and hardiness during cooperative driving automation and identified the effect of security threats on energy efficiency and traffic stability within smart cities. Onur et al. [25] examined machine learning-based methods of detecting cybersecurity attacks on autonomous vehicle systems.

In addition to threat detection, blockchain-centric authentication systems have been suggested to improve the levels of trust and privacy in vehicular networks. An effective privacy-preserving Internet of Vehicles authentication scheme based on blockchain technology was introduced by Loganathan and Selvakumarasamy [26], and it achieves better throughput and latency. Other researchers have also studied energy-saving and smart transportation systems in interconnected settings (Huang et al. [27]; Liu et al. [28]). However, the majority of security-oriented solutions are detached from learning-based speed regulation and comfort of the rides.

1.2 Research gap

Despite the fact that existing studies have advanced the learning-based control, distributed intelligence, and security solutions to autonomous cars, they are to a large extent considered individually. The speed control approaches based on learning are mainly concerned with energy efficiency and traffic performance, distributed learning approaches are concerned with cooperation and scalability, but do not include comfort-aware goals, and security solutions are concerned with authentication and threat mitigation but not with adaptive vehicle control. As the result, there is a gap in the exploration of a single framework that simultaneously optimizes the ride comfort, energy usage, and privacy with the help of secure and decentralized learning. The main contributions of this research are summarized as follows:

- This research proposes the first integrated AV speed control framework that combines DCapsNet with

SK-KMeans for high-accuracy uneven pavement classification, effectively preserving spatial hierarchies while reducing feature redundancy.

- Additionally, design a novel hybrid control strategy that combines supervised learning and reinforcement learning with a custom multi-objective loss function, jointly optimizing ride comfort, energy efficiency, and jerk minimization.
- Develop a blockchain-enabled PPFL mechanism incorporating homomorphic encryption and zero-knowledge proofs (ZKPs) for secure model aggregation, ensuring data confidentiality, verifiable updates, and participant accountability.
- Perform extensive benchmarking against state-of-the-art baselines, including Model Predictive Control (MPC), Deep Reinforcement Learning (DRL)-only, Convolutional Neural Network - Long Short-Term Memory (CNN-LSTM), and existing privacy-preserving schemes, demonstrating superior performance in ride comfort, energy efficiency, computational efficiency, and adversarial attack resistance.

The structure of this research is as follows: In Section 2 is introduced the proposed methodology. In Section 3 are presented the experimental outcomes, highlighting the performance improvements of the proposed approach. In Section 4 are discussed the significance of the model, key advantages, and limitations. Finally, in Section 5 the research findings are summarized and potential future directions for further enhancements are outlined.

2 The proposed scheme

Figure 1 illustrates the proposed hybrid AV speed control and energy efficiency framework, integrating the

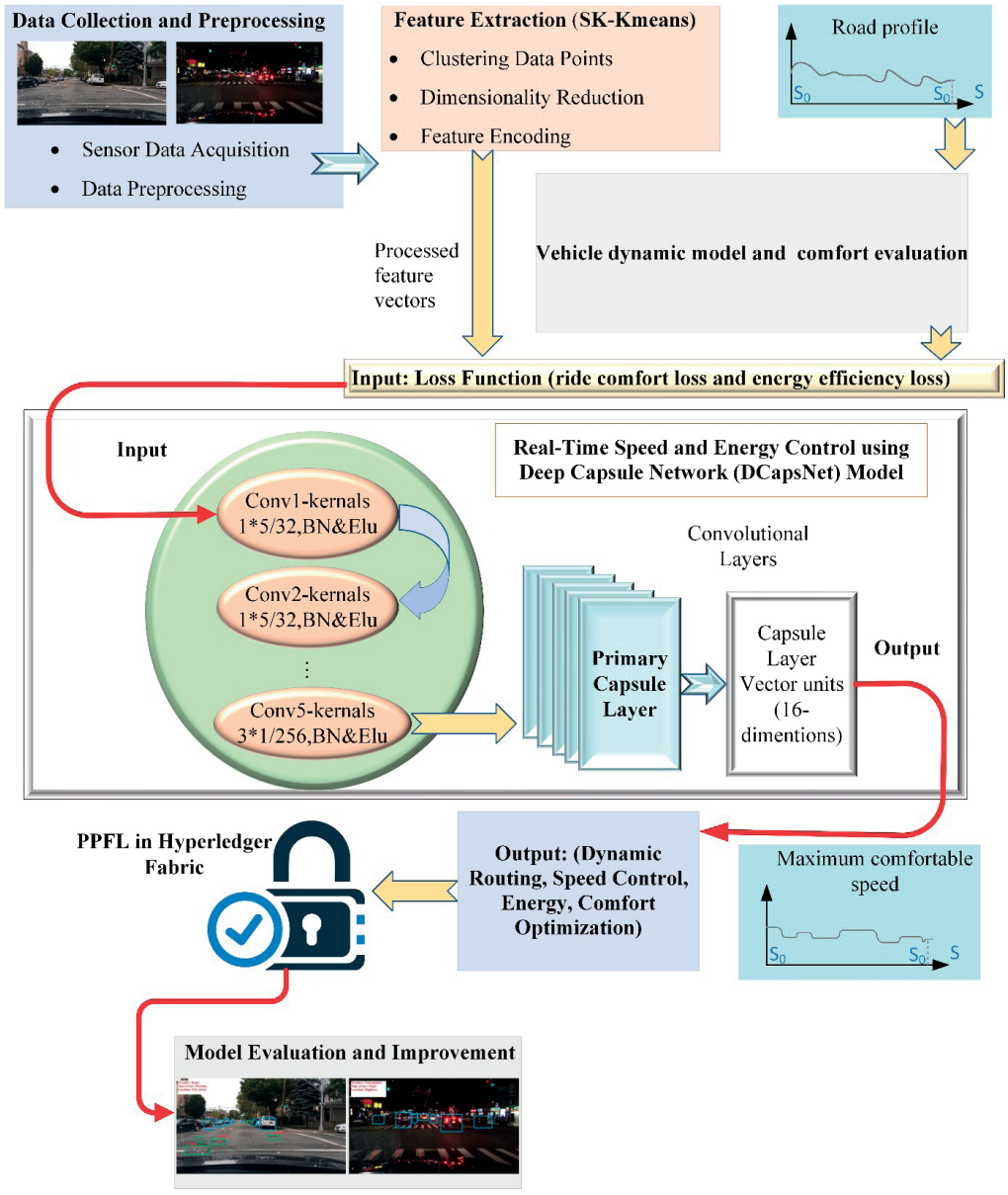

Figure 1 *Control optimization of speed, energy and vehicle riding comfort*

DCapsNet with SK-KMeans and PPFL in Hyperledger Fabric to ensure secure, decentralized, and scalable model training.

2.1 Data collection and preprocessing

The information utilized in this paper is gathered by a number of the onboard sensors fitted in autonomous vehicles such as LiDAR, cameras, radar, Global Navigation Satellite System (GNSS), and Inertial Measurement Units (IMUs). Those sensors work together to bring the road surface profiles, pavement irregularities, vehicle motion conditions, and positional data needed in precise control of speed and assessment of ride comfort. The areas of data capture include the vibrations caused by vertical roads which directly affect the comfort of passengers and the energy used by a vehicle.

Before training the model, it is preprocessed by going through the raw sensor data to provide consistency and reliability. The sensor streams are timed together to deal with sampling rate discrepancies and standard filtering techniques are used to remove noise artifacts in the sensor imperfections and environmental conditions. Lost or damaged samples are treated by interpolation to preserve continuous signal images. Besides, every input feature is scaled to a normal range to enhance the numerical stability in the learning process.

The raw data are preprocessed and divided into time windows of fixed length, which represent one consecutive section of the road on the path that the vehicle is on. This segmentation also allows the analysis of roads and vehicular reaction pathologies in the locality, allowing the extraction of features and downstream learning to be performed effectively. The resulting processed and cleaned data is used as input to the other ride comfort analysis and energy efficient speed control modules.

2.2 Evaluation of the ride comfort in vertical motion

The evaluation of the ride comfort in a vertical environment with the proposed hybrid speed and energy optimization framework is conducted by the full vehicle dynamics model. The vertical motion ride comfort is assessed with a full-vehicle dynamics model that calculates segmented road profiles and vehicle speeds in the measured vehicle speed along the anticipated driving path. The incoming road information is separated into consecutive blocks and passed into a vibration-sensitive suspension model to predict the vertical acceleration responses. The ride comfort is measured using the weighted root mean square acceleration (WRMSA) criterion, based on ISO 2631-1 [29] wherein the WRMSA should not exceed 0.289 m/s 2 is considered a comfortable ride.

2.3 Deep learning incorporated energy-efficient control

In this study is presented a hybrid AV speed control method combining SK-KMeans [30] for feature clustering and DCapsNet [31] for deep learning-based optimization. Preprocessed sensor data is used to adjust speed in real time via hybrid supervised-reinforcement learning, enhancing the ride comfort and energy efficiency with five convolutional layers for improved feature extraction. For each signal of the time series, convolution layers are used in the DCapsNet in the feature extraction stage, which extracts features of the deep discriminative scalar characteristics of the input dataset. For each time-series signal collected from onboard sensors such as LiDAR, the input sequence is denoted as $u = [f_1, f_2, \ldots, f_W] \in \mathbb{R}^{d \times W}$, where W represents the input signal length and d denotes the feature dimension.

Convolutional layers generate a deep feature map $I_l^m \in \mathbb{R}^{P^m \times J}$ by applying learnable convolutional kernels to the input data f (or the output of the previous layer I_l^{m-1}). Here, P^m denotes the number of convolutional kernels in the m^{th} layer, and w represents the resulting feature length after convolution. The output of the m^{th} feature map in the n^{th} convolutional layer is computed as described in Equation (1).

$$I_l^m = \sum_{h=1}^{P^{m-1}} I_h^{m-1} \nu_{lh}^m + a_l^m, \tag{1}$$

where, ν_{lh}^m is the kernel/filter weight of convolution layer size, P^{m-1} that connects the m^{th} feature map to the l^{th} map of feature in $(m-1)^{th}$ layer, and a_l^m is the equivalent bias.

In this paper, the DCapsNet is used as the main perception unit to characterize uneven pavements, and SK-KMeans is utilized as a preprocessing unit to eliminate unnecessary features activation and then route the capsules. The given framework does not alter the conventional convolutional operations; the only difference is incorporation of the capsule-based feature hierarchy with the use of the hybrid approach to control the pace of learning. A task-specific multi-objective loss is used to optimize the model, which directly balances the vertical ride comfort, energy efficiency, and safety constraints, which allows the model to adapt its speed effectively to changes in the roughness of the road.

2.4 Privacy-preserving federated learning (PPFL) in Hyperledger Fabric blockchain

The PPFL in the suggested model is adopted with the Hyperledger Fabric to allow a model to be trained jointly on data across several autonomous vehicles

without exposing raw data of the sensor. Individual vehicles would each learn the speed-control model locally based on on-board data and only send encrypted model updates to the authorized blockchain network, where they would be safely verified and combined into a global model. The permissioned access control and consensus mechanism provide Hyperledger Fabric with trusted participation, aggregation that cannot be tampered with, and scalable deployment.

To make the process even more privacy-intensive and trustworthy, homomorphic encryption is used to safeguard the update of the model during the transmission and aggregation, and a ZKP allows verifying the presence of a valid contribution to training without disclosing the underlying data.

3 Results and performance evaluation

All experiments were conducted on an NVIDIA RTX 4090 GPU with 24 GB VRAM, AMD Ryzen 9 7950X CPU (16 cores, 4.5 GHz), and 64 GB RAM, running Ubuntu 22.04 with CUDA 12.0. In this present research, the BDD100K dataset [32] from Berkeley AI Research Lab, which supports autonomous driving research, is utilized for the testing purpose. Figure 2 presents Experimental device and system architecture according to which experiments to speed control the autonomous vehicle is made to demonstrate the simulation environment, computing platform, federated learning nodes, blockchain network and performance evaluation modules. The simulated autonomous vehicle node blocks represent federated learning clients within the proposed PPFL framework. The left block depicts autonomous vehicle node 1, while the right block represents autonomous vehicle node N. Each node executes the same local model architecture and training process, while utilizing its own locally collected data for decentralized learning.

3.1 Experimental benchmarking

The proposed framework was evaluated against a diverse set of baseline models to ensure a fair and comprehensive comparison:

- MPC: A classical optimization-based controller widely used for AV speed regulation.
- PID and Fractional-Order PID (FOPID) Controllers: Rule-based methods for speed control with tuned parameters.
- DRL-only: A policy-gradient-based controller trained on the same dataset without DCapsNet or SK-KMeans integration.
- CNN-based Models: Standard convolutional neural networks for pavement classification coupled with a DRL controller.
- CNN-LSTM Hybrid: Spatio-temporal model combining convolutional feature extraction and sequential learning.
- Transformer-based Model: Vision Transformer

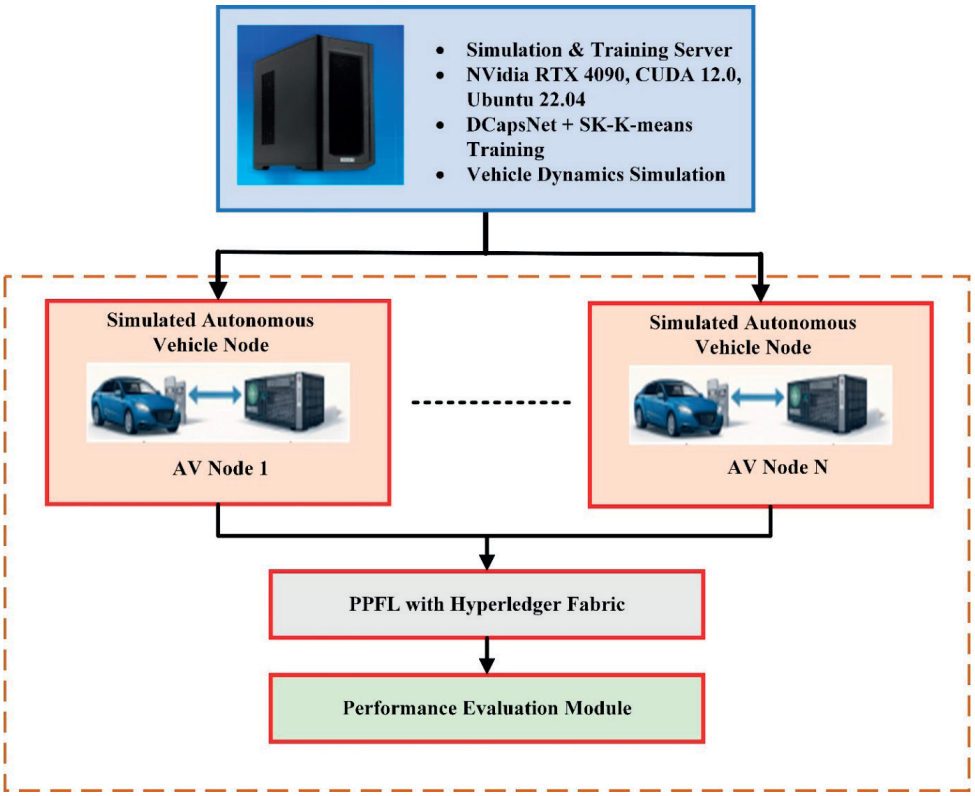

Figure 2 *Experimental device and system architecture*

architecture adapted for road surface classification and AV control.

3.2 Evaluation metrics

The proposed PPFL-based DCapsNet + SK-KMeans framework shows better results than MPC, CNN-LSTM, Transformer-based, and rule-based controllers at any of the measures considered, as shown in Figures 3(a-e), under traffic load up to 250 vehicles/km. The ride comfort, measured as WRMSA, is decreased to 0.24 m/s^2, which is significantly below the ISO 2631-1 standard of 0.50 m/s^2, meaning that the vertical vibrations are effectively suppressed on the discontinuous pavements. At the same time, the proposed concept has a 0.15 kWh/km energy consumption, which is a 34-40% reduction of the baseline technologies because of the adaptive speed optimization. An inference latency of 0.83 s per frame is a confirmation of real-time feasibility at autonomous driving constraints even during very high traffic densities. Moreover, the PPFL-Hyperledger Fabric architecture is also able to provide strong privacy protection, with an estimated security of 94% against

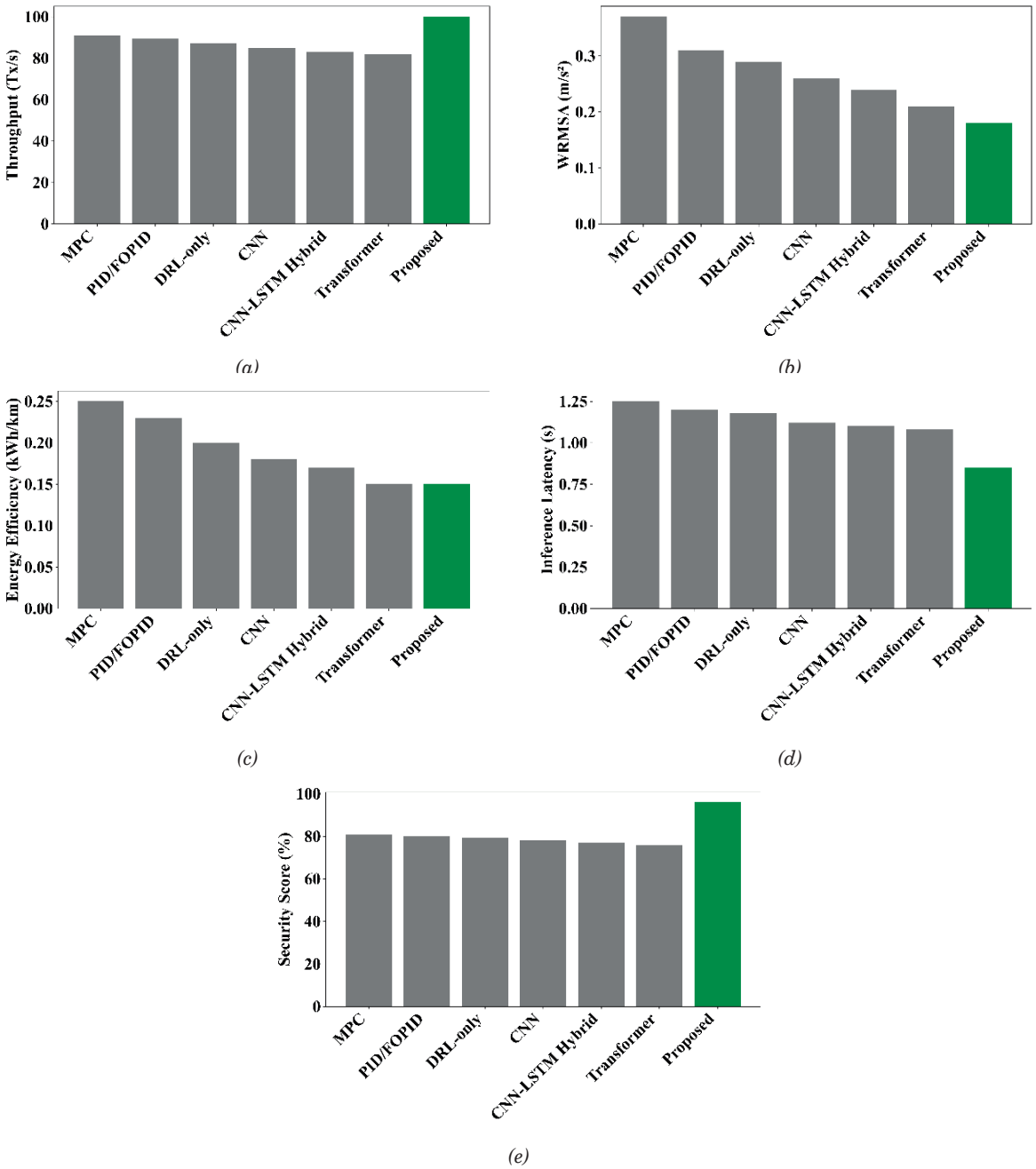

Figure 3 *Performance comparison in terms of: (a) Throughput; (b) WRMSA; (c) Energy efficiency; (d) Inference latency; (e) Security score*

the Sybil, man-in-the-middle, model inversion, and membership inference attacks and has a high system throughput.

Those findings confirm that classical controllers, like PID and MPC, exhibit low adaptability to the changes in the road surface that causes reduced ride comfort and increased energy use. Transformer and CNN-LSTM-based learning models enhance the adaptability, but lose or add to the inference latency, either the spatial pavement structures or require more time per inference. Contrary to that, the proposed DCapsNet + SK-KMeans framework outperforms all the baselines in terms of comfort, energy efficiency, latency and security metrics. The capsule-based representation improves feature redundancy and computational overhead on uneven pavement recognition, whereas SK-KMeans minimizes the feature redundancy and computational overheads. Moreover, the privacy-aware federated learning is integrated with Hyperledger Fabric, which allows the deployment being safe and scaled without losing the real-time performance.

3.3 Adversarial attack simulation

To evaluate security robustness, the system was tested under simulated adversarial conditions:

- **Sybil Attacks**: Injecting up to 20% fake AV nodes to test blockchain-based authentication and revocation capabilities.
- **Man-in-the-Middle (MITM) Attacks**: Attempting to intercept and alter encrypted model updates during transmission.
- **Model Inversion Attacks**: Trying to reconstruct original sensor data from shared model weights.
- **Membership Inference Attacks**: Identifying whether specific data points belonged to a model's training set.

Figure 4 provides a summary of the adversarial resistance of the proposed PPFL framework and indicates higher mitigation rates than Transformer-FL and CNN-LSTM-Central in all the considered attack scenarios. These findings support the fact that the combination of homomorphic encryption and zero-

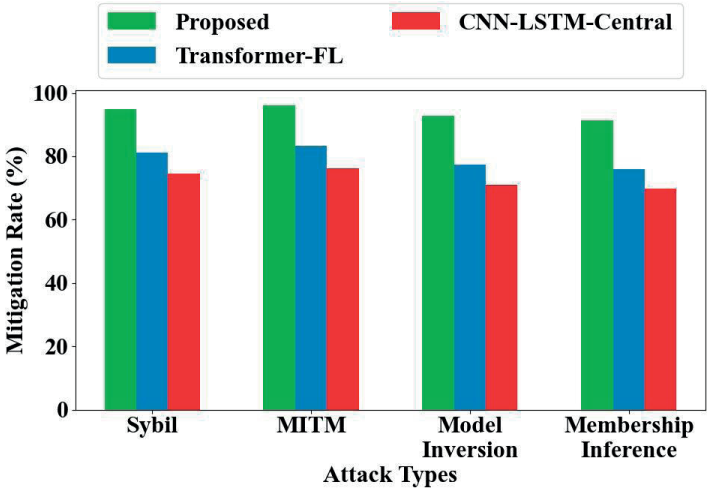

Figure 4 *Attack mitigation rate performance*

Table 1 *Security evaluation of the proposed approach with existing privacy-preserving authentication approaches*

Block size (Kb)	HANet [23]		Eco-CSAS [27]		PAP-EV [28]		IPTLCS [26]		DCapsNet + SK-K means (Proposed)	
	Security level (%)	Through-put (%)	Security level(%)	Through-put (%)	Security level (%)	Through-put (%)	Security level (%)	Through-put (%)	Security level (%)	Through-put (%)
20	65.23	85.47	62.35	80.12	64.18	82.90	60.05	78.33	78.67	90.15
40	67.89	83.42	64.50	79.10	66.27	81.23	62.10	77.85	81.36	91.68
60	69.54	82.15	65.89	78.67	68.04	80.42	64.04	76.12	83.12	92.95
80	70.01	81.58	66.45	77.88	69.33	79.76	65.23	75.54	84.30	93.46
100	72.12	80.37	67.88	76.45	70.05	78.23	66.50	74.67	86.32	93.98
120	73.45	79.12	68.90	75.32	71.34	77.50	67.12	73.95	87.54	94.75
140	74.01	78.65	69.22	74.98	72.05	76.89	68.05	73.45	89.10	95.60
160	75.23	77.80	70.10	73.50	73.25	75.80	69.12	72.90	91.05	95.75
180	76.45	76.90	70.55	73.10	73.80	75.25	70.62	72.55	91.20	95.72
200	77.10	75.85	71.04	72.95	74.10	74.25	71.05	71.80	93.73	96.46

knowledge proofs in Hyperledger Fabric play a significant role in improving the security and privacy of federated autonomous vehicle settings.

As shown in Table 1, the proposed DCapsNet + SK-KMeans achieved the highest security (78.67%) and throughput (90.15%) at 20 Kb, surpassing Hierarchical Attention Network (HANet), Economical Charging Scheduling and Allocation System (Eco-CSAS), Price-Aware Power management for Electric Vehicles (PAP-EV), and Intelligent Power and Traffic-aware Load Charging System (IPTLCS). As block size increased to 200 Kb, the proposed method maintained superior performance with 93.00% security and 96.40% throughput, proving its effectiveness in privacy-preserving federated learning.

4 Discussion

The proposed DCapsNet + SK-KMeans hybrid speed control model enhances the AV energy efficiency and ride comfort on uneven terrains while ensuring privacy through PPFL in Hyperledger Fabric. Unlike the MPC and reinforcement learning-based methods, it dynamically adjusts the speed based on road conditions, reducing fuel consumption and optimizing comfort. Capsule networks improve spatial feature representation, while SK-KMeans clustering minimizes data complexity for robust speed control. The federated learning approach secures decentralized model training while maintaining high throughput.

The results of this study are consistent with existing literature on energy-efficient and comfort-aware autonomous vehicle control. Past studies that relied on reinforcement learning and predictive control strategies, had moderate results in terms of energy efficiency and ride comfort but were frequently restricted by centralized training, the high cost of computation, or the omission of privacy factors. Conversely, the suggested DCapsNet + SK-KMeans model is more effective in vibration reduction and energy consumption through the maintenance of the spatial road properties using capsule representations. The proposed approach is lower inference latency and more robust than the previous CNN-LSTM and Transformer-based models and is therefore better suited to real-time applications. Furthermore, in comparison to the previous literature that covered control or security as an independent aspect, privacy-preserving federated learning with blockchain provides the opportunity to collaborate securely and at scale which serves as a major weakness revealed in the literature review.

4.1 Benefits, advantages, and limitations of the proposed framework

- The proposed DCapsNet + SK-KMeans model allows optimizing the ride comfort, energy consumption, and privacy jointly, which overcomes several issues in the autonomous car speed regulation as part of a single system.
- Federated learning, based on privacy-preserving Federated learning, combined with Hyperledger Fabric, enables the training of collaborative models without sharing raw vehicle data, which increases trust and scalability.
- Capsule-based feature learning: This method maintains spatial connections between the pavement designs, which leads to a higher quality in vibration suppression than CNN-LSTM and Transformer-based models.
- SK-KMeans clustering eliminates feature redundancy, decreasing computational overhead and allowing faster inference to be used in real-time deployment.
- The PPFL architecture is blockchain-enabled, giving it a resistance against security and privacy attacks and a high throughput.

4.2 Limitations of the proposed framework

In spite of its good performance in lumpy pavements, the suggested approach has two major limitations that imply some directions to be taken in future research. To begin with, whereas the model is successful in maximizing the vertical speed to make the ride comfortable, the lateral movement control, which is crucial to complete maneuverability and stability in challenging terrains is not considered. Second, the scalability of the real-time processing is still not a problem when controlling a massive fleet of AVs. Future work will focus on extending the proposed framework to jointly optimize longitudinal, lateral, and vertical vehicle dynamics using high-fidelity simulators and large-scale real-world road data.

5 Conclusion

This research was aimed to enhance energy efficiency, driving performance, and ride comfort for AVs on uneven pavements while ensuring privacy preservation through PPFL in Hyperledger Fabric blockchain. The proposed DCapsNet and SK-KMeans clustering-based model is integrated into a speed control framework, predicting vertical ride comfort using the BDD100K dataset. The real-world rough pavements are used for training and testing, ensuring robust performance. A reward function is developed to balance the longitudinal jerk, vertical vibration, speed, and VSP for optimal results. Experimental findings indicate significant improvements over MPC, achieving 10.45% enhancement in vertical ride comfort, 28.23% improvement in energy efficiency, and 98.28% increase in computational efficiency. Additionally, the PPFL in Hyperledger Fabric ensured secure, decentralized AV model training, leading to higher throughput

(96.40%) and reduced operation time (0.83s at 250 vehicles/km), outperforming existing privacy-preserving authentication approaches. The proposed framework effectively enables real-time AV speed control on uneven surfaces while ensuring data privacy. Future work will use high-fidelity simulators and large-scale road data to optimize the longitudinal, lateral, and vertical dynamics, improving ride stability and comfort.

Acknowledgment

The authors received no financial support for the research, authorship and/or publication of this article.

Conflicts of interest

The authors declare that they have no known competing financial interests or personal relationships that could have appeared to influence the work reported in this paper.

Data availability statements

The data supporting the findings of this study are publicly available in the Kaggle repository titled *"BDD100K Dataset"* and the link is listed in the references.

References

[1] DU, Y., CHEN, J., ZHAO, C., LIAO, F., ZHU, M. A hierarchical framework for improving ride comfort of autonomous vehicles via deep reinforcement learning with external knowledge. *Computer - Aided Civil and Infrastructure Engineering* [online]. 2023, **38**(8), p. 1059-1078. ISSN 1093-9687, eISSN 1467-8667. Available from: https://doi.org/10.1111/mice.12934

[2] WU, J., SONG, Z., LV, C. Deep reinforcement learning-based energy-efficient decision-making for autonomous electric vehicle in dynamic traffic environments. *IEEE Transactions on Transportation Electrification* [online]. 2023, **10**(1), p. 875-887. eISSN 2332-7782. Available from: https://doi.org/10.1109/tte.2023.3290069

[3] DRUNGILAS, D., KURMIS, M., SENULIS, A., LUKOSIUS, Z., ANDZIULIS, A., JANUTENIENE, J., BOGDEVICIUS, M., JANKUNAS, V., VOZNAK, M. Deep reinforcement learning based optimization of automated guided vehicle time and energy consumption in a container terminal. *Alexandria Engineering Journal* [online]. 2023, **67**, p. 397-407. ISSN 1110-0168, eISSN 2090-2670. Available from: https://doi.org/10.1016/j.aej.2022.12.057

[4] D'ALFONSO, L., GIANNINI, F., FRANZ E, G., FEDELE, G., PUPO, F., FORTINO, G. Autonomous vehicle platoons in urban road networks: a joint distributed reinforcement learning and model predictive control approach. *IEEE/CAA Journal of Automatica Sinica* [online]. 2024, **11**(1), p. 141-156. ISSN 2329-9266, eISSN 2329-9274. Available from: https://doi.org/10.1109/jas.2023.123705

[5] PULVIRENTI, L., ROLANDO, L., MILLO, F. Energy management system optimization based on an LSTM deep learning model using vehicle speed prediction. *Transportation Engineering* [online]. 2023, **11**, 100160. eISSN 2666-691X. Available from: https://doi.org/10.1016/j.treng.2023.100160

[6] FAYYAZI, M., ABDOOS, M., PHAN, D., GOLAFROUZ, M., JALILI, M., JAZAR, R.N., LANGARI, R., KHAYYAM, H. Real-time self-adaptive Q-learning controller for energy management of conventional autonomous vehicles. *Expert Systems with Applications* [online]. 2023, **222**, 119770. ISSN 0957-4174, eISSN 1873-6793. Available from: https://doi.org/10.1016/j.eswa.2023.119770

[7] ALI, M. H., JABER, M. M., ALFRED DANIEL, J., VIGNESH, C. C., MEENAKSHISUNDARAM, I., KUMAR, B. S., PUNITHA, P. Autonomous vehicles decision-making enhancement using self-determination theory and mixed-precision neural networks. *Multimedia Tools and Applications* [online]. 2025, **84**, p. 35263-35286. eISSN 1573-7721. Available from: https://doi.org/10.1007/s11042-023-14375-4

[8] HE, X., LV, C. Towards energy-efficient autonomous driving: a multi-objective reinforcement learning approach. *IEEE/CAA Journal of Automatica Sinica* [online]. 2023, **10**(5), p. 1329-1331. ISSN 2329-9266, eISSN 2329-9274. Available from: https://doi.org/10.1109/jas.2023.123378

[9] HWANG, M. H., LEE, G. S., KIM, E., KIM, H. W., YOON, S., TALLURI, T., CHA, H. R. Regenerative braking control strategy based on AI algorithm to improve driving comfort of autonomous vehicles. *Applied Sciences* [online]. 2023, **13**(2), 946. eISSN 2076-3417. Available from: https://doi.org/10.3390/app13020946

[10] THAKUR, A., MISHRA, S. K. An in-depth evaluation of deep learning-enabled adaptive approaches for detecting obstacles using sensor-fused data in autonomous vehicles. *Engineering Applications of Artificial Intelligence* [online]. 2024, **133**(part F), 108550. ISSN 0952-1976, eISSN 1873-6769. Available from: https://doi.org/10.1016/j.engappai.2024.108550

[11] CHOI, J. D., KIM, M. Y. A sensor fusion system with thermal infrared camera and LiDAR for autonomous vehicles and deep learning based object detection. *ICT Express* [online]. 2023, **9**(2), p. 222-227. eISSN 2405-9595. Available from: https://doi.org/10.1016/j.icte.2021.12.016

[12] KWAK, J., LEE, Y., CHOI, M., LEE, S. Deep learning based approaches to enhance energy efficiency in autonomous driving systems. *Energy* [online]. 2024, **307**, 132625. ISSN 0360-5442, eISSN 1873-6785. Available from: https://doi.org/10.1016/j.energy.2024.132625

[13] MOHAMMADPOUR, M., KELOUWANI, S., GAUDREAU, M. A., ZEGHMI, L., AMAMOU, A., BAHMANABADI, H., ALLANI, B., GRABA, M. Energy-efficient motion planning of an autonomous forklift using deep neural networks and kinetic model. *Expert Systems with Applications* [online]. 2024, **237**, 121623. eISSN 1873-6793. Available from: https://doi.org/10.1016/j.eswa.2023.121623

[14] LI, D., ZHANG, H., CHENG, J., LIU, B. Improving efficiency of DNN-based relocalization module for autonomous driving with server-side computing. *Journal of Cloud Computing* [online]. 2024, **13**(1), 25. eISSN 2192-113X. Available from: https://doi.org/10.1186/s13677-024-00592-1

[15] KHANMOHAMMADI, F., AZMI, R. Time-series anomaly detection in automated vehicles using D-CNN-LSTM Autoencoder. *IEEE Transactions on Intelligent Transportation Systems* [online]. 2024, **25**(8), p. 9296-9307. ISSN 1524-9050, eISSN 1558-0016. Available from: https://doi.org/10.1109/tits.2024.3380263

[16] ELALLID, B., BENAMAR, N., BAGAA, M., KELOUWANI, S., MRANI, N. Improving reinforcement learning with expert demonstrations and vision transformers for autonomous vehicle control. *World Electric Vehicle Journal* [online]. 2024, **15**(12), 585. eISSN 2032-6653. Available from: https://doi.org/10.3390/wevj15120585

[17] KAZMI, S., AKBER, S. GRouteNet: A GNN-based model to optimize pathfinding and smart charging management for autonomous guided vehicles. *Symmetry* [online]. 2024, **16**(12), 1573. eISSN 2073-8994. Available from: https://doi.org/10.3390/sym16121573

[18] COSKUN, S., YAZAR, O., ZHANG, F., LI, L., HUANG, C., KARIMI, H. R. A multi-objective hierarchical deep reinforcement learning algorithm for connected and automated HEVs energy management. *Control Engineering Practice* [online]. 2024, **153**, 106104. ISSN 0967-0661, eISSN 1873-6939. Available from: https://doi.org/10.1016/j.conengprac.2024.106104

[19] WANG, Q., JU, F., WANG, H., QIAN, Y., ZHU, M., ZHUANG, W., WANG, L. Multiagent reinforcement learning for ecological car-following control in mixed traffic. *IEEE Transactions on Transportation Electrification* [online]. 2024, **10**(4), p. 8671-8684. eISSN 2332-7782. Available from: https://doi.org/10.1109/tte.2024.3383091

[20] BARRIOS, F. A., BISWAS, A., EMADI, A. Deep learning-based motion prediction leveraging autonomous driving datasets: state-of-the-art. *IEEE Access* [online]. 2024, **12**, p. 93318-93332. eISSN 2169-3536. Available from: https://doi.org/10.1109/access.2024.3423809

[21] CHENG, S., HU, B.-B., WEI, H.-L., LI, L., LV, C. Deep learning-based hybrid dynamic modelling and improved handling stability assessment for autonomous vehicles at driving limits. *IEEE Transactions on Vehicular Technology* [online]. 2025, **74**(4), p. 5582-5593. ISSN 0018-9545, eISSN 1939-9359. Available from: https://doi.org/10.1109/tvt.2024.3515209

[22] UD DIN, I., ALMOGREN, A., RODRIGUES, J. J. AIOT integration in autonomous vehicles: Enhancing road cooperation and traffic management. *IEEE Internet of Things Journal* [online]. 2024, **11**(22), p. 35942-35949. eISSN 2327-4662. Available from: https://doi.org/10.1109/jiot.2024.3387927

[23] LIU, C., SHENG, Z., LI, P., CHEN, S., LUO, X., RAN, B. A distributed deep reinforcement learning-based longitudinal control strategy for connected automated vehicles combining attention mechanism. *Transportation Letters - The International Journal of Transportation Research* [online]. 2024, **17**(2), p. 183-199. ISSN 1942-7867, eISSN 1942-7875. Available from: https://doi.org/10.1080/19427867.2024.2335084

[24] KHATTAK, Z. H. Cybersecurity vulnerability and resilience of cooperative driving automation for energy efficiency and flow stability in smart cities. *Sustainable Cities and Society* [online]. 2024, **106**, 105368. ISSN 2210-6707, eISSN 2210-6715. Available from: https://doi.org/10.1016/j.scs.2024.105368

[25] ONUR, F., GONEN, S., BARIŞKAN, M. A., KUBAT, C., TUNAY, M., YILMAZ, E. N. Machine learning-based identification of cybersecurity threats affecting autonomous vehicle systems. *Computers and Industrial Engineering* [online]. 2024, **190**, 110088. ISSN 0360-8352, eISSN 1879-0550. Available from: https://doi.org/10.1016/j.cie.2024.110088

[26] LOGANATHAN, R., SELVAKUMARASAMY, S. An efficient privacy-preserving authentication scheme for internet of vehicles based on blockchain technology with hybrid adaptive network. *Peer-to-Peer Networking and Applications* [online]. 2025, **18**(3), 99. ISSN 1936-6442, eISSN 1936-6450. Available from: https://doi.org/10.1007/s12083-024-01864-y

[27] HUANG, J., YU, T., ZHU, X., YANG, F., LAI, X., ALFARRAJ, O., YU, K. Energy Efficiency Maximization in UAV-assisted intelligent autonomous transport system for 6G networks with energy harvesting. *IEEE Transactions on Intelligent Transportation Systems* [online]. 2025, **26**(10), p. 17212 - 17222. ISSN 1524-9050, eISSN 1558-0016. Available from: https://doi.org/10.1109/tits.2024.3445088

[28] LIU, H., YUAN, T., ZENG, X., GUO, K., WANG, Y., MO, Y., XU, H. Eco-driving strategy for connected automated vehicles in mixed traffic flow. *Physica A: Statistical Mechanics and its Applications* [online]. 2024, **633**, 129388. ISSN 0378-4371, eISSN 1873-2119. Available from: https://doi.org/10.1016/j.physa.2023.129388

[29] Mechanical vibration and shock-evaluation of human exposure to whole-body vibration. Part 1: general requirements.
[30] SEZAVAR, A., ATTA, R., GHANBARI, M. DCapsNet: deep capsule network for human activity and gait recognition with smartphone sensors. *Pattern Recognition* [online]. 2024, **147**, 110054. ISSN 0031-3203, eISSN 1873-5142. Available from: https://doi.org/10.1016/j.patcog.2023.110054
[31] ZHANG, Z., CHEN, X., WANG, C., WANG, R., SONG, W., NIE, F. Structured multi-view K-means clustering. *Pattern Recognition* [online]. 2025, **160**, 111113. ISSN 0031-3203, eISSN 1873-5142. Available from: https://doi.org/10.1016/j.patcog.2024.111113
[32] Kaggle repository [online]. Available from: https://www.kaggle.com/datasets/solesensei/solesensei_bdd100k

DEVELOPMENT AND RESEARCH OF SPECIAL EXCAVATOR BUCKETS FOR MINING OIL-BITUMINOUS ROCKS

Yerbol Kaliyev[1], Shynbolat Tynybekov[2], Rashida Duisen[2], Abish Torgayev[1], Nurbol Kamzanov[2], Kazyna Ashim[3], Rustem Kozbagarov[1,*]

[1]Mukhametzhan Tynyshbayev ALT University, Almaty, Republic of Kazakhstan
[2]Satbayev University, Almaty, Republic of Kazakhstan
[3]Nazarbayev Intellectual Schools of Chemistry and Biology, Almaty, Republic of Kazakhstan

*E-mail of corresponding author: ryctem_1968@mail.ru

Yerbol Kaliyev 0000-0002-1961-4809,
Rashida Duisen 0009-0009-2992-717X,
Nurbol Kamzanov 0000-0002-2420-8362,
Rustem Kozbagarov 0000-0002-7258-0775
Shynbolat Tynybekov 0009-0002-6146-2076,
Abish Torgayev 0000-0002-8263-6779,
Kazyna Ashim 0009-0002-1496-1278,

Resume

Given the shortage of petroleum bitumen in the Republic of Kazakhstan, the use of local bitumen-containing rocks is becoming increasingly relevant, which requires the development of specialized mechanization tools. In this paper are discussed the special excavator buckets designed for year-round extraction of rocks with a bitumen content of up to 25%. The design features of the bucket that reduce resistance during digging and unloading are described. Calculations of resistance, chip thickness, operation duration, and productivity of the EO-4121 excavator at different temperatures and bitumen contents were performed. It is shown that unloading becomes more difficult when the bitumen content exceeds 18.2%. A comparison of the calculated and experimental data confirmed the high accuracy of the models used.

Article info

Received 5 January 2026
Accepted 10 April 2026
Online 20 April 2026

Keywords:

excavator
bucket
bitumen
productivity
rocks

Available online: https://doi.org/10.26552/com.C.2026.025

ISSN 1335-4205 (print version)
ISSN 2585-7878 (online version)

1 Introduction

Production of means for mechanization development, transportation and use of bitumen-containing rocks in the Republic of Kazakhstan is still episodic [1]. At the same time, the road organizations of the country require 1.7 million tons of bitumen annually for construction, repair and maintenance of highways. They receive less than half of the required amount, because bitumen, a heavy residue of oil refining, is a scarce material.

Regardless of how much its production increases, practice shows that the lack of bitumen will remain acute. In large volumes bitumen is used in industrial, civil, agricultural and other construction sites, in the production of roofing, thermal and waterproofing materials, in nuclear power engineering as a means of protection against radioactive radiation, in the paint and electrical industry, as well as in other sectors of the economy. In general, the need for bitumen is now estimated at several million tons per year. The current deficit can be largely balanced by expanding the use of domestic bitumen-containing rocks [2].

Progress in the use of bitumen-containing rocks in various sectors of the national economy depends crucially on creation of the new special tools and machine systems for development, transportation and processing, in which the fundamental scientific and technical ideas are materialized.

Special means of mechanization lay the foundation for a wide access to fundamentally new, resource-saving technologies based on the bitumen-containing rocks, increase in labor productivity and product quality. Production persistently raises questions of improvement and creation of mechanization means, as success in the use of rocks is primarily determined by the efficiency and productivity of the tools used [3]. It should be noted that the rock properties make the existing tools inoperable and work with a sharp decrease in productivity precisely in the process of their interaction with the working bodies of the applied means of mechanization.

The performed work was aimed at creation of special excavator buckets, allowing extraction of bitumen-containing rocks with bitumen content up to 25% in year-round operation. The use of such equipment would allow to extract bitumen-containing rocks directly by excavators without powerful bulldozers.

It should be noted that the subject of this study is closely related to the field of "Mechanical Engineering in the Transport Industry" and the objectives of the automotive industry, since the development of specialized buckets and working parts for excavators is aimed at increasing the efficiency of extracting bitumen-containing raw materials, which are the basis for the production of road construction materials. Modern transport engineering considers construction and quarry machinery to be an important link in the technological chain of transport infrastructure development. Improving the productivity and reliability of earthmoving equipment directly affects the pace of construction and repair of motorways, the performance characteristics of road surfaces, and the economic sustainability of the motor transport system as a whole.

2 Materials and methods

Oil-bituminous rocks have high strength characteristics, especially at low positive temperatures, which makes it difficult to extract them mechanically using standard mining and construction equipment [4]. At sub-zero temperatures or in early spring and late autumn conditions, the strength of these rocks increases, making it impossible to break them down effectively without the use of specialized equipment. In view of this, to ensure stable extraction of these materials, it is necessary to use slow-moving or slow-moving transport machines equipped with hydraulic drives. This allows the speed of the working parts to be adjusted depending on the level of resistance encountered, thus ensuring more stable and energy-efficient operation.

Currently available single-bucket excavators are equipped with buckets with teeth that are well suited for breaking up dense and hard soils such as loam, gravel, frozen or rocky soil. In such cases, the force is concentrated on the teeth, which allows the load to be concentrated and the material to be broken up effectively [5]. However, the oil-bituminous rocks differ significantly in structure. They are elastic-viscoplastic materials that are not prone to brittle fracture like mineral rocks. When cutting these rocks with a bucket, the so-called drain-type chips are formed-an elongated, viscous, and sticky mass.

When using a bucket with teeth in such conditions, cutting efficiency is significantly reduced. This is due to the fact that the material is destroyed between the teeth by the blunt part of the bucket, known as the gum. The gum has a large contact area with the rock, creating excessive resistance and increasing the energy consumption of the mining process. Moreover, due to the accumulation of material on the inner surfaces of the teeth and gums, friction increases, which negatively affects the performance of the equipment, as well.

To increase the efficiency of cutting oil-bituminous rocks, it is recommended to use buckets with a continuous cutting edge sharpened along the entire length [6]. This design allows for a uniform and directed force across the entire width of the cut chips. The reduced thickness of the edge and sharpening achieve an oblique cutting effect, in which the forces are distributed more evenly and the resistance of the material is reduced. This not only improves the performance of the excavator, but reduces wear on the cutting elements, as well.

The standard excavator buckets were originally designed for working with loose or loose materials that have a small natural slope angle, typically up to 30-40°. In such cases, the bucket is made in the form of a vessel with one open side, through which both material intake and subsequent unloading are carried out. However, the oil-bituminous rocks have a significantly larger natural slope angle-up to 80°, which eliminates the possibility of material spillage. In this regard, there is no need for side walls on the bucket. Moreover, the presence of such walls only increases the contact area between the bucket and the rock, which leads to increased resistance during unloading.

It should be noted that oil-bituminous rocks tend to adhere strongly to metal surfaces, especially at elevated temperatures and when the bitumen content exceeds 18-20% [7]. This significantly complicates the process of unloading material from the bucket, often making it impossible without the use of auxiliary means such as vibrators, mechanical scrapers, or manual labor. In the design of the proposed buckets, the absence of side walls significantly reduces the area of contact between the material and the surface, thereby facilitating unloading even at high levels of stickiness.

In addition, the oil-bituminous rocks have the high moisture content, which contributes to formation of a monolith inside the bucket. This, in turn, simplifies the task of retaining material in the bucket even if there are slots or holes in its walls. Therefore, solid side and rear walls are not required. To reduce the weight of the equipment, increase maneuverability, and reduce energy consumption, it is proposed to manufacture the rear wall and side elements of the bucket perforated or with longitudinal slits oriented in the direction of chip movement [8]. Such slits not only serve to lighten the structure, but also create conditions for mechanical cleaning of the bucket from adhering material.

The proposed ladle consists only of a bottom and a back wall. To simplify manufacturing, they should represent a single surface of cylindrical shape. To ensure that the capacity of the proposed bucket is equal to that of a standard bucket, it should be slightly larger in width or height. Bucket designs are shown in Figure 1.

The bucket EO-AT-01 consists of the following main

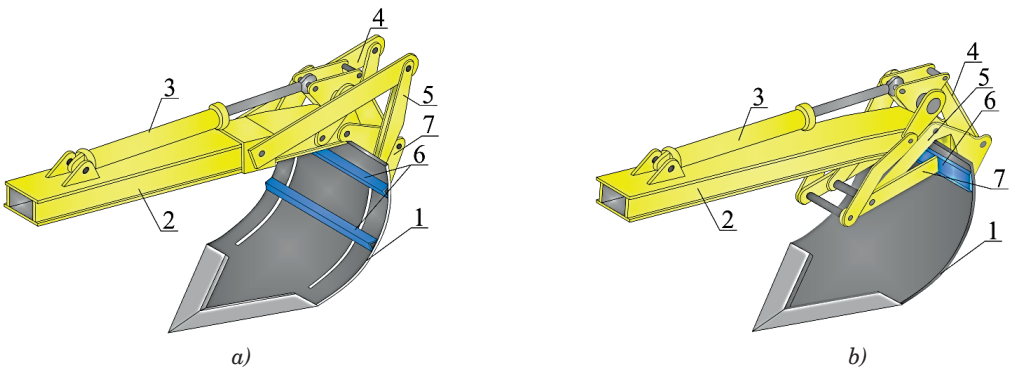

Figure 1 *Excavator working equipment: a) with two cleaning devices; b) with one cleaning device; 1 - bucket; 2 - handle; 3 - hydraulic cylinder; 4 - linkage system; 5 - tie rod; 6 - tie rod; 7 - cleaning frame*

parts (Figure 1, a). Bucket 1 is connected to the handle 2 and is driven by hydraulic cylinder 3 through the lever system 4. One end of the rod 5 is rigidly connected to the bucket body 1, and the rod 6 to the lever system 4. The other end of the link 5 and the link 6 are articulated with the cleaning frame 7. In the initial position, the cleaning frame is behind the bucket.

When turning the bucket for scooping the material, the link 5 turns together with the bucket, and the cleaning frame 7 turns with the link 6 in relation to the joints of the link 5 and in the final stage approaches the handle 2 (Figure 1, b). When unloading, the bucket is rotated in the opposite direction, the cleaning frame moves along the cylindrical bottom of the bucket and cleans it.

Working equipment of EO-AT-02 (Figure 2, a) includes a bucket 1 fixed on the handle 2 and driven by a hydraulic cylinder 3. Levers 4 are rigidly fixed on the handle by means of clamps, which are connected with the cleaning frame 6 through rods 5. The frame is attached to the rods through slots in the bucket bottom.

The working equipment of the excavator works as follows. When the bucket moves along the face, the cutting edge cuts the rock chips. As the bucket is filled with rock (Figure 2, b), it is rotated by hydraulic cylinder 3, and the cleaning device is moved in the direction of rock movement by means of rods 5. After the bucket is filled with rock, the excavator bucket is moved to the unloading position (Figure 2, c), rotated, and the bucket is unloaded under the action of gravity. Part of the rock, adhering to the inner surface of the bucket is cut off by cleaning frame 6, which, when the bucket is turned towards the cutting edge, slides along the inner walls to ensure the complete discharge of the sticky material. This mechanism prevents the accumulation of bitumen and maintains the high volumetric efficiency of the bucket throughout the working cycle. After that, the working equipment of the excavator is transferred to the initial position and the work cycle is repeated.

Oil-bituminous rocks adhere to the surface of the bottom and rear wall of the proposed bucket. Its cleaning is the most expedient to be carried out mechanically by movement of a special cleaning element [9]. To avoid an increase in the equipment costs, without reducing its reliability, it is advisable to move the cleaning element not by a special drive (hydraulic cylinder), but with the help of levers fixed on the handle. When turning the bucket for unloading, the lever located on the back side of the bucket should move the cleaning element, and for this purpose it is advisable to use longitudinal slots made to reduce the weight of the bucket.

3 Results and discussions

Increase of working capacity of developing machines is possible at reduction of resistances to movement of the working body, and also saving the technological operations performance time. Next is considered the possibility of application in the development of oil-bituminous rocks excavator EO-4121, which has the following indicators: cutting force 145 kN, bucket movement speed 0.03 - 0.4 m/s, unloading rotation time 4 s, capacity 1000 mm^3, cutting angle 30° [10].

The working capacity of the equipment is reduced due to difficulties in overcoming resistances during digging and releasing the working bodies from the rock. Resistances arising during the rock development can be calculated based on the parameters of working bodies and properties of the medium, using dependencies obtained from interaction models.

The combinations of parameters, at which the excavator operation is possible, are to be found next. As it was shown earlier, the resistance can be determined from [11]:

$$P = 1.24 \cdot b \cdot h \cdot \left(\frac{1}{2}\gamma \cdot h \cdot A_1 + K_{v1} \cdot \rho_1 \cdot A_2 + \right. \\ \left. + K_{v2} \cdot \rho_2 \cdot A_3\right), N, \quad (1)$$

where P - digging resistance, N; b - bucket width, mm; γ - material density, N/m^3; A_1, A_2, A_3- analytical ratios; ρ_1 - stickiness, Pa; ρ_2 - coupling, Pa; K_{v1} - coefficient of influence of load application speed on stickiness value; K_{v2} - coefficient of influence of the load application speed on the adhesion value.

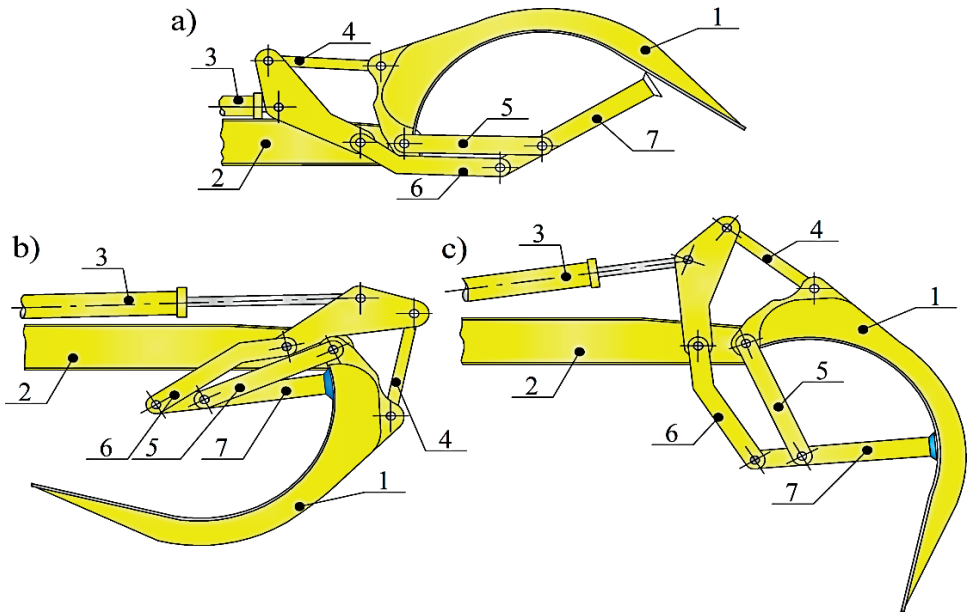

Figure 2 *Excavator working equipment: a) start of operation; b) bucket filling process; c) unloading position; 1 - bucket; 2 - arm; 3 - hydraulic cylinder; 4 - linkage system; 5 - link; 6 - link; 7 - scraper frame*

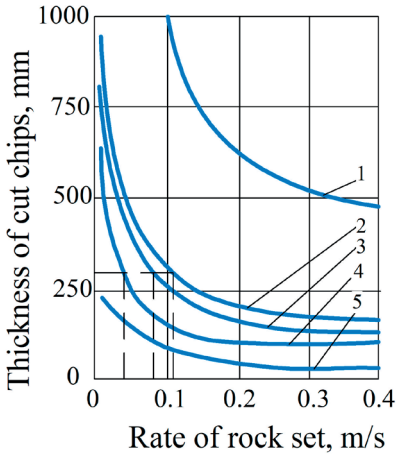

Figure 3 *Effect of speed on possible chip thickness: 1 - bitumen content 25%,temperature 20 °C; 2 - 18.5% and 20°C; 3 - 18.5% and 10°C; 4 - 10% and 20°C; 5 - 10% and 0°C.*

The maximum force on the cutting edge of the excavator bucket is 145 kN. Taking into account this (limit force) according to:

$$P_{01} = b \cdot h \cdot \left(\frac{\gamma \cdot h}{2} \cdot A_1 + K_{v1} \cdot \rho_1 \cdot A_2 + \right. \\ \left. + K_{v2} \cdot \rho_2 \cdot A_3\right), N \quad (2)$$

For the rock with bitumen content of 10 and 30% at temperatures of 0 and 40 °C the influence of cutting speed on the possible thickness of cut chips was established (Figure 3).

At the bucket set path length L, the required thickness of the cut chips can be found from [12]:

$$h = \frac{q \cdot K_n}{L \cdot b}, \text{ mm} \quad (3)$$

where q - bucket capacity equal to 1 m^3; K_n - rock recruitment loss factor, K_n = 1.2; L- material path length, L = 4000 mm; b - bucket width (b = 1000 mm).

For the single scooping, the thickness of the cut chip is 300 mm. Based on this it is possible to find optimal cutting speeds of rock (Figure 3) for specific conditions. Thus, the optimum rock cutting speed with bitumen content at 0 °C is 0.003, with 30 % - 0.08, and at 40 °C - 0.11 and 0.6 m/s.

Based on the constant length of the rock picking path at the optimum speed of the implemented movement, the duration of this operation can be determined depending on the temperature and cohesion value (Figure 4). The limit value of adhesion, at which the equipment operation is irrational, depends on the bitumen content,

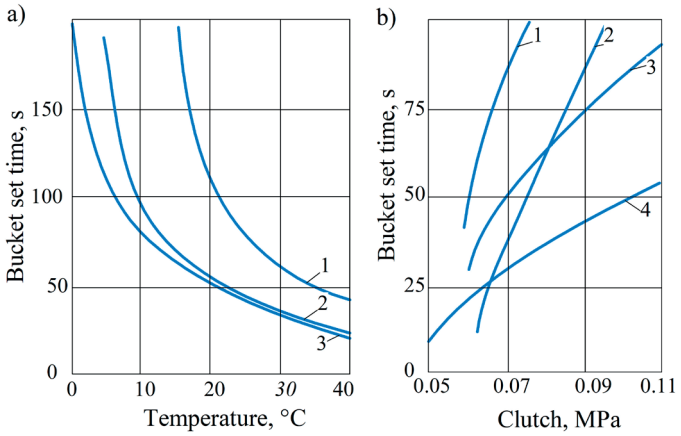

Figure 4 *Impact: a) rock temperatures: 1 - bitumen 10%; 2 - bitumen 18.5; 3 - bitumen 20; b) of the clutch on the bucket take-up time: 1 - bitumen 10%; 2 - bitumen 18.5%; 3 - bitumen 25%*

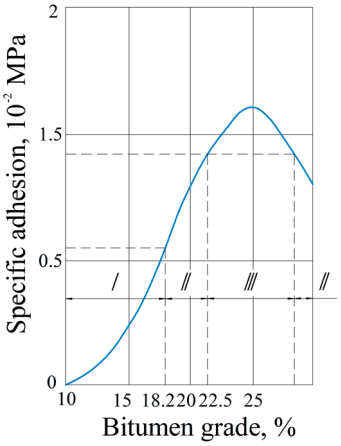

Figure 5 *Zones of workability of excavator EO-4121 on bucket unloading depending on bitumen content in rock: I - smooth unloading, II - longer operation, III - unloading is impossible*

temperature and the maximum possible duration of the operation [13].

The specific adhesion, depending on the bitumen content of the rock and temperature, is evaluated with respect to contact duration and pressure. The inner surface of the excavator bucket contacts the rock in the following way. During the rock recruitment, the cut chip exerts a pressure on the cutting edge and bottom that is larger than the static pressure of its gravity. As the bucket is filled, the pressure from the gravity of the material increases and is transmitted to the side walls, i.e., its magnitude in the rock contact zone changes as the bucket is filled. At the end of filling and after turning the bucket for unloading, the pressure stabilizes [14]. For practical calculations, it is assumed that the pressure value in the contact zone can be determined by Equation (4), and it acts during the bucket filling and bucket rotation for unloading.

The value of pressure in the contact zone can be determined as

$$N = (0.5 - 0.7) \cdot C \cdot S\,, \tag{4}$$

where C - soil developability index by DorNII impactor, blow count; S - half of the bucket projection area in the direction of travel when digging, mm².

Specific adhesion of oil-bituminous rock, which determines the equipment operability, depends on design and technological parameters. The influence of bitumen content in the rock on the workability of the EO-4121 excavator is of interest (Figure 5). At 20°C the rock of the Munaily-Mola deposit can be developed by the excavator with unobstructed bucket unloading if the bitumen content is less than 18.2%. At a higher amount of bitumen, unloading becomes difficult, and at 22.5% it becomes impossible.

Unloading of the rock with bitumen content more than 18.2% is possible, but it will be significantly stretched in time, which leads to a decrease in productivity and the use of manual labor to clean the working bodies. Duration of unloading operation of on rock with specific adhesion above the limit can be determined from the expression

$$t_2 = \frac{\rho_2 \cdot t_1}{2\rho_2 - \rho}, s\,, \tag{5}$$

where ρ_2 - specific adhesion at which the productivity is not reduced, N/mm²; t_1 - bucket turning time for

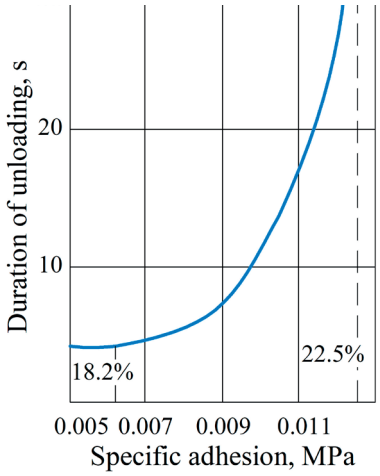

Figure 6 *Dependence of excavator bucket unloading time on specific adhesion of oil-bituminous rock*

unloading, s; ρ - specific rock adhesion for the conditions under consideration, N/mm^2.

The influence of specific adhesion of oil-bituminous rock with different bitumen content, at 20°C, on duration of unloading the excavator bucket is shown in Figure 6. The limiting value of specific adhesion, when unloading of the rock is impossible even when the bucket is held for a long time after its rotation, is 0.0124 N/mm^2.

From the data on duration of the operations, the productivity of the machine as a whole can be determined. Operating capacity of the excavator is:

$$P_e = \frac{60 \cdot q \cdot K_H}{t_s - K_r} \cdot K_b, N\,, \tag{6}$$

where q - excavator bucket capacity equal to 1 m^3; K_H - bucket fill factor; K_r - rock loosening factor (1.1); K_b - excavator time utilization factor (0.85-0.9); t_s - duration of the excavator working cycle, equal to $t_s = t_k + t_n + t_b + t_{nz}$ (t_k, t_n, t_b, t_{nz} - duration of digging, turning to unloading, unloading, turning into the face, respectively), s.

It is assumed that taking into account acceleration and stops during normal operation of the excavator $t_n + t_{nz} = 0.6t_s$. When the excavator is rotated by 90° during the rock unloading, the minimum cycle duration is 18 s, i.e., the duration of rotation to unload and back to the face is 10.8 s.

The duration of the working cycle during extraction of oil-bituminous rocks is determined mainly by the duration of digging and unloading, which depends on the properties of the rock. The change in time spent on these operations affects the excavator productivity (Figure 7).

The standard productivity of the excavator is 91.3 m^3/h. The analysis of the change of excavator productivity at extraction of oil-bituminous rocks allows to note that with the growth of adhesion (at temperature decrease from 40 to 0°C) the excavator productivity at development of rock with bitumen content of 10% decreases due to the increase of bucket filling duration. At development of rock with bitumen content of 25% up to adhesion value of 0.077 N/mm^2 (15°C) the excavator operation is impossible, because the rock is not discharged from the bucket. As the temperature decreases, the stickiness of the rock decreases, which leads to an increase in productivity by reducing the duration of unloading. But since the duration of bucket recruitment increases simultaneously, productivity decreases after 0.0 95 N/mm^2.

Thus, the possibility of development of oil-bituminous rocks depends on strength indicators characterized by adhesion and stickiness. Moreover, material destruction can be ensured by reducing the speed of movement of the working body, while it is impossible to realize bucket unloading under unfavorable conditions without additional improvements of the working body.

The timing of work of excavator E0-4121 at extraction of oil-bituminous rock of Munaily-Mola deposit (Kazakhstan) with bitumen content of 19.4% at 33°C has shown that the duration of working cycle and productivity differ significantly from these indicators at soil development (Table 1).

The angle of internal friction is found by the following equation [15-16]

$$\varphi = 0.019 \cdot B^2 - 1.7 \cdot B + 0.0084 \cdot T^2 + \\ + 0.24 \cdot T - 44,^{\circ} \tag{7}$$

where B - bitumen content, %; T - temperature of oil-bituminous rock, °.

The clutch value is determined by [15-16]:

$$C = 0.000025 \cdot B^2 - 0.00265 \cdot B + \\ + 0.0000075 \cdot T^2 - 0.001 \cdot T + 0.086, \text{MPa}. \tag{8}$$

The stickiness value is found as [15-16]:

$$P_2 = 0.0000575 \cdot T^2 - 0.0038 \cdot T - \\ - 0.000075 \cdot B^2 + 0.00295 \cdot B + 0.107, \text{MPa}. \tag{9}$$

The average rock set path was 4200 mm, bucket travel speed was 0.13 m/s, the thickness of cut chips was 310 mm, and the duration of rock contact with the bucket surface was 42.1 s. Using the field device P10-SU1, the grip and angle of internal friction of the material were determined in the field, which are equal

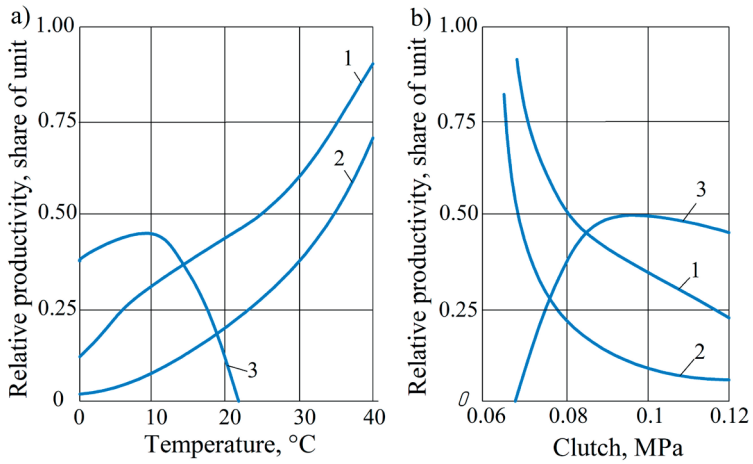

Figure 7 *Dependence of productivity of excavator E0-4121 on: a) rock temperatures: 1 - bitumen content 18.5%; 2 - bitumen content 10%; 3 - bitumen content 25%); b) of petroleum-bituminous rock adhesion: 1 - bitumen content 18.5%; 2 - bitumen content 10%; 3 - bitumen content 25%*

Table 1 *Timekeeping of working cycle of excavator EO-4121*

Operation	Average duration, s	Standard deviation	Coefficient of variation	Confidence interval
Rock set in the bucket	31.2	3.49	11.2	± 2.5
Turning the bucket for unloading	10.9	0.52	4.8	± 0.9
Unloading rock from the bucket	7.8	1.05	13.4	± 0.6
Turning the bucket into the face	7.3	0.31	4.3	± 0.6
Working cycle time	57.2	-	-	-

Table 2 *Correspondence between the production data and those derived from theoretical models*

Indicator	Unit of measurement	Significance		Absolute deviation	Divergence, %
		valid	estimated		
Duration of rock intake into the bucket	s	31.2	32.3	1.1	3.5
Unloading duration	s	7.8	6.2	-1.6	20.5
Cycle duration	s	57.2	56.7	-0.5	0.9
Capacity	m^3/h	55.1	55.4	0.3	0.5

to 0.072 MPa and 18.1°; calculated by Equations (8) and (9), respectively, 0.066 and 16.95° [17-19].

The value of specific adhesion, determined by calculation, at the moment of rock recruitment into the bucket (pressure 0.06 MPa, contact duration 10 s) was 0.0076 N/mm^2, for the moment of bucket unloading (respectively 0.06 and 42.1) - 0.0084 N/mm^2.

As a result of calculation of resistance to bucket displacement (cutting angle $\alpha = 30^{\circ}$) the following values were obtained: when using in the calculation the shear characteristics determined in the fields, 141805 N, when using the calculated values - 132149 N. Discrepancies with the passport characteristic of the force on the cutting edge of the bucket are respectively 2.2 and 8.9%.

The predicted duration of material unloading from the bucket is 6.2 s, which is 20.5% different from the timing data due to the unevenness of unloading. Comparison of calculated values of indicators of the working cycle elements and productivity of the excavator with the actual ones is given in Table 2 [20-22].

The calculated value of working cycle time is 0.9% lower than the actual value, and the calculated productivity is 0.5% higher than the actual value.

4 Conclusion

The conducted studies and calculations confirm the relevance and prospects of development and implementation of specialized excavator buckets for effective extraction of oil bituminous rocks in the conditions of the Republic of Kazakhstan. Taking into account the chronic deficit of oil bitumen in the country and the growing needs of road and construction sector, the use of natural bitumen-containing rocks can become

a significant reserve to replace the scarce material.

The developed bucket designs adapted to the physical and mechanical characteristics of oil-bituminous rocks allow to significantly reduce the cutting forces and resistance during unloading, as well as to increase the productivity of excavator machines. An important advantage is the refusal to use an additional drive for bucket cleaning - the movement of the cleaning frame is realized by the kinematics of the bucket itself, which increases reliability and reduces the cost of equipment.

Modelling of the technological process of rock cutting and unloading allowed to reveal the dependence between the bitumen content, rock temperature and duration of operations. Limit values of rock stickiness and adhesion were determined, at which the use of a standard excavator becomes ineffective or impossible. In those cases it is necessary to use new technical solutions or change the machine operation mode.

Comparison of the calculated data to results of timing observations showed a high degree of coincidence - the differences do not exceed 1%, which confirms the reliability of the proposed model and the possibility of its application in the design and selection of operating modes of excavators.

Thus, the proposed technical solutions and approaches can become a basis for creation of a new generation of machines capable of efficient development of bitumen-containing rocks, reducing operating costs and increasing productivity in conditions of complex geological and climatic factors.

Acknowledgements

The authors received no financial support for the research, authorship and/or publication of this article.

Conflicts of interest

The authors declare that they have no known competing financial interests or personal relationships that could have appeared to influence the work reported in this paper.

References

[1] KAMZANOV, N., TYNYBEKOV, S., BAIKENZHE, N., NAIMANOVA, G., KYRGYZBAY, B., KOZBAGAROV, R. An analytical model for calculating the active interaction forces of the working body of earthmoving machines with sticky soils. *Communications - Scientific Letters of the University of Zilina* [online]. 2026, **28**(1), p. B1-B8. ISSN 2585-7878, eISSN 1335-4205. Available from: https://doi.org/10.26552/com.C.2026.002

[2] LUKASHUK, O. A., LIBERMAN, Y. L. *Rotary trench excavators: design and calculation*. Ekaterinburg: Ural University Publishing House, 2022. ISBN 978-5-7996-3548-0.

[3] DOTSENKO, A. I., KARASEV, G. N., KUSTAREV, G. V., SHESTOPALOV, K. K. *Machines for earthworks*. Moscow: Bastet, 2012. ISBN 978-5-903178-28-5.

[4] MACHNIAK, L., KOZIOL, W. Method of assessment of hard rock workability using bucket wheel excavators. *Archives of Mining Sciences* [online]. 2017, **62**(1), p. 73-82. ISSN 1689-0469, eISSN 0860-7001. Available from: https://doi.org/10.1515/amsc-2017-0006

[5] NURAKOV, S. N., AWWAD, T. Investigation on soil cutting by non-bucket bottom rotor end chisels. *International Journal of GEOMATE* [online]. 2019, **16**(53), p. 231-237. ISSN 2186-2982, eISSN 2186-2990. Available from: https://doi.org/10.21660/2019.53.96902

[6] BURIY, G. G., SHHERBAKOV, V. S., SKOBELEV, S. B., KOVALEVSKIY, V. F. Improvement of the hydraulic excavator bucket design. *Bulletin SibADI* [online]. 2019, **16**(3), p. 202-213. ISSN 2071-7296, eISSN 2658-5626. Available from: https://doi.org/10.26518/2071-7296-2019-3-202-213

[7] WANG, Y., ZHANG, L., LIU, X. Viscosity reduction and drag reduction performance analysis of bionic excavator buckets based on discrete element method. *Bionimetics* [online]. 2024, **9**(11), 686. eISSN 2313-7673. Available from: https://doi.org/10.3390/biomimetics9110686

[8] KOZBAGAROV, R. A., ZHIYENKOZHAYEV, M. S., KAMZANOV, N. S., TSYGANKOV, S. G., BAIKENZHEYEVA, A. S. Design of hydraulic excavator working members for development of mudslides. *News of the National Academy of Sciences of the Republic of Kazakhstan, Series of Geology and Technical Sciences* [online]. 2023, **2**(458), p. 134-141. ISSN 2224-5278, eISSN 2518-170X. Available from: https://doi.org/10.32014/2023.2518-170X.288

[9] SHARMA, D., BARAKAT, N. Evolutionary Bi-objective optimization for bulldozer and its blade in soil cutting. *Journal of The Institution of Engineers (India)*: *Series C* [online]. 2019, **100**(2), p. 295-310. ISSN 2050-0553, eISSN 2050-0545. Available from: https://doi.org/10.1007/s40032-017-0437-z

[10] MAKAROVA, V. V., LAGUNOVA, Y. A., KOVYAZIN, R. A., NESTEROV, V. I. A new approach to creation of hydraulic excavators. *Mining Equipment and Electromechanics* [online]. 2021, **6**, p. 9-14. ISSN 1816-4528, eISSN 2949-0634. Available from: https://doi.org/10.26730/1816-4528-2021-6-9-14

[11] LUKASHUK, O. A., KOMISSAROV, A. P., LETNEV, K. Y. *Machines for soil development. Design and calculation*. Ekaterinburg: Ural University Publishing House, 2018. ISBN 978-5-7996-2386-9.

[12] ABRAMOV, B. N., LUKASHUK, O. A. *Multi-bucket excavators: design and calculation tutorial*. Ekaterinburg: Ural University Publishing House, 2012. ISBN 978-5-321-0205-4.

[13] YANG, CH., HUANG, K., LI, Y., WANG, J., ZHOU, M. Review for development of hydraulic excavator attachment. *Energy Science and Technology* [online]. 2012, **3**(2), p. 93-97. ISSN 1923-8460, eISSN 1923-8479. Available from: https://doi.org/10.3968/j.est.1923847920120302.386

[14] LIBERMAN, Y. L., LUKASHUK, O. A., MAALAOUI, H. Algorithmization of operation of a rotary quarry excavator equipped with a software control system. *Mining Equipment and Electromechanics* [online]. 2025, **6**(182), p. 42-50. ISSN 1816-4528, eISSN 2949-0634. Available from: https://doi.org/10.26730/1816-4528-2025-6-42-50

[15] HE, Q.-H., ZHANG, D.-Q., HAO, P., ZHANG, H.-T. Modeling and control of hydraulic excavator arm. *Journal of Central South University of Technology* [online]. 2006, **13**(4), p. 422-427. ISSN 1005-9484, eISSN 1993-0666. Available from: https://doi.org/10.1007/s11771-006-0061-1

[16] MASAKAZU, H.,WATANABE, H., KAZUO, F. Digging control system for hydraulic excavator. *Mechatronics* [online]. 2001, **11**(6), p. 665-676. ISSN 2326-2885, eISSN 2326-2893. Available from: https://doi.org/10.1016/S0957-4158(00)00043-X

[17] DOVGYALO, V. A., BOCHKAREV, D. I. *Road construction machines. Part I: Machines for earthworks.* Gomel: Belarusian state University of Transport, 2010. ISBN 978-985-468-741-4.

[18] KOZBAGAROV, R. A., AMANOVA, M., KAMZANOV, N., BIMAGAMBETOVA, L., IMANGALIYEVA, A. Investigation of wear of cutting part of polygonal knife car graders in different ground conditions. *Communications - Scientific letters of the University of Zilina* [online]. 2022, **24**(4), p. D229-D238. ISSN 2585-7878, eISSN 1335-4205. Available from: https://doi.org/10.26552/com.C.2022.4.D229-D238

[19] KOZBAGAROV, R. A., ZHUSSUPOV, K. A., KALIYEV, Y. B., YESSENGALIYEV, M. N., KOCHETKOV, A. V. Determination of energy consumption of high-speed rock digging. *News of the National Academy of Sciences of the Republic of Kazakhstan, Series of Geology and Technical Sciences* [online]. 2021, **6**(450), p. 85-92. ISSN 2585-7878, eISSN 1335-4205. Available from: https://doi.org/10.32014/2021.2518-170X.123

[20] TOGIZBAYEVA, B. B., SAZAMBAYEVA, B. T., KENESBEK, A. B., KINZHEBAYEVA, A. S. Calculation method of the working body of a hydraulic excavator. *Bulletin of L. N. Gumilyov Eurasian National University, Technical Science and Technology Series* [online]. 2018, **125**(4), p. 75-80. ISSN 2616-7263, eISSN 2663-1261. Available from: https://doi.org/10.32523/2616-7263-2018-125-4-75-80

[21] KOZBAGAROV, R. A., SHALBAYEV, K. K., ZHIYENKOZHAYEV, M. S., KAMZANOV, N. S., NAIMANOVA, G. T. Design of cutting elements of reusable motor graders in mining. *News of the National Academy of Sciences of the Republic of Kazakhstan, Series of Geology and Technical Sciences* [online]. 2022, **3**(453), p. 128-141. ISSN 2585-7878, eISSN 1335-4205. Available from: https://doi.org/10.32014/2022.2518-170X.185

[22] MUSTAFAYEV, O. B., RAXMONOV, I. I., AXMEDOV, S. T., SHUKUROV, A. R., HUSANOV, L. M. Experimental results on the effectiveness of an improved excavator bucket tooth design. *Web of Technology: Multidimensional Research Journal* [online]. 2024, **2**(2), p. 66-71. eISSN 2938-3757. Available from: https://webofjournals.com/index.php/4/article/view/809

THE STRENGTH ASSESSMENT OF THE HORIZONTAL LEVER IN THE BRAKE TRANSMISSION OF A FREIGHT WAGON BOGIE

Juraj Gerlici[1], Alyona Lovska[1,*], Vasyl Ravlyuk[2], Patrik Slušňák[1]

[1]University of Zilina, Zilina, Slovak Republic
[2]Ukrainian State University of Railway Transport, Kharkiv, Ukraine

*E-mail of corresponding author: Alyona.Lovska@fstroj.uniza.sk

Juraj Gerlici 0000-0003-3928-0567,
Vasyl Ravlyuk 0000-0003-4818-9482,
Alyona Lovska 0000-0002-8604-1764,
Patrik Slusňak 0009-0007-2463-3370

Resume

In this article are discussed the features of selecting the geometric parameters and calculating the strength of the horizontal lever in the brake lever transmission of a freight wagon bogie. The results of the research show that the greatest stresses are concentrated in the areas where the holes for the rollers are located. Since the design stresses are 22% lower than the permissible value, thus the strength of the horizontal lever is obeyed.
This research results could be useful in the design of modern brake lever transmission systems.

Article info

Received 8 August 2025
Accepted 23 November 2025
Online 21 April 2026

Keywords:

railway transport
brake lever transmission system
horizontal lever
strength calculation for a horizontal lever

Available online: https://doi.org/10.26552/com.C.2026.026

ISSN 1335-4205 (print version)
ISSN 2585-7878 (online version)

1 Introduction

The railway traffic safety is a key factor in the efficiency of railway transport [1-3]. Brakes are the most critical unit of the rolling stock, upon the reliability of which the train traffic safety depends. Most modern 1,520-mm gauge freight rolling stock is equipped with single-acting brake lever systems using wheel-mounted brake pads [4-5]. Importantly, the horizontal lever of the brake lever transmission is one of its most critical components (Figure 1). The horizontal lever is designed to transfer force from the brake cylinder rod to the brake pads. It forms a part of the system that applies the brakes the wagon, allowing pads to press against wheels. The horizontal lever provides the reliable and efficient force transmission, which is a key component of the braking system.

In operation, the horizontal lever is subjected to bending stresses due to its fastening diagram and the load applied to it. To ensure the traffic safety, it is important to study the strength of the horizontal lever under operational loads, to identify the most heavily loaded components of its structure and propose solutions aimed at improving it.

To assess the current state of the research into the strength of horizontal levers, an analysis of scientific publications on this topic was carried out.

The operating processes of the brake lever transmission, as well as the wear of the wheel and brake pads in the wheel-shoe braking system of freight wagons using composite pads, are investigated in [6]. The tribological interaction is analysed by means of a bench simulation of the brake lever transmission under the actual braking conditions. The results obtained demonstrate that the use of high-friction composite pads changes the distribution of contact stresses and can lead to accelerated wear of specific areas of the wheel. However, the study does not address the issue of studying the strength of the brake lever transmission components in operation.

The operation of the brake assembly and thermal processes in cast iron pads during the braking is investigated in [7]. Using the numerical simulation, the thermal behaviour of the brake assembly at various braking modes is analysed. The influence of speed, braking duration and the thermal conductivity of the material on the temperature distribution in the contact zone is examined. The achieved results show the formation of significant temperature gradients in the brake pad, which can cause thermal deformations

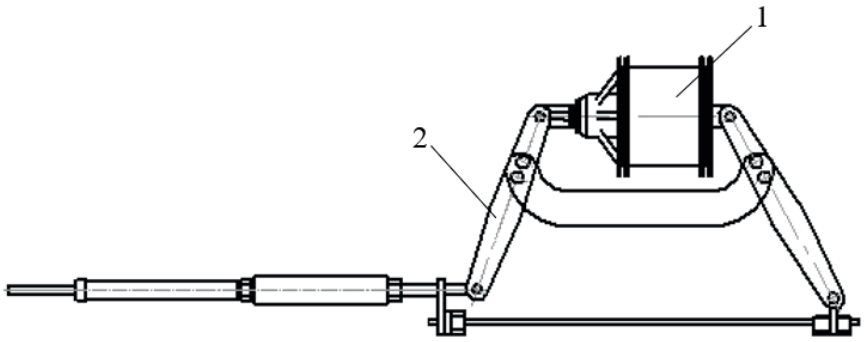

Figure 1 *A location of the horizontal lever in the brake system: 1 - brake cylinder; 2 - horizontal lever*

and accelerated wear of the friction surface. The study was focused on thermal processes, but the strength of the components of the brake lever transmission is not considered.

The operational issues of using the brake lever transmission and composite pads in freight wagons are analysed in [8]. The authors studied their interaction with wheels, the impact of operating conditions on the wear intensity and potential negative consequences of using composite materials. Particularly, it is noted that such brake pads are more sensitive to braking patterns and uneven load distribution, which can lead to accelerated localised wear and changes in the friction coefficient. However, the study does not address the issue of the strength of the brake lever transmission components under operational loads.

The braking system parameters and the conditions governing the generation of the pressing force between the brake pads and the wheel surface are analysed in [9], where the influence of structural and operational factors on the braking efficiency and stability of brake equipment were studied, particularly, the issue of ensuring the necessary brake pressure in the brake systems of freight wagons. The results obtained are used to determine the dependencies between the pressure in the brake cylinder and the pressing force of the pads. However, the authors did not research the strength of the elements of the brake lever transmission that bear the load when braking forces are applied.

The results of numerical optimization and experimental verification of the disc brakes for the freight wagons are presented in [10]. The distribution of stresses and temperatures in the disk under braking is investigated, and a modified profile is proposed using numerical simulation, that improves the heat dissipation and reduces stress concentrations. The experimental tests conducted confirmed an increase in durability and a decrease in the risk of thermal damage to the brake disc. However, the issue of strength and load on the brake components was not studied.

The factors influencing the braking force, transmitted by the brake lever transmission, and the effect of the brake pad material type on the wear rate are described in [11]. The obtained results demonstrate that an increase in the braking force significantly accelerates wear, while the choice of the brake pad material determines the nature of the tribological interaction. However, in the study was not examined the operation of the brake lever transmission components that transmit braking forces to the wheel set.

An experimental study of properties of the organic composite brake pads with a modified friction composition is presented in [12]. It describes a series of laboratory tests to determine the material's mechanical, tribological and thermal properties. It is found that changes in the composition of the friction material can significantly affect the friction coefficient, braking stability and wear intensity. The results obtained confirmed that it is possible to increase the service life of brake pads by optimizing their material composition. However, the authors did not analyse the strength of the brake lever transmission components that transfer braking forces to the wheel set.

The way the elements of the shoe brake affect the wear and fatigue damage of wheels made of different steel grades and used in high-speed railway transport is investigated in [13]. Authors conducted the experimental tribological tests to determine the wear intensity and progression of microdamage in the surface layers of the wheel. It is found that the wheel material significantly affects the nature of the damage and the service life of the wheel-pad interaction. The results obtained made it possible to assess the wear resistance of various steels under braking conditions. However, the strength of the brake lever transmission components under braking conditions was not investigated.

The specifics of conducting the field experiments and numerical modelling of temperature processes are presented in [14]. The authors measured the temperatures of the wheel surface during braking and compare them with the results of numerical calculations. It is established that the contact surface temperature can reach significant values, which profoundly affects the wear intensity and formation of the friction layer. However, the authors did not analyse the strength of the brake lever transmission components.

A comprehensive analysis of the causes of brake system failures associated with the use of metal and composite materials is covered in [15]. It presents a technical and economic analysis of failures of components

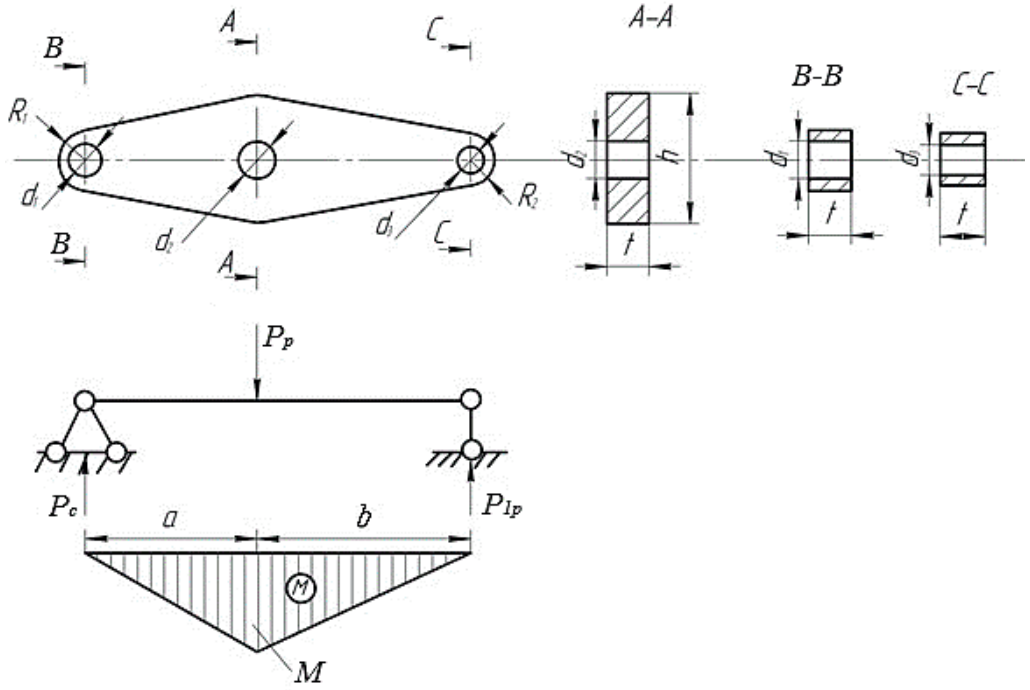

Figure 2 *The design diagram of the horizontal lever: a and b are the lever arms; h is the maximum width; t is the thickness; d_1, d_2, d_3 are the hole diameters; R_1 and R_2 are the end radii; P_c is the cylinder rod force; P_{1P} is the reaction of the brake transmission of the wagon; P_p is the reaction force of the horizontal levers*

of the mechanical part of brakes, particularly brake pads, considering their design features and material. The main factors leading to a reduction in braking efficiency were identified; they include wear, overheating and deterioration of the frictional properties of materials. However, the issue of the strength of the mechanical brake components was not analysed.

An overview and development of mathematical models of pneumatic brake systems of freight trains is presented in [16]. The authors generalized modern approaches to modelling the operation of the brake cylinders and the generation of braking forces in the train. The models designed can be used to analyse the braking dynamics of the train and assess the pneumatic system efficiency. Meanwhile, the study was focused on modelling the pneumatic processes, while the mechanics of the brake lever transmission components subjecting to operational loads during braking was not considered.

The review of scientific publications [6-16] makes it possible to conclude that at present the issue of studying the strength of horizontal levers of the brake lever transmission has yet to be given due attention. Therefore, there is a need for research in this area. This article is devoted to assessing the strength of the horizontal lever of the brake lever transmission. The following research objectives were set:

- to substantiate the geometric parameters of the horizontal lever, and
- to investigate the strength of the horizontal lever using the finite element method (FEM).

2 The substantiation of the geometrical parameters of a horizontal lever

The loading diagram of the horizontal lever in operation was considered, provided that it is a rod on two supports [17]. The design diagram of the horizontal lever and its cross-section shown in Figure 2.

The width h of the lever is determined from

$$[\sigma] \geq \frac{M}{W}, \tag{1}$$

where $[\sigma]$ is the permissible stress arising in the lever during bending, MPa; M is the bending moment in the dangerous cross-section of the lever, Nm; W is the moment of resistance in the cross-section A-A, m^3.

The bending moment can be written as

$$M = P_c \cdot a = P_{1p} \cdot b. \tag{2}$$

For a two-plate lever, the bending moment must be halved.

Then,

$$M = 0.5 \cdot P_c \cdot a = 0.5 \cdot P_{1p} \cdot b. \tag{3}$$

For the section A-A the resistance moment is

$$W = \frac{t \cdot (h^3 - d_2^3)}{6 \cdot h}, \tag{4}$$

in turn, the moment of resistance can be determined from Equation (1) as:

$$W = \frac{M}{[\sigma]}. \quad (5)$$

Then, equating Equations (4) and (5), one obtains

$$\frac{t \cdot (h^3 - d_2^3)}{6 \cdot h} = \frac{M}{[\sigma]}. \quad (6)$$

After the corresponding transformations, an algebraic cubic equation for the width is obtained:

$$h^3 = \frac{6 \cdot M}{t \cdot [\sigma]} h + d_2^3. \quad (7)$$

According to Tartaglia's rule, the root of this equation is

$$h = \sqrt[3]{U} + \sqrt[3]{V}, \quad (8)$$

where U and V is the system solution

$$\begin{aligned} U + V &= d_2^3; \\ U \cdot V &= \left(\frac{6 \cdot M}{3 \cdot t \cdot (\sigma)}\right)^3 = \left(\frac{2 \cdot M}{t \cdot [\sigma]}\right)^3. \end{aligned} \quad (9)$$

Equation (8) can be written as $h^3 + p \cdot h + q = 0$,

where $p = -\frac{6 \cdot M}{t \cdot [\sigma]}, q = -d_2^3$.

When solving Equation (9), the discriminant of the cubic equation can be negative $\Delta = \frac{q^2}{4} + \frac{p^3}{27} < 0$.

In that case, h is calculated as $h_1 = 2\left|\sqrt[3]{r}\right|\left(\cos\frac{\varphi}{3}\right)$,

$h_2 = 2 \cdot \left|\sqrt[3]{r}\right|\left(\cos\frac{\varphi + 2 \cdot \pi}{3}\right)$,

$h_3 = 2 \cdot \left|\sqrt[3]{r}\right|\left(\cos\frac{\varphi + 4 \cdot \pi}{3}\right)$,

where $r = \left|\sqrt{-\frac{p^3}{27}}\right|$ $\varphi = \arccos\left(-\frac{q}{2 \cdot r}\right)$.

It is possible to determine the width h by specifying the standard thickness t of a sheet from the rolled steel product range and the diameter d_2 of an opening from Equations (1) and (8).

Thus, it is possible to determine its geometric parameters for given force effects based on the bending moment acting in the cross-section of the horizontal lever.

The main parameters were determined (Table 1) considering the fact that the lever is a component of the brake lever transmission of the open wagon bogie equipped with an air distributor (No. 483-000). The symbols shown in the header of Table 1 correspond to those shown in Figure 3.

However, the localized effects of the rollers, stress concentrations around the horizontal lever holes, and possible out-of-plane effects on it are not considered in this analytical approach of determining the geometric parameters of the horizontal lever. This is a limitation of this approach.

The next stage of the study included the construction of a spatial model of the horizontal lever and calculation of its strength.

3 The investigation into the horizontal lever strength using the FEM

The strength of the horizontal lever was calculated using the FEM in SolidWorks Simulation. The model of the horizontal lever was built in SolidWorks (Figure 4).

The continual model of the horizontal lever was constructed with tetrahedra (Figure 5). This choice was based on the fact that the mesh was created on a solid body [18-19].

The graph analytical method was used to determine the optimal number of model's elements [20-22]. The model had 4,280 elements. The number of nodes was 7,718. The construction material of the horizontal lever

Table 1 *The main parameters of the horizontal lever, mm*

l	$h \times t$	a	b	d_1	d_2	R
574	110 × 14	195	305	40	45	32

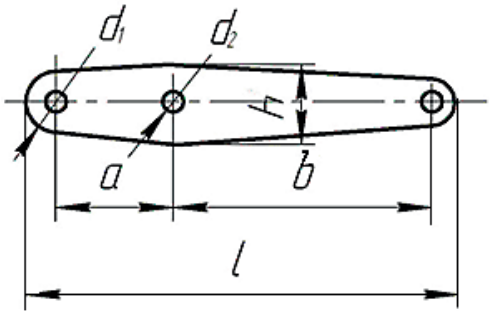

Figure 3 *The geometric parameters of the horizontal lever*

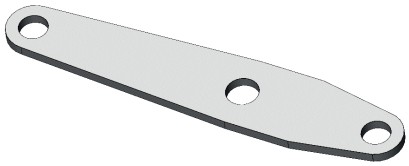

Figure 4 *The spatial model of the horizontal lever*

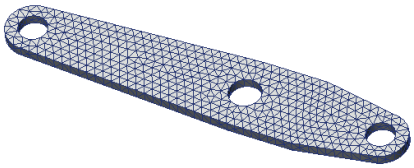

Figure 5 *The finite element model of the horizontal lever*

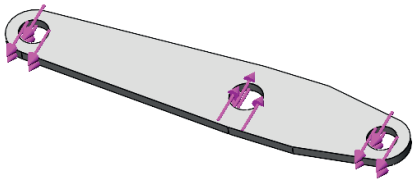

Figure 6 *A calculation scheme of the horizontal lever*

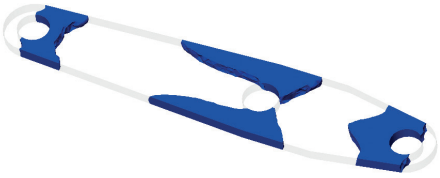

Figure 7 *Concentration zones of the stresses in the horizontal lever*

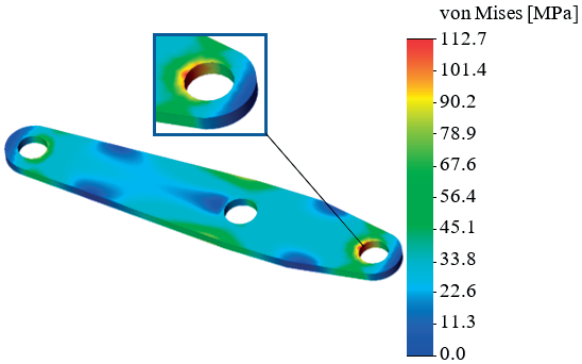

Figure 8 *The stress state of the horizontal lever*

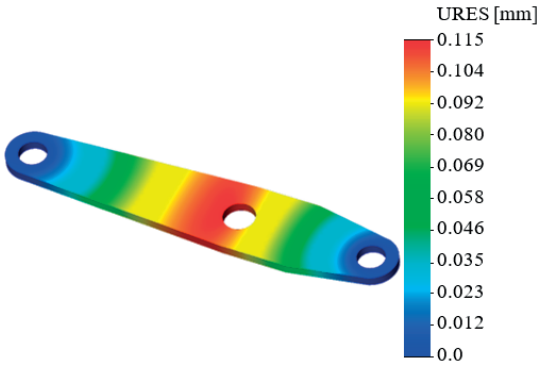

Figure 9 *The displacements in the horizontal lever assemblies*

was steel St. 3 with permissible stresses of 145 MPa [23].

Rigid connections were installed at the points of contact with the rollers. The diagram of the application of forces to the model is shown in Figure 6.

Calculations showed that maximum stresses occur in the areas where the roller holes were located (Figure 7). The maximum stresses were 112.7 MPa (Figure 8). Thus, the calculated stresses are 22% lower than the permissible ones.

The middle part of the lever is subjected to the greatest displacement, which is 0.1 mm (Figure 9).

The calculations made it possible to conclude that the strength of the horizontal lever with the specified geometric parameters was obeyed.

It is important to say that the above approach to calculating the horizontal lever can be used for any type of freight car. Since currently all the types of freight cars with a gauge of 1520 mm are equipped with air distributors of the No. 483-000, which have certain operating modes depending on the loading of the rolling stock: empty, average or loaded, therefore, taking into account the application of a load to the lever that corresponds to one of these modes, the appropriate calculation can be carried out.

At the same time, in conditions of excessive load modes that are not specified in regulatory documents, this approach must be adjusted. In the event of wear of the horizontal lever, its actual geometric dimensions must be taken into account when building a spatial model. In the event of the use of a material with properties different from that of steel of St. 3, the stress calculation criterion according to the finite element method must be replaced by the appropriate one.

The advantage of this study over existing ones is that the authors not only calculated the horizontal lever of the brake system lever, but also identified specific features that influence the determination of its geometric dimensions.

However, the study has its drawbacks. The main one is that the fixing of the horizontal lever was modelled as rigid, that is, the potential friction forces in the areas where the horizontal lever interacted with the rollers were not considered. This will be addressed in the further research.

The research will be useful in the design of modern brake lever transmission systems.

4 Conclusions

1. The rationale for the selection of the geometric parameters of the horizontal lever in the brake lever transmission is presented. It is considered that the lever is a component of the brake lever transmission on the bogie of an open wagon equipped with air distributor No. 483-000. According to the results of the calculations, the geometric parameters of the horizontal lever are determined and its spatial model is built.
2. The strength of the horizontal lever is studied by the FEM. It is established that the stresses are mainly concentrated in the areas where the holes for the rollers are located. The maximum design stress is 112.7 MPa, 22% lower than the permissible value. The greatest displacement is experienced by the middle section of the horizontal lever, with the maximum displacement being 0.1 mm. Therefore, the strength of the horizontal lever is obeyed.

Acknowledgment

This research was supported by the following projects: KEGA 024ZU-4/2024 and VEGA 1/0602/26.

Conflict of interest

The authors declare that they have no conflict of interest in relation to this research, whether financial, personal, authorship or otherwise, that could affect the research and its results presented in this paper.

References

[1] DIZO, J., STEISUNAS, S., BLATNICKY, M. Vibration analysis of a coach with the wheel-flat due to suspension parameters changes. *Procedia Engineering* [online]. 2017, **192**, p. 107-112. ISSN 1877-7058. Available from: https://doi.org/10.1016/j.proeng.2017.06.019

[2] DIZO, J., HARUSINEC, J., BLATNICKY, M. Multibody system of a rail vehicle bogie with a flexible body. *Manufacturing Technology* [online]. 2015, **15**(5), p. 781-788. ISSN 1213-2489, eISSN 2787-9402. Available from: https://doi.org/10.21062/ujep/x.2015/a/1213-2489/MT/15/5/781

[3] DIZO, J., BLATNICKY, M., STEISUNAS, S., SKOCILASOVA, B. Assessment of a rail vehicle running with the damaged wheel on a ride comfort for passengers. *MATEC Web of Conferences* [online]. 2018, **157**, 03004. eISSN 2261-236X. Available from: https://doi.org/10.1051/matecconf/201815703004

[4] RAVLYUK, V., ELYAZOV, I., AFANASENKO, I., RAVLIUK, M. Determination of forces in the elements of the brake rigging of bogies of freight cars. *E3S Web of Conferences* [online]. 2020, **166**, 07003. eISSN 2267-1242. Available from: https://doi.org/10.1051/e3sconf/202016607003

[5] PANCHENKO, S., GERLICI, J., LOVSKA, A., VATULIA, G., RAVLYUK, V., RYBIN, A. Method for determining the factor of dual wedge-shaped wear of composite brake pads for freight wagons. *Communications - Scientific Letters of the University of Zilina* [online]. 2023, **26**(1), p. B31-B40. ISSN 1335-4205, eISSN 2585-7878. Available from: https://doi.org/10.26552/com.C.2024.006

[6] LU, B. H., CHEN, X. Y., QU, B. Z., ZHANG, H. B. Research on wheel-shoe wear for high friction composite brake shoes based on foundation brake rigging in railway wagon. *Key Engineering Materials* [online]. 2015, **667**, p. 530-535. ISSN 1662-9795. Available from: https://doi.org/10.4028/www.scientific.net/KEM.667.530

[7] SOMA, A., AIMAR, M., ZAMPIERI, N. Simulation of the thermal behavior of cast iron brake block during braking maneuvers. *Applied Sciences* [online]. 2021, **11**(11), 5010. eISSN 2076-3417. Available from: https://doi.org/10.3390/app11115010

[8] NISIEWICZ, P., SAWCZUK, W. Composite brake blocks in railway freight wagons: operational problems. *Rail Vehicles/Pojazdy Szynowe* [online]. 2025, **1-2**, p. 9-17. ISSN 0138-0370, eISSN 2719-9630. Available from: https://doi.org/10.53502/RAIL-209083

[9] SHELEIKO, T., SHELEIKO, I. Providing braking pressure for freight train wagons. *Transport Systems and Technologies* [online]. 2018, **1**(32), p. 154-165. ISSN 2617-9040, eISSN 2617-9059. Available from: https://doi.org/10.32703/2617-9040-2018-32-1-154-165

[10] GRIVC, U., DERZIC, D., MUHIC, S. Numerical optimisation and experimental validation of divided rail freight brake disc crown. *Railway Engineering Science* [online]. 2019, **27**, p. 1-10. ISSN 2662-4745, eISSN 2662-4753. Available from: https://doi.org/10.1007/s40534-018-0174-x

[11] SULISTYO, H., VIYUS, V. Simulation on the effect of braking force and brake shoe material type on the wear rate of railway bogie brake block. *Journal of Mechanical Engineering, Industrial, Electrical Engineering and Information Technology* [online]. 2024, **3**(3), p. 378-394. ISSN 2963-8208, eISSN 2963-7805. Available from: https://doi.org/10.55606/jtmei.v3i3.4277

[12] WASILEWSKI, P. Experimental study on the effect of formulation modification on the properties of organic composite railway brake shoe. *Wear* [online]. 2017, **390-391**, p. 283-294. ISSN 0043-1648, eISSN 1873-2577. Available from: https://doi.org/10.1016/j.wear.2017.08.007

[13] MAZZU, A., PROVEZZA, L., ZANI, N., PETROGALLI, C., GHIDINI, A., FACCOLI, M. Effect of shoe braking on wear and fatigue damage of various railway wheel steels for high speed applications. *Wear* [online]. 2019, **434-435**, 203005. ISSN 0043-1648, eISSN 1873-2577. Available from: https://doi.org/10.1016/j.wear.2019.203005

[14] WALIA, M. S., VERNERSSON, T., LUNDEN, R., BLENNOW, F., MEINEL, M. Temperatures and wear at railway tread braking: field experiments and simulations. *Wear* [online]. 2019, **440-441**, 203086. ISSN 0043-1648, eISSN 1873-2577. Available from: https://doi.org/10.1016/j.wear.2019.203086

[15] MUFLIKHUN, M. A., ADYUDYA, M., RAHMAN, N. F., SENTANUHADY, J., RAGHU, S. N., V. Comprehensive analysis and economic study of railway brake failure from metal-based and composite-based materials. *Engineering Failure Analysis* [online]. 2023, **12**, 100223. eISSN 2666-3597. Available from: https://doi.org/10.1016/j.finmec.2023.100223

[16] WU, Q., COLE, C., SPIRYAGIN, M., CHANG, CH., WEI, W., URSULYAK, L., SHVETS, A., MURTAZA, M. A., MIRZA, I. M., ZHELIEZNOV, K., MOHAMMADI, S., SERAJIAN, H., SCHICK, B., BERG, M., SHARMA, R. CH., ABOUBAKR, A., SHARMA, S. K., MELZI, S., DI GIALLEONARDO, E., BOSSO, N., ZAMPIERI, N., MAGELLI, M., ION, C. C., ROUTCLIFFE, I., PUDOVIKOV, O., MENAKER, G., MO, J., LUO, S., GHAFOURIAN, A., SERAJIAN, R., SANTOS, A. A., PAVANI TEODORO, I., JAVORSKI ECKERT, J., PUGI, L., SHABANA, A., CANTONE, L. Freight train air brake models. *International Journal of Rail Transportation* [online]. 2023, **11**(1), p. 1-49. ISSN 2324-8378, eISSN 2324-8386. Available from: https://doi.org/10.1080/23248378.2021.2006808

[17] RAVLYUK, V. G., AFANASENKO, I. M. Assignments for a course project with methodological instructions on the discipline "Automatic brakes and traffic safety". Kharkiv: UkrSART, 2012.

[18] KOWALSKI, S., CIESLIKOWSKI, B., BARTA, D., DIZO, J., DITTRICH, A. Analysis of the operational wear of the combustion engine piston pin. *Lubricants* [online]. 2023, **11**(3), 100. eISSN 2075-4442. Available from: https://doi.org/10.3390/lubricants11030100

[19] BLATNICKY, M., STAUDEROVA, M., DIZO, J. Numerical analysis of the structure girder for vehicle axle scale calibration. *Procedia Engineering* [online]. 2017, **177**, p. 510-515. ISSN 1877-7058. Available from: https://doi.org/10.1016/j.proeng.2017.02.253

[20] PANCHENKO, S., GERLICI, J., LOVSKA, A., RAVLYUK, V., DIZO, J., HARUSINEC, J. Analysis of asymmetric wear of brake pads on freight wagons despite full contact between pad surface and wheel. *Symmetry* [online]. 2024, **16**(3), 346. eISSN 2073-8994. Available from: https://doi.org/10.3390/sym16030346

[21] PANCHENKO, S., GERLICI, J., LOVSKA, A., RAVLYUK, V., DIZO, J., HARUSINEC, J. Study on the strength of the brake pad of a freight wagon under uneven loading in operation. *Sensors* [online]. 2024, **24**(2), 463. eISSN 1424-8220. Available from: https://doi.org/10.3390/s24020463

[22] KONDRATIEV, A., PISTEK, V., GAJDACHUK, V., KHARCHENKO, M., NABOKINA, T., KUCERA, P., KUCERA, O. Effect of ply orientation on the mechanical performance of carbon fibre honeycomb cores. *Polymers* [online]. 2023, **15**(11), 2503. eISSN 2073-4360. Available from: https://doi.org/10.3390/polym15112503

[23] DSTU 7598:2014. Freight wagons. General requirements for calculations and design of new and modernized wagons of 1520 mm track (non-self-propelled). Kiev: Ukrainian Research Institute of Carriage Building, 2015.

DEVELOPMENT AND RESEARCH OF WORKING PARTS OF JOINT CUTTING MACHINES WITH CYCLOIDAL MOTION

Yerbol Kaliyev[1], Turly Dyussengaliyeva[1], Beibitbek Zhunisbekov[2], Manarbek Yessengaliyev[1], Nurbol Kamzanov[2], Zhuldyz Dainova[3], Rustem Kozbagarov [1,*]

[1]Mukhametzhan Tynyshbayev ALT University, Almaty, Republic of Kazakhstan
[2]Satbayev University, Almaty, Republic of Kazakhstan
[3]Ekibastuz Engineering and Technical Institute named after academician K. Satpayev, Ekibastuz, Republic of Kazakhstan

*E-mail of corresponding author: ryctem_1968@mail.ru

Yerbol Kaliyev 0000-0002-1961-4809,
Beibitbek Zhunisbekov 0009-0005-0067-2178,
Nurbol Kamzanov 0000-0002-2420-8362,
Rustem Kozbagarov 0000-0002-7258-0775
Turly Dyussengaliyeva 0000-0002-0844-0807,
Manarbek Yessengaliyev 0000-0002-6905-5208,
Zhuldyz Dainova 0000-0003-3061-4858,

Resume

The development of a country's economy largely depends on the pace and efficiency of construction work, which, in turn, is determined by the extent to which innovative technologies and techniques are used. This work is devoted to justification of the basic parameters and the development of a new working body for a machine for cutting joints in road surfaces. A design with cycloidal motion is proposed, which intensifies the destruction process due to the vibrational impact of the cutters on the material being processed. The use of such a working body provides a vibrational effect, increases the cutting speed, and reduces the energy consumption of the process. As a result of intensifying the interaction between the working body and the material, it was possible to reduce the energy consumption of cutting by 1.13 times, and increase productivity by 1.18 times compared to analogues.

Article info

Received 5 January 2026
Accepted 10 April 2026
Online 21 April 2026

Keywords:

working body
slitting machine
cycloidal motion
energy consumption
cutting force

Available online: https://doi.org/10.26552/com.C.2026.027

ISSN 1335-4205 (print version)
ISSN 2585-7878 (online version)

1 Introduction

In Kazakhstan, a number of important tasks related to creation of new and highly productive equipment, and the modernization of existing technical means in road construction, are to be solved in the shortest possible time to improve the quality of work in the construction and repair of motorways. The mechanization of the construction, repair, and reconstruction of urban and road facilities is linked to the implementation of measures to reduce the energy and material costs of their implementation, which requires new, high-performance, and less energy-intensive equipment [1-3].

In this regard, the great importance is devoted to machines designed for cutting joints in road surfaces. The main disadvantages of existing machines are: low productivity and reliability of the machine's working body, high energy consumption, and significant dimensions and weight of the working body. Based on an analysis of scientific and technical literature [2-4], it has been established that existing joint cutting machines are inefficient, have high energy consumption, and low reliability of chain working parts. According to the analysis of existing machine designs and theoretical and experimental studies of soil cutting processes, it has been established that existing cutter machines have practically exhausted their potential for further productivity improvements, creating a need for more efficient, high-performance, and less energy-intensive cutter machines.

The main idea of this work was to use the principle of cycloidal motion to cut slots in road surfaces, which allows for more intense interaction between the working body and the material being processed. In addition, the working bodies of the slot cutting machine are made according to mutually enveloping cycloidal curves, which allow for the minimum possible specific energy consumption of the working process.

The cycloidal (planetary-rotary) motion of the working parts of machines significantly reduces their weight and dimensions and expands their technological capabilities. A positive feature of machines with cycloidal motion of working parts is that they can operate at speeds significantly exceeding those calculated for traditional machines [5-7].

It is precisely in these areas that the development of a new design for a road cutting machine with cycloidal movement of the working body is justified. This machine design makes it possible to intensify the process of road surface destruction by means of the vibrational impact of the cutters on the material being worked on, reduce the energy intensity of the cutting process, and expand the technological capabilities of the machine. Thus, the justification of the parameters and development of the working body of the machine for cutting joints is a very urgent task aimed at finding and creating new innovative technology [4].

The subject matter of this study is directly related to the field of "Mechanical Engineering in the Transport Industry" and the development of the automotive industry, since the design solutions considered in this work relate to the creation and improvement of working parts for road construction machines used in the formation and restoration of transport infrastructure. The proposed design and kinematic solutions are aimed at improving the efficiency of equipment operation, reducing energy consumption, and increasing the productivity of machines used in transport construction. Thus, the results of the work are directly relevant to the development of transport engineering, in particular to the improvement of technological equipment for the automotive industry, ensuring the improvement of road surfaces and the reliability of transport communications.

An analysis of existing road-cutting machine designs has shown that their main drawbacks - low productivity, insufficient reliability of working components, and high energy consumption - are due to the fact that the potential of traditional cutting schemes has been exhausted. It has been established that further improvements in the efficiency of road construction equipment require a transition to innovative kinematic solutions capable of intensifying the material destruction process through dynamic forces. Thus, there is a need for research aimed at scientifically substantiating the parameters of a working body with a cycloidal motion type, which would allow for overcoming existing technological limitations and significantly reducing energy consumption.

The objective of this study was to improve the performance of road milling machines by justifying the design parameters and developing an innovative working body with cycloidal motion.

To achieve this goal, the following tasks were addressed:

1. Justifying the application of the cycloidal motion principle to intensify the interaction between the working body and the road surface.
2. Developing a mathematical model of the working body's dynamics and derive equations for determining the cutting force, taking into account vibrational effects.
3. Conducting a comparative analysis of the proposed design's efficiency against existing counterparts (such as the DFM-40, DFM-RMT, etc.) in terms of productivity and specific energy consumption.
4. Experimentally verifying the operational capability of the developed device on a physical model and validate the adequacy of the derived theoretical relationships.

2 Materials and methods

A well-known machine for cutting joints in road pavements comprises a hollow frame with a rectangular cross-section. A drive kinematic transmission in the form of a chain gear transmission, with a chain and drive and driven sprockets, is housed within the frame cavity.

The eccentric shaft comprises a main section and, on either side of it, eccentrically offset sections. The driven sprocket is coaxially aligned and rigidly connected to the main section of the shaft.

Disc cutters are mounted on the eccentrically offset sections of the shaft. They are oriented parallel to each other and perpendicular to the shaft axis. The disc cutters are polygonal in shape with equal convex sides, and removable cutting edges are secured at the vertices of the polygons.

On the sides of the frame facing the cutters, coaxial with the eccentrically offset sections of the eccentric shaft, are attached the planetary gears with an internal gear ring [4-8]. Satellite gears with an external gear ring are located and rigidly attached to the side surfaces of the disc cutters. The external gear ring of the satellite gear meshes with the internal gear ring of the planetary gear.

The disadvantages of the known device include limited functionality, namely, the inability to cut joints in road surfaces, dense and frozen soils, and other surfaces with a minimum number of working strokes.

The study is based on a theoretical justification of the main parameters of the working body of machines for cutting joints with cycloidal motion of cutting discs, which intensifies the interaction of the cutting elements of the working body with the material being processed. When analyzing the laws of motion of the working body, the method of interaction of the working body with the material being processed and the trajectory of the working body's motion were taken into account [5-9].

The technical result of using the proposed design is an expansion of functional capabilities, namely, cutting joints of various widths in different surfaces with high quality of their surfaces and high-performance cutting with a minimum number of working strokes.

The eccentric shaft is prefabricated and consists of a prefabricated main section in the form of a cylindrical sleeve with two spring-loaded coaxial main sections of equal length, spring-loaded coaxial main sections of the eccentric shaft, connected by their side edges to eccentrically offset sections of the eccentric shaft, which are synchronously extended in opposite directions from the center of this section. At the same time, the cylindrical sleeve of the main section of the eccentric shaft is rigidly connected with the opening of the driven star by its outer surface. A holder oriented perpendicular to the shaft axis is attached to the outer surface of the sleeve, which is additionally introduced into the drive device for axial displacement of the side edges of the eccentric shaft, for example, in the form of a hydraulic cylinder, the extendable rod of which interacts with the side face of the eccentric shaft with the possibility of synchronous multidirectional extension of its sections and subsequent fixation of the achieved level of extension of the side faces of the eccentric shaft, together with its eccentrically displaced sections, wherein the inner rims of the planetary gear wheels are elongated along the axis by the amount of the drive rod stroke.

The device is mounted on a vehicle, such as a truck, by means of a frame 1 (Figure 1). Rotation is transmitted from the drive to a chain gear consisting of a drive sprocket, chain 2, and driven sprocket 3, and from the driven sprocket 3, rotation is transmitted to the eccentric shaft 4, and from it to the disc cutters 6. At the same time, the inner rims of the planetary gears 8 are in internal meshing with the outer rims of the satellite gears 9 (the wheels 9 roll inside the wheels 8). Disc cutters 6 perform a rotational movement around the axis O_1-O_1 of eccentrically displaced sections 5 of the eccentric shaft. The points of the cutters 7 with the same name move along complex trajectories representing hypotrochoids. Moving along the branches of the hypotrochoid, when in contact with the road surface, the

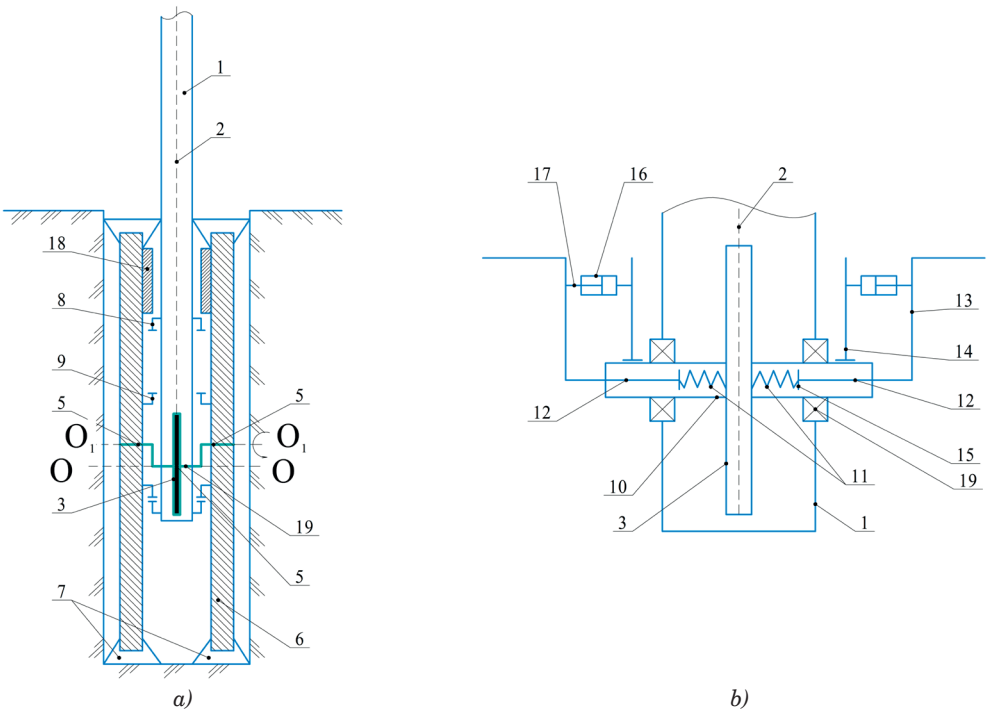

a) b)

1 - frame
2 - chain gear transmission with chain
3 - trailing star
4 - eccentric shaft with main section
5 - eccentrically displaced areas
6 - disc cutters
7 - removable cutters
8 - planetary gears with internal gear rim
9 - satellite gears
10 - cylindrical bushing
11 - elastic element
12 - main section of the eccentric shaft
13 - side edges
14 - holder
15 - washer
16 - hydraulic cylinder
17 - sliding rod
18 - counterweight
19 - bearing
O-O - axis of rotation of the main section of the eccentric shaft together with the driven star 3
O_1-O_1 - rotation axis of disc cutters 6

Figure 1 *Device for cutting joints in road surfaces: a - general view of the device; b - enlarged image of the eccentric shaft*

cutters 7 of the cutters 6 make a cut, penetrating the road surface to the full cutting depth. At the same time, the speed of the cutter moving along the hypotrochoid does not remain constant, since its movement from the top to the middle of the hypotrochoid branch is slowed down and, conversely, from the middle of the branch to the next top, it is accelerated, resulting in a vibration-force impact on the road surface. To reduce vibrations on eccentrically offset sections of the shaft, counterweights 18 are used. Their use reduces the wear on the bearings 19 of the eccentric shaft. The cut soil is removed to the road surface by cutters 6.

When it is necessary to automatically increase the cutting width, the microprocessor control device sends a command to activate the drives that axially shift the side edges 13 of the eccentric shaft. Their displacement causes the displacement of elements 11. The achieved position of the drive rods 17 is fixed. After the cutting is complete, under the action of elastic deformations of elements 11, the drive rods 17 return to their initial equilibrium state.

The device is effective in operation and has extended functionality, namely, it allows cutting the joints of different widths with a minimum number of working strokes.

The cross section of the machine's working body is a flat triangular shape, the points of which, when rotating around two parallel axes (O-O, O_1-O_1), describe the curved lines-hypotrochoids with straight branches, and the side generatrices of the sections roll along these branches as if along guides.

To determine the main parameters of the working body, the kinematic diagram of its movement was considered (Figure 2).

The cutting trajectory of the rotary working body with cycloidal motion of the discs is formed as a result of the combination of the translational motion of the machine at a speed of υ_{mash} and the complex rotational motion of the rotor at a speed of ω_r shown by dotted lines in Figure 1. The direction of rotational movement in the lower part of the rotor coincides with the direction of the machine's translational movement, and in the upper part, it is opposite to it.

The coordinates of the cutting path are determined as follows [5-9]:

$$\left.\begin{aligned} x &= \upsilon_{masch} \cdot t - c + e \cdot \cos(\omega_1 \cdot t) + a \cdot \cos(\omega \cdot t) \\ z &= -H_{o.p.} + e \cdot \sin(\omega_1 \cdot t) + a \cdot \sin(\omega \cdot t) \end{aligned}\right\}, \quad (1)$$

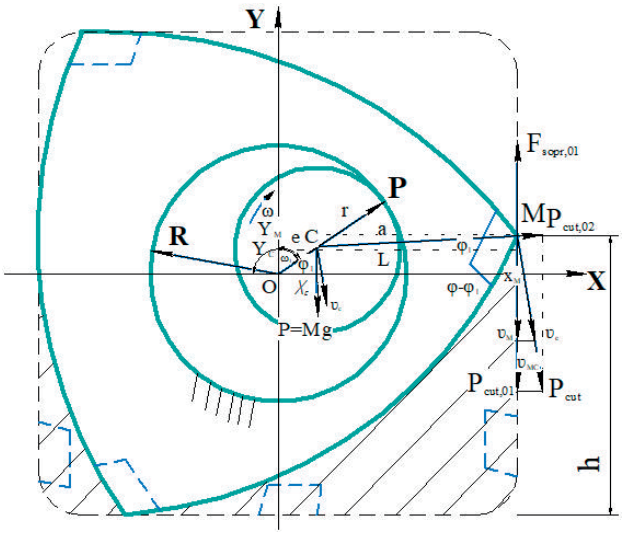

CM - distance from the satellite axis to the cutting element

X_m, Y_m - coordinates of point M of the cutting element

φ_1, ω_1 - angle of rotation and angular velocity of the driver

φ, ω - angle of rotation and angular velocity of the satellite

$P^k_{cut,01}$ - tangential component of cutting force P_{rez}, N

$P^n_{cut,02}$ - the normal component of the cutting force is P_{cut}, N

$F^k_{sopr,01}$ - tangential component of total resistance force F_{sopr}, N

υ_{MC} - speed of point M (cutting element of the disc working body) relative to point C of the satellite center

υ_M - absolute speed of point M (cutting element of the disc working body) relative to point O, the center of the wheel shaft

O - wheel hub

C - satellite center

CM = a, OC = e (eccentricity)

R - the radius of the large stationary wheel

r - satellite radius

X_c, Y_c - coordinate points C

h - cutting depth, mm

υ_c - speed of point C relative to point O, the center of the wheel shaft

***Figure 2** Diagram for determining the kinematic parameters and cutting force of a disc-type working body with cycloidal motion*

where υ_{masch} - vehicle speed, m/s; t - time spent by the cutting edges of the working tool in the cutting process, s; c - rotor shaft offset, mm; $H_{o.p.}$ - difference between the levels of the machine platform and the axis of rotation of the working body, mm; ω_1 - angular velocity of the driver, rad/s; e - eccentricity, mm; a - distance from the satellite axis to the cutting element, mm.

The cutting force when penetrating the road surface, with certain assumptions, can be determined based on the theorem of kinetic energy of a material point. This theorem is expressed by the equation [5-9]:

$$\frac{J_c \cdot \omega^2}{2} + \frac{M \cdot \upsilon_c^2}{2} = A = P_{cut,01} \cdot L_{cut}\,, \tag{2}$$

where J_c - moment of inertia of rotor and satellite discs, kg·mm^2; υ_c - satellite rotation speed, m/s; A - work expended in cutting the road surface, J; ω - rotor angular velocity, rad/s; L_{cut} - cutting path, mm; $P_{cut,01}$- tangential component of cutting force P_{cut}, N.

After transformations, based on the theorem on the change in kinetic energy, one obtains the cutting force [5-9]:

$$P_{cut,01} = \frac{\left(\frac{M \cdot r^2}{2} + \frac{J_c}{2}\right) \cdot \left[\frac{(R-r)}{r}\right]^2 \cdot \omega_1^2}{L_{\text{rez}}}, \tag{3}$$

where R - gear wheel radius, mm; r - satellite radius, mm; ω_1 - angular velocity of the driver, sec^{-1}; M - mass of the disc and the cut road surface, $M = m_{rot} + m_s$, kg.

The tangential component of the cutting force, when the working body is introduced into the road surface, takes the form [5-9]:

$$P_{cut,01} = \frac{\left(\frac{(m_{rot} + F_{cr} \cdot L_{cut} \cdot \gamma) r^2}{2} + \frac{J_c}{2}\right) \cdot \left[\frac{(R-r)}{r}\right]^2 \cdot \omega_1^2}{L_{\text{rez}}}, \tag{4}$$

or

$$P_{cut,01} = \frac{\left(\frac{\left(m_{rot} + F_{cr} \cdot \lambda \cdot \gamma \cdot \frac{\sin(\delta+\theta)}{\sin\theta}\right) r^2}{2} + \frac{J_c}{2}\right) \cdot \left[\frac{(R-r)}{r}\right]^2 \cdot \omega_1^2}{L_{\text{rez}}}. \tag{5}$$

After transforming Equation (5), taking into account that $P_{cut.01} = 0.85 P_{cut}$, one obtains

$$P_{cut} = \frac{0.06 \cdot \omega_1^2 \left[m_{rot} + F_{cr} \cdot \lambda \cdot \gamma \cdot \frac{\sin(\delta+\theta)}{\sin\theta}\right] \cdot (r^2 + J_c)}{L_{cut}}, \tag{6}$$

where δ - cutting angle, degrees; θ - angle between the chip trajectory and the cutting surface, degrees; λ - length of cut section, mm; F_{cr} - average cross-sectional area of the cut, mm^2; γ - asphalt concrete density, kg/mm^3.

To verify the theoretical dependencies and evaluate the performance, experiments were conducted on a physical model of a disc working body with cycloidal motion (Figure 3). To determine the cutting force, the bending stresses on the rotor shaft were measured using the strain gauges. Using the similarity theory,

Figure 3 *Experimental setup with cycloidal motion of the working body*

Figure 4 *Material cut made by the proposed design*

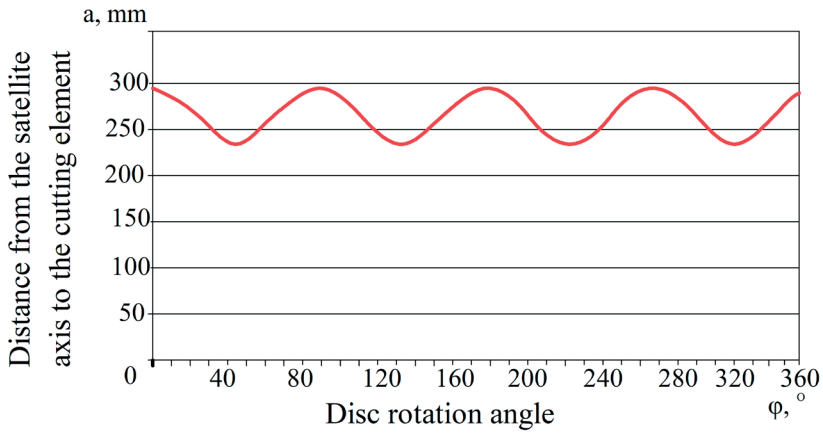

Figure 5 *Graph showing the dependence of CM = a on the satellite's angle of rotation*

the experimental values of the model were converted to full-scale results.

During experimental studies conducted on a physical model, a visual and instrumental analysis was performed on the cross-sections of the asphalt concrete pavement. Unlike the traditional cutting with disc cutters, where the cut surface is smooth, the cut produced by the cycloidal motion of the working body is characterized by the presence of microcracks, indicating that the tensile deformations predominate over shear deformations.

This confirms the hypothesis that the variable speed of the cutters along the hypotrochoid (from a minimum at the start of contact to a maximum during the active fracture phase) creates a "dynamic impact" effect (Figure 4). Zones of cyclic loading are clearly visible on the sample cross-section, which correlate with the calculated cycloid pitch. This fracture mechanism made it possible to achieve a cutting depth of up to 200 mm while significantly reducing the forces on the cutting tool. A comparison of the cut profile showed that the width of the slot remains stable along its entire length, which meets the requirements for expansion joints in road pavements.

3 Results and discussions

The trajectories of the cutting elements are shown in Figures 5 and 6.

Figure 6 shows that the trajectory of the cutters in polar coordinates has the shape of a regular quadrilateral square with smooth transitions at the vertices. When the rotor rotates, the speed of movement on each branch of the trajectory changes from a minimum to a maximum value.

Under the action of the cycloidal cutting force, vibrations are transmitted to the material being cut, which allows additional energy to be supplied, increasing the machine productivity and workflow

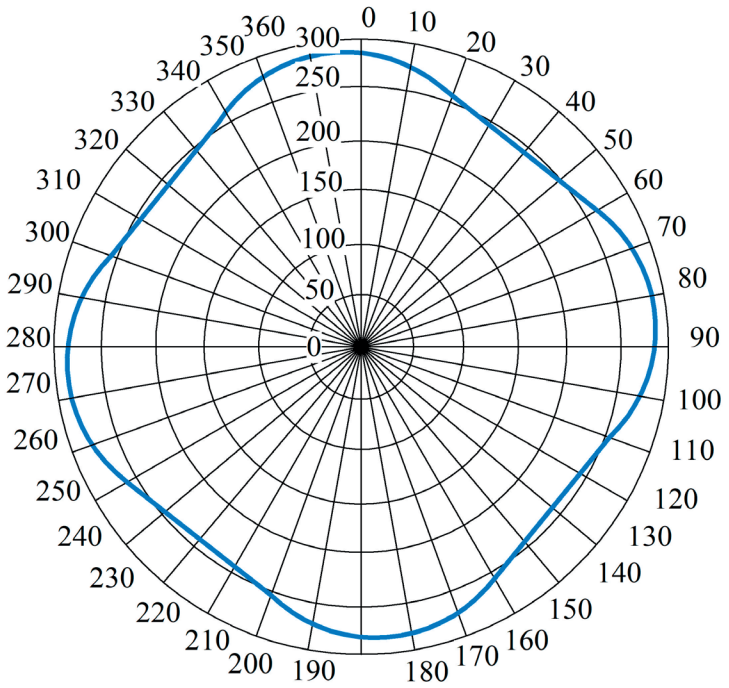

Figure 6 *Trajectory of cutter movement in polar coordinates of a disc-shaped working body with cycloidal movement of cutting elements (degree)*

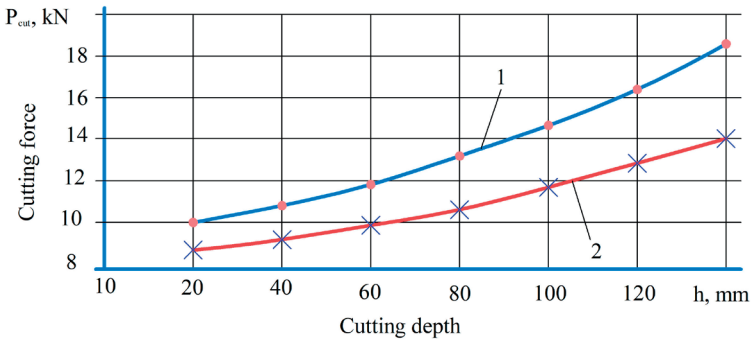

Figure 7 *Dependence of the cutting force on the thickness of the road surface being cut: 1-theoretical; 2-experimental*

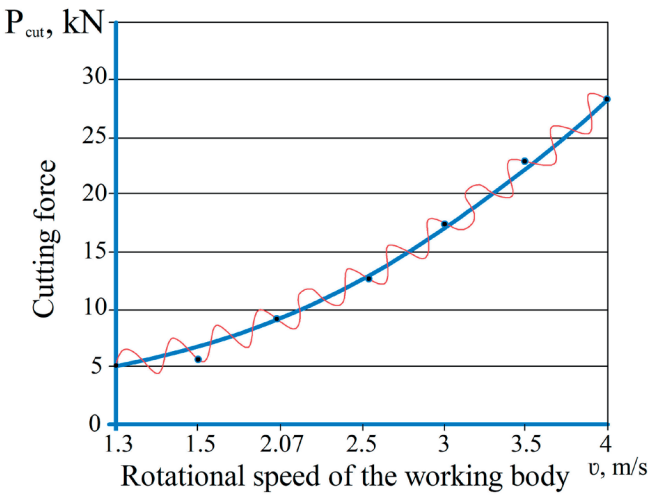

Figure 8 *Dependence of the cutting force on the rotational speed of the disc working body at a cutting width of 15 mm and a cut layer thickness of 140 mm*

Table 1 *Comparative analysis of slitting machines*

No.	Device	Productivity, mm/minutes	Installed capacity, kW	Specific energy consumption, kW-h/m
1	DFM-40	7100	40	5.63
2	DFM-RMT	6500	37	5.69
3	DFM-64	6200	35	5.65
4	New ZRM-1 machine	8700	35	4.02

efficiency. The cycloidal movement of the disc makes it possible to intensify the interaction of the cutting elements with the material being developed.

The results of experimental studies of the dependence of cutting forces on the thickness of the road surface being cut are shown in Figure 7.

Analysis of the experimental results shows that at shallow cutting depths, the discrepancy between the theoretical and experimental cutting force values is small, then increases to 15%, which does not exceed the permissible experimental error limits.

Figure 8 shows a graph of the cutting force dependence on the rotational speed of the disc working body.

The dependence of the cutting force on the rotational speed of the working body has been confirmed experimentally. In all the experiments, the cutting force increased with increasing cutting speed. This pattern can be explained by the specific mechanical conditions of the road surface cutting process, which result from the cyclical change in the speed at which the cutting elements impact the asphalt concrete [10-12].

Analysis of the results obtained reveals the key relationships between the kinematics of motion and the force parameters of the process. It has been established that the nature of the change in cutting force correlates directly with the trajectory of the cutters (hypotrochoid). The change in velocity along each branch of the trajectory, from the minimum to the maximum value, creates the effect of a cyclic dynamic impact [4-6].

The relationship between rotational speed and material resistance is confirmed by the fact that the cycloidal motion generates forced vibrations that are transmitted to the fracture zone. This intensifies the process: the additional kinetic energy of the vibrational impact reduces the static cutting resistance. As experimental data show, at a speed of n=150 rpm, the cutting force is 30 kN, which is 40% lower than that of machines with a bar chain (50 kN) and 33% lower than that of discs with uniform rotation (45 kN) [13-14].

The observed trend of increasing the cutting force with increasing penetration depth (up to a 15% deviation from theory) is explained by the increase in the cross-sectional area of the cut and the density of the asphalt concrete in the contact zone. Nevertheless, it is precisely the use of a cycloidal trajectory that allows for maintaining an advantage in energy efficiency across all tested operating modes, resulting in a 1.13-fold reduction in specific energy consumption compared to mass-produced counterparts such as the DFM-40 and DFM-64.

A comparative analysis of the most common slot cutting machines and the new machine is presented in Table 1.

The results presented in this paper were obtained under certain assumptions. In particular, when developing the mathematical model of the cutting tool's dynamics (Equations (1)-(4)), it was assumed that the cutting process takes place in a homogeneous asphalt concrete medium, without accounting for large foreign inclusions. Experimental studies were conducted on a physical model under laboratory conditions, where the variation of parameters was limited to a range of rotational speeds up to n=150 rpm and a cutting depth of up to h = 200 mm. Furthermore, the assessment of the cutter wear resistance was not considered in this work; the main focus was on the force and energy efficiency of the kinematic scheme.

Further research in this area should focus on studying the effect of various geometric shapes of the cutting segments on the stability of the cycloidal trajectory [15-18]. An important step in the development of this topic will be conducting field tests of a full-scale prototype of the ZRM-1 type road-cutting machine under real road conditions on various types of pavement (cement concrete, reinforced concrete). In addition, of scientific interest is the optimization of vibration modes to minimize the dynamic loads on the base machine's frame, which will further enhance the operational reliability of the proposed design, which has already demonstrated a 1.18-fold performance advantage in current tests.

4 Conclusions

In this study was addressed a pressing scientific and technical challenge involving the justification of design parameters and the development of a working component for a slot-cutting machine with cycloidal motion. Based on the theoretical and experimental data obtained, the following main conclusions were drawn:

1. Scientific findings: It has been established that the use of the cycloidal motion principle (movement of the cutters along a hypotrochoid) enhances the process of asphalt concrete fragmentation through the vibro-impact action. The theoretically derived dependencies of the cutting force (Equations (1)-

(4)) have been experimentally confirmed with a correlation of 85%, which proves the adequacy of the proposed mathematical model of the working process dynamics.

2. Technical and Economic Efficiency: A comparative analysis of the developed design with existing counterparts (DFM-40, DFM-64) demonstrated a significant advantage of the proposed method. The use of a cycloidal cutting tool reduces the energy consumption of the cutting process by a factor of 1.13 and increases productivity by a factor of 1.18. Under optimal operating conditions (n = 150 rpm), a reduction in cutting force to 30 kN was recorded, compared to 45-50 kN in conventional machines.
3. Practical significance: The results of this study can be applied in the design of new models of the road construction equipment, specifically the ZRM-1 expansion joint cutting machine. The implementation of this technology would improve the quality of the expansion joints cut and reduce operational costs in the construction and repair of highways in Kazakhstan.
4. Areas for future research: Further development of this topic involves studying the wear resistance of cutting elements when working with high-strength cement-concrete pavements, as well as optimizing the mass and dimensional characteristics of the vibration exciter to minimize dynamic loads on the base chassis frame.

Acknowledgements

The authors received no financial support for the research, authorship and/or publication of this article.

Conflicts of interest

The authors declare that they have no known competing financial interests or personal relationships that could have appeared to influence the work reported in this paper.

References

[1] STOPKA, O., KUCERKA, D., KAMPF, R., LIZBETIN, J., BARTUSKA L., KMEC, J., GOMBAR, M., WEISS,V. Heavy machinery required for the proper application of geosynthetic products in the implementation of transport constructions. *Procedia Engineering* [online]. 2016, **161**, p. 445-450. ISSN 1877-70587. Available from: https://doi.org/10.1016/j.proeng.2016.08.588

[2] DOVGYALO, V. A., BOCHKAREV, D. I. *Road construction machines. Part I: Machines for earthworks.* Gomel: Belarusian state University of Transport, 2010. ISBN 978-985-468-741-4.

[3] DOVGYALO, V. A., BOCHKAREV, D. I. *Road construction machines. Part II. Machines for the construction and repair of road surfaces.* Gomel: Belarusian state University of Transport, 2018. ISBN 978-5-7996-2386-9.

[4] FEDOROV, D. I. *Working bodies of earth-moving machines*. Moscow: Mechanical Engineering, 1977. ISBN 5-217-00490-8.

[5] VOLKOV, D. P., KRIKUN, V. Y., TOTOLIN, P. E., GAEVSKAYA, K. S. *Earthwork machines.* Moscow: Mechanical Engineering, 1992. ISBN 5-217-01973-5.

[6] BALOVNEV, V. I. *Modeling of interaction processes with the environment of working bodies of road construction machines*. Moscow: Higher School, 1981, ISBN 5-217-02343-0.

[7] SHERBAKOV, A. P., PUSHKAREV, A. E., MAKSIMOV, S. E. Replacement working body material as a way to increase reliability of road construction machines. *The Russian Automobile and Highway Industry Journal* [online]. 2021, **18**(6), p. 646-661. ISSN 2071-7296, eISSN 2658-5626. Available from: https://doi.org/10.26518/2071-7296-2021-18-6-646-661

[8] BURGONUTDINOV, A. M. *Machines for the construction, repair and maintenance of highways. Part 3: Machinery and equipment for the repair and maintenance of road.* Perm: Perm National Research Polytechnic University, 2011. ISBN 978-5-398-00900-2.

[9] LUKASHUK, € €, KOMISSAROV, A. P., LETNEV, K. Y. *Machines for soil development. Design and calculation*. Ekaterinburg: Ural University Publishing House, 2018. ISBN 978-5-7996-2386-9.

[10] KOZBAGAROV, R. A., KAMZANOV, N. S., AKHMETOVA, S. D., ZHUSSUPOV, K. A., DAINOVA, Z**.** K**.** Improving the methods of milling gauge on highways. *News of the National Academy of Sciences of the Republic of Kazakhstan, Series of Geology and Technical Sciences* [online]. 2021, **3**(447), p. 87-93. ISSN 2224-5278, eISSN 2518-170X. Available from: https://doi.org/10.32014/2021.2518-170X.67

[11] ILGE, I. Model of selection of a road miller. *Bulletin of Kharkov National Automobile and Highway University* [online]. 2021, **1**(92), p. 103-108. ISSN 2219-5548, eISSN 2521-1773. Available from: https://doi.org/10.30977/BUL.2219-5548.2021.92.0.103

[12] KAMZANOV, N., AMANOVA, M., BAIKENZHEYEVA, A., NAIMANOVA, G., KOZBAGAROV, R. Automated road milling cutter for repair of the road surfaces with variable trackage. *Communications - Scientific letters of*

the University of Zilina [online]. 2023, **25**(2), p. B157-B164. ISSN 2224-5278, eISSN 2518-170X. Available from: https://doi.org/10.26552/com.C.2023.039

[13] TCHUFISTOV, E. A., TCHUFISTOV, O. E., BLAGOJEVIC, M., VASIC, M. Simulation of motion in a cycloidal gear. Part II. Loaded gear (in Russian). *University Proceedings. Volga Region. Engineering Sciences* [online]. 2025, **1**, p. 92-105. ISSN 2072-3059. Available from: https://doi.org/10.21685/2072-3059-2025-1-8

[14] TCHUFISTOV, E. A., TCHUFISTOV, O. E., BLAGOJEVIC, M. Loads in the planetary-pinion gear with modification of the tooth profile and eccentricity of the satellites [online]. In: *Latest advancements in mechanical engineering*. *ISIEA 2024. Lecture Notes in Networks and Systems, vol 1124*. CONCLI, F., MACCIONI, L., VIDONI, R., MATT, D. T. (Eds.). Cham: Springer, 2024. ISBN 978-3-031-70461-1, eISBN 978-3-031-70462-8, p. 84-95. Available from: https://doi.org/10.1007/978-3-031-70462-8_8

[15] KOZBAGAROV, R. A., SHALBAYEV, K. K., ZHIYENKOZHAYEV, M. S., KAMZANOV, N. S., NAIMANOVA, G. T. Design of cutting elements of reusable motor graders in mining. *News of the National Academy of Sciences of the Republic of Kazakhstan, Series of Geology and Technical Sciences* [online]. 2022, **3**(453), p. 128-141. ISSN 2224-5278, eISSN 2518-170X. Available from: https://doi.org/10.32014/2022.2518-170X.185

[16] KOZBAGAROV, R., AMANOVA, M., KAMZANOV, N., BIMAGAMBETOVA, L., IMANGALIYEVA A. Investigation of wear of cutting part of polygonal knife car graders in different ground conditions. *Communications - Scientific letters of the University of Zilina* [online]. 2022, **24**(4), p. D229-D238. ISSN 2224-5278, eISSN 2518-170X. Available from: https://doi.org/10.26552/com.C.2022.4.D229-D238

[17] KAKINUMA, Y., IGARASHI, K., KATSURA, S., AOYAMA, T. Development of 5-axis polishing machine capable of simultaneous trajectory, posture, and force control. *CIRP Annals* [online]. 2013, **62**(1), p. 379-382. ISSN 0007-8506, eISSN 1726-0604. Available from: https://doi.org/10.1016/j.cirp.2013.03.135

[18] ZAKHAROV, O. V, KOCHETKOV, A. V. Minimization of the systematic error in centerless measurement of the roundness of parts. *Measurement Techniques* [online]. 2016, **589**(12), p. 1317-1321. ISSN 1573-8906. Available from: https://doi.org/10.1007/s11018-016-0892-6

DESIGN AND PERMANENT MAGNETS REDUCTION OF LINEAR OSCILLATORY MACHINE FOR RECIPROCATING DRIVES IN TRANSPORT

Matúš Horník[1,*], Pavol Rafajdus[1], Hao Chen[2], Yassen Gorbounov[3], Gojko Joksimović[4]

[1]University of Zilina, Department of Power System and Electric Drives, Zilina, Slovakia
[2]China University of Mining and Technology, School of Electrical Engineering, Xuzhou, China
[3]New Bulgarian University, Department of Informatics, Sofia, Bulgaria
[4]University of Montenegro, Faculty of Electrical Engineering, Podgorica, Montenegro

*E-mail of corresponding author: matus.hornik@feit.uniza.sk

Matúš Horník 0009-0008-0885-5704,
Yassen Gorbounov 0000-0002-2936-951X,
Pavol Rafajdus 0000-0003-2903-3394,
Gojko Joksimović 0000-0002-2764-1540

Resume

Electric vehicles (EVs) require efficient compressors for air-conditioning and battery thermal management, typically driven by a dedicated electric motor. In this paper is dealt with the design and optimization of a stator-magnet transverse-flux linear oscillatory machine (SMTLOM) intended for such compressor applications. The topology employs permanent magnets embedded in the stator, enabling simplified assembly, improved vibration robustness, and reduced dependence on rare-earth materials. A detailed 3D finite element analysis was conducted to maximize the performance, while minimizing the volume of permanent magnets. The results demonstrate the feasibility of SMTLOM for EV compressor drives and highlight the trade-offs between force capability, efficiency, and magnet usage.

Article info

Received 12 February 2026
Accepted 28 March 2026
Online 17 April 2026

Keywords:

Linear compressor
electric vehicle
stator-magnet moving-iron
transversal-flux linear machine
three-dimensional finite-element analysis
dual-mode current excitation
rare-earth magnet reduction
force profile optimization

ISSN 1335-4205 (print version)
ISSN 2585-7878 (online version)

Available online: https://doi.org/10.26552/com.C.2026.024

1 Introduction

With climate changes and environmental pollution becoming more critical than ever, the electric vehicles (EVs) offer possibilities of more eco-friendly transportation solution. Electric vehicles are already used a lot in transportation, though the research on them is far from over. Their efficiency and driving range are the biggest focus. By optimizing components used in the EVs it is possible to make them more appealing for the world. One such component used in every type of EV are the compressors. They are mainly used in air conditioning units and battery thermal management systems. Research in [1] provided a review on air conditioning systems (ACS) used in electric vehicles. In the EVs, the AC unit is separately supplied in contrast to the combusting engine vehicles. A separate electric motor is needed for their operation. As is mentioned in [2], the ACS have high power consumption in EVs. This is affected by weather conditions as well and in winter when the ACS can have the biggest power consumption in vehicles. In most cases rotational electric motors are used, for their simple design as can be seen in [3-4]. This leads to a necessary transmission from rotary motion of electric motor to linear motion of the piston in the ACS. Therefore, a direct linear motion without the transmission would be preferable for transmission losses reduction.

Linear oscillatory machines (LOMs) have been the cornerstone of numerous industrial applications due to their ability to directly convert electromagnetic forces into linear motion without the need for mechanical transmissions and are particularly advantageous in scenarios where oscillatory motion with high efficiency is required. Therefore, their usage in compressor applications is possible, and they are already being used in this field, such as in [5].

Nowadays the transfer flux linear oscillatory

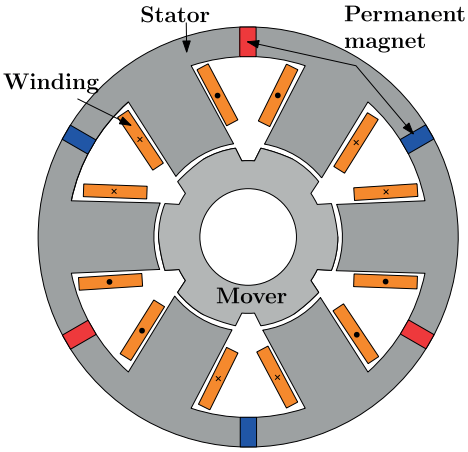

Figure 1 *Radial cross section of SMTLOM*

Table 1 *Specific maximum parameters of SMTLOM*

Description	Parameter	Value	Unit
Voltage RMS	V	145	[V]
Current RMS	I	0.3&1.7	[A]
Frequency	f	75	[Hz]
Total Width	W	60	[mm]
Stator Diameter	D_{so}	120	[mm]
Mover Diameter	D_{si}	46	[mm]

machine with permanent magnets (PMs) on the mover are the most used type [6]. Those machines are highly efficient, with high power density. However, they suffer on the reliability side. Since their magnets are placed on the moving part, the magnets are susceptible to vibration and high temperatures. Thus, to evade some of these deficiencies, similar machine with PMs on the stator was introduced by Boldea [7] to improve the motor reliability. This model was later modified to a stator-magnet transverse-flux linear oscillatory machine (SMTLOM) in [8-9], to keep the reliability and boost the efficiency of the machine. By moving the PMs to the outer part of the stator, the magnets can be better cooled, and easier to install.

The main contribution of this paper is the systematic reduction of stator-mounted rare-earth magnet volume in an SMTLOM, while maintaining the full-stroke force coverage for EV compressor applications.

2 Design requirements and specifications

As it is demonstrated in Figure 1, the SMTLOM was selected for the present study. The machine contains magnets embedded in the stator yoke. The incorporation of rare-earth permanent magnets (PM) composed of NdFeB within the stator yoke confers two primary advantages: facilitation of installation and replacement of the PM, and enhancement of protection against vibrations induced by the mover.

The incorporation of the PM modifies the flux path configuration, transitioning frosm a series to a parallel structure. Consequently, this approach results in a substantial reduction in the PM usage. The SMTLOM is operated with twin stators that generate magnetomotive forces (MMFs) when energized by current. These MMFs interact with the permanent magnet's field, creating a flux imbalance that drives the mover toward the stator with higher flux density. The machine's operation is facilitated by single-phase sinusoidal currents, thereby generating an oscillatory magnetic field that drives the mover axially. This resonant motion, synchronized with the power supply frequency, facilitates precise oscillatory motion, which is well-suited for applications such as compressors.

For the design of the SMTLOM, several key parameters must be defined, as this forms the initial step in the development of any electric machine. The requirements and constraints applied in this work are summarised in Table 1. These values were selected to ensure that the proposed SMTLOM is suitable for use in compressor applications.

According to the operating principle of the SMTLOM, described in the previous section, the machine performs an oscillatory motion whose frequency corresponds to the frequency of the applied voltage. The relationship is expressed as:

$$v_m = l_{st} f \,, \tag{1}$$

where v_m denotes the linear velocity of the mover, l_{st} represents the full bidirectional stroke length, and f

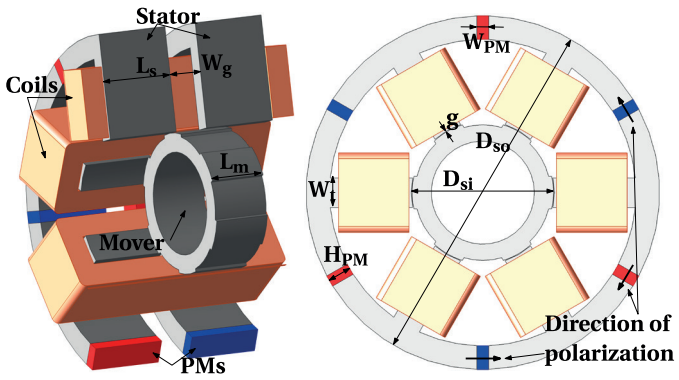

Figure 2 *Illustration of the front view of the SMTLOM and its partial section without the mechanical springs*

is the excitation frequency. This expression does not consider the effects of mechanical springs. The stroke length is particularly important, as it directly influences the mover velocity and consequently affects the overall performance of the compressor.

2.1 Influence of stroke length

The stroke length has a substantial influence on both the performance and energy demand of a linear compressor. A longer stroke enables a larger volume change inside the compression chamber, which allows the system to reach higher pressures and achieve greater compression ratios. However, an extended stroke must be controlled with high precision, as excessive displacement may result in over-compression and reduced efficiency. In contrast, a shorter stroke requires the machine to operate at a higher number of cycles to reach the same pressure level, increasing the mechanical wear and overall energy consumption.

2.2 Force and current requirement

In linear compressor operation, the piston is driven by a linear electric actuator and oscillates directly along a single axis, eliminating the need for a crankshaft mechanism. As a result, the electromagnetic force and phase current vary significantly between the compression and decompression strokes. During the compression, a considerable amount of force is necessary to counteract the resistance of the working fluid and the existing chamber backpressure. Although the decompression typically demands less force, additional thrust may still be required to overcome the stiffness of mechanical springs. Rapid switching between the two phases calls for brief periods of increased current to accelerate or decelerate the mover. Mechanical springs help to reduce the required electrical current during these transitions, increasing system efficiency.

For this reason, a dual-mode current strategy is implemented. Figure 2 illustrates the SMTLOM geometry and the principal parameters included in the design.

2.3 Low-current and high-current modes

In the low-current operation, hereafter referred to as the efficiency mode, the system operates with minimal electrical input, maintaining oscillations close to their natural resonance. This operational mode is suitable for maintaining system pressure under light load. By delivering only the current necessary to offset mechanical losses such as friction and damping, the mover can oscillate with very low energy consumption. This reduces mechanical and thermal stress, prolongs the service life, and ensures that the transition to high-current operation can be performed immediately when required.

The high-current operation, hereafter referred to as the power mode, is engaged when the compressor must deliver significantly higher force, for instance when facing elevated backpressure, compressing liquid refrigerant, or achieving higher compression ratios. Increasing the supplied current strengthens the magnetomotive force in the armature winding and thus raises the electromagnetic thrust required for demanding operating points. One practical approach for switching between the current modes is modifying the electrical properties of the armature winding through the use of a tapped winding structure.

Both operational modes, efficiency and power, are incorporated into the SMTLOM design to ensure optimal force generation in dependence on the compressor's mechanical requirements. The detailed specifications for each mode are given in Table 1.

3 Reference force determination

Before optimizing the linear oscillatory motor, it is necessary to determine the required mechanical force that the motor must generate during operation. In this section, therefore, the focus is not on the motor itself, but

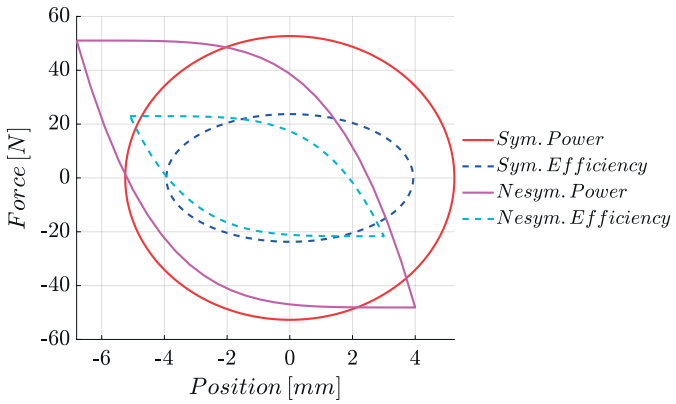

Figure 3 *Theoretical forces required from electric motor in compressor*

on the mechanical load it must drive - the reciprocating compressor of the cooling system. It is described how the target force profiles used in the optimization of the linear oscillatory machine were derived. Such a force can be seen in Figure 3.

By analyzing the gas pressure difference acting on the piston and the resulting displacement, the corresponding force profile $F(x)$ required to perform the compression and suction strokes can be obtained. This force profile serves as the design target for the electromagnetic optimization of the motor, ensuring that the motor produces sufficient thrust over the entire motion range while maintaining efficiency. Two main models were used: a non-symmetric profile that emulates the real pressure behavior in the compressor, and a symmetric (pressure-based) profile that corresponds to idealized sinusoidal operation. The non-symmetric formulation allows to reproduce the different compression and expansion forces that occur in the reciprocating cycle.

3.1 Non-symmetric force model

The non-symmetric force profile $F(x)$ is described by a nonlinear interpolation law using an exponent α_{ns}. It provides an adjustable shape that can be tuned to reproduce realistic asymmetric compression behavior.

The extended range of piston displacement can be defined as:

$$x_{\min,ext} = x_{\min} - \Delta_{ext}, \tag{2}$$

$$x_{\max,ext} = x_{\max} + \Delta_{ext}, \tag{3}$$

$$L = x_{\max,ext} - x_{\min,ext}, \tag{4}$$

where $x_{\min}$ and $x_{\max}$ represent the nominal stroke limits, and Δ_{ext} slightly enlarges this range to ensure that boundary effects are included during optimization. This prevents numerical clipping when generating the full cycle trajectory.

The interpolation shape is defined as:

$$s(x) = \left(\frac{x - x_{\min}}{L}\right)^{\alpha_{ns}}. \tag{5}$$

The interpolation function $s(x)$ is defined over the displacement interval $x \in [x_{\min,ext}, x_{\max,ext}]$, with $\alpha_{ns} > 0$ being a shape exponent controlling the degree of force asymmetry. In Figure 3 the $\alpha_{ns} = 4.5$.

The actual force function is:

$$F(x) = F_{\max} + (F_{\min} - F_{\max})s(x). \tag{6}$$

Alternatively:

$$F(x) = (1 - s(x))F_{\max} + s(x)F_{\min}. \tag{7}$$

To determine $F_{\max}$ and $F_{\min}$, two target points are used:

$$(x_1, F_1), (x_2, F_2). \tag{8}$$

Then, one can calculate:

$$s_1 = s(x_1), s_2 = s(x_2). \tag{9}$$

Substituting the calculated interpolation values s_1 and s_2 into the force expression leads to the following linear system:

$$\begin{bmatrix} 1 - s_1 & s_1 \\ 1 - s_2 & s_2 \end{bmatrix} \begin{bmatrix} F_{\max} \\ F_{\min} \end{bmatrix} = \begin{bmatrix} F_1 \\ F_2 \end{bmatrix}. \tag{10}$$

The solutions are:

$$F_{\max} = \frac{F_1 s_2 - F_2 s_1}{s_2 - s_1}, \tag{11}$$

$$F_{\min} = \frac{F_2(1 - s_1) - F_1(1 - s_2)}{s_2 - s_1}. \tag{12}$$

These equations provide explicit values for the maximum and minimum forces of the nonlinear asymmetric curve. They are used to generate the complete forward and backward motion profiles for dynamic analysis.

Table 2 *Properties of NdFeB PM at 25°C*

Parameter	Value	Unit
H_{cj}	1592	kA/m
H_c	901	kA/m
B_r	1.35	T

3.2 Symmetric pressure-based model

For comparison, a symmetric sinusoidal model is developed based purely on the pressure difference acting on the piston. This model represents the ideal power mode of the compressor, where the compression and expansion are balanced.

The piston area is:

$$A = \pi\left(\frac{D_{pist}}{2}\right)^2. \tag{13}$$

The theoretical maximum force:

$$F_{\max} = \Delta p \cdot A \cdot reserve\,. \tag{14}$$

To model the efficiency mode, reduced amplitude values are introduced:

$$F_{\max,ext} = \eta_F F_{\max}\,, \tag{15}$$

$$x_{\max,ext} = \eta_x x_{\max}\,. \tag{16}$$

Assuming sinusoidal motion at frequency f:

$$x_{power}(t) = x_{\max,ext}\sin(2\pi ft), \tag{17}$$

$$F_{power}(t) = F_{\max,ext}\cos(2\pi ft). \tag{18}$$

Efficiency mode is:

$$x_{eff}(t) = x_{\max,ext}\sin(2\pi ft), \tag{19}$$

$$F_{eff}(t) = F_{\max,ext}\cos(2\pi ft). \tag{20}$$

These sinusoidal expressions are used for reference simulations and energy evaluation.

3.3 Scaling of the non-symmetric profile to efficiency mode

To combine both models:

$$x_{ns,eff}(t) = \eta_x x_{ns}(t), \tag{21}$$

$$F_{ns,eff}(t) = \eta_F F_{ns}(t). \tag{22}$$

This preserves the shape of the asymmetric force curve while reducing its amplitude and stroke. Such scaling enables direct comparison of realistic and idealized excitation modes under identical frequency conditions.

4 Design priorities

As can be seen in Figure 3, the force is in fact required during the whole stroke and not just at a peak. Any further optimization of the proposed machine will reflect this. To know what parameters to focus on, it is important to set goals for the optimization. As there is more than one requirement, it is also good to set priorities among them. For that purpose, a list of requirements is compiled:

1. Achievement of forces in Efficiency and Power modes,
2. Adherence to the dimensions,
3. Reduction of rare-earth materials in magnets,
4. Efficiency above 92% in efficiency mode.

As mentioned before, the force must be applied throughout the entire stroke, or at least the majority of it, to ensure sufficient power for compression and decompression. As the Power mode is easier to achieve thanks to the higher current and because efficiency is not required, the optimization can focus on Efficiency mode. As mentioned in the previous section, a positive change in efficiency mode force also has a positive effect on Power mode.

Adherence to the dimensions is important, as the entire motor must fit within the compressor system. If this requirement is not met, the linear motor cannot be used for the compressor, which requires the force specified above. The maximum width of the machine cannot exceed 60 mm, not including the winding, and the diameter cannot exceed 120 mm.

Reducing rare-earth magnets is important due to their high costs, limited supply, and environmental impact. Where possible, they can be replaced with more abundant alternatives, such as ferrites.

The compressor should work continuously to maintain resonance, even when cooling is not exactly necessary. In this case, the linear motor is required to be highly efficient. Therefore, a required efficiency at least 92% was set. The referred efficiency applies only to the linear electric machine and not to the entire system.

To optimize the model, a replica of the model created by the Chinese scientists was utilized [8]. The current was selected to be 0.3 A for Efficiency mode and 1.7 A for Power mode. The NdFeB permanent magnet parameters are given in Table 2.

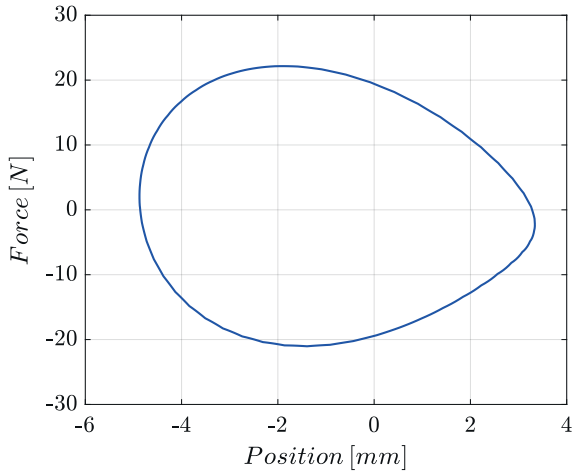

Figure 4 *Required reference force in Efficiency mode*

The coercivity H_c is the magnetic field strength at which the magnetic flux density B becomes zero, while the intrinsic coercivity H_{cj} corresponds to the field at which the magnetic polarization J (or magnetization M) vanishes. Unlike H_c, which is affected by demagnetizing effects, H_{cj} directly indicates the resistance of a permanent magnet to irreversible demagnetization.

All the possible modifications and curves with which the optimisation was conducted are depicted in Figure 3. It has been established that any alterations made to the Efficiency mode would be reflected in the Power mode, due to the work that had been completed during research. It was therefore determined that the Efficiency mode should be prioritised as the most significant, based on that, in this mode, efficiency was deemed to be a prerequisite. The reference Efficiency mode curve is presented in Figure 4. This curve was obtained through collaboration with an industrial partner, BSH Drives and Pumps s.r.o., utilising the theoretical equations, and reflects the reality to a greater extent than curves in Figure 3.

It is imperative to note that, given the utilisation of this curve as a point of reference, a comparison of the simulation results against it is essential. The objective is to attain a force that is greater throughout the entirety of the movement, or that encompasses the majority of the curve.

5 Methods used for optimization

For the optimization, Parametric and Mixed-Integer Sequential Quadratic Programming (Gradient and Discrete Optimization) methods were employed. Both optimization strategies are integrated within the Ansys Maxwell 3D simulation environment, enabling automated design exploration and performance improvement of electromagnetic systems. To establish a basis for comparison, the simulated force was evaluated in relation to the reference curve.

The Parametric optimization approach involves systematical varying selected design parameters - such as geometric dimensions, material properties, or excitation values to evaluate their influence on key performance metrics. By defining those parameters as variables within the simulation model, Ansys Maxwell can automatically perform parametric sweeps or response surface optimizations, allowing the identification of optimal configurations and sensitivity relationships between input parameters and output performance. This method provides a clear understanding of how each variable affects the overall machine behavior, facilitating efficient design refinement.

The Mixed-Integer Sequential Quadratic Programming (MISQP) method, on the other hand, extends the traditional gradient-based Sequential Quadratic Programming (SQP) by incorporating discrete or integer variables. The algorithm iteratively solves a series of quadratic programming subproblems that approximate the nonlinear objective function and constraints using gradient and Hessian information. While continuous variables are optimized through the gradient-based search, the discrete variables are handled via branch-and-bound or enumeration techniques. This hybrid structure enables simultaneous optimization of both continuous and discrete design variables such as slot numbers, magnet arrangements, or dimensional parameters resulting in a globally efficient and physically feasible design solution.

6 Optimization of the stator-magnet transverse flux linear oscillatory machine

A final dimensional model was selected from the set of simulated models. The parameters of the final dimension are delineated in Table 3. Given these parameters, the stator-magnet transverse flux linear oscillatory machine is consistent with the maximum dimensional requirements for its diameter, width, and inner space in the mover, thereby allowing for the accommodation of a piston.

Table 3 *Dimensions of the chosen SMTLOM*

Variable Name	Parameter	Value
Mover width	L_m	24 mm
Mover diameter	D_{si}	39.6 mm
Mover inside diameter	D_{in}	31 mm
Mover tooth height	H_{Mt}	5 mm
Mover tooth width	L_{Mt}	19.7 mm
Mover tooth depth	W_{Mt}	15 mm
Stator diameter	D_{so}	120 mm
Stator width	L_s	24 mm
Stator tooth height	H_t	33.7 mm
Stator tooth width	W_t	19.7 mm
Stator air gap	W_g	6 mm
Air gap	g	0.3 mm
PM height	H_{PM}	13 mm

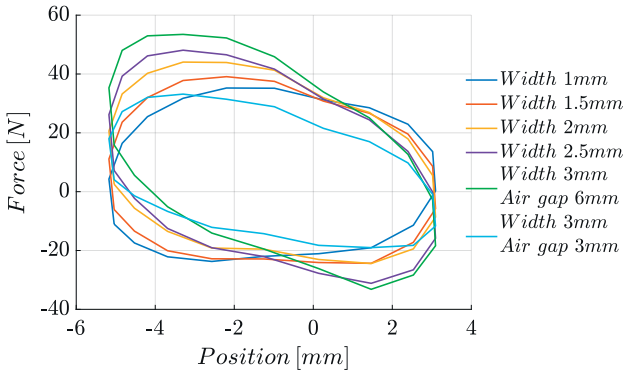

Figure 5 *Force-position characteristics for different permanent magnet widths in efficiency mode*

The first step is to find a model which will produce desired force curve during the whole operation of the SMTLOM. Therefore a machine was simulated with a width of magnet of 3 mm. This was done for two different stator air gaps of 3 mm and 6 mm. As previously mentioned these changes lead to a different distribution of forces during movement. In Figure 5, these curves can be observed, along with further magnet reduction, which was done at stator air gap of 6 mm, as it provided higher forces during the complete movement, compared to 3 mm stator air gap.

Upon examination of the Figure 5, two notable facts emerge. The initial observation is that an increased quantity of NdFeB magnets results in a higher peak force. The latter is of utmost importance for the optimization. As is evident from the maximum and minimum values observed at the limit point of the position axis, this effect is not without its drawbacks for the model in question.

At this point, the electric motor reaches its maximum mobility limit, leading to a change in direction. The force that would be optimal is then opposite to the force it was producing during movement in the previous direction. When comparing the obtained force result, it is not sufficient to consider only the peak.

As demonstrated by Figure 5, it is evident that increasing the width of the magnet results in higher force amplitudes in both directions of motion. This behavior is characteristic of configurations with a stronger magnetic flux, as a larger volume of magnetic material enables the machine to generate higher peak attractive and repulsive forces. However, as the width of the magnet increases, the symmetry of the force with respect to the zero level on the force axis becomes significantly worse. The initial oval shape of the curves gradually becomes distorted, resulting in a narrower and less balanced appearance.

This imbalance signifies that the force exerted on the mover is not uniformly distributed over the entire stroke. In the context of linear compressor applications, force symmetry is of paramount importance. An asymmetric force profile has the potential to exert a negative influence on the dynamics and the overall energy efficiency of the drive. As demonstrated in Figure 4, the force should be symmetrical about the zero level of the Y-axis. Consequently, configurations with reduced magnet widths, which exhibit enhanced symmetry even at decreased amplitudes, are more appropriate for meeting the compressor requirements.

Given the extensive array of simulations conducted, a precise selection process was imperative. For the purpose of comparison, a comparison of simulated results and theoretical force was conducted.

7 Comparison of simulation results to theoretical forces

As previously indicated, the selection of the appropriate model was conducted by a comprehensive consideration of the entire moving process. A comparative analysis was conducted among numerous models.

Given the movement's bidirectional nature, both the simulated and theoretical curves were divided according to the movement direction. The theoretical force is divided into two components: one that is directed forward and one that is directed backward. This approach was similarly implemented in the context of the simulated models in Figure 6, where the number in the legend is the width of the magnets.

The segmentation was performed at the extreme mover positions, where the direction changes. Since the theoretical force curve contained more data points than the simulated results, interpolation was used to align both datasets. The simulation step size was relatively large due to computational limits, which caused visibly discrete force points and required smoothing.

A common position vector x_{common} was created over the overlapping region of both datasets, and all the curves were linearly interpolated onto this grid. This ensured a direct point-wise comparison, while avoiding nonphysical extrapolation. Invalid or incomplete simulation curves were automatically skipped.

The comparison evaluated the percentage of the stroke where the simulated force magnitude exceeded

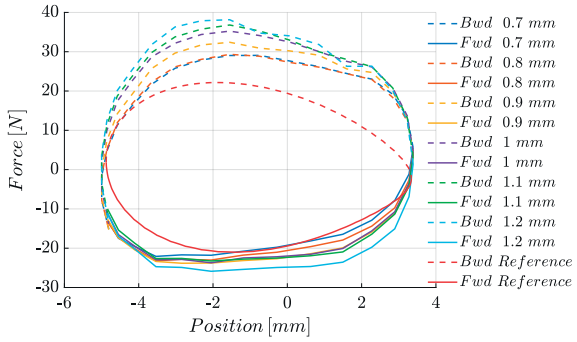

Figure 6 *Force-position characteristics for different permanent magnet widths including the reference model*

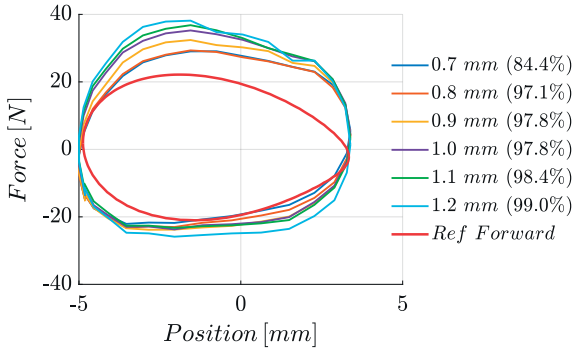

Figure 7 *Forces comparison of efficiency mode*

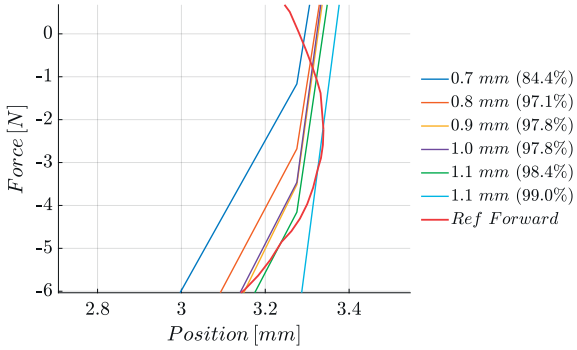

Figure 8 *Forces coparison at maximum movement of the piston of efficiency mode*

the theoretical reference. The resulting values, shown in Figure 7, indicate that magnet widths below 1.2 mm lead to a rapid drop in performance. A 99 % match is considered sufficient, as interpolation was involved. The detail in Figure 8 shows a small region where the simulated force did not fully cover the theoretical curve, likely due to coarse simulation resolution. The chosen model was therefore selected as the most suitable candidate for further detailed evaluation.

8 Final results of optimized linear motor

The final model of the SMTLOM, shown in Figure 2, was chosen and its parameters are listed in Table 4. As described in the previous sections, this model fulfils the dimensional goal, the force requirement, explained in section 2, and the reduction of rare-earth magnets that has been done in section 6. Only the efficiency goal remains unknown.

Table 4 *Dimensions of the final SMTLOM model*

Variable Name	Label	Value
Mover width	L_m	24 mm
Mover diameter	D_{si}	39.6 mm
Mover diameter inside	D_{in}	31 mm
Mover tooth height	H_{Mt}	5 mm
Mover tooth width	L_{Mt}	19.7 mm
Mover tooth depth	W_{Mt}	15 mm
Stator diameter	D_{so}	120 mm
Stator width	L_s	24 mm
Stator tooth height	H_t	33.7 mm
Stator tooth width	W_t	19.7 mm
Stator air gap	W_g	6 mm
Air gap	g	0.3 mm
PM height	H_{PM}	13 mm
PM width	W_{PM}	1.2 mm

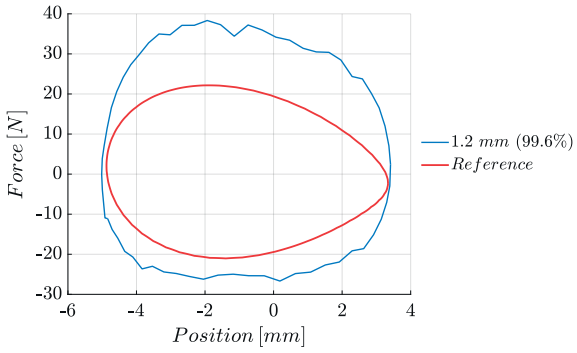

Figure 9 *Efficiency mode force curve of the final model*

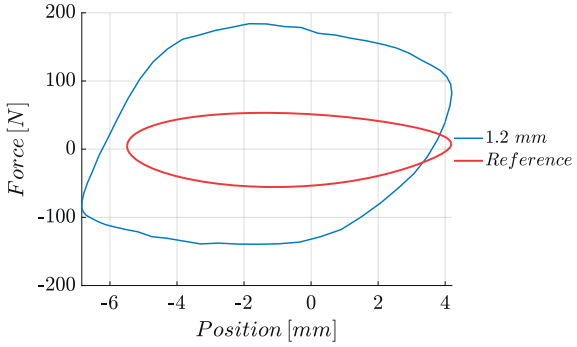

Figure 10 *Power mode force curve of the final model*

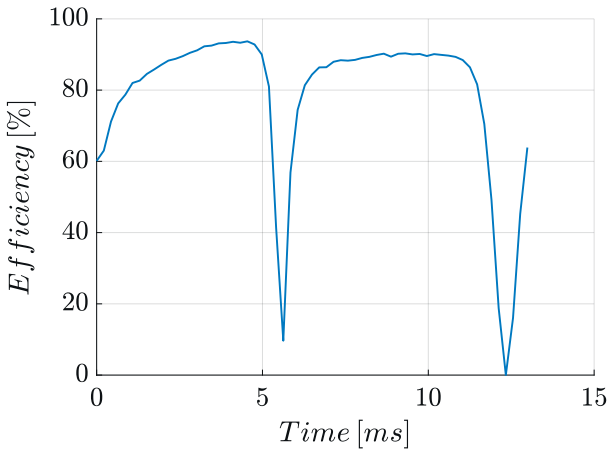

Figure 11 *Efficiency of the efficiency mode during one period*

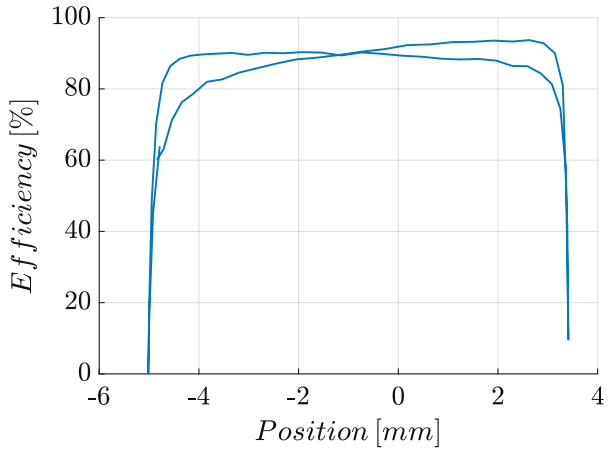

Figure 12 *Efficiency of the efficiency mode during one period for position of the mover*

As previously stated, the SMTLOM with a permanent magnet measuring 1.2 mm in width generates sufficient force to envelop the theoretical force. Despite the initial results exhibiting a reduced number of steps in the simulation, the final model was selected, consequently necessitating a simulation with a greater number of steps. The results for Efficiency mode are available in Figure 9. The Power mode force is visualized in Figure 10.

The produced force, in the efficiency mode, exceeds the theoretical reference throughout the entire movement of the SMTLOM. This indicates that the enhanced simulation precision has led to the elimination of the error that occurred in Figure 8, due to the reduced step size in the simulation.

In the power mode, the force exerted during movement typically exceeds the reference value by a significant margin. It is worth noting that, at its maximum point of movement, the object may not fully cover the reference point. However, this is not necessarily problematic, as the object generates sufficient force during its movement to compress the medium.

With the exception of the efficiency goal, all other objectives were successfully achieved. Therefore, an investigation was conducted into the efficiency of this model. The process of SMTLOM is illustrated in Figure 11.

This phenomenon is more readily apparent in Figure 12, in which the entire movement is displayed.

The maximum achieved efficiency for the efficiency mode during a single periodic movement was 93.692%. According to the operational principle, it is evident that the machine's efficiency will fluctuate. The root mean square (RMS) value of the efficiency is 81.647%. It is imperative to acknowledge that this valuation exclusively encompasses accounts that are associated with electromagnetic efficiency of the standalone linear machine, it does not extend to accounts that incorporate mechanical components. As illustrated in Figures 11 and 12, two significant declines in efficiency are evident, attributable to alterations in direction.

The efficiency of the linear oscillatory machine was evaluated in Ansys Maxwell 3D based on the instantaneous mechanical output power and electromagnetic losses. The instantaneous output power is defined as

$$P_{out}(t) = F(t)\,v(t), \tag{23}$$

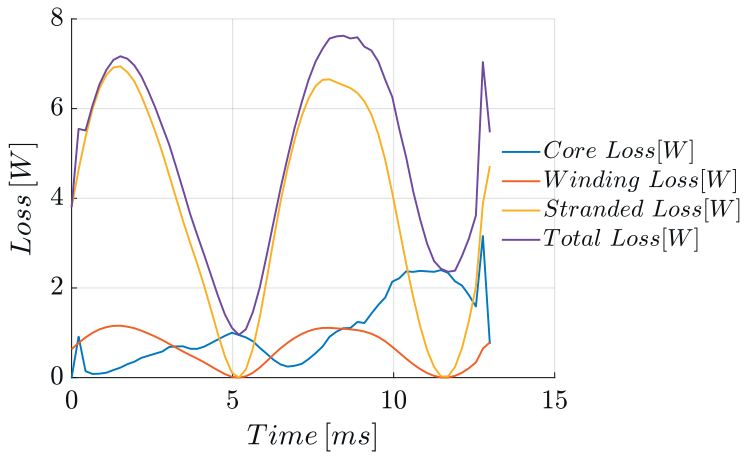

Figure 13 *Losses in the SMTLOM in efficiency mode*

where $F(t)$ is the electromagnetic force acting on the mover and $F(t)$ is its instantaneous velocity. The efficiency is calculated as

$$\eta(t) = \frac{|P_{out}(t)|}{|P_{out}(t)| + P_{loss}(t)} \cdot 100\% . \tag{24}$$

The absolute value of the output power is used due to the oscillatory motion, during which the velocity and power change sign within one period. In this case, the negative power does not represent a loss but a reversal of energy flow. The losses $P_{\text{loss}}(t)$ include only electromagnetic losses of the machine, namely copper and iron losses, while the mechanical and fluid losses are not considered. This efficiency definition is intended for comparative electromagnetic evaluation of different SMTLOM designs and does not represent the overall compressor system efficiency.

In oscillatory systems, such as linear compressors, springs are utilized to maintain resonance. This configuration enables the machine to undergo directional changes with reduced losses, thereby maintaining elevated operational efficiency throughout its function. Therefore, it can be concluded that these substantial declines in efficiency will not be observed in the compressor system. However, some loss of efficiency may still occur in the points during directional changes.

At this stage of the research, the mechanical system had not yet been incorporated into the machine's design. Therefore, it can be concluded that all the figures and values are exclusively applicable to the electromagnetic efficiency of the standalone linear machine. This includes all the forces, which did not take into account weight of the piston and the fluid, the efficiency curves and all the losses. As illustrated in Figure 13, the losses are exclusively those of the machine, excluding any mechanical load. In this particular instance, the greatest proportion of total losses is attributable to stranded losses. The occurrence of stranded losses can result in the heat-related issues, a phenomenon that is characteristic of this particular type of machine. Due to the positioning of the magnets on the exterior surface of the SMTLOM, they are likely to be insulated from elevated temperatures. However, a more comprehensive temperature assessment is necessary to verify this hypothesis.

9 Conclusion

The presented study demonstrates that the proposed SMTLOM is a suitable candidate for driving linear compressors in electric vehicle applications. Through a combination of analytical modelling, 3D finite-element simulations, and multi-stage optimization, the machine was designed to satisfy strict dimensional constraints while achieving the required bidirectional force across the full stroke. The systematic reduction of rare-earth magnet volume, enabled by relocating the magnets to the stator, and employing a transverse-flux topology, proved effective, yielding a final configuration that maintains adequate thrust despite a magnet width of only 1.2 mm. The optimized machine consistently exceeded the theoretical force reference in both efficiency and power modes, confirming that the electromagnetic design is capable of meeting demanding compressor load conditions.

The evaluation of efficiency revealed that, while the instantaneous efficiency varies due to the oscillatory nature of the system, the peak efficiency reaches 93.7%. The efficiency is expected to improve when mechanical springs are included, as resonant operation reduces electrical power demand near reversal points. Losses analysis showed that stranded losses represent the dominant component, highlighting the need for future thermal assessment and potential mitigation strategies. Overall, the results validate the feasibility of the SMTLOM concept and establish a solid foundation for future work involving mechanical integration, thermal modelling, and prototype development.

Acknowledgment

The authors would like to thank BSH Drives and Pumps s.r.o. for their support during this research. This research was funded by the Slovak Research and Development Agency APVV No. DS-FR-24-0056 and KEGA K-25-010-00.

Conflicts of interest

The authors declare that they have no known competing financial interests or personal relationships that could have appeared to influence the work reported in this paper.

References

[1] ZHANG, Z., WANG, J., FENG, X., Chang, L., Chen, Y., Wang, X. The solutions to electric vehicle air conditioning systems: a review. *Renewable and Sustainable Energy Reviews* [online]. 2018, **91**, p. 443-463. ISSN 1364-0321, eISSN 1879-0690. Available from: https://doi.org/10.1016/j.rser.2018.04.005

[2] ZHANG, Z., WANG, D., ZHANG, CH., CHEN, J. Electric vehicle range extension strategies based on improved AC system in cold climate - a review. *International Journal of Refrigeration* [online]. 2018, **88**, p. 141-150. ISSN 0140-7007, eISSN 1879-2081. Available from: https://doi.org/10.1016/j.ijrefrig.2017.12.018

[3] KIM, S.-I., LEE, G.-H., HONG, J.P., JUNG, T.-U. Design process of interior PM synchronous motor for 42-V electric air-conditioner system in hybrid electric vehicle. *IEEE Transactions on Magnetics* [online]. 2008, **44**(6), p. 1590-1593. ISSN 0018-9464, eISSN 1941-0069. Available from: https://doi.org/10.1109/TMAG.2007.916136

[4] JUNG, T.-U., LEE, S.-H., KIM, S.-I., PARK, S.-J., HONG, J.-P. The development of hybrid electric compressor motor drive system for HEV. In: 2007 IEEE Vehicle Power and Propulsion Conference: proceedings [online]. IEEE. 2007. ISSN 1938-8756, ISBN 978-0-7803-9760-6, p. 802-807. Available from: https://doi.org/10.1109/VPPC.2007.4544234

[5] XUE, X., CHENG, K. W. E., ZHANG, Z. Model, analysis, and application of tubular linear switched reluctance actuator for linear compressors. *IEEE Transactions on Industrial Electronics* [online]. 2018, **65**(12), p. 9863-9872. ISSN 0278-0046, eISSN 1557-9948. Available from: https://doi.org/10.1109/TIE.2018.2818638

[6] ZHANG, Y., LU, Q., YU, M., YE, Y. A novel transverse-flux moving-magnet linear oscillatory actuator. *IEEE Transactions on Magnetics* [online]. 2012, **48**(5), p. 1856-1862. ISSN 0018-9464, eISSN 1941-0069. Available from: https://doi.org/10.1109/TMAG.2011.2178077

[7] BOLDEA, I., NASAR, S.A., PENSWICK, B., ROSS, B., OLAN, R. New linear reciprocating machine with stationary permanent magnets. In: IAS '96. Conference Record of the 1996 IEEE Industry Applications Conference Thirty-First IAS Annual Meeting: proceedings [online]. Vol. 2. 1996. ISSN 0197-2618, ISBN 0-7803-3544-9, p. 825-829. Available from: https://doi.org/10.1109/IAS.1996.560179

[8] LI, X., XU, W., LIAO, K., WU, X. Design of stator-magnet moving-iron transverse-flux linear oscillatory machine considering asymmetric saturation. *IEEE Transactions on Transportation Electrification* [online]. 2022, **8**(3), p. 3464-3477. eISSN 2332-7782. Available from: https://doi.org/10.1109/TTE.2022.3152909

[9] LI, X., JIANG, M., XU, W., WU, T., ZHANG, D. Design and test of a less-rare-earth stator-magnet moving-iron transverse-flux linear oscillatory machine for reciprocating drive. *IEEE Transactions on Industrial Electronics* [online]. 2024, **71**(3), p. 2831-2841. ISSN 0278-0046, eISSN 1557-9948. Available from: https://doi.org/10.1109/TIE.2023.3269472

EXTERNAL MONITORING SYSTEM FOR BATTERY CONDITION AND STATE OF HEALTH OF LITHIUM-ION BATTERIES

Milan Havelka[1], Matúš Nečas[2], Dušan Maga[3], Juraj Duďák[1,2,*]

[1]Slovak University of Technology in Bratislava, Faculty of Materials Science and Technology in Trnava, Institute of Applied Informatics, Automation and Mechatronics, Trnava, Slovak Republic
[2]University of Zilina, Research Centre, Zilina, Slovak Republic
[3]Czech Technical University in Prague, Faculty of Electrical Engineering CTU in Prague, Prague, Czech Republic

*E-mail of the corresponding author: juraj.dudak@stuba.sk

Milan Havelka 0009-0005-1706-155X,
Dusan Maga 0000-0001-8176-2151,
Matus Necas 0009-0002-5145-2835,
Juraj Dudak 0000-0002-5570-5150

Resume
Lithium-ion batteries power light electric vehicles such as electric bicycles, but end users typically lack reliable information about true battery health and instead rely on misleading indicators of remaining charge. In this paper is introduced a novel external plug-and-play diagnostic module that connects between the standard charger and a battery of a light electric vehicle. The system uses a precise discrete-time energy integration method during standard charging. It captures dynamic current fluctuations and estimates battery health from the partial charging data. Experimental validation on multiple battery packs demonstrates that the proposed algorithm reliably distinguishes between healthy and degraded batteries. This non-invasive system adds diagnostics to conventional charging, enabling users to assess actual capacity without full discharge cycles.

Article info
Received 2 March 2026
Accepted 28 March 2026
Online 22 April 2026

Keywords:
capacity fade
condition monitoring
energy integration
light electric vehicles
ithium-ion batteries
state of health

Available online: https://doi.org/10.26552/com.C.2026.028

ISSN 1335-4205 (print version)
ISSN 2585-7878 (online version)

1 Introduction

The development of modern transportation systems, along with the need to reduce greenhouse gas emissions in urban areas, has driven the widespread adoption of electrically powered vehicles in daily life. The shift to electric transport has become central to sustainable transportation, with its success depending on the availability, performance, and lifespan of energy storage systems, especially lithium-ion (Li-Ion) batteries. Efforts to maximize battery lifespan hold immense economic value and critical ecological significance, as the production and recycling of battery cells represent a considerable environmental burden and require advanced lifecycle management. From the standpoint of technological complexity and infrastructure requirements, electric mobility can be divided into three main categories: mass and freight transport (electric buses and trucks), standard passenger transport (electric vehicles), and simple personal micromobility, commonly called light electric vehicles, such as e-bicycles and e-scooters [1]. While passenger EVs and public transport systems use sophisticated Battery Management Systems (BMS) with active thermal management and precise State of Health (SOH) diagnostics, the LEV category significantly lags in this area. In simple personal micromobility, BMS architectures are often limited to basic overcharge and overdischarge protection. The LEV users typically lack access to reliable information about the actual health and remaining capacity of their batteries. Instead, they must rely on a basic and often misleading State of Charge (SOC) indicator, usually based only on instantaneous terminal voltage [2]. This significant disparity in battery management underscores the urgent need for improved diagnostics in the LEV category. The lack of accurate SOH information leads to improper charging habits, which accelerate battery degradation and reduce overall lifespan. Therefore, there is a growing demand for diagnostic devices that are accessible, external, and flexible.

Accumulators, such as rechargeable batteries (also called secondary batteries), are a key technology in energy storage, enabling repeated charging and discharging through reversible electrochemical

reactions. While this work primarily focuses on Li-Ion batteries, understanding their market position and scientific context requires a brief overview of the main competing technologies. Currently, Li-Ion batteries are among the most widely used energy storage systems in portable electronics, electromobility, and industrial applications. Their widespread adoption is mainly due to their high energy density, low weight, and relatively long lifespan compared to traditional accumulators. These characteristics have made Li-Ion batteries the standard choice for devices that require low weight, compact design, and high energy efficiency, including smartphones, laptops, electric vehicles, drones, and renewable energy systems. The energy density of Li-Ion batteries is approximately 150 to 250 Wh/kg, a significant advantage over older technologies [3]. In addition, they have relatively low self-discharge rates, making them suitable for the long-term storage.

Although the charging and discharging process of a Li-Ion battery is theoretically reversible, practical applications involve gradual losses caused by side chemical reactions, the formation of passivation layers, and mechanical degradation of electrodes. These phenomena result in capacity fade, increased internal resistance, and a gradual reduction in the battery's lifespan. Li-Ion batteries are produced in various mechanical designs. The most commonly used are cylindrical cells with a metal casing, prismatic cells with a rigid shell, and pouch cells with a flexible enclosure. Each type has specific characteristics regarding mechanical durability, cooling options, and integration into battery systems [4]. The selection of an appropriate cell type depends on the specific application, required power output, available space, and safety requirements.

The life cycle of Li-Ion batteries includes all phases from manufacturing, through operation, to end-of-life disposal. A proper understanding of the individual life cycle phases is essential for designing systems capable of effectively monitoring, protecting, and extending battery longevity. In battery monitoring systems, it is particularly important to track operational conditions, as these have a direct impact on battery degradation [5].

The operational phase is the longest and most significant part of the life cycle of a Li-Ion battery. During this phase, the battery is repeatedly charged and discharged depending on the application. Each charge-discharge cycle contributes to the gradual degradation of the cell, which appears as a decrease in capacity, an increase in internal resistance, and a deterioration of performance parameters [6]. The rate of degradation is significantly influenced by operating conditions, particularly temperature, charging and discharging current magnitudes, the operating voltage range, and the Depth of Discharge (DoD). Adverse conditions can substantially shorten the battery's lifespan and increase the risk of failure.

The aging of a Li-Ion battery is a complex process involving a combination of chemical, electrochemical, and mechanical phenomena within the cell. A distinction is made between calendar aging, which occurs even when the battery is not cycled, and cyclic aging, which is caused by repeated charging and discharging. The main manifestations of aging include the loss of active lithium inventory, degradation of electrode materials, an increase in internal resistance, and a reduction in the battery's ability to deliver high currents. These processes are largely irreversible [7] and gradually limit the battery's usability in its primary application.

1.1 Safety aspects during the life cycle

The safety of Li-Ion batteries is critical throughout their entire life cycle. Improper operation, mechanical damage, or exceeding permissible temperature and voltage limits can lead to hazardous events such as overheating, cell swelling, or, in extreme cases, thermal runaway [8]. For these reasons, modern applications increasingly use protection and monitoring systems that continuously track key battery parameters and, if necessary, alert the user or restrict the operation of the system. Such continuous monitoring throughout the life cycle significantly improves the safety, reliability, and lifespan of battery systems.

The end of life for a Li-Ion battery is generally considered to be the point at which its usable capacity drops below a specified threshold, most commonly around 70 % to 80 % of its initial nominal capacity. In this state, the battery may no longer meet the requirements of its original application; however, it can still be repurposed for less demanding systems [9]. The conclusion of primary use is followed by a secondary use phase (second life) or recycling, aimed at minimizing the environmental footprint while recovering valuable materials. Efficient life cycle management of Li-Ion batteries is therefore crucial not only from a technical and safety standpoint but also from an ecological perspective.

The SOC represents the ratio of the currently available battery capacity to its nominal capacity, usually expressed as a percentage. It is one of the most important parameters for both the user and the management system, as it indicates the remaining energy in the battery. However, the SOC cannot be measured directly and must be estimated using various computational methods. One of the most common methods is current integration, known as Coulomb counting, which tracks the amount of electrical charge supplied to or drawn from the battery during operation [10]. The main drawback of this method is the gradual accumulation of errors due to current measurement inaccuracies

and the absence of a precise initial SOC value. An alternative approach uses voltage-based methods, where the instantaneous voltage is compared to the cell's characteristic open-circuit voltage (OCV) curve. While simple to implement, this method has limited accuracy, especially under load or during dynamic current fluctuations [11].

In addition to the SOC, another key parameter is the SOH, which quantifies the degree of battery degradation compared to a new cell. The SOH is typically defined as the percentage ratio of the current maximum available capacity to the original nominal capacity. The decline in SOH is a natural result of battery aging and long-term operation. The primary degradation mechanisms include chemical degradation of electrodes, loss of active lithium, and an increase in the internal resistance of the cell. Monitoring the SOH is essential for estimating the Remaining Useful Life (RUL) of the battery, enhancing operational safety, and planning for battery replacement or repurposing in less demanding applications. The SOH is estimated based on long-term observation of charging and discharging cycles, capacity measurements, or analysis of changes in the battery's internal resistance [12].

The primary motivation for this study stems from the need to determine the actual remaining capacity of commonly used lithium-ion batteries, since this key indicator of battery health is typically not available to end users. Therefore, the objective of this research was to design and implement an SOH estimation algorithm embedded within a dedicated health-monitoring device for standard light LEVs, such as e-bicycles and e-scooters. The proposed system is designed to operate continuously during standard charging cycles. By analyzing dynamic charging parameters and specific battery characteristics, the device can accurately estimate the actual battery capacity.

The main goals of this research were:

- Design and implementation of a flexible, external data acquisition system: Development of a non-invasive condition monitoring device capable of logging main operational parameters (voltage, current, temperature) for LEV lithium-ion batteries without interfering with the internal BMS.
- Comprehensive experimental evaluation of battery cycling: Execution of repeated charging and discharging cycles on standard micromobility battery packs (e.g., e-bicycles, e-scooters) to capture real-world degradation patterns and capacity fade over time.
- Development and validation of a practical SOH estimation algorithm: Proposal of an algorithm to accurately estimate the SOH and evaluate the remaining useful life of the batteries, validated against the collected experimental dataset.

2 Materials and methods

Determining the SOH in practical applications is significantly more challenging than estimating the SOC, as it is a slowly varying parameter that cannot be directly measured by conventional physical sensors. The accuracy of SOH estimation depends heavily on the chosen mathematical model and the quality of the input data. Currently, the Li-Ion battery diagnostics primarily use methods based on tracking capacity degradation and internal resistance growth. The most straightforward approach is the direct capacity measurement method (Ah-method) [13], which compares the actual charge transferred during a full cycle with the nominal capacity of a new battery. Although highly accurate, this method requires a complete discharge and charge cycle under controlled conditions, which is often unfeasible in real-world operation. An alternative is monitoring the increase in Direct Current Internal Resistance (DCIR) [14], calculated based on the voltage response to a step change in current. The rise in internal resistance is a direct consequence of electrolyte aging and the formation of passivation layers on the electrodes. For applications requiring real-time SOH estimation, advanced model-based approaches, running directly within the BMS control unit, are employed [15]. These algorithms use Equivalent Circuit Models (ECM) that simulate the dynamic behavior of the battery with a network of resistors and capacitors. In state-of-the-art systems, data-driven methods are gaining traction; these leverage neural networks to identify nonlinear correlations between operational data and battery degradation, eliminating the need for an in-depth understanding of the internal electrochemical processes of the cell [16].

2.1 Basic quantities and principles of Li-Ion battery monitoring

Monitoring operational variables is a fundamental prerequisite for the safe and efficient operation of Li-Ion batteries. The most critical monitored parameters include electrical quantities - primarily voltage and current - as well as battery temperature. These data points provide vital information regarding the instantaneous state of the battery, its load, and potential operational risks. External monitoring devices are a distinct category of solutions connected to the battery without intruding into its internal architecture. These devices enable the measurement of voltage, current, and temperature during battery operation and often feature a visual user interface. The primary advantage of external solutions is their versatility and compatibility across various battery types.

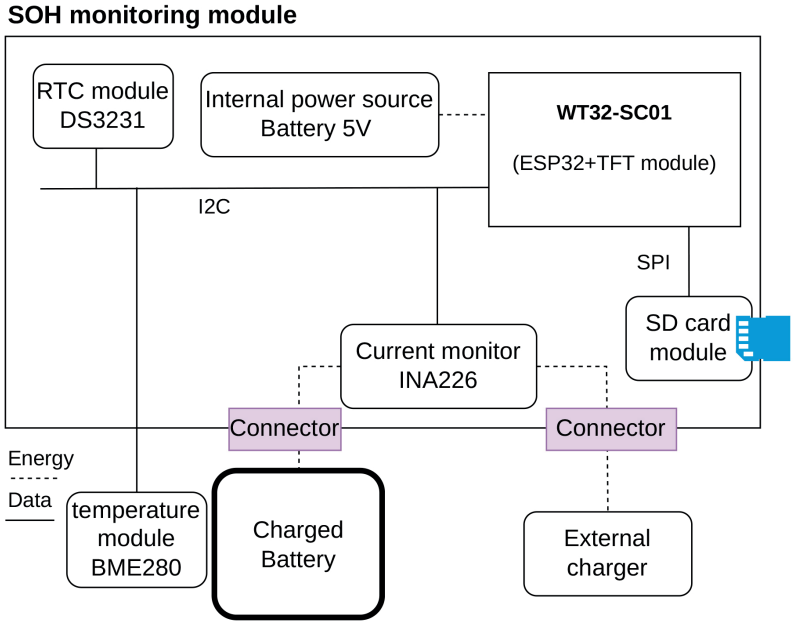

Figure 1 *Principal block connection diagram*

Table 1 *List of used batteries*

Label	Battery	Volage	Capacity
B1..B4	CNHL 4S	16.8 V	22.2 Wh
B5	Turnigy 2S	7.4 V	13.32 Wh

System architecture and hardware setup

The proposed external condition monitoring system was designed as an independent, non-invasive diagnostic unit. The core of the hardware architecture is the ESP32 microcontroller, selected for its robust processing capabilities and the extensive peripheral interface support. The ESP32 microcontroller is a part of the WT32-SC01 development board with a 3.5-inch color touch screen with a resolution of 320x480 pixels. To ensure the high-precision data acquisition during the battery charging process, a dedicated ADS1015 analog-to-digital converter (ADC) was used, rather than the microcontroller's internal ADC.

The electrical parameters are monitored using an INA226 power monitor integrated circuit (IC), which is connected via the I²C bus. This sensor continuously measures the charging current and battery voltage with high accuracy. The temperature of the battery pack and the ambient environment is monitored using the BME280 sensor. To ensure accurate time integration for capacity calculations and precise temporal data logging, a DS3231 Real-Time Clock (RTC) module is included in the system.

During the charging cycle, all monitored parameters - voltage, current, temperature, and elapsed time - are sampled continuously and logged to an external microSD card via the SPI interface. This comprehensive dataset forms the primary input for the subsequent SOH estimation algorithm. The system also includes a graphical touch interface for the real-time visualisation of the charging status, current SOC, and the estimated SOH (for example, tested on a 4S Li-Po configuration).

Battery specifications and charging protocol

The following batteries (Table 1) were used for this experiment.

A SkyRC[1] charger was used for charging. It is used to manage LiPo/LiHV/LiFe/LiIon (1-6S), NiMH/NiCd (1-15S) and Pb (2-20 V) batteries with capacities ranging from 100 to 50,000 mAh. The device provides a continuously adjustable charging current from 0.1 to 10 A and a balancing current of max. 300 mA per cell. The charging power with DC power supply reaches 2 x 100 W, while with an AC mains power supply it offers a total of 100 W with the possibility of asymmetrical distribution between the two outputs. Secondary, the device can be used as a laboratory power supply with a fixed voltage of 13.8 V and a power of up to 100 W [17].

For lithium (LiPo, LiHV, LiIon, LiFe) and lead (Pb) cells, the charger uses a CC/CV (Constant Current / Constant Voltage) algorithm. In the first phase, it applies a constant current (CC) until the maximum threshold voltage is reached. It then switches to the constant voltage (CV) phase, during which the charging current asymptotically approaches zero. Voltage balancing: For

[1] https://www.skyrc.com/D100_v2_Charger

lithium kits (from 2S to 6S), the voltage of individual cells is monitored and balanced via JST-XH ports using a passive balancing method with a limit current of 300 mA.

Data acquisition and SOH estimation algorithm

To accurately estimate the initial State of Charge (SOC_{start}), the proposed system requires the battery to be in a resting state before charging. The external device measures the Open-Circuit Voltage (OCV), allowing the microcontroller to derive SOC_{start} using a known dependency model [18]. This resting state measurement mitigates estimation errors caused by voltage drops across the internal resistance.

Energy Integration

Once the charging process is initiated, the system samples the instantaneous terminal voltage U_k and the charging current I_k at a frequency of 1 Hz. The total delivered electrical energy, $E_{delivered}$ (in Wh), is calculated using discrete time integration:

$$E_{delivered} = \sum_{k=1}^{N} U_k I_k \Delta t \tag{1}$$

where N is the total number of samples during the charge cycle, and Δt represents the sampling period converted to hours [19].

Capacity extrapolation and SOH calculation - The measurement concludes when the charging current drops below a predefined cutoff threshold (e.g., 0.3 A during the Constant Voltage phase), indicating that the battery has reached approximately 100 % SOC. The change in the State of Charge (ΔSOC), supplied during the measured cycle, is defined as:

$$\Delta SOC = 1 - \frac{SOC_{start}}{100}. \tag{2}$$

Based on the partially delivered energy and the corresponding ΔSOC, the system extrapolates the estimated maximum actual capacity of the battery, $E_{estimated}$:

$$E_{estimated} = \frac{E_{delivered} \cdot \eta}{\Delta SOC}, \tag{3}$$

where η represents the Coulombic and energy efficiency factor to account for thermal losses during charging. Finally, the State of Health is quantified by comparing the extrapolated real capacity to the nominal capacity ($E_{nominal}$) provided by the user configurations:

$$SOH = \left(\frac{E_{estimated}}{E_{nominal}}\right) \times 100. \tag{4}$$

To account for initial manufacturing variances, where the new cells might slightly exceed their nominal specifications, the algorithm caps the maximum SOH output at 105 %.

When measuring the total SOC, it is important to identify when the battery has reached its maximum charge. The battery charging process was terminated when the following conditions were met: $OCV \geq 4.2$ V and charging current I ≤ 0.3 A The actual battery capacity is then calculated (according to Equation (1)) and the battery health is evaluated according to Equation (4).

3 Results and discussion

As was stated at the beginning of this paper, the aim of this project was to design and implement of a flexible, external data acquisition system with a practical SOH estimation algorithm. The basic architecture is shown in Figure 1. The design uses an ESP32 microcontroller with a built-in display, which is used as an information module during battery charging (Figure 2).

To verify the functionality of the proposed device, 5 batteries were used (Table 1). The charger used had accurate power output measurements, which were used as reference values for the device.

The Final SOC values in Table 2 are calculated according to Equation (4). In the calculation, is considered a capacity of 22.2 Wh for batteries B1 to B4 and a capacity of 13.32 Wh for battery B5.

Graphs in Figure 3 present comprehensive charging profiles - specifically, charging voltage and current as functions of time - for all five batteries

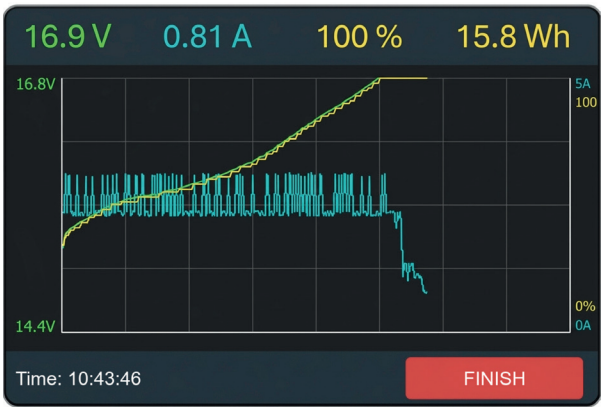

Figure 2 *Monitoring of battery charging process*

Table 2 *Charging results*

Battery	Start level	Delivered E	Final SOH
B1	0 %	18.95 Wh	89.8 %
B2	0 %	20.65 Wh	93.0 %
B3	15 %	18.8 Wh	99.6 %
B4	5 %	19.9 Wh	94.4 %
B5	33 %	4.8 Wh	53.8 %

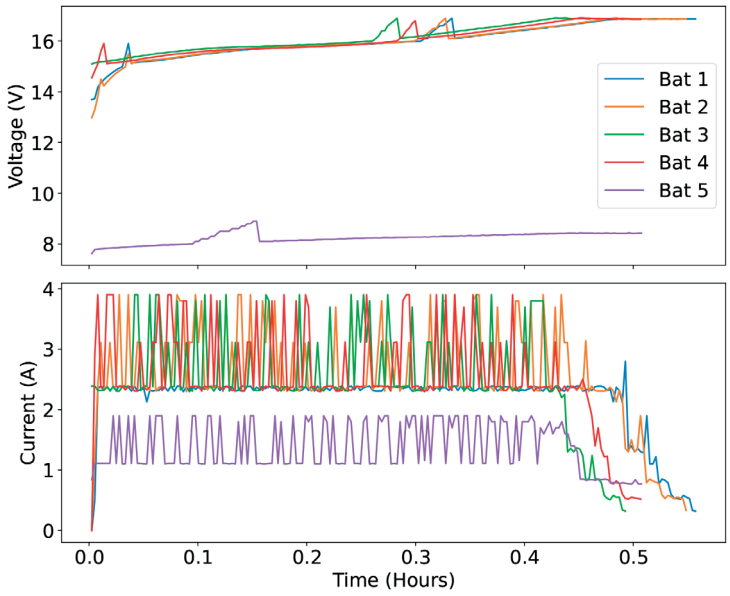

Figure 3 *The charging process monitored by our device*

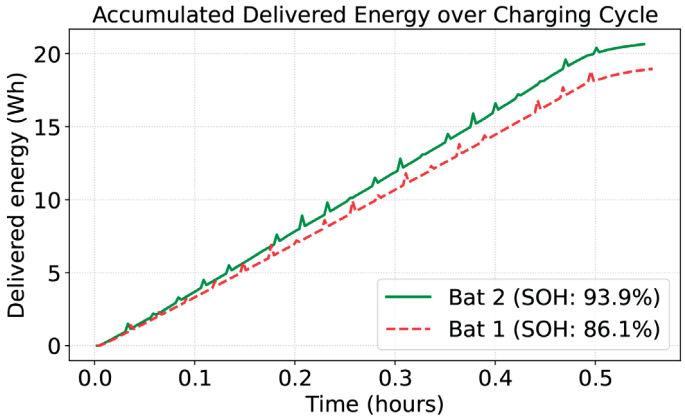

Figure 4 *Accumulated delivered energy over time during a charging cycle for a healthy (Bat 2) and a degraded (Bat 1) battery, both starting from 0 % SOC*

tested. The data confirm that the external monitoring system reliably records the standard constant current and constant voltage (CC-CV) charging protocol across different operating conditions and battery configurations. The voltage graph (top section) clearly distinguishes the architectures of the individual batteries. Batteries 1 to 4 have a 4S configuration, gradually approaching their maximum cut-off voltage of approximately 16.8 V during charging. In contrast, battery 5 has a 2S configuration and operates at a significantly lower voltage level, with a maximum limit of around 8.4 V.

The graph in Figure 3 (bottom) clearly highlights the transition between the CC and CV phases. During the initial CC phase, the charging current remains relatively high and stable until it reaches the battery's

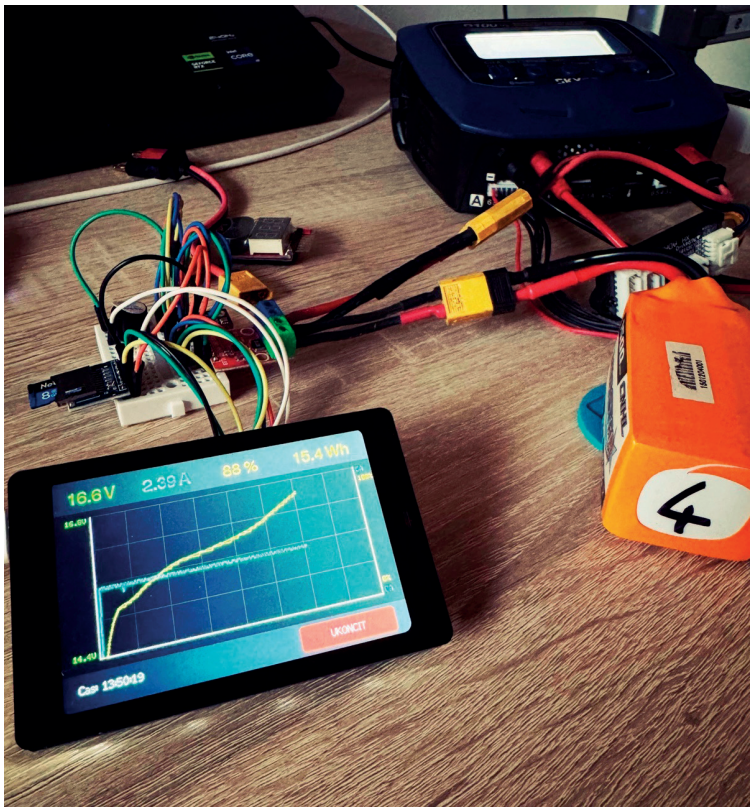

Figure 5 *Prototype of the external condition monitoring module, functioning as an intermediary diagnostic interface between a standard charger and the Li-Ion battery*

cut-off voltage. The charging process then transitions to the CV phase, where the current decreases exponentially until it falls below a predefined limit (e.g., 0.3 A), at which point charging is terminated.

In addition, different lengths of the charging cycles directly reflect the different initial charge states (e.g., battery 3 started the measurement at 15 % SOC, while battery 2 started at 0 % SOC), as well as the different levels of degradation and capacity loss of the individual cells.

Graph in Figure 4 shows the accumulation of delivered electrical energy during a charging cycle for two different battery packs, both starting from a completely discharged state (0 % SOC). As charging progresses, continuous discrete integration of electrical power reveals a significant difference in the total absorbed energy.

Although the charging cycle for both batteries ends when the current drops below the cutoff threshold - indicating 100 % relative SOC-the absolute energy capacity differs substantially. The healthy battery (Bat 2) accumulates a total of 20.65 Wh, while the slightly degraded battery (Bat 1) absorbs only 18.95 Wh before reaching the maximum voltage limit.

This 1.7 Wh difference clearly demonstrates capacity fade caused by battery aging. More importantly, it highlights the critical limitation of relying solely on the standard SOC indicator. While the BMS reports a *fully charged* state for both batteries, the degraded cell holds significantly less actual usable energy for the electric vehicle. This finding strongly supports the need for the proposed external monitoring device, which addresses this information gap by calculating the true SOH based on actual energy integration.

Furthermore, the experimental data revealed discrete fluctuations and step changes in the charging current, particularly during the Constant Current (CC) phase. These variations are primarily due to the discrete regulation mechanisms of commercial switch-mode power supply (SMPS) chargers typically used for micromobility, which do not provide an ideal, continuous current output. The presence of these real-world anomalies strongly underscores the necessity and robustness of the proposed high-frequency (1 Hz) discrete-time energy integration method. The used method of continuous sampling approach effectively captures dynamic fluctuations, ensuring high accuracy in calculating the total delivered energy and the subsequent SOH.

To demonstrate the practical applicability of the proposed solution, the physical monitoring module was constructed as a standalone, plug-and-play add-on device. Figure 5 shows the final hardware prototype in operation.

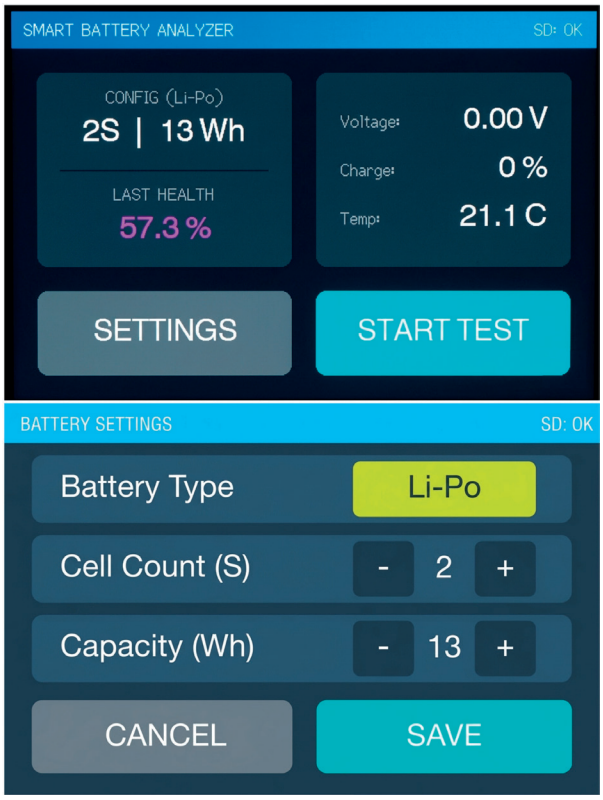

Figure 6 *Graphical user interface of proposed solution - setting of parameters*

Figure 6 shows the app's settings: battery type selection (Li-Po or Li-Ion), number of cells, and total battery capacity specified by the manufacturer.

The system is designed to connect in series directly between a conventional charger and the lithium-ion battery pack. A significant economic and practical advantage of this topology is its versatility. It operates on the premise that a basic, standard charger, serving solely as a power supply, is sufficient for the charging process, as all intelligent monitoring, data acquisition, and diagnostic algorithms are fully handled by the proposed external module.

During the charging cycle, the integrated graphical user interface (GUI) provides the end user with continuous, real-time feedback. It displays the instantaneous charging parameters, the dynamically calculated SOC, and the total accumulated energy delivered to the battery. By making these previously hidden metrics visible, the module transforms any standard charging setup into an advanced diagnostic station, giving users a clear, real-time understanding of their battery's actual condition.

4 Conclusion and future work

In this paper are presented the design, implementation, and practical validation of a flexible external condition monitoring system for lithium-ion batteries, specifically targeting light electric vehicles such as e-bikes and e-scooters. By serving as an independent diagnostic interface between the standard power supply and the battery pack, the proposed module effectively addresses the lack of operational transparency in conventional charging setups. The implemented SOH estimation algorithm, based on partial charging extrapolation and discrete energy integration, demonstrated high reliability. It successfully distinguished between healthy battery packs and those with significant capacity fade, without requiring the user to perform time-consuming full discharge cycles.

While the current hardware prototype with a large graphical interface validates the concept, future development will focus on optimizing the device for broader practical deployment. Proposed improvements for future iterations include:

Cloud-Based Analytics. Leveraging IoT capabilities for remote data collection and implementing data-driven predictive models to estimate the Remaining Useful Life (RUL) with even greater precision.

Mobile Application Integration. Exploiting the native Bluetooth Low Energy (BLE) and Wi-Fi capabilities of the ESP32 microcontroller to transmit data to a dedicated smartphone application (iOS/Android). This app would serve as the primary user interface, offering detailed diagnostic insights, long-term charging history, and degradation trends.

The proposed external monitoring concept transforms a standard charging routine into a reliable diagnostic process, empowering users to maximize the lifespan, safety, and performance of their micromobility energy storage systems.

Future development will include further discussion of specific calibration requirements and device durability under various environmental conditions to streamline integration with commercial charging systems. Additionally, to validate the general applicability and evaluate measurement uncertainties, subsequent research will involve sensitivity analysis, testing on a broader dataset of diverse battery chemistries, and a direct comparative assessment with integrated BMS solutions.

Acknowledgements

This work was supported by KEGA through the Teaching and development of methodology for the use of microcontrollers in automation using practical examples and laboratory exercises for engineering students under Grant 024STU-4/2024.

Conflicts of interest

The authors declare that they have no known competing financial interests or personal relationships that could have influenced the work reported in this paper.

References

[1] DYCZKOWSKA, J. A., CHAMIER-GLISZCZYNSKI, N., MURAWSKI, J. Assessment of micromobility infrastructure from the perspective of electromobility development. *Applied Sciences* [online]. 2025, **15**(22), 12276. eISSN 2076-3417. Available from: https://doi.org/10.3390/app152212276

[2] MOHAMMADI, F. Lithium-ion battery state-of-charge estimation based on an improved coulomb-counting algorithm and uncertainty evaluation. *Journal of Energy Storage* [online]. 2022, **48**, 104061. ISSN 2352-152X, eISSN 2352-1538. Available from: https://doi.org/10.1016/j.est.2022.104061

[3] PHOGAT, P., DEY, S., WAN, M. Powering the sustainable future: a review of emerging battery technologies and their environmental impact. *RSC Sustainability* [online]. 2025, **3**(8), p. 3266-3306. ISSN 2753-8125. Available from: https://doi.org/10.1039/D5SU00127G

[4] TRAN, M.-K., FOWLER, M. A review of cloud-based battery management systems for lithium-ion batteries in electric vehicles. *IEEE Access* [online]. 2022, **10**, p. 99263-99277. elSSN 2169-3536. Available from: https://doi.org/10.1109/ACCESS.2024.3446880

[5] ARABSALMANABADI, B., TASHAKOR, N., JAVADI, A., AL-HADDAD, K. Charging techniques in lithium-ion battery charger: review and new solution. In: 44th Annual Conference of the IEEE Industrial Electronics Society IECON 2018: proceedings. IEEE. 2018. eISSN 2577-1647, eISBN 978-1-5090-6684-1, p. 5731-5738. Available from: https://doi.org/10.1109/IECON.2018.8591173

[6] OTHMAN, A., HRAD, J., HAJEK, J., MAGA, D. Control strategies of hybrid energy harvesting - a survey. *Sustainability* [online]. 2022, **14**(24), 16670. eISSN 2071-1050. Available from: https://doi.org/10.3390/su142416670

[7] EDGE, J. S., O'KANE, S., PROSSER, R., KIRKALDY, N. D., PATEL, H. C., HALES, A., GHOSH, A., AI, W., CHEN, J., YANG, J., LI, S., PANG, M.-CH., DIAZ, L. B., TOMASZEWSKA, A., MARZOOK, M. V., RADHAKRISHNAN, K. N., WANG, H., PATEL, Y., WUBD, B., OFFER, G. J. Lithium ion battery degradation: what you need to know. *Physical Chemistry Chemical Physics* [online]. 2021, **23**(14), p. 8200-8221. Available from: https://doi.org/10.1039/D1CP00359C

[8] DUAN, J., TANG, X., DAI, H., YANG, Y., WU, W., WEI, X., SUN, Z. Building safe lithium-ion batteries for electric vehicles: areview. *Electrochemical Energy Reviews* [online]. 2020, **3**, p. 1-42. ISSN 2520-8489, eISSN 2520-8136. Available from: https://doi.org/10.1007/s41918-019-00060-4

[9] GAO, W., THOO, A. C., SARKER, M., LEE, N., DENG, X., YANG, Y. Secondary use of retired lithium-ion traction batteries: a review of health assessment, interface technology, and supply chain management. *Batteries* [online]. 2026, **12**(1), 1. eISSN 2313-0105. Available from: https://doi.org/10.3390/batteries12010001

[10] MOVASSAGH, K., RAIHAN, A., BALASINGAM, B., PATTIPATI, K. A critical look at coulomb counting approach for state of charge estimation in batteries. *Energies* [online]. 2021, **14**, 4074. eISSN 1996-1073. Available from: https://doi.org/10.3390/en14144074

[11] PISANI ORTA, M. A., GARCIA ELVIRA, D., VALDERRAMA BLAVI, H. Review of state-of-charge estimation methods for electric vehicle applications. *World Electric Vehicle Journal* [online]. 2025, **16**, 87. eISSN 2032-6653. Available from: https://doi.org/10.3390/wevj16020087

[12] BERECIBAR, M., GANDIAGA, I., VILLARREAL, I., OMAR, N., VAN MIERLO, J., VAN DEN BOSSCHE, P. Critical review of state of health estimation methods of Li-ion batteries for real applications. *Renewable*

and Sustainable Energy Reviews [online]. 2016, **56**, p. 572-587. eISSN 1364-0321. Available from: https://doi.org/10.1016/j.rser.2015.11.042

[13] AL-HAJ HUSSEIN, A., BATARSEH, I. A review of charging algorithms for nickel and lithium battery chargers. *IEEE Transactions on Vehicular Technology* [online]. 2011, **60**(3), p. 830-838. ISSN 0018-9545, eISSN 1939-9359. Available from: https://doi.org/10.1109/TVT.2011.2106527

[14] MUN, T., NOH, C., LEE, S.-E. Comparative analysis of DCIR and SOH in field-deployed ESS considering thermal non-uniformity using linear regression. *Energies* [online]. 2025, **18**(21), 5640. eISSN 1996-1073. Available from: https://doi.org/10.3390/en18215640

[15] CHENG, K. W. E., DIVAKAR, B. P., WU, H., DING, K., HO, H. F. Battery-management system (BMS) and SOC development for electrical vehicles. *IEEE Transactions on Vehicular Technology* [online]. 2011, **60**(1), p. 76-88. ISSN 0018-9545, eISSN 1939-9359. Available from: https://doi.org/10.1109/TVT.2010.2089647

[16] TIAN, H., QIN, P., LI, K., ZHAO, Z. A review of the state of health for lithium-ion batteries: research status and suggestions. *Journal of Cleaner Production* [online]. 2020, **261**, 120813. ISSN 0959-6526, eISSN 1879-1786. Available from: https://doi.org/10.1016/j.jclepro.2020.120813

[17] D100v2 AC/DC dual balance charger/discharger/power supply - SkyRC Technology Co., Ltd. [online]. 2022. Available from: https://www.skyrc.com/D100_v2_Charger

[18] PATTIPATI, B., BALASINGAM, B., AVVARI, G., PATTIPATI, K., BAR-SHALOM, Y. Open circuit voltage characterization of lithium-ion batteries. *Journal of Power Sources* [online]. 2014, **269**, p. 317-333. ISSN 0378-7753, eISSN 1873-2755. Available from: https://doi.org/10.1016/j.jpowsour.2014.06.152

[19] LAVIGNE, L., SABATIER, J., MBALA, F., GUILLEMARD, F., NOURY, A. Lithium-ion open circuit voltage (OCV) curve modelling and its ageing adjustment. *Journal of Power Sources* [online]. 2016, **324**, p. 694-703. ISSN 0378-7753, eISSN 1873-2755. Available from: https://doi.org/10.1016/j.jpowsour.2016.05.121

ASSESSMENT OF VEHICULAR PASSENGER OCCUPANCY AND ITS EFFECT ON LOS

Rashmi Ranjan Samal[1], Kundan Samal[1], Sitansu Kumar Das[2], Satya Ranjan Samal[1], Malaya Mohanty[1,*]

[1]Kalinga Institute of Industrial Technology (KIIT) Deemed to be University, School of Civil Engineering, Bhubaneswar, India
[2]Government College of Engineering, Department of Civil Engineering, Keonjhar, India

*E-mail of corresponding author: malaya.mohantyfce@kiit.ac.in

Kundan Samal 0000-0003-2142-0656,
Satya Ranjan Samal 0000-0001-8675-453X,
Sitansu Kumar Das 0000-0003-3472-2792,
Malaya Mohanty 0000-0002-6116-782X

Resume

The expansion of infrastructure in developing countries have led to a surge in car ownership. Although cars offer greater safety, their less passenger occupancy has contributed to reduced level of service (LOS). The present study was aimed to investigate the effect of passenger occupancy of various modes of transport on LOS. Detailed on-field surveys, including video recordings and questionnaires have been used to collect data, which is subsequently analyzed. The study findings suggest that a huge improvement in LOS and congestion can be achieved if public transportation is used more. Even usage of 3Ws and 2Ws can reduce congestion compared to usage of cars. While a person using a bus uses just 0.48 m^2 of the road space, a person using car uses 2.23 m^2 of the road space. The findings of this research are intended to inform traffic engineers and practitioners in developing more balanced traffic management strategies.

Article info

Received 18 November 2025
Accepted 9 March 2026
Online 18 March 2026

Keywords:

Level of Service (LOS)
congestion
passenger occupancy
vehicular occupancy
traffic engineering
transportation management

Available online: https://doi.org/10.26552/com.C.2026.018

ISSN 1335-4205 (print version)
ISSN 2585-7878 (online version)

1 Introduction

Transportation systems are integral part to the economic and social fabric of any society. The efficiency and effectiveness of these systems depend on various factors, including the mode of choice, vehicle occupancy, and the level of service (LOS) provided [1]. The LOS is the service provided to the road users in terms of comfort and safety, which is usually categorized using Volume to Capacity (V/C) ratio. The choice of vehicle mode/category that is preferred by the road users, along with vehicle occupancy and level of service are critical factors that influence the efficiency and sustainability of transportation systems. Understanding these elements helps in planning and implementing strategies to improve mobility, reduce congestion, minimize environmental impacts and sustainability of transportation networks.

The mode of choice refers to the type of a vehicle, which individuals/groups select for their transportation needs. Examples include private cars (4W), public buses (Bus), private motorized two-wheelers (2W), bicycles, or walkers/pedestrians. The choice of transportation mode is influenced by various factors, including individual preferences, socioeconomic status, environmental concerns, and the availability of infrastructure [2-3]. In a developing country like India, the use of different types of vehicles varies significantly among the population. As of recent data [4], the trends in sales of the two-wheelers (2Ws), three-wheelers (3Ws), cars, and buses in India show significant growth and transformation. Motorized 2 Wheelers remain the most common form of personal transportation in India, with approximately 70-75% of households owning at least one [4-6]. On average, public buses are used by around 10-15% of the population for daily commuting [6]. Another very commonly used public mode of transportation in developing countries like India are 3 Wheelers/autorickshaws (3W) [6-8]. They cater to around 5-10% of the urban population, providing a flexible and relatively affordable alternative to buses and personal vehicle. Next are the cars/jeeps, which can be termed as LMVs/4 Wheelers too. In India, the ownership and use of private cars (4W) are

Figure 1 *Snapshots of Video Recordings*

increasing rapidly, but they are still less prevalent as compared to 2W [6-8]. On an average, 7.5% (ranging from 4.4% in rural areas to 13.8% in urban areas) of households are found to be owning private car [7-9]. These statistics highlight the diversity in transportation preferences in India, which is dynamically shifting towards private cars or 4W [10]. However, the occupancy of these vehicles poses a threat to congestion as well as air quality [11-13].

Vehicle occupancy refers to the number of people in a vehicle at a given time [13]. This concept is significant in transportation planning, environmental analysis, and urban development. Understanding vehicle occupancy helps in assessing traffic congestion, fuel efficiency, and pollution levels [14-16]. Indians are heavily dependent on private vehicles as compared to public transportation. Even in private vehicle possession, gradually a shift from 2Ws to cars is being observed. If 100 people commuting to workplace using 2Ws shift towards cars, the space required for 100 cars would be 4-5 times more than for the 2Ws. This shall lead to undesirable delay and congestion on the road. Many studies were devoted to the usage of public transport [16-22], which can improve the effectiveness of traffic flow and improve air quality. Increased areas occupied by private vehicles with less occupants may lead to increased travel times, cause congestion and reduce the level of service (LOS) on road. The LOS of a road describes the quality of service that a roadway facility is providing to its users encompassing aspects such as travel time, frequency, reliability, and user comfort [21]. Although studies have been conducted to evaluate the mode of choice and vehicular occupancy individually by various researchers [6-8], combined effect of both the factors have been rarely studied. Further, studies in developing countries are limited.

The present study has been conducted to explore the preferences and behaviors of road users regarding their mode of choice, analyze the vehicle occupancy patterns for different categories of vehicles, and examine how these factors affect the level of service on road. The research provides valuable insights into current transportation trends and identifies potential areas for improvement in transportation systems to reduce congestion, delays, etc., thereby improving LOS on roads.

2 Data collection, extraction and methodology

The objectives of the present study have been attained by the collection of data from various road locations. The present study has been conducted in the city of Bhubaneswar, India on the urban arterials, which are 4-lane divided roads. Bhubaneswar is a Tier - II developing smart city in India. The cities across India have been divided into three categories [22].

- Category X (population of 5 million and above),
- Category Y (population between 0.5 and 5 million), and
- Category Z (population below 0.5 million).

Usually, these are indicated as tier-I, tier-II, and tier-III cities, respectively. The present study has been conducted in a tier - II city considering its varied qualities concerning people, their economic standards, education standard, job status, family type, etc., leading to a much large spectrum of driving behavior. Further, Tier II cities in India are experiencing many developmental changes in recent times [22]. Furthermore, majority of the cities in India belong to the category of tier-II. Thus, to achieve the motive of the research, Bhubaneswar, which is one of the tier-II cities of India and the capital city of Odisha has been chosen as the study area. However, the methodology used in the study can be used at various tier-I and tier-III cities to get the findings for them. Due to difference in demography and living standards, the results will vary, mainly in terms of vehicular composition leading to difference in congestion and LOS levels. Video recordings have been conducted for various road mid-block sections across the city. Few snapshots from various locations are provided in Figure 1.

The collected videos are played on a TV monitor and the classified traffic volume is extracted. In case of 2 Wheelers, the vehicle occupancy is noted from the collected videos. For buses, physical inspection and driver interrogation has been conducted to ascertain the average vehicle occupancy. Similarly, for 3 wheelers and 4 wheelers, the vehicle occupancy is determined based on both, observation from videos and field along with cross-examination from riders. Thereafter, the collected traffic volumes across different times of day are converted to Passenger car Units (PCUs) for further

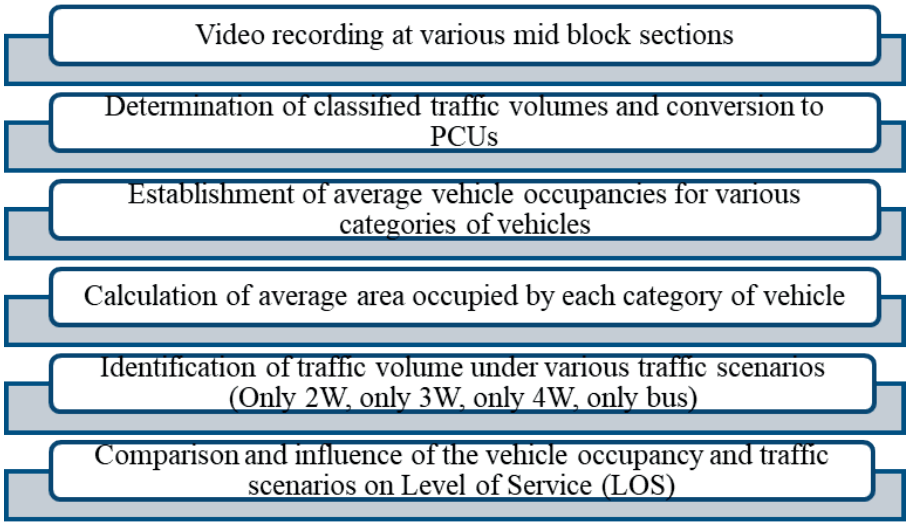

Figure 2 *Flow chart depicting methodology*

Table 1 *Classified vehicle count with percentage composition and PCU*

Time	2W	3W	4W	Buses	Total	Total PCU
8:00-9:00 AM	840	192	210	16	1258	937.6
9:00-10:00 AM	1008	252	264	24	1548	1176
10:00-11:00 AM	1440	260	400	24	2124	1564.8
11:00-12:00 PM	1500	312	620	32	2464	1938.8
12:00-01:00 PM	1600	404	496	36	2536	1959.2
01:00-02:00 PM	980	224	460	12	1676	1337.2
02:00-03:00 PM	1352	240	580	24	2196	1712.8
03:00-04:00 PM	1548	344	720	12	2624	2077.2
04:00-05:00 PM	1592	304	740	16	2652	2084
Total Volume	11860	2532	4490	196	19078	14788
Vehicle Composition (%)	62.1	13.3	23.6	1	100	

Table 2 *Median PCU Units used for the present study*

Vehicles	PCU
Two-Wheeler (2W)	0.50
Four-Wheeler (4W)	1.00
Big Cars/LCV (4W)	1.40
Three-Wheeler (3W)	1.20
Bus	2.20

analyses. Figure 2 shows the methodology that has been used in the present study.

3 Results

Traffic data has been extracted from over 9 hours of recorded video across various traffic volumes on various mid-block sections of Bhubaneswar city. The data comprised of more than 15000 vehicles. The vehicles were first classified into 4 categories as follows.

- Two Wheelers (2W)
- Three Wheelers (3W)
- Cars and jeeps (4W), and
- Buses

Trucks were not considered for the study as their number is small on road and they are used for transport of goods and not passengers. Therefore, they do not serve as a mode choice for road users. Further, 4W comprises both passenger cars and big cars. They have been clubbed in one category as the vehicle occupancy is same in both. Table 1 show cases of the consolidated classified counts of various categories of vehicles over 9 AM to 5 PM period, with percentage composition of each

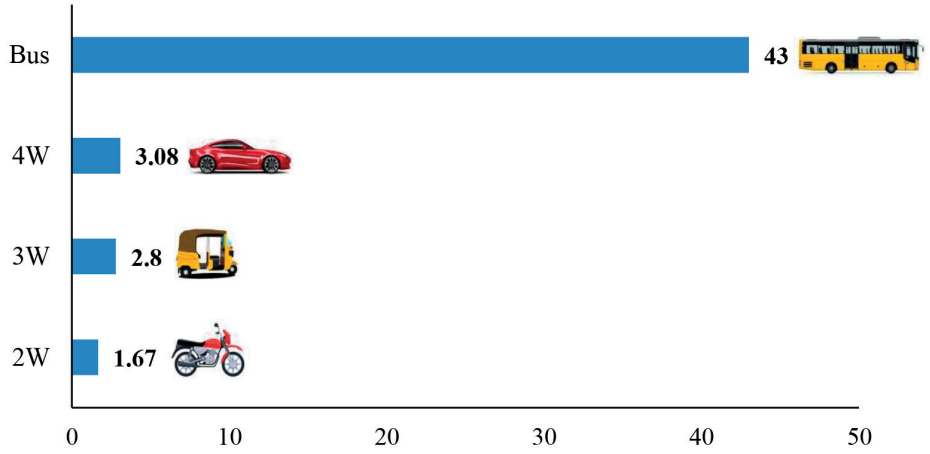

Figure 3 *Average occupancy per vehicle*

Table 31 *Determination of mode choice ratio among road users*

Category of vehicle	Number of vehicles on road (considering 100 vehicles plying on road)	Number of people using them (considering the avg. vehicle occupancy)	Percentage of road users using the specific vehicle category
2W	62	104	40.3
3W	13	37	14.3
4W	24	74	28.7
Bus	1	43	16.7
Total	100	258	

vehicle category. The vehicle counts are converted to PCUs (Passenger Car Units) based on the IRC 106-1990 (Guidelines for capacity of urban roads in plain areas) [23] as shown in Table 2. The PCU for any vehicular category is defined as the equivalent factor as compared to passenger car (which is 1.00), which is determined based on vehicle dimensions and its speed. In the case of 4W, as mentioned earlier, it comprises both passenger and big cars. Therefore, the PCU values for 4W is considered as 1.2 for the study.

As can be seen from Table 1, the average traffic volume on the studied 2-lane one way (one direction of 4-lane divided road) ranged from 938 PCUs to 2084 PCUs on a typical working day. The vehicle composition shows excessive use of private vehicles, both 2W and 4W, while commuting by the road users. Similarly, the 3W too account for 13.3%, which are known for their slow speeds and the public buses account just 1% on the road. However, this does not reflect the number of people using the public and private transport, since the occupancy of all modes is not the same. To understand this, the occupancy of various categories of vehicles have been collected through the field survey and have been extracted from recorded data as well. Figure 3 shows the average vehicle occupancy based on category of vehicles.

As can be observed from Figure 3, the average occupancy of 2W is the smallest and rightfully so, at 1.67, whereas, the 4W (cars and jeeps) even though have a minimum seating capacity of 5, are observed to have an average occupancy of around 3.08. Roughly, it can be stated that if 100 vehicles are plying on road, roughly 62 of them are 2W, 13 vehicles are 3W, 24 are 4Ws, and only 1 vehicle is a bus. From this data, the number of road users using various modes can be determined using their occupancy as stated in Table 3. The conclusion from Table 3 is that around 83% of people are opting for 2W, 3W, or car usage (as pillion/rider, or as driver/passenger), while only 16.7% are opting for bus.

From Table 3 can also be noticed that although 62% of trips on roads are made by 2Ws and 23.6% of trips are made by cars and jeeps (4Ws), which accounts for around 86% of trips on roads, however, the people using them comprise only 69%. This showcases that these vehicles might be augmenting traffic congestion leading to increased delays, since they occupy more space on the road, but their occupancy is less. Thus, a smaller number of people are using more space on road, which also varies between 2W, Cars, 3W and Buses. Many articles on social media present this event as a graphic image comparing cars and buses but it is not scientific/technically correct. Moreover, it also varies from category to category. To put a perspective of Indian conditions to the study, at first the top best-selling 2Ws, 3Ws, 4Ws and common buses observed on the road have been considered. The areas occupied by them on the road has been obtained (dimensions of vehicles) and their average has been considered for the said category for the study. Table 4 presents the details.

Average area obtained from Table 4 for different categories have been used in the present study for further

Table 4 *Area covered by commonly sold/observed vehicles of different categories*

Category of vehicle	Area occupied (m^2)	Average area occupied (m^2)
	2W	
Hero Splendor	1.48 (2.00 X 0.74)	1.38
Honda Activa	1.3 (1.833 X 0.697)	
Bajaj Pulsar	1.55 (2.035 X 0.765)	
TVS Jupiter	1.2 (1.834 X 0.650)	
	4W	
Tata Nexon	7.2 (3.995×1.804)	6.87
Maruti Suzuki Swift	6.7 (3.845×1.735)	
Maruti Suzuki Dzire	6.9 (3.995×1.735)	
Tata Punch	6.7 (3.827×1.742)	
	3W	
Bajaj Auto	3.4 (2.635×1.300)	3.67
Piaggio	3.7 (2.700×1.370)	
Atul Auto	3.9 (2.765×1.420)	
	BUS	
Ashok Leyland Sunshine	20.7 (9.415×2.200)	20.8
Mahindra Cruzio Grande Staff	21 (8.950×2.350)	
Eicher Starline	20.7 (9.584×2.164)	

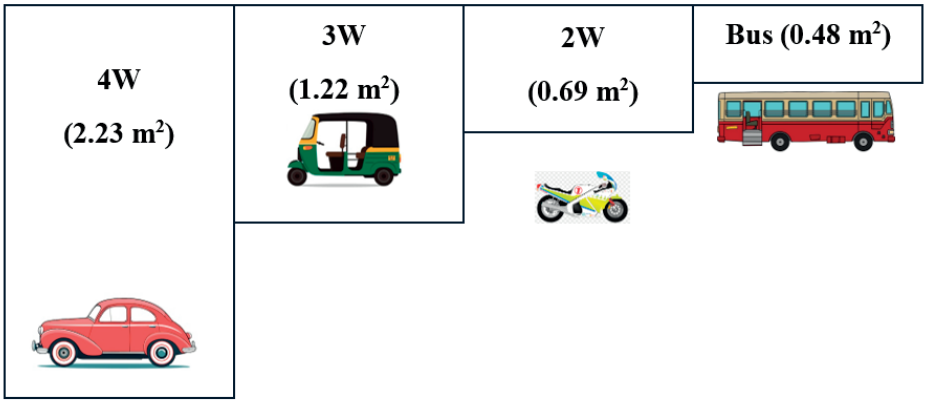

Figure 4 *Area occupied by each road user using a specific category of vehicle*

analysis on assessing the increased congestion on road. Based on the earlier results of vehicle occupancy, the area occupied by each road user using a specific category has been determined and is shown graphically in Figure 4. It clearly shows how people travelling in buses occupy the least space on the road (0.48 m^2) while people travelling in cars take up the highest space on road (2.23 m^2). In other words, the area occupied by around 5 people in a bus, is occupied solely by a car user.

In an ideal scenario, if people start using cars only, it will lead to dangerous levels of traffic congestion. To identify the effect of specific vehicle type on traffic volume, which is a major indicator of the LOS on roads (Indo HCM, 2017; IRC 106-1990), 4 ideal scenarios have been created as follows.

- All road users use Bus.
- All road users use 2W.
- All road users use 3W.
- All road users use 4W/Car.

The effect of these ideal scenarios on LOS of the road is compared to the existing traffic scenario with prevailing vehicle proportions. Now, to analyze and compare, traffic counts from field data, as provided in Table 1, have been utilized. For instance, during 10-11 AM, which is one of the peak time periods, a total of 1440-2W, 260-3W, 400-4W, and 24 buses are travelling on the road. Based on average vehicle occupancy, during this time total number of people travelling on the surveyed road can be calculated, which comes out to be 5397 $\cong$ 5400 (1440*1.67 + 260*2.8 + 400*3.08 + 24*43). Considering the above data, the number of vehicles required if they travel only by 2W, 3W, Car/4W or bus (the 4 ideal scenarios listed earlier) is determined and then converted into PCUs (as per data from Table 2), to

Table 5 *Determination of traffic volume under various traffic scenarios*

Time (h)	Avg. occupancy	Only Bus		Only 2W		Only 3W		Only 4W		Ex. PCU
		No.	PCU	No.	PCU	No.	PCU	No.	PCU	
8-9	3276	76	167.2	1962	981	1170	1404.0	1064	1276.8	937.6
9-10	4235	98	215.6	2536	1268	1513	1815.6	1375	1650.0	1176
10-11	5397	126	277.2	3232	1616	1928	2313.6	1753	2103.6	1564.8
11-12	6665	155	341.0	3992	1996	2381	2857.2	2164	2596.8	1938.8
12-13	6879	160	352.0	4120	2060	2457	2948.4	2234	2680.8	1959.2
13-14	4197	98	215.6	2514	1257	1499	1798.8	1363	1635.6	1337.2
14-15	5749	134	294.8	3443	1721.5	2054	2464.8	1867	2240.4	1712.8
15-16	6282	146	321.2	3762	1881	2244	2692.8	2040	2448.0	2077.2
16-17	6478	151	332.2	3880	1940	2314	2776.8	2104	2524.8	2084
Avg. Volm.	5462	127	279.4	3272	1636	1952	2342.4	1774	2128.8	1643.1

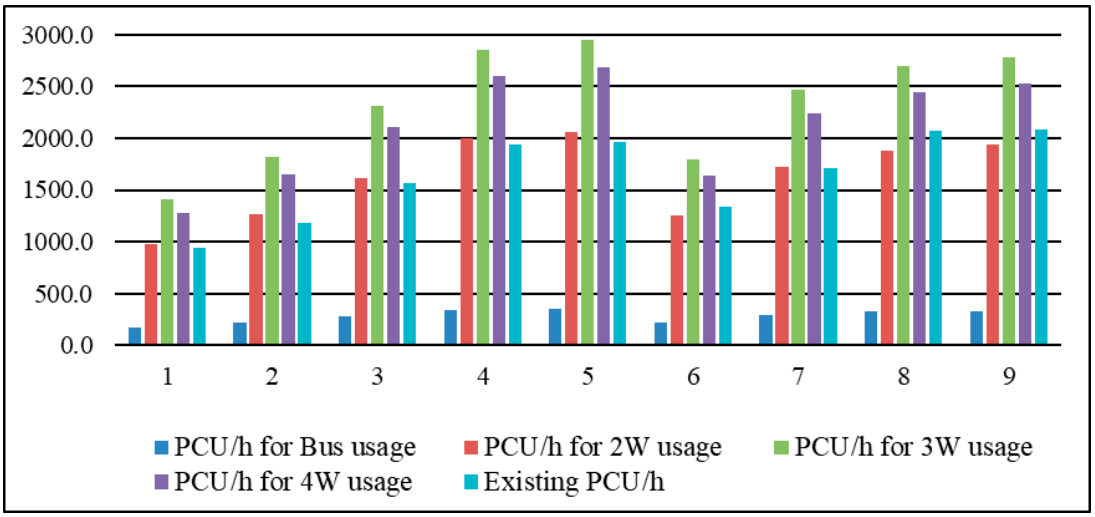

5(b) *Comparison of existing traffic flow with specific vehicle usage scenarios*

Figure 5 *Graphs displaying traffic flow for specific vehicle usage scenarios and existing traffic volume*

know how the traffic flow can be reduced/increased if a specific category of vehicle is used by road users. These traffic flows are compared to the existing traffic flows (Existing PCU in Table 1) during that time interval. The detailed analysis and comparison of PCUs is shown in Table 5.

It can be observed that the usage of 3W, and Cars increase the PCUs of road as compared to existing traffic, whereas the usage of buses can decrease the PCU. In the context of the present study, the percentage decrease/increase in the traffic volume/accommodation of more/less road user, with the existing traffic volume, with respect to usage of specific category of vehicle is presented in Figures 5 (a) and (b).

5(a) Traffic volume in terms of PCU/h from 8 AM to 5 PM for specific vehicle usage compared to existing traffic flow

As can be seen from the Figure 5, the usage of Bus only, can decrease the traffic flow on roads by 83%, whereas the usage of cars/3W only shall increase the traffic flow by 30-43%. The present study is conducted on a 2-lane one way road where the capacity is 2400 PCU/h based on IRC 106-1990 and Indo-HCM (2017) [23-28]. According to IRC guidelines, for urban roads, the design level of service (LOS) should be C where V/C ratio lies between 0.56-0.70. Indo-HCM (2017) suggests new lane or any other measures if the existing volume regularly exceeds 1680 PCU/h, which is also termed as Design Service Volume (DSV). In the present study, it is observed that although the average existing traffic volume is 1643 PCU/h, however, there are instances like 11 AM - 1 PM and 3 PM - 5 PM where the volume exceeds DSV (Table 5). As can be seen from Table 5, if only buses are used, the LOS can decrease largely on road improving the quality of traffic movement. Table 6 shows the LOS ranges based on Indo-HCM (2017) [26] guidelines, and thereafter Table 7 presents the LOS while using a particular vehicle category under

Table 6 *LOS of Two lane Undivided Urban Roads [26]*

LOS level	V/C ratio
A	< 0.35
B	0.36 - 0.55
C	0.56 - 0.70
D	0.71 - 0.85
E	0.86 - 1.00
F	> 1.00

Table 7 *Determination of LOS under various traffic scenarios*

Time (h)	Only Bus		Only 2W		Only 3W		Only 4W		Actual PCU	Actual V/C (LOS)
	PCU	V/C (LOS)	PCU	V/C (LOS)	PCU	V/C (LOS)	PCU	V/C (LOS)		
8-9	167.2	0.07 (A)	981	0.41 (B)	1404.0	0.59 (C)	1276.8	0.53 (B)	937.6	0.39 (B)
9-10	215.6	0.09 (A)	1268	0.53 (B)	1815.6	0.76 (D)	1650.0	0.69 (C)	1176	0.49 (B)
10-11	277.2	0.12 (A)	1616	0.67 (C)	2313.6	0.96 (E)	2103.6	0.88 (E)	1564.8	0.65 (C)
11-12	341.0	0.14 (A)	1996	0.83 (D)	2857.2	1.19 (F)	2596.8	1.08 (F)	1938.8	0.81 (D)
12-13	352.0	0.15 (A)	2060	0.86 (E)	2948.4	1.23 (F)	2680.8	1.12 (F)	1959.2	0.82 (D)
13-14	215.6	0.09 (A)	1257	0.52 (B)	1798.8	0.75 (D)	1635.6	0.68 (C)	1337.2	0.56 (C)
14-15	294.8	0.12 (A)	1721.5	0.72 (D)	2464.8	1.03 (F)	2240.4	0.93 (E)	1712.8	0.71 (D)
15-16	321.2	0.13 (A)	1881	0.78 (D)	2692.8	1.12 (F)	2448.0	1.02 (F)	2077.2	0.87 (E)
16-17	332.2	0.14 (A)	1940	0.81 (D)	2776.8	1.16 (F)	2524.8	1.05 (F)	2084	0.87 (E)
Avg. volm.	279.4	0.12 (A)	1636	0.68 (C)	2342.4	0.98 (E)	2128.8	0.89 (E)	1643.1	0.68 (C)

particular traffic scenarios. Table 7 is an extension to Table 5.

In Table 7, it can be observed that LOS A is achieved only when buses are used for transport by all the road users. Similarly, even usage of only 2Ws will keep the LOS levels to mostly B/C. However, more usage of 3W and cars can lead to congestion and deteriorate the quality of traffic flow as compared to the actual traffic conditions on the road. Similarly, more usage of bus can help to alleviate the traffic congestion and improve the driving conditions. Previous studies by various authors [29-31] have examined changes in traffic conditions using historical data from cities such as Bhopal and Delhi, and have highlighted the challenges, and strategies associated with achieving sustainable urban mobility in India. The findings from the present study provides further insights into this issue by proposing strategic solutions to address the growing problem of traffic congestion in Indian cities, which has resulted in reduced LOS and increased congestion.

4 Conclusion

The traffic congestion is a major issue in many of the developing countries including India. Many studies are being conducted to tackle the issue. However, one of the most pertinent issues of mode use or vehicle passenger occupancy is less discussed and studied. In the present study was investigated the reduction of LOS on the road due to stubbornness of road users to use a particular category of a vehicle. Traffic survey was conducted on assessing the impact of different vehicle categories (Bus, Car, 3 Wheeler, and 2 Wheeler) on traffic volume and road capacity on various road stretches in Bhubaneswar. By analyzing existing traffic conditions and evaluating ideal scenarios where only one type of vehicle dominates the road, the study has yielded critical insights into the road space usage, traffic volume, and the overall quality of traffic flow.

The current analysis indicates that the existing traffic conditions, characterized by a diverse mix of vehicle types, result in moderate congestion. Although the Passenger Car Unit (PCU) values suggest that the traffic movement is generally manageable, there are noticeable signs of congestion during the peak hours. It was an insightful finding that the buses, which contribute just 1% of total vehicular categories for passenger transport, carry 16% of total road users. However, 2Ws, which comprise around 64% of total road traffic only carry 43% of total road users. Similarly, it was underwhelming to see that only 30% (16% buses, 14% 3Ws) of total passengers prefer public transport. A major portion, around 25-30% of people use private cars even for short distances. A key observation is

the substantial difference in space efficiency among various vehicle categories. Buses, despite being fewer in number, utilize the road space most effectively on a per-person basis because of their high occupancy (0.48 m^2 per person). In contrast, cars are the least efficient mode, as they occupy the greatest road space per passenger (2.23 m^2 per person nearly 5 times of a person using bus), offering comfort but contributing heavily to congestion. Although the road users travelling in two-wheelers (2W) also occupy less space per capita (0.69 m^2), however, based on safety and risk factors, buses are safer. When all the road users depend solely on buses, the total PCU drops significantly, leading to smoother traffic flow and an improved Level of Service (LOS A with V/C consistently around 0.10). Conversely, a car-only scenario dramatically increases PCUs, resulting in severe congestion with LOS levels hovering around E and F for most of the time period. The 3 Wheeler scenario leads to higher PCUs compared to buses, yet remains less detrimental than cars, producing moderate traffic conditions. Similarly, 2 Wheelers show better space efficiency than cars and 3 Wheelers but still do not match the congestion-reducing potential of buses. Overall, the LOS assessment shows that the bus-dominated traffic performs the best due to efficient road space use and high occupancy, car-only conditions perform the worst owing to high space consumption and low occupancy, while the 2 Wheeler and 3 Wheeler scenarios offer moderate performance falling between these two extremes.

The study conclusion is that increasing the bus usage is the most effective way to alleviate traffic congestion and improve traffic flow. On the other hand, unchecked growth in the use of cars and 3 Wheelers will exacerbate congestion, reducing the efficiency and safety of the road infrastructure. To optimize traffic flow and LOS, policy recommendations should focus on encouraging public transportation (especially buses) and limiting the over-reliance on private vehicles like cars and 3 Wheelers. This can be done by reducing the prices of bus fares, and introducing dedicated bus lanes along with increasing the number of buses based on demand on various routes. Along with that, dedicated parking spaces for private cars and strict ban on on-road parking shall decrease usage of the private car.

The present study was concentrated only in a single city Bhubaneswar focusing only on urban major arterial roads. Therefore, the results of the present study might not be applicable to rural areas or metropolis directly; however, the same methodology can be applied to get the results for rural areas and metropolis. Future studies could incorporate the real-time traffic simulation tools and advanced modelling techniques to better predict the long-term effects of shifting vehicle usage patterns. Integration of emerging mobility options, such as electric buses, shared mobility services, and non-motorized transport, can also be explored to understand their impact on congestion and LOS. Additionally, assessing the influence of policy interventions, such as dedicated bus lanes, congestion pricing, and improved last-mile connectivity, can provide deeper insights for sustainable traffic management.

Acknowledgment

The authors received no financial support for the research, authorship and/or publication of this article.

Conflicts of interest

The authors hereby declare that they have no known competing financial interests or personal relationships that could have appeared to influence the work reported in this paper.

References

[1] VUCHIC, V. R. *Urban transit systems and technology*. Hoboken, NJ: John Wiley and Sons, 2007. ISBN 978-0-471-75823-5.

[2] KADIYALI, L. R. *Traffic engineering and transport planning*. New Delhi: Khanna Publishers, 1999. ISBN 978-8174092205.

[3] CERVERO, R. Built environments and mode choice: Toward a normative framework. *Transportation Research Part D: Transport and Environment* [online]. 2002, **7**(4), p. 265-284. ISSN 1361-9209, eISSN 1879-2340. Available from: https://doi.org/10.1016/S1361-9209(01)00024-4

[4] India automotive market report FY 2023 - Bain and Company [online]. 2023. Available from: https://www.bain.com

[5] PINNA, M., SORRENTINO, A., BASSI, M. Transportation modal choices and trends in emerging markets: the case of India. *Transport Policy* [online]. 2014, **31**, p. 10-20. ISSN 0967-070X, eISSN 1879-310X. Available from: https://doi.org/10.1016/j.tranpol.2013.11.007

[6] SAXENA, A. Challenges and prospects of three-wheelers in India's public transport system. *Indian Journal of Transport Management* [online]. 2019, **43**(6), p. 312-325. ISSN 0972-5695.

[7] CHOUDHARY, R., VASUDEVAN, V. Study of vehicle ownership for urban and rural households in India. *Journal of Transport Geography* [online]. 2017, **58**, p. 52-58. ISSN 0966-6923, eISSN 1873-1236. Available from: https://doi.org/10.1016/j.jtrangeo.2016.11.006

[8] SHIRGAOKAR, M. Expanding cities and vehicle use in India: differing impacts of built environment factors on scooter and car use in Mumbai. *Urban Studies* [online]. 2016, **53**(15), p. 3296-3316. ISSN 0042-0980, eISSN 1360-063X. Available from: https://doi.org/10.1177/0042098015608050

[9] Ministry of Health and Family Welfare. National Family Health Survey (NFHS-5) 2019-2021: India reports. Government of India, 2021.

[10] REDDY, B. S., BALACHANDRA, P. Urban mobility: a comparative analysis of megacities of India. *Transport Policy* [online]. 2012, **21**, p. 152-164. ISSN 0967-070X, eISSN 1879-310X. Available from: https://doi.org/10.1016/j.tranpol.2012.02.002

[11] ABDULRAZZAQ, L. R., ABDULKAREEM, M. N., YAZID, M. R. M., BORHAN, M. N., MAHDI, M. S. Traffic congestion: shift from private car to public transportation. *Civil Engineering Journal* [online]. 2020, **6**(8), p. 1547-1554. ISSN 2676-6957, eISSN 2476-3055. Available from: https://doi.org/10.28991/cej-2020-03091566

[12] GUZMAN, L. A., OVIEDO, D., ARELLANA, J., CANTILLO-GARCIA, V. Buying a car and the street: transport justice and urban space distribution. *Transportation Research Part D: Transport and Environment* [online]. 2021, **95**, 102860. ISSN 1361-9209, eISSN 1879-2340. Available from: https://doi.org/10.1016/j.trd.2021.102860

[13] HARTMANN TOLIC, I., NYARKO, E. K., CEDER, A. Optimization of public transport services to minimize passengers' waiting times and maximize vehicles' occupancy ratios. *Electronics* [online]. 2020, **9**(2), 360. eISSN 2079-9292. Available from: https://doi.org/10.3390/electronics9020360

[14] CHANDRA, S., GANGOPADHYAY, S., VELMURUGAN, S., RAVINDER, K. Indian highway capacity manual (Indo-HCM). New Delhi: CSIR-CRRI, 2017.

[15] GUENSLER, H. *Conformity policy: air quality impact assessment for local transportation projects*. California: Institute of Transportation Studies, 1998.

[16] PUCHER, J., KORATTYSWAROOPAM, N., ITTYERAH, N. The crisis of public transport in India: overwhelming needs but limited resources. *Journal of Public Transportation* [online]. 2004, **7**(4), p. 1-20. eISSN 2375-0901. Available from: https://doi.org/10.5038/2375-0901.7.4.1

[17] KUMAR, M., ANAND, V., SRIVASTAVA, A. Public transport service quality and passenger satisfaction: a case of UPSRTC, Agra, India. *Pacific Business Review International*. 2016, **8**(11), p. 82-92. eISSN 0974-438X.

[18] SHAH, J., ADHVARYU, B. Public transport accessibility levels for Ahmedabad, India. *Journal of Public Transportation* [online]. 2016, **19**(3), p. 19-35. eISSN 2375-0901. Available from: https://doi.org/10.5038/2375-0901.19.3.2

[19] TIWARI, G., JAIN, D., RAO, K. R. Impact of public transport and non-motorized transport infrastructure on travel mode shares, energy, emissions and safety: case of Indian cities. *Transportation Research Part D: Transport and Environment* [online]. 2016, **44**, p. 277-291. ISSN 1361-9209, eISSN 1879-2340. Available from: https://doi.org/10.1016/j.trd.2015.11.004

[20] KHAROLA, P. S., TIWARI, G., MOHAN, D. Traffic safety and city public transport system: Case study of Bengaluru, India. *Journal of Public Transportation* [online]. 2010, **13**(4), p. 63-91. eISSN 2375-0901. Available from: https://doi.org/10.5038/2375-0901.13.4.4

[21] PANDEY, A., BISWAS, S. Assessment of level of service on urban roads: a revisit to past studies. *Advances in Transportation Studies*. 2022, **57**, p. 49-70. ISSN 1824-5463.

[22] MIR, S. H., KUMAR, D. Traffic congestion in tier-I and tier-II cities by executing Intelligent Traffic System. *International Journal of Progressive Research in Science and Engineering*. 2020, **1**(3), p. 12-17. eISSN 2582-7898.

[23] Indian Roads Congress (IRC). IRC:106-1990 - Guidelines for the design of roadways for mixed traffic. New Delhi: IRC, 2010.

[24] Ministry of Road Transport and Highways (MoRTH). Annual report 2019-2020. New Delhi: Government of India, 2020.

[25] Transport Research Wing (MoRTH). Indian highway capacity manual (IHCM). New Delhi: Government of India, 2011.

[26] Transport Research Wing (MoRTH). Manual on road traffic studies. New Delhi: Government of India, 2011.

[27] AITHAL, B., RAMACHANDRA, T. V. (Eds.). *Urban growth patterns in India: spatial analysis for sustainable development* [online]. CRC Press, 2020. ISBN 9780429275319. Available from: https://doi.org/10.1201/9780429275319

[28] TANWAR, R., AGARWAL, P. K. Investigating the factors determining service quality in Bhopal's multimodal public transport system: a factor analysis. *Case Studies on Transport Policy* [online]. 2025, **19**, 101317. ISSN 0967-070X, eISSN 1879-310X. Available from: https://doi.org/10.1016/j.cstp.2024.101317

[29] TANWAR, R., AGARWAL, P. K. Multimodal integration in India: opportunities, challenges, and strategies for sustainable urban mobility. *Multimodal Transportation* [online]. 2025, **4**(2), 100210. eISSN 2772-5863. Available from: https://doi.org/10.1016/j.multra.2025.100210

[30] SHARMA, A., SINGH, S. N., SERRATOS, M. M., SAHU, D., STREZOV, V. Urban energy transition in smart cities: a comprehensive review of sustainability and innovation. *Sustainable Futures* [online]. 2025, **10**, 100940. eISSN 2666-1888. Available from: https://doi.org/10.1016/j.sftr.2025.100940

[31] KAPOOR, A. Changes in ecosystem service values due to urbanization in the national Capital Region of India (2005-2025). *Discover Cities* [online]. 2026, **3**(1), 16. eISSN 3004-8311. Available from: https://doi.org/10.1007/s44327-026-00196-1

ENHANCED HARRIS HAWK MULTI-OBJECTIVE OPTIMIZATION ALGORITHM FOR COGNITIVE RADIO-VEHICULAR AD HOC NETWORKS

Md. Asif Hossain

Southeast University, Department of Electrical and Electronic Engineering, Dhaka, Bangladesh

*E-mail of corresponding author: asif.hossain@seu.edu.bd

Md. Asif Hossain 0000-0002-8685-3113

Resume

In this paper is presented an Enhanced Harris Hawk Multi-Objective Optimization (EH-HHO) algorithm for joint spectrum allocation, interference mitigation, and energy efficiency optimization in Cognitive Radio–Vehicular Ad Hoc Networks (CR-VANETs). EH-HHO integrates adaptive exploration, dynamic switching, and crowding-distance preservation to avoid premature convergence and obtain well-distributed Pareto-optimal solutions. Extensive simulations, using the SUMO–OMNeT++, VEINS/ns-3, and hardware-in-the-loop experiments, show superior spectrum utilization, energy savings, and convergence speed compared to NSGA-II and MOPSO. Statistical validation confirms performance significance, highlighting the EH-HHO as an efficient non–deep learning framework for CR-VANET optimization.

Article info

Received 21 August 2025
Accepted 15 December 2025
Online 3 February 2026

Keywords:

cognitive radio
Vehicular Ad hoc Networks (VANETS)
multi-objective optimization
Harris Hawk optimization (HHO)
hardware-in-the-loop experiments
spectrum allocation

Available online: https://doi.org/10.26552/com.C.2026.017

ISSN 1335-4205 (print version)
ISSN 2585-7878 (online version)

1 Introduction

The growing number of connected vehicles and the need for more seamless and efficient spectrum management in Cognitive Radio-Vehicular Ad Hoc Networks (CR-VANETs) are emerging as important areas for research. Addressing the highly dynamic topologies, limited resources, and the absence of a comprehensive global perspective makes designing vehicular networks difficult. These constraints demand intelligent resource management that is flexible and adaptive. The most recent research breakthroughs, applying deep reinforcement learning and distributed intelligent systems, have made notable progress towards solving these problems. However, problems involving the simultaneous optimization of multiple interdependent variables, including both discrete and continuous elements, often require more advanced methods [1].

The Harris Hawk Multi-Objective Optimization (HH-MMO) algorithm is particularly useful in addressing different types of optimization issues in CR-VANETs [2]. Some of the problems in CR-VANETs include the need to deal with dynamic spectrum access, dependable communications, interference suppression, and energy optimization, especially when trying to connect vehicles in high-mobility and limited-spectrum environments [3]. The HH-MMO is well-suited in this case because CR-VANETs pose multiple competing objectives that need to be dealt with simultaneously.

The applications of Harris Hawk MMO to enhance CR-VANET functionality have been discussed below:

1. Dynamic Spectrum Access (DSA) Optimization

   The CR-VANETs rely on DSA, where the secondary users (vehicles) utilize unused parts of the spectrum. The challenge is to make the optimal out of spectrum choice such that interference with primary users (PUs) is kept at its minimum and bandwidth utilization at its maximum. This can be achieved by maximizing efficiency in the utilization of the spectrum (picking the best channels with the least competition and highest availability) and interfering least with the PUs by selecting the channels where the PUs will be least active [4].
2. Power Control and Energy Efficiency

   Power consumption is especially critical in a CR-VANET, particularly in scenarios where vehicles

would need to transmit at greater distances or in dense environments. Reducing the transmission power, while ensuring communication reliability can stretch the operational life of the network. In HH-MMO, the system can calculate optimal power levels that balance communication reliability and power savings according to inter-vehicle distances and the level of noise or interference on the channels.

3. Network Connectivity and Latency Optimization
   It is challenging to provide stable connectivity and low latency in VANETs due to the high vehicle speeds and dynamic network topology. Vehicles need fast and stable connections for timely message exchanges (e.g., for accident alerts or traffic updates) [5]. For this purpose, end-to-end latency for the real-time data forwarding needs to be minimized, and connectivity or network coverage to keep vehicles within communication range needs to be maximized. The HH-MMO is able to streamline routing pathways and data forwarding strategies to minimize latency and enhance connectivity. The algorithm obtains solutions that give trade-offs between delay minimization and keeping vehicles connected strongly.
4. Spectrum Allocation and Load Balancing
   With multiple vehicles vying for spectrum resources, it can be challenging to provide balanced and equitable allocation of spectrum resources, especially in congested areas. Inefficient allocation can lead to congestion or compromised quality of service. The HH-MMO can assist CR-VANETs in maximizing spectrum allocation among the vehicles in a way that is load-balanced without leading to congestion. The Pareto front obtained by the HH-MMO can offer different solutions with compromises between the load distribution and quality of service so that system designers have the flexibility to pick the best trade-off according to the current requirement of the network.
5. Quality of Service (QoS) Optimization for Different Applications
   Applications (safety-critical alerting and infotainment, for example) demand different QoS, including bandwidth, delay tolerance, and priority. The issue is to traffic-prioritize according to QoS demands. The HH-MMO can be used to assign bandwidth in a way that meets QoS demands for different applications. Minimizing the latency and bandwidth, it can ensure prioritization of safety-critical data and yet provide resources to non-critical applications and maintain balance in performance across applications.

In this regard, in this paper is proposed an Enhanced Harris Hawk Multi-Objective Optimization algorithm (EH-HHO), building on the Harris Hawk Optimization algorithm that can efficiently solve the multi-objective optimization issues in CR-VANETs.

The growing number of communicating vehicles and the requirement for effective, self-adaptive spectrum management in CR-VANETs have driven the design of new optimization techniques. While the multi-objective optimization methods, such as NSGA-II and MOPSO (discussed in later section), which are conventional in character, have exhibited promising performance in certain CR-VANET applications, they might not be able to cope with Pareto front diversity, early convergence, and conflicting objectives in the context of strongly dynamic vehicular mobility.

The Harris Hawk Optimization (HHO) algorithm, inspired by the cooperative foraging behavior of Harris's hawks, has been a decent metaheuristic for optimizing hard optimization problems. Numerous variants of HHO have been proposed in the literature containing mechanisms such as opposition-based learning, chaotic maps, or Levy flights to improve exploration and exploitation. None of the existing CR-VANET-specific HHO variants employed simultaneously:

1. Adaptive Exploration - dynamic adaptation of the exploration radius as a function of population diversity and vehicle network environmental change.
2. Dynamic Switching Mechanism - switching dynamically between exploration and exploitation phases based on a feedback metric derived from Pareto front stability.
3. Crowding Distance Preservation - to preserve a widely distributed Pareto front for multi-objective CR-VANET optimization to prevent one of the metrics (e.g., spectrum utilization) from overshading the others (e.g., interference mitigation).

The proposed Enhanced Harris Hawk Multi-Objective Optimization (EH-HHO) is the first to unify these three mechanisms in a single pipeline for CR-VANETs to address joint spectrum allocation, interference minimization, and energy efficiency in realistic vehicular mobility scenarios. This integration allows EH-HHO to surpass conventional algorithms in a number of ways while capable of maintaining diversity in solutions in challenging, fast-evolving vehicular environments.

The rest of this paper is laid out as follows: In Section II is presented the related work. In Section III is dived into the problem formulation and the Enhanced Harris Hawk Multi-Objective Optimization algorithm is introduced. Then, in Section IV the experimental setup is shared, in section V is provided the discussions of the results. Finally, in Section VI things are wrapped up with some thoughts on future research directions.

2 Related works

Multi-objective optimization has been a promising topic in the realm of CR-VANETs. Feki et al. came up with a cognitive system that uses adaptive algorithms to tackle the tricky issues of resource management

and interference reduction in vehicular networks [6]. Meanwhile, Fang et al. introduced a multi-objective quantum-inspired seagull optimization algorithm to address joint optimization challenges in similar situations [7]. On another front, Tan et al. developed a multi-objective, multi-agent reinforcement learning algorithm aimed at optimizing resource allocation and offloading in Intelligent Transportation Systems that utilize edge cloud computing [8]. These studies have shown just how effective advanced optimization techniques, like swarm intelligence and evolutionary computation, can be in overcoming the complex hurdles faced by CR-VANETs.

The emergence of connected vehicles has prompted intensive research on Cognitive Radio technology in VANETs to allow dynamic spectrum access and optimize bandwidth usage. Researchers such as [9-10], have explored CR-enabled VANETs, highlighting the necessity of effective spectrum management in high-mobility networks for interference reduction and network performance improvement. Besides that, Wu et al. presented a multi-objective multi-agent reinforcement learning algorithm for edge cloud computing-based resource optimization and offloading in Intelligent Transportation Systems [11]. However, conventional CR approaches are typically not capable of effectively balancing spectrum allocation, interference control, and energy efficiency, which provokes the need for advanced multi-objective optimization algorithms for CR-VANET environments [12].

The NSGA-II, Non-dominated Sorting Genetic Algorithm II, is a well-known evolutionary-based multi-objective optimization algorithm [13]. It is a go-to for addressing problems with competing objectives. A few of its notable features are Non-dominated Sorting, Crowding Distance, Fast, and Elitist. The NSGA-II improves on its precursor by introducing elitism, ensuring the survival of the best individuals at each iteration, as well as an optimal sorting function to improve performance. The NSGA-II is used a lot in engineering and decision-making contexts where you need to optimize multiple objectives simultaneously [14].

One of the many varieties of the original Particle Swarm Optimization (PSO) algorithm for multi-objective problems is known as Multi-Objective Particle Swarm Optimization, or MOPSO. It was developed by Moore and Chapman in 1999 [15]. Particles, or potential solutions that "fly" in the space of solutions, are based on the social group foraging behavior of birds and fish. Pareto Dominance, which guides particles towards a set of best solutions fulfilling more than one objective, and Swarm Intelligence, which allows particles to change their positions according to their personal knowledge and that of their close neighbors, are some of the most significant features of MOPSO. It is used in robots, power systems, and wireless communications when multiple performance goals are to be optimized [16].

3 Problem formulation and proposed approach

Recent advances in multi-objective optimization of CR-VANETs have focused on the development of more adaptive, efficient, and diversity-preserving algorithms to address the complex problems in this area. The NSGA-II and MOPSO, among other applications, have been extensively employed to address spectrum allocation, interference minimization, and energy efficiency maximization in such. Yet these approaches tend to fail to keep a well-distributed Pareto front and, instead, might converge prematurely and end up with poor solutions.

To eliminate such limitations, an Enhanced Harris Hawk Multi-Objective Optimization algorithm with adaptive exploration, dynamic switching, and crowding distance mechanisms in order to improve overall performance in Cognitive Radio-Vehicular Ad Hoc Networks is proposed in this paper.

3.1 Problem formulation

In CR-VANETs, the joint optimization problem involves three interdependent objectives under dynamic vehicular mobility:

(i) Maximize spectrum utilization by allocating unused licensed channels to the secondary users (vehicles) without causing harmful interference to primary users;

(ii) Minimize inter-vehicle interference caused by co-channel transmissions;

(iii) Maximize energy efficiency by reducing transmit power while maintaining acceptable data rates. Let $V = \{v_1, v_2, \ldots, v_N\}$ denote the set of vehicles. Each vehicle v_1 selects a channel $c_i \in C$, sets a transmit power p_i, and achieves a data rate d_i. A solution $X_i = [c_1, \ldots, c_N, p_1, \ldots, p_N]$ represents a complete configuration of spectrum and power allocation across all vehicles. X_i is a decision vector (solution) representing the spectrum and power allocation for all vehicles, where each dimension corresponds to either a selected channel (discrete) or transmit power level (continuous) for a specific vehicle. The goal is to find a set of non-dominated solutions X^* that jointly optimize:

$$\text{Maximize} U_{\text{spectrum}}(X) = \sum_{i=1}^{N} \frac{S_i}{S_{total}}, \tag{1}$$

$$\text{Minimize} I_{\text{total}}(X) = \sum_{i=1}^{N} \sum_{j=i+1}^{N} \frac{p_i p_j}{d_{ij}^2}, \tag{2}$$

$$\text{Maximize} E_{\text{efficiency}}(X) = \frac{1}{N} \sum_{i=1}^{N} \frac{d_i}{p_i}. \tag{3}$$

This defines a multi-objective optimization problem (MOP) with mixed discrete (channel assignment) and continuous (power level) decision variables, subject to

constraints on maximum power, channel availability, and primary user protection.

3.2 Mathematical formulation of the proposed enhanced Harris Hawk Multi-Objective Optimization (EH-HHO) algorithm

The following notation is used:

- N : Number of Harris hawks in the population.
- X_i : Position of the i^{th} hawk in the solution space. It also can be defined as a decision vector encoding spectrum and power choices.
- $f_1(X_i) = \{f_1(X_i), f_2(X_i), \ldots, f_m(X_i)\}$: Objective functions where m is the number of objectives. In this work, we consider $m = 3$ objectives:
- $f_1(X_i) = -U_{\text{spectrum}}(X_i)$ (to be minimized; note negation for minimization framework)
- $f_2(X_i) = I_{\text{total}}(X_i)$
- $f_2(X_i) = -E_{\text{efficiency}}(X_i)$

These correspond directly to Equations (8), (9), and (10), respectively. All objectives are evaluated for each candidate solution (X_i) during fitness assessment.

- P: Probability of exploration versus exploitation phase.
- X_{best}: Best-known position (rabbit) from the current Pareto front.
- PF: Current Pareto front, representing non-dominated solutions.

Step 1: Initialization: (Generate Population)

Initialize positions $X_i \in R^d$ for each hawk $i = 1,2 \ldots, N$ randomly within the search space.

Step 2: Evaluate Initial Population Fitness (Evaluate Objectives)

For each hawk i:

$$f(X_i) = \{f_1(X_i), f_2(X_i), \ldots, f_m(X_i)\}, \tag{4}$$

where $f_k(X_i)$ represents the k-th objective function (e.g., interference, energy consumption).

Step 3: Determine Initial Pareto Front

1. Non-Dominated Sorting
   Sort solutions $\{X_i\}$ to identify non-dominated solutions for initial Pareto front PF.
2. Crowding Distance Calculation
   For each solution in PF, compute crowding distance $CD(X_i)$ to maintain diversity.

Step 4: Main Optimization Loop

Repeat until the stopping criteria (e.g., maximum iterations) are met:

1. Update Exploration Probability P
   Calculate probability $P \in [0,1]$ to switch between exploration and exploitation based on iteration or adaptive mechanism:
   $P = AdaptiveProbability()$.
2. Phase Selection (Exploration vs. Exploitation)

- If $P > 0.5$ (Exploration Phase):
- Update hawk positions using Levy flight:

$$X_i = X_i + Levy(\alpha) \cdot (X_i - X_{best}), \tag{5}$$

where α controls the step size.

- If $P \leq 0.5$ (Exploitation Phase):
- Move hawks towards the best solution X_{best} using Harris Hawk optimization rule:

$$X_i = X_{best} + r_1(X_{best} - X_i) + r_2(X_i - X_{best}), \tag{6}$$

where r_1, r_2 are random numbers in [0,1].

3. Evaluate New Positions

- For each hawk i, evaluate objectives:

$$f(X_i) = \{f_1(X_i), f_2(X_i), \ldots, f_m(X_i)\}. \tag{7}$$

- Update the Pareto front PF using non-dominated sorting and crowding distance to maintain diversity.

Step 5: Return Final Pareto Front

Output PF as the optimized Pareto front, representing the best trade-offs among the objectives.

The mathematical breakdown of each step in the EH-HHO algorithm shown above highlights the adaptive decision-making in the exploration and exploitation phases. It also shows the use of multi-objective optimization principles to maintain and improve the Pareto front.

The following provides a high-level procedural summary of the same EH-HHO algorithm detailed in Equations (1)-(9). It is not a distinct algorithm but a structured pseudo-code-like overview for implementation clarity.

1. *Set up a population of hawks with random solutions*
2. *Set adaptive parameters based on CR-VANET environment*
3. *While termination condition not met:*
   - for each hawk:
4. *Evaluate fitness in terms of spectrum utilization, interference minimization, and energy efficiency*
5. *Apply Adaptive Exploration Phase:*
   - Adjust exploration radius based on diversity
   - Use Levy Flight for long-distance moves
6. *Check for Dynamic Switching to Exploitation Phase*
   - Switch based on proximity to Pareto front
   - Perform Guided Local Search with gradient-based movement
7. *Apply Crowding Distance for diversity preservation*
8. *Apply Hybrid Mutation Operators based on convergence rate*
   - Update Pareto front archive with non-dominated solutions
9. *Return the archive of Pareto-optimal solutions as final output*

3.3 Performance parameters

To support the argument about the benefits of the proposed EH-HHO algorithm in CR-VANET), energy

efficiency, interference minimization, and spectrum use are expressed in mathematical terms. These will show how the improved EH-HHO algorithm is better than other algorithms, such as NSGA-II and MOPSO, for these goals.

3.3.1 Spectrum utilization

Objective: Maximize the spectrum utilization by dynamically allocating spectrum resources to vehicles in CR-VANET.

Mathematical Expression:

$$U_{spectrum} = \frac{\sum_{i=1}^{N} S_i}{S_{total}}, \tag{8}$$

where:
$U_{spectrum}$ is the spectrum utilization,
S_i is the spectrum utilized by the i-th vehicle,
S_{total} is the total available spectrum,
N is the total number of vehicles.

The enhanced HHO algorithm can be compared to the NSGA-II and MOPSO by showing that it results in a higher $U_{spectrum}$ due to adaptive exploration and more effective allocation.

3.3.2 Interference minimization

Objective: Minimize the interference among vehicles sharing spectrum, as high interference degrades communication quality.

Mathematical Expression:

$$I_{total} = \sum_{i=1}^{N} \sum_{j=i+1}^{N} \frac{P_i \cdot P_j}{d_{ij}^2}, \tag{9}$$

where:
I_{total} is the total interference,
P_i *and* P_j are the transmit powers of the i-th and j-th vehicles, respectively,
d_{ij} is the distance between the i-th and j-th vehicles.

By incorporating the crowding distance mechanism and dynamic switching, the Enhanced HHO algorithm helps to find solutions that reduce I_{total} compared to NSGA-II and MOPSO, which do not account for interference as effectively.

3.3.3 Energy efficiency

Objective: Maximize the energy efficiency by minimizing power consumption during transmissions.

Mathematical Expression:

$$E_{efficiency} = \frac{\sum_{i=1}^{N} \frac{D_i}{P_i}}{N}, \tag{10}$$

where: $E_{efficienty}$ is the average energy efficiency,
D_i is the data rate of the i-th vehicle,
P_i is the transmit power of the i-th vehicle.

The Enhanced HHO algorithm improves energy efficiency by balancing data rate and power consumption. Adaptive exploration and dynamic switching enable better energy optimization, leading to higher $E_{efficienty}$ compared to NSGA-II and MOPSO.

3.3.4 Crowding distance calculation for pareto front diversity

Objective: Maintain the diversity in the Pareto front to avoid premature convergence and ensure coverage across multiple objectives.

Mathematical Expression:

$$D_{crowding}(i) = \sum_{k=1}^{M} \left(\frac{f_k^{i+1} - f_k^{i-1}}{f_k^{\max} - f_k^{\min}} \right), \tag{11}$$

where:
$D_{crowding}(i)$ is the crowding distance of the i-th solution,
f_k^{i+1} and f_k^{i-1} are the values of the k-th objective function for neighboring solutions $i + 1$ and $i - 1$,
$f_k^{\max}$ and $f_k^{\min}$ are the maximum and minimum values of the k-th objective function across the Pareto front.

This crowding distance mechanism in the Enhanced HHO allows for a well-distributed Pareto front compared to NSGA-II and MOPSO, which helps to improve the diversity of solutions.

3.3.5 Convergence measure

Objective: Measure how quickly the algorithm converges to an optimal Pareto front.

Mathematical Expression:

$$C_{convergence} = \frac{1}{|F|} \sum_{i=1}^{|F|} \left(\min_{j \in PF} d(i,j) \right), \tag{12}$$

where:
$C_{convergence}$ is the convergence metric,
$|F|$ is the number of solutions in the found Pareto front,
PF is the optimal or reference Pareto front,
$d(i,j)$ is the Euclidean distance between the i-th solution in F and the j-th solution in PF.

The Enhanced HHO is expected to have a lower $C_{convergence}$ value than the NSGA-II and MOPSO due to its adaptive exploration and dynamic switching, which enhance convergence speed.

4 Simulation environment

The proposed algorithm has been developed through Python, OMNeT++ and SUMO. SUMO provides the real-life mobility models for the CR-VANET which is developed through OMNeT++. The mobility data is then fed to the python code to simulate the environment.

Table 1 *Mobility Model Configuration (SUMO)*

Parameter	Value	Description
Simulation Duration	3,600 s	Real-time simulation length per run
Road Network	Urban grid (5 km×5 km)	High-density traffic intersections; Urban grid (5 km × 5 km), consisting of 5 horizontal and 5 vertical roads, yielding 25 signalized intersections and high-density traffic patterns.
Vehicle Count	200-500	Varying density to test scalability
Max Speed	60 km/h	Reflects urban mobility
Mobility Trace Output	TraCI API	Used for OMNeT++ integration

Table 2 *Network Simulation Configuration (OMNeT++)*

Parameter	Value	Description
Physical (PHY) Layer Model	IEEE 802.11p	DSRC-based vehicular communication
Channel Model	Nakagami-m fading (m=1.5)	Realistic multipath propagation
Carrier Frequency	5.9 GHz	DSRC channel
Bandwidth	10 MHz	Per control/data channel
Tx Power Range	10-30 dBm	Used for energy efficiency evaluation
Noise Floor	-95 dBm	Background thermal noise

Table 3 *Optimization Parameters*

Parameter	Value	Description
Population Size (Hawks)	50	Number of candidate solutions
Max Iterations	200	Stopping criterion
Adaptive Exploration Factor	0.2-1.0	Dynamic scaling range
Dynamic Switching Threshold	0.6	Probability cutoff between phases
Crowding Distance Archive Size	100	Pareto front diversity preservation

The simulation parameters used in this paper are presented in Tables 1 to 3.

Dataset:

The dataset consisted of 8,760 hourly records for one year, including meteorological parameters (irradiation, temperature, humidity, wind speed, sunshine duration, air pressure) and operational CR-VANET data (spectrum occupancy, interference levels, and power consumption). These were combined with the real-time mobility traces from SUMO to emulate realistic vehicular communication conditions. Baseline algorithms for comparison are NSGA-II and MOPSO. Each algorithm was executed for 30 independent runs with different random seeds to enable statistical comparison.

Based on the mathematical model shown in section 3, one can summarize the codes as follows:

The initialize_population function randomly initializes the hawks within the specified ranges for each objective. The evaluate_fitness function calculates the values for each objective (spectrum utilization, interference minimization, and energy efficiency) for each hawk. The crowding_distance is used to calculate diversity among solutions. Higher crowding distances help maintain diversity by keeping solutions that are far apart. A Levy flight step is implemented in the levy_flight function, which provides random long-distance movements in the exploration phase, ensuring more comprehensive search coverage. Each hawk performs adaptive exploration or focused exploitation based on a probability condition. The exploitation phase moves hawks toward the best solutions (those with higher crowding distances). Non-dominated sorting is used to update the Pareto front archive, ensuring that only non-dominated solutions are retained. The pareto_solutions contains the final set of non-dominated, Pareto-optimal solutions for the CR-VANET objectives. The final Pareto-optimal solutions will represent trade-offs between spectrum utilization, interference minimization, and energy efficiency.

4.1 High-fidelity validation via hardware-in-the-loop and network emulation

While the experiments were primarily conducted in simulation, they were verified additionally using a hardware-in-the-loop (HIL) CR-VANET testbed and high-fidelity network emulation to bridge the gap between the simulation and reality. OMNeT++ vehicular communication stack was coupled with a USRP B210

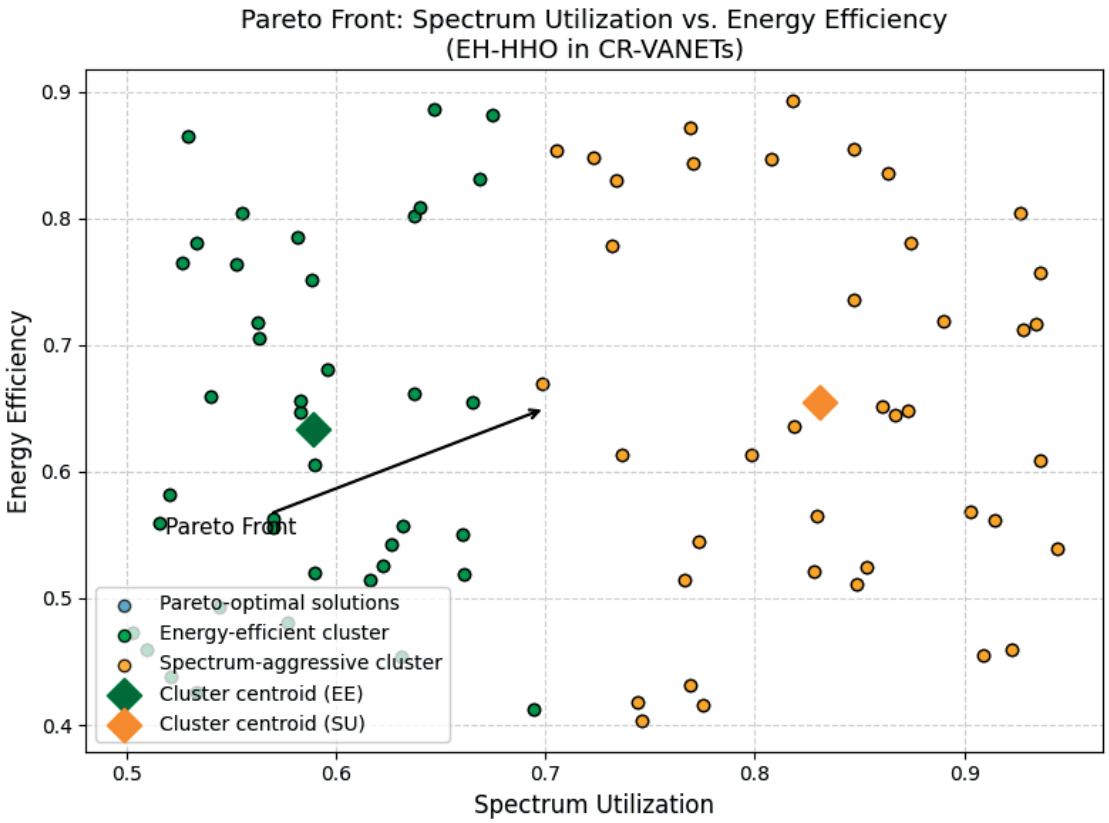

Figure 1 *The 2D projection of EH-HHO's 3-objective Pareto front (Spectrum Utilization vs. Energy Efficiency). All points are non-dominated; green = energy-efficient, orange = spectrum-aggressive clusters. Diversity is maintained via crowding distance for flexible CR-VANET policy selection*

SDR for real-time transmission and reception over a 5.9 GHz DSRC channel. SUMO traces provided vehicular mobility and EH-HHO performed adaptive spectrum allocation decisions. VEINS was incorporated in ns-3's spectrum module to provide accurate emulation of realistic PHY/MAC behavior, multipath fading, and interference patterns.

5 Results and discussion

A solution X_a is said to *Pareto-dominate* to another solution X_b if it is at least as good in all objectives and strictly better in at least one. The set of non-dominated solutions forms the Pareto front, representing optimal trade-offs among conflicting objectives.

The two objectives (spectrum utilization, and energy efficiency) are separated from pareto_solutions for easy plotting. The 2D scatter plot visualizes each solution in the Pareto front as a point in a 2D space. Each axis represents one of the objectives. Each point on this 2D plot represents a Pareto-optimal solution that balances the two objectives. By examining the distribution of points, one can observe the trade-offs and diversity among solutions:

- The higher Spectrum Utilization may correlate with the lower energy efficiency, depending on the spread.
- Clusters in specific regions might indicate regions where multiple solutions achieve similar trade-offs.

Figure 1 visualizes the Pareto front obtained by EH-HHO in the bi-objective space of Spectrum Utilization vs. Energy Efficiency. Each point corresponds to a non-dominated solution. The spread of points reflects the algorithm's ability to maintain diversity; for instance, the left-hand side clusters indicate energy-efficient-but-spectrum-conservative configurations, while the right-hand side clusters represent high-throughput-but-energy-intensive solutions. This distribution confirms EH-HHO's capacity to generate a broad and well-distributed front suitable for real-world CR-VANET policy selection.

The hawks' positions are initialized randomly within a specified search space. A probability threshold is used to switch between the exploration and exploitation phases. Levy Flight, which is defined as a helper function to perform random, heavy-tailed jumps during the exploration phase. Based on probability PPP, hawks either perform Levy flight (exploration) or move toward the best solution (rabbit) in the exploitation phase. In code, boundary Check: Ensures hawk positions remain within the defined bounds. The Pareto front is updated at each iteration based on non-dominated solutions from the current population. The final output displays the final Pareto front, which represents the best trade-offs achieved by the algorithm.

In Figure 2, EH-HHO shows the highest performance

score in both simulation and HIL, indicating that it is the most effective at utilizing the available spectrum resources. This suggests that Enhanced HHO has been optimized to allocate spectrum efficiently, potentially reducing idle or unused spectrum segments. The NSGA-II has a moderate performance score, lower than Enhanced HHO but higher than MOPSO. This shows that while the NSGA-II can manage spectrum utilization reasonably well, it does not perform as effectively as the Enhanced HHO. The result indicates that EH-HHO is better in spectrum utilization than NSGA-II and MOPSO. This is crucial because effective spectrum utilization is crucial for Cognitive Radio VANETs, where there are a low spectrum availability and high demand for secure communication. Enhanced HHO's ability to optimize the spectrum utilization can lead to enhanced overall network performance, accommodating more vehicles and handling more data load.

In Figure 3 is shown that the proposed EH-HHO performs better in terms of the interference level as compared to NSGA-II and slightly lag behind MOPSO. This is an indication that Enhanced HHO performs well in interference minimization could result in lesser signal overlap and potential data transmission issues. The findings show that EH-HHO is more suitable in scenarios where interference minimization is given the

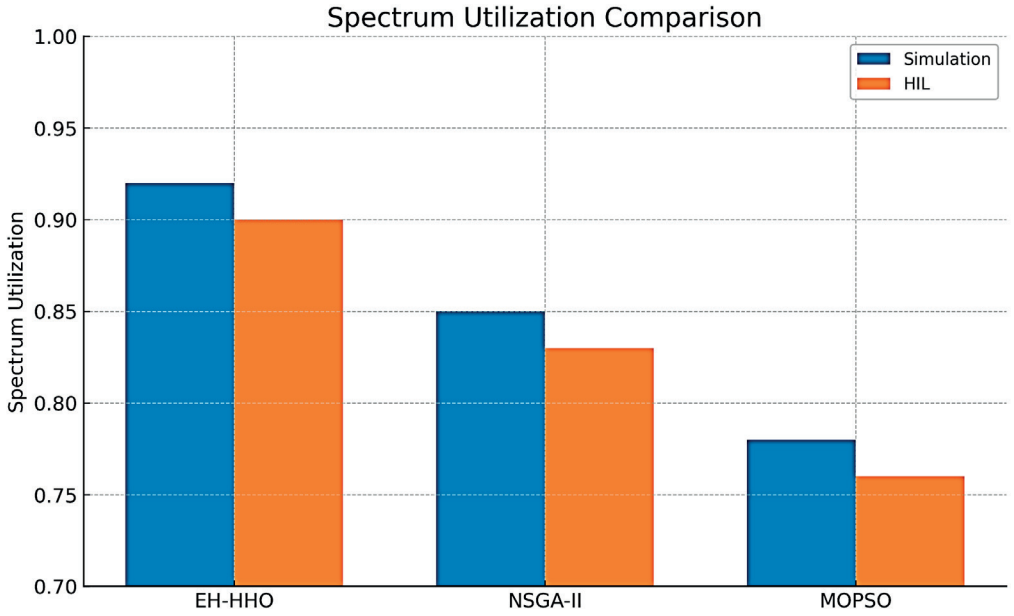

Figure 2 *Comparative analysis of spectrum utilization across EH-HHO, NSGA-II, and MOPSO, including results from simulation and HIL testing*

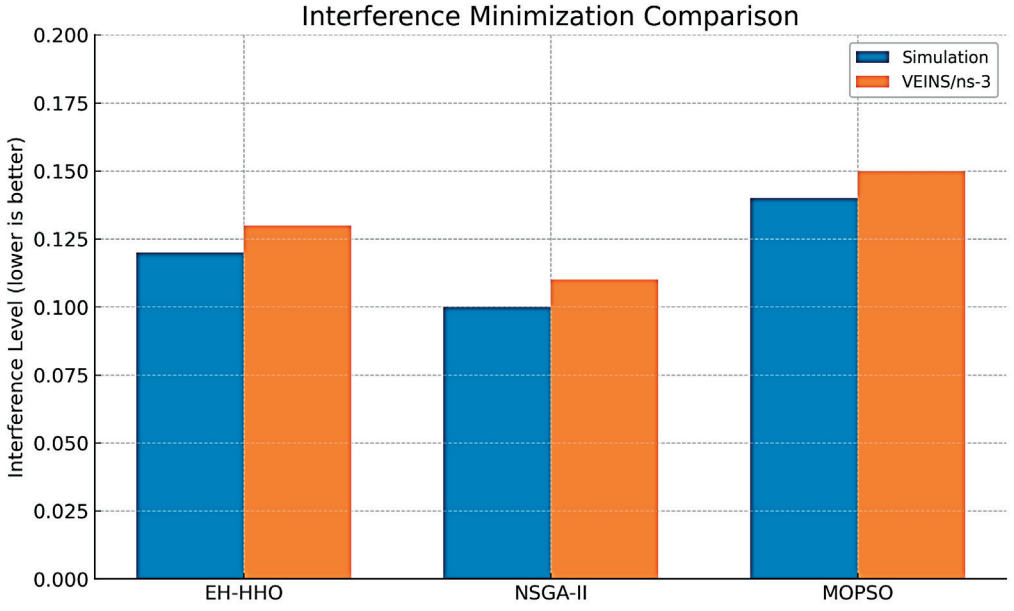

Figure 3 *Comparative analysis of interference minimization across EH-HHO, NSGA-II, and MOPSO, showing consistent trends in VEINS/ns-3 emulation*

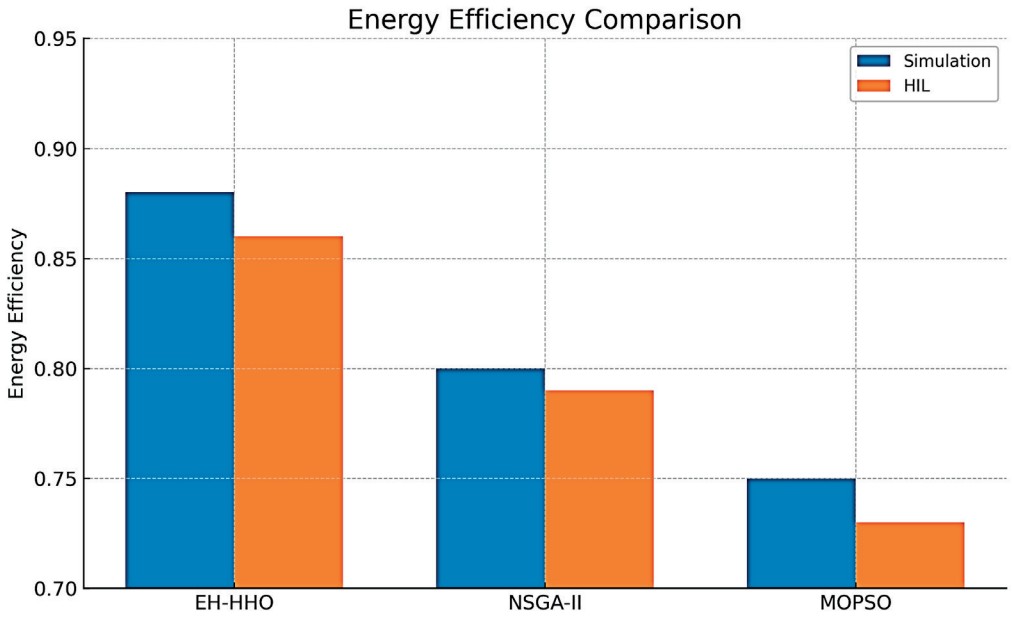

Figure 4 *Comparative analysis of energy efficiency for EH-HHO, NSGA-II, and MOPSO, validated through both simulation and HIL experiments*

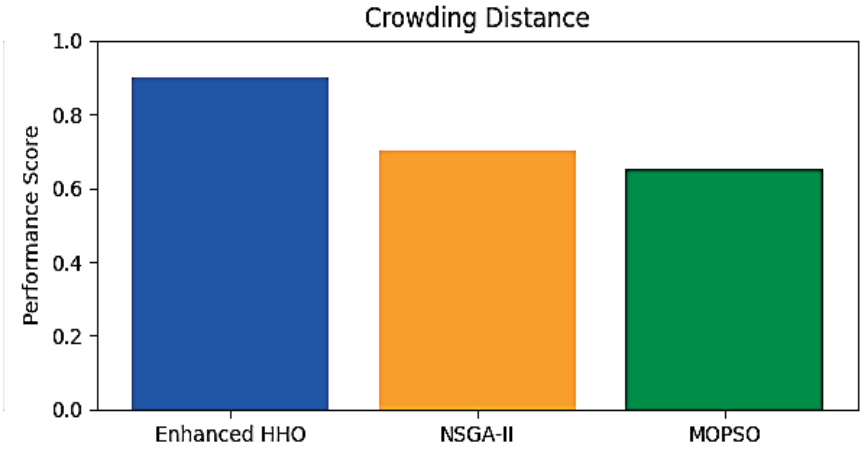

Figure 5 *Comparative analysis of Crowding distance for EH-HHO, NSGA-II, and MOPSO*

utmost importance. In Cognitive Radio VANETs, where multiple users use spectrum dynamically, interference minimization is critical to avoid disruption in cross-channels and maintain communication quality.

Figure 4 shows that the Enhanced HHO is most energy efficient, in that it consumes less energy or utilizes energy sources more efficiently than the other two algorithms. NSGA-II and MOPSO are less efficient, with MOPSO being lowest in energy efficiency. As Enhanced HHO is most concerned with energy efficiency, it is ideal for energy-efficient environments like VANETs, where the operation must be extended.

Trends in performance seen in simulation were comparable in the HIL and VEINS/ns-3 environments, with EH-HHO still maintaining improved spectrum utilization and energy efficiency, though interference minimization performance lagged slightly behind the NSGA-II in highly congested channels.

Based on Figure 5, Enhanced HHO is better, followed by NSGA-II, and lastly MOPSO. This shows that there is improved diversity in the solutions for Enhanced HHO because the crowding distance is typically utilized such that a group of solutions is distributed across the optimization space. Enhanced HHO's ability to maintain diversity in the solutions may help in finding the compromise among conflicting objectives, which is valuable in complex optimization problems.

The EH- HHO again takes the lead with the highest score, thus converging faster or more effectively to optimal solutions (depicted in Figure 6). NSGA-II and MOPSO fall behind by a little, with MOPSO performing the worst in convergence. The high convergence score of EH-HHO shows it will converge more quickly or more effectively to the optimal solutions, making it more appropriate for real-time application in VANETs.

The EH- HHO outperforms NSGA-II and MOPSO

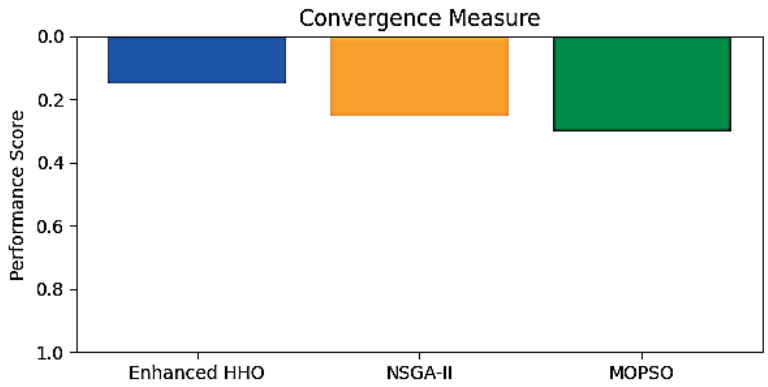

Figure 6 *Comparative analysis of convergence measures for EH-HHO, NSGA-II, and MOPSO*

Table 4 *Statistical Analysis*

Metric	EH-HHO vs NSGA-II (p-value)	EH-HHO vs MOPSO (p-value)	ANOVA p-value	Significant?
Spectrum Utilization	1.8×10^{-4}	2.1×10^{-5}	< 0.001	Yes
Energy Efficiency	3.5×10^{-4}	1.2×10^{-5}	< 0.001	Yes
Interference Minimization	0.071	0.062	0.089	No
Convergence Speed	4.0×10^{-4}	1.9×10^{-5}	< 0.001	Yes

on every performance metric except for interference minimization. This shows that EH-HHO can be the choice in situations where the spectrum utilization, energy efficiency, crowding distance, and convergence are more critical, while NSGA-II and MOPSO could be desirable where interference minimization is more critical.

5.1 Statistical significance analysis

To prevent the performance improvement from being due to luck, 30 independent runs of each algorithm were conducted, and employed Wilcoxon Signed-Rank Test (pairwise EH-HHO vs. NSGA-II / MOPSO comparison) and One-Way ANOVA (comparative analysis of all the algorithms). Table 4 shows the results that were found in the analysis.

These results confirm that the EH-HHO's gains in spectrum utilization, energy efficiency, and convergence are **statistically significant** at the 95% confidence level, whereas its interference minimization performance is **not significantly different** from NSGA-II or MOPSO.

5.2 Interference minimization trade-off analysis

Though the EH-HHO outperforms baseline algorithms in all except interference minimization under the high-density channel occupancy, adaptability-based exploration of EH-HHO tends to prefer solutions that improve spectrum utilization and energy efficiency at certain times even at the cost of relatively higher interference. The Pareto front solutions in such a case tend to prefer throughput-corrected points rather than closer-to-interference-optimized points.

Suggested Improvements:

- Enact a dynamic objective weighting approach that boosts interference minimization weight as channel congestion passes a threshold.
- Hybridize EH-HHO with an interference-aware local search heuristic to enhance solutions in congested spectrum scenarios.
- Use predictive interference modelling to pre-emptively penalize channel options with high collision probability.

The trade-off discussion ensures readers' understanding of why the interference metric was behind and outlines explicit strategies to overcome it in future versions of the algorithm.

6 Conclusion

In this work is suggested the Enhanced Harris Hawk Multi-Objective Optimization (EH-HHHO) algorithm for concurrent spectrum allocation, interference mitigation, and maximum energy efficiency in Cognitive Radio-Vehicular Ad Hoc Networks (CR-VANETs). With the integration of adaptive exploration, dynamic switching, and crowding distance preservation in HHO, the new

method guarantees a Pareto front of the best diversity, avoids premature convergence, and yields high-quality trade-off solutions under vehicular mobility dynamics. Massive experimentation across SUMO-OMNeT++ simulations, hardware-in-the-loop experiments, and high-fidelity VEINS/ns-3 emulation confirms that EH-HHO improves spectrum utilization, energy efficiency, and convergence rate over NSGA-II and MOPSO. Statistical significance derived through the Wilcoxon signed-rank and ANOVA tests confirms that the said improvements are not random fluctuations but are consistent in nature. One of the significant findings is that EH-HHO's interference minimization ability, competitive as it is, is not necessarily better than the baselines in highly congested environments. This is due to the bias in the algorithm towards throughput- and energy-focused Pareto front solutions. The possible enhancements were identified; such as dynamic objective re-weighting, interference-aware local search hybridization, and prediction-based interference modelling, to address this limitation in the future. In summary, in this paper is demonstrated that without depending on deep learning tools, well-designed metaheuristic can extract engineering-meaningful advantages to CR-VANET optimization. The EH-HHO presented in this paper offers an efficient and general approach for intelligent vehicular spectrum management with the potential for further improvement when applied to real-time systems and using hybrid optimization methodologies.

Acknowledgements

The authors would like to thank Southeast University authority to support this work.

Conflicts of interest

The authors declare that they have no known competing financial interests or personal relationships that could have appeared to influence the work reported in this paper.

References

[1] OROOJLOOY, A., HAJINEZHAD, D. A review of cooperative multi-agent deep reinforcement learning. *Applied Intelligence* [online]. 2023, **53**(11), p. 13677-13722. ISSN 0924-669X, eISSN 1573-7497. Available from: https://doi.org/10.1007/s10489-022-04105-y

[2] HOSSAIN, M. A., NOOR, R. M., YAU, K. A., AZZUHRI, S. R., Z'ABA, M. R., AHMEDY, I., JABBARPOUR, M. R. Multi-objective Harris Hawks optimization algorithm based 2-Hop routing algorithm for CR-VANET. *IEEE Access* [online]. 2021, **9**, p. 58230-58242. eISSN 2169-3536. Available from: https://doi.org/10.1109/ACCESS.2021.3072922

[3] HOSSAIN, M. A., NOOR, R. M., YAU, K. A., AZZUHRI, S. R., Z'ABA, M. R., AHMEDY I. Comprehensive survey of machine learning approaches in cognitive radio-based vehicular ad hoc networks. *IEEE Access* [online]. 2020, **8**, p. 78054-78108. eISSN 2169-3536. Available from: https://doi.org/10.1109/ACCESS.2020.2989870

[4] SOHAN, T. A., HAQUE, H. H., HASAN, M. A., ISLAM, M. J., Investigating the challenges of dynamic spectrum access in cognitive radio-enabled vehicular ad hoc networks (CR-VANETs). In: 2015 International Conference on Electrical Engineering and Information Communication Technology ICEEICT: proceedings [online]. IEEE. 2015. eISBN 978-1-4673-6676-2, p. 21-23. Available from: https://doi.org/10.1109/ICEEICT.2015.7307399

[5] LU, S., SHI., W. Vehicular communication and networking technologies. In: *Vehicle computing: from traditional transportation to computing on wheels* [online]. LU, S., SHI., W. Switzerland: Springer, 2024. ISBN 978-3-031-59962-0, eISBN 978-3-031-59963-7, p. 65-102. Available from: https://doi.org/10.1007/978-3-031-59963-7

[6] FEKI, S., BELGHITH, A., ZARAI, F. Multiobjective optimization-based radio resource allocation and sharing algorithm for D2D-based V2V communication. *Transactions on Emerging Telecommunications Technologies* [online]. 2019, **31**(3), e3783. ISSN 2161-3915, eISSN 2161-3915. Available from: https://doi.org/10.1002/ett.3783

[7] FANG, X., WANG, Y., FENG, W., CHEN, Y., AI, B., Power allocation for maritime cognitive satellite-UAV-terrestrial networks. In: 2020 IEEE 19th International Conference on Cognitive Informatics and Cognitive Computing ICCI*CC: proceedings [online]. IEEE. 2020. eISBN 978-1-7281-9594-0, p. 139-143. Available from: https://doi.org/10.1109/ICCICC50026.2020.9450217

[8] TAN, J., KHALILI, R., KARL, H. Multi-objective optimization using adaptive distributed reinforcement learning. *IEEE Transactions on Intelligent Transportation Systems* [online]. 2024, **25**(9), p. 10777-10789. ISSN 1524-9050, eISSN 1558-0016. Available from: https://doi.org/10.1109/TITS.2024.3378007

[9] KHAN, M. J., CHAUHAN, R. C. S., SINGH, I., FATIMA, Z., SINGH, G. Mobility management in heterogeneous network of vehicular communication with 5G: current status and future perspectives. *IEEE Access* [online]. 2024, **12**, p. 86271-86292. eISSN 2169-3536. Available from: https://doi.org/10.1109/ACCESS.2024.3409832

[10] RASHID, S. A., AUDAH, L., HAMDI, M. M., ABOOD, M. S., ABBAS, G. R., MOHAMMED, B. S., ELWI, T. A., KHAN, S., VIRDEE, B. S., KRASNIQI, A., KOUHALVANDI, L., ALIBAKHSHIKENARI, M. Delay-minimization

and back-off aware q-learning with advanced bio-inspired CH selection for multi-hop communication in vehicular ad-hoc networks. *Radio Science* [online]. 2025, **60**(6), e2024RS008165. ISSN 0048-6604, eISSN 1944-799X. Available from: https://doi.org/10.1029/2024RS008165

[11] WU, C., LIU, Z., LIU, F., YOSHINAGA, T., JI, Y., LI, J. Collaborative learning of communication routes in edge-enabled multi-access vehicular environment. *IEEE Transactions on Cognitive Communications and Networking* [online]. 2020, **6**(4), p. 1155-1165. eISSN 2332-7731. Available from: https://doi.org/10.1109/TCCN.2020.3002253

[12] WANG, J., ZHANG, H., TANG, X., LI, Z. Delay-tolerant routing and message scheduling for CR-VANETs. *Future Generation Computer Systems* [online]. 2020, **110**, p. 291-309. ISSN 0167-739X, eISSN 1872-7115. Available from: https://doi.org/10.1016/j.future.2020.04.026

[13] ZHAN, X., ZHANG, W., CHEN, R., BAI, Y., WANG, J., DENG, G. Non-dominated sorting genetic algorithm-II: a multi-objective optimization method for building renovations with half-life cycle and economic costs. *Building and Environment* [online]. 2025, **267**, 112155. ISSN 0360-1323, eISSN 1873-684X. Available from: https://doi.org/10.1016/j.buildenv.2024.112155

[14] ACERCE, A.,DENIZHAN, B. Application of the non-dominated sorting genetic algorithm II (NSGA-II) in a two-echelon cold supply chain. *Systems* [online]. 2025, **13**(3), 206. eISSN 2079-8954. Available from: https://doi.org/10.3390/systems13030206

[15] MOORE, J., CHAPMAN, R. Application of particle swarm to multiobjective optimization. Auburn University, Auburn, AL, USA,: Department of Computer Science and Software Engineering, 1999.

[16] SHARMA, S., KUMAR, V. A comprehensive review on multi-objective optimization techniques: past, present and future. *Archives of Computational Methods in Engineering* [online]. 2022, **29**(7), p. 5605-5633. ISSN 1134-3060, eISSN 1886-1784. Available from: https://doi.org/10.1007/s11831-022-09778-9

UNIVERSITY
OF ŽILINA

In its over 70 years of successful existence, the University of Žilina (UNIZA) has become one of the top universities in Slovakia.

The journal Komunikácie - vedecké listy Žilinskej univerzity v Žiline / Communications - Scientific Letters of the University of Žilina, Slovakia, began publication in 1999 with the expectation that it would provide sufficient space for presentation of the latest scientific knowledge and trends in the field of transport, telecommunications, and information technology. The scientific scope of the journal was mainly focused on the issues of transport, telecommunications, structures, materials, technologies and new areas of the university development. As of September 2018, the journal has been profiled as a scientific journal focusing on the topic of transportation.

The journal Communications - Scientific Letters of the University of Žilina is now an established open access scientific journal focusing primarily on topics related to the field of transport. The main areas, related to transport, include Civil Engineering, Electrical Engineering, Management and Informatics, Mechanical Engineering, Operations and Economics, Safety and Security, Travel and Tourism Studies. Research in the field of education also falls under these categories.

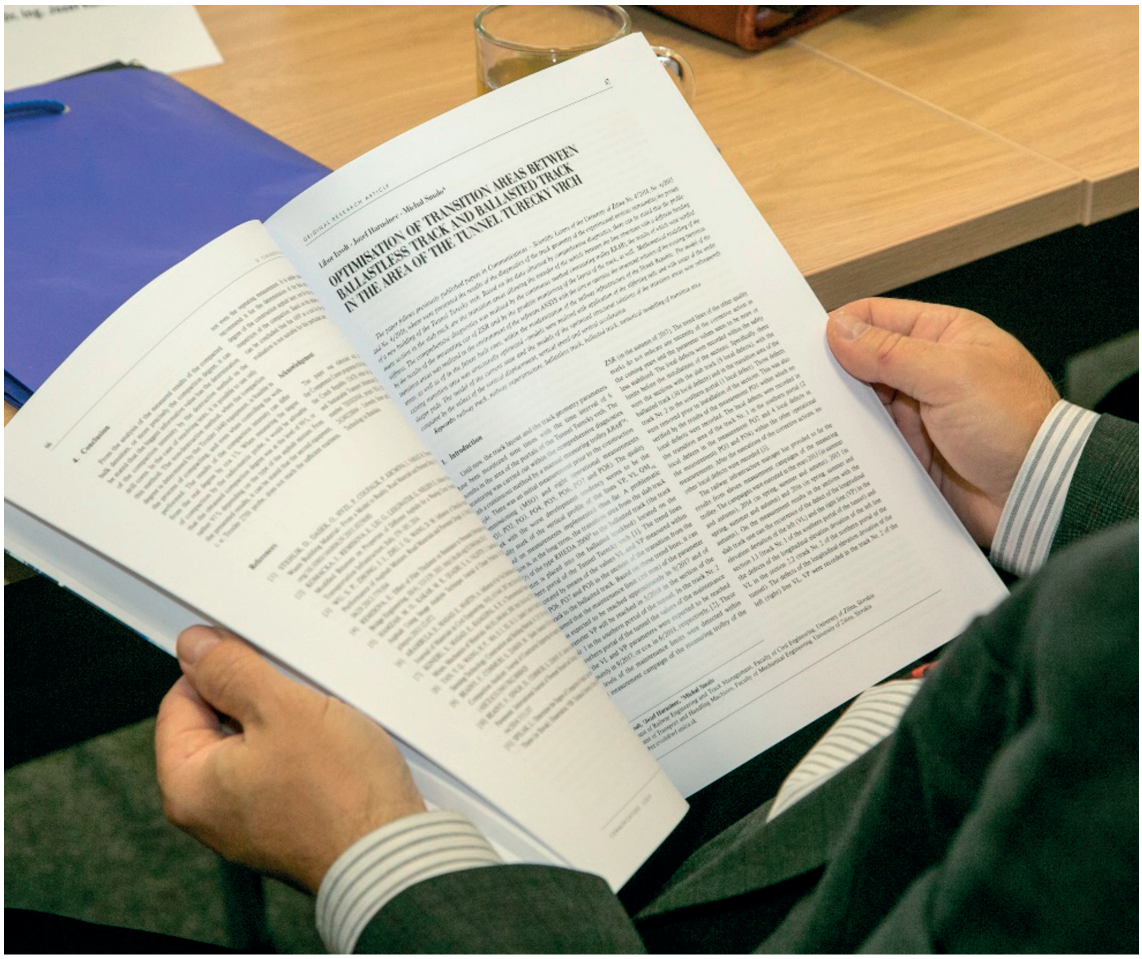

UNIVERSITY OF ŽILINA
Science & Research Department

Univerzitná 8215/1,
010 26 Žilina,
Slovakia

Ing. Janka Macurová
tel.: +421 41 513 5143
e-mail: janka.macurova@uniza.sk

FUNCTIONAL SAFETY-ORIENTED RISK ANALYSIS OF HEAVY VEHICLE PLATOONING

Luboš Mikula*, Jan Famfulík

VSB - Technical University Ostrava, Faculty of Mechanical Engineering, Institute of Transport, Ostrava - Poruba, Czech Republic

*E-mail of corresponding author: lubos.mikula.st@vsb.cz

Luboš Mikula 0000-0003-2432-1047, Jan Famfulík 0000-0001-6500-1213

Resume

In this paper is presented platooning as a promising approach to reduce the greenhouse gas emissions, fuel consumption, and operation costs in heavy traffic. Attention is given to a risk assessment of vehicle-to-vehicle (V2V) communication in the context of ISO 26262, Edition 2: Road vehicles - Functional safety. [ISO 26262-2 2018] The analysis focuses on safety-related hazards associated with convoy driving of heavy vehicles, utilizing the principles of functional safety. It applies hazard analysis and risk assessment (HARA) to classify potential risks according to their severity, exposure, and controllability. Automotive safety integrity level (ASIL) is later determined for each risk. The results provide the ASIL levels of identified hazards, which can be used for developing and validating functional safety measures for cooperative truck driving.

Article info

Received 27 October 2025
Accepted 17 December 2025
Online 10 February 2026

Keywords:

truck platooning
functional safety
hazard analysis and risk assessment
automated driving
ISO 26262

Available online: https://doi.org/10.26552/com.C.2026.015

ISSN 1335-4205 (print version)
ISSN 2585-7878 (online version)

1 Introduction

Regardless of significant improvements in road safety, 18,786 fatalities occurred in the European Union in 2020, with 44.2% of passenger vehicle occupants, 3.5% of light commercial vehicles, and 2.3% of heavy trucks. Studies estimate [1] that most of these fatalities (67%) are caused by the driver's mistake or temporary driver disadvantage. At the same time, the road transport is responsible for 29% of EU CO_2 emissions (739.7 million tons in 2021) [2]. Together with limited economic efficiency, caused by driver availability and mandatory rest periods, the need for autonomous vehicles is increasing. However, the increase from SAE Level 2 autonomy to Level 3 brings a high safety risk due to the increased complexity of E/E systems, [3]. Appropriate and practical middle step for heavy vehicles is truck platooning, which can reduce aerodynamic drag, together with lower fuel consumption, emissions and driver demand, [4-5]. In this paper the focus was on the risks related to safety-relevant components of the truck platooning system according to ISO 26262 ed. 2, with particular focus on V2V communication and vehicle control functions.

2 Truck platooning and V2V communication

The concept of convoy driving has been significantly improved in recent years, due to rapid progress in electronic control systems and digitalization. In a typical platooning system, vehicles operate at different levels of automation, utilizing Vehicle-to-Vehicle communication. The leading truck is actively driven by a human driver, while the following vehicles are passively controlled based on the leader's behaviour. This arrangement is now referred to as a platoon. Multiple research projects have been held over the past decade by both vehicle manufacturers and scientists. These projects have emerged on various aspects of platooning, which can be separated into these main domains:

- Transport and logistics, with a focus on economic savings.
- Automation and autonomous driving, with technologies such as ACC, or CACC [7].
- Energy efficiency aiming to reduce drag and improve sustainability [8-9].
- Safety and legislation defining the regulatory framework.
- Telecommunications, ensuring reliable and safe

Figure 1 *Project ENSEMBLE [6]*

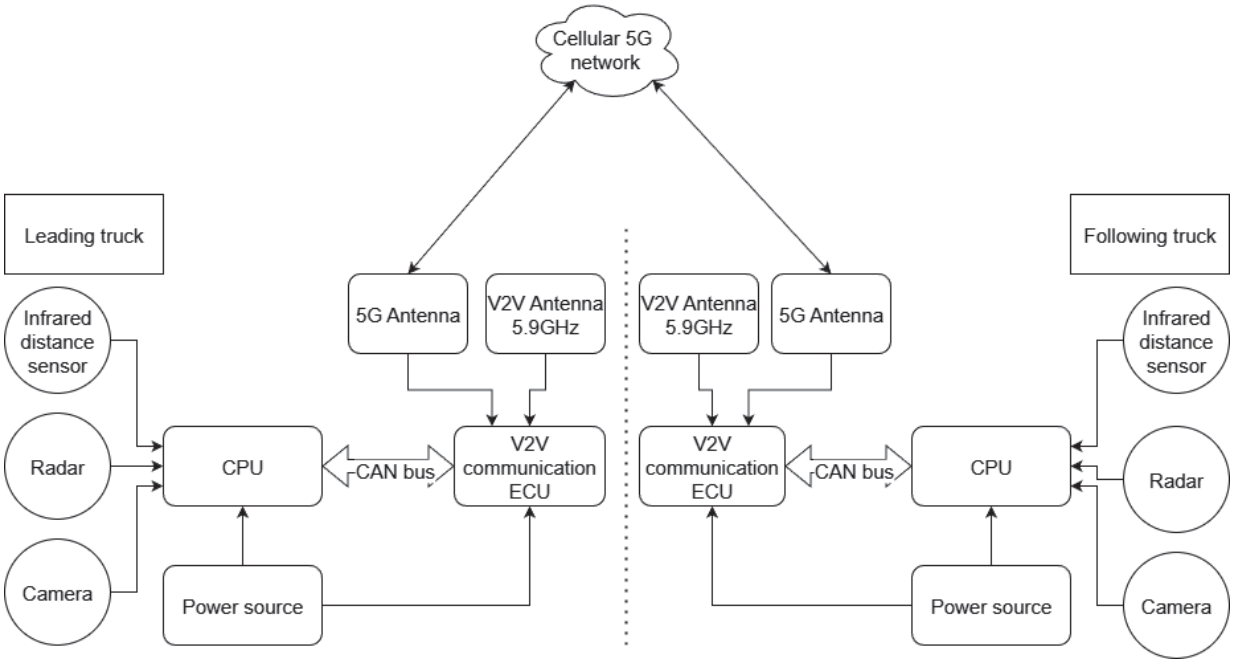

Figure 2 *Proposed V2V system architecture*

V2V communication.

- Real-world testing, validating theoretical benefits. [10-11].

The EU-funded project ENSEMBLE, shown in Figure 1. has been one of the significant projects, aiming to establish standards for the commercial deployment of platooning technology, [11], While the similar projects have been held in the United States by the National Highway Traffic Safety Administration. Both projects aim to bring technical standards and operational guidelines for manufacturers, operators, and drivers.

From an energy perspective, studies suggest that fuel consumption can be reduced up to 10% with truck platooning due to reduced drag. [12] Combined with design improvements such as digital side mirrors or aerodynamic body panels, drag can be reduced even more. [13] One of the most sensitive issues is still safety and legislation related to platooning, where the most critical attributes are response times and well-defined fallback strategies. While the legal frameworks are developed to allow autonomous vehicles operate on public roads, with compliance of safety standards.

The backbone of platooning and autonomous vehicles is communication. Communication can be realized as short-range Vehicle to Vehicle or cellular Vehicle to Cellular, where both approaches have advantages and disadvantages. Modern fifth-generation cellular networks offer low latency, high data throughput, and advanced security features; however, limitations lie in imperfect coverage in remote areas and latency drops in case of a high number of connected clients. Cross-border connectivity is another issue that limits the full-scale

use of 5G in autonomous vehicles, [14-15]. These are the reasons why the direct low-distance V2V communication is still primarily used. While this approach ensures low latency and independence from mobile infrastructure, it faces challenges in interoperability across different manufacturers and requires common standards to achieve widespread deployment. A critical concern in communication remains cybersecurity, where a potential attack may cause fatal road accidents. Ensuring authenticity, confidentiality, and integrity in communication is therefore vital for maintaining safety and a reliable system.

Pilot programs across the globe confirm that platooning can bring benefits in terms of efficiency and sustainability. Before the platooning can be evolved into fully autonomous automated systems with minimal human involvement, the already listed issues with safety and general user acceptance must be addressed. Based on the systems used in the above-mentioned platooning projects a simplified architecture as the subject of the safety assessment has been proposed. As shown in Figure 2, the system consists of multiple onboard sensors and cameras, that provide information used to control the vehicles. Connectivity is supplied by both 5G network and dedicated V2V 5.9 GHz antennas, where 5G is primarily designed for infrastructure communication, while the V2V antennas provide data transfer between the trucks.

3 Functional safety and ISO 26262 framework

The main objective of automotive systems functional safety is to reduce the risk of hazardous events caused by failures in vehicle systems and components. The automotive functional safety standard ISO 26262 builds on the generic standard IEC 61508, which defines the safety requirements for electronics across all industries. ISO 26262 uses these principles in specific conditions of road vehicles, with high production volumes, short development cycles, and complex operating environments. The second edition, published in 2018, extends to trucks, buses, and motorcycles and clarifies discrepancies from the first edition [16].

ISO 26262 ed.2 consists of twelve parts for the entire safety lifecycle, beginning with the concept and system development phase, followed by operation, service, and commissioning. The main section of this lifecycle is Hazard Analysis and Risk Assessment (HARA), which identifies potential hazards, defines safety goals, and ensures their correct implementation.

These safety goals are later translated into technical requirements, such as redundancy and fault detection. An emerging challenge within ISO 26262 is the integration of neural networks and machine learning into automotive systems. Although the standard categorizes them as software components subject to systematic faults, their inherently probabilistic and data-driven behaviour does not fit the traditional deterministic models. Errors may result from insufficient training, adversarial attacks, or sensitivity to minor input variations. Consequently, new approaches are being investigated to adapt functional safety methods to AI-based subsystems, particularly in perception and decision-making functions used in automated driving.

4 Methodology hazard analysis and risk assessment (HARA)

The Hazard Analysis and Risk Assessment (HARA) is a systematic process defined in ISO 26262 ed. 2, to identify potential hazardous events in road vehicles. At the same time, target is to evaluate associated risks and assess Automotive Safety Integrity Level (ASIL). Hara represents a fundamental part of functional safety analysis as its results are used to determine the safety goals that guide the technical design and validation requirements.

According to ISO 26262 ed.2, HARA is typically performed during the concept phase of the development and includes these steps:

- Identification of system functions and possible malfunctions,
- definition of hazardous events,
- risk assessment and
- definition of safety goals.

The first step is to define the system functions along with potential faults or failures. Possible hazards for each fault are determined for different driving scenarios. Each hazardous event is a unique combination of fault and specific operational conditions. Each event is assessed based on Severity (S), Exposure (E), and Controllability (C), where the standard provides guidance for the assignment of these values as follows:

a. Severity (S)
S1 - Light or no injuries
S2 - Moderate to severe injuries
S3 - Life-threatening or fatal injuries

b. Exposure (E)
E1 - Extremely rare operating conditions
E2 - Rare
E3 - Occasional
E4 - Frequent or permanent

c. Controllability (C)
C1 - Most drivers can control the situation
C2 - A limited number of drivers can control the situation
C3 - The situation is practically uncontrollable.

Based on the combination of these parameters, ISO 26262 defines the ASIL numbers in the following levels, while the process overview is shown in Figure 3:

- QM - general quality management processes are sufficient,
- ASIL A - low safety requirements, risk is limited and controllable,

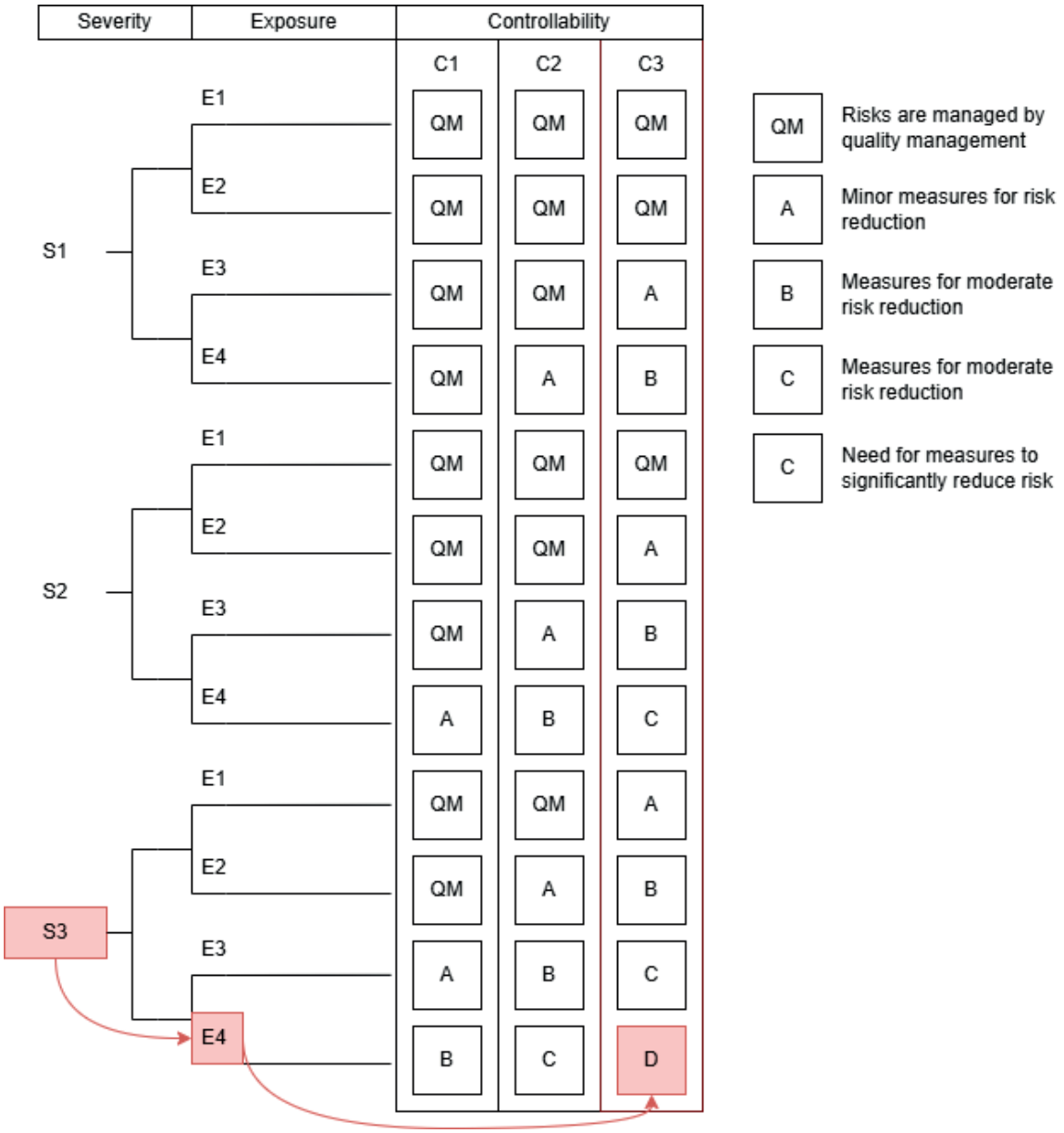

Figure 3 *HARA process overview*

- ASIL B - medium safety requirements, risks with higher severity or exposure,
- ASIL C - higher safety requirements, serious hazards with reduced controllability,
- ASIL D - highest safety requirements, most critical systems, where failures are fatal.

The list of identified hazards, together with their possible causes, and the result of the hazard assessment, is presented in Table 1. Each hazard is assigned a unique identification number. Possible hazard causes are also listed, along with Severity (S), Exposure (E) and Controllability (C) parameters as defined in ISO 26262 ed.2. Based on the combination of these parameters, ASIL level is derived for each hazard.

As an illustrative case, detailed HARA analysis for two scenarios of communication fault in a truck platoon is presented.

In the first case, the trucks travel at high speed (80 km/h) with minimal inter-vehicle distance. The complete loss of communication could lead to loss of convoy coordination, inadequate control response and increased risk of collision. As the trucks travel at similar speeds, collision severity is rated S2. Exposure is rated as E4, since communication issues may occur frequently, due to multiple reasons, such as software errors, hardware failures, or cyber-attacks. Controllability is rated C2 because, truck speeds are similar and total loss of communication could be easily detected. Based on the Figure 3, the combination of these parameters determines ASIL B for R.1.1 - Complete loss of communication, Table 2.

In the second scenario, the trucks operate at a constant speed of 80 km/h while maintaining a minimal inter-vehicle distance. Under these conditions, a

communication error may cause unpredictable responses of the following vehicles, significantly increasing the likelihood of a collision with severe consequences. Therefore, the severity of this hazard is assessed as S3, as unexpected braking or acceleration can result in life-threatening or fatal injuries. The exposure is again classified as E4, since communication disturbances can occur at any time during the platoon operation.

Table 1 *List of identified hazards and possible causes*

HAZARD NO.	HAZARD	POSSIBLE CAUSES	S/E/C ASIL
R.1.1	Complete loss of communication	Power supply failure, antenna hardware malfunction, excessive distance between vehicles, radio band interference, encryption error, hacker attack	S2/E4/C2 ASIL B
R.1.2	Erroneous communication	Antenna hardware failure, signal interference, encryption error, hacker attack	S3/E4/C3 ASIL D
R.2.1	Total loss of braking effect	Failure of wheel brake, retarder, or parking brake	S3/E4/C3 ASIL D
R.2.2	Reduced braking effect	Decreased efficiency of wheel brake, retarder, or parking brake	S2/E4/C3 ASIL C
R.2.3	Unintended braking	Incorrect brake activation without driver input	S3/E4/C3 ASIL D
R.2.4	Failure to release brakes	Malfunction of the wheel brake release mechanism	S2/E4/C1 ASIL A
R.3.1	Complete loss of tractive force	Powertrain failure	S2/E4/C2 ASIL B
R.3.2	Reduced tractive force	Reduced powertrain performance	S1/E4/C1 QM
R.3.3	Unintended tractive force	Malfunction in drive force regulation	S2/E4/C3 ASIL C
R.4.1	Complete unavailability of HMI (Human Machine Interface)	HMI power supply failure, hardware or software error	S2/E4/C2 ASIL B
R.4.2	Limited availability of HMI	Limited functionality due to hardware failure, software error, or cyberattack	S1/E4/C2 ASIL A
R.4.3	Unintended HMI commands	Incorrect inputs generated by system error or malicious attack	S3/E4/C2 ASIL C
R.5.1	Complete unavailability of control system	Power supply failure, ECU hardware failure, software error, or cyberattack	S3/E4/C3 ASIL D
R.5.2	False-positive control output	Incorrect signal from sensors or software fault triggering an unnecessary reaction	S2/E4/C3 ASIL C
R.5.3	False-negative control reaction	Failure to detect a critical situation due to incorrect evaluation of inputs	S3/E4/C3 ASIL D

Table 2 *Detailed analysis for Complete loss of communication*

HAZARD NO.	R.1.1
HAZARD	Complete loss of communication
POSSIBLE CAUSES	Power supply failure, antenna hardware malfunction, excessive distance between vehicles, radio band interference, encryption error, hacker attack
POSSIBLE CONSEQUENCES	Loss of convoy coordination, inadequate control response, increased risk of collision
SEVERITY	S2
EXPOSURE	E4
CONTROLLABILITY	C2
ASIL LEVEL	ASIL B
SAFETY GOAL	Detection of unavailable communication, fault signalling, transition to a safe state
SAFE STATE	Driver takeover, increased spacing between vehicles, controlled platoon dissolution

Table 3 *Detailed analysis of Erroneous communication*

HAZARD NO.	R.1.2
HAZARD	Erroneous communication
POSSIBLE CAUSES	Power supply failure, antenna hardware malfunction, excessive distance between vehicles, radio band interference, encryption error, hacker attack
POSSIBLE CONSEQUENCES	Antenna hardware failure, signal interference, encryption error, hacker attack
SEVERITY	S3
EXPOSURE	E4
CONTROLLABILITY	C3
ASIL LEVEL	ASIL D
SAFETY GOAL	Detect erroneous or corrupted communication, prevent unsafe control actions, and ensure reliable fallback operation.
SAFE STATE	Driver takeover with system alert, automatic platoon dissolution, and restoration of safe vehicle spacing

Due to the short spacing between vehicles and the limited ability to promptly recognize and compensate for the fault, the controllability is rated as C3. As illustrated in Figure 3 and summarized in Table 3, the combination of these parameters leads to an ASIL D classification for the communication subsystem. This assessment highlights that erroneous communication, whether caused by technical failures or malicious interference, represents one of the most critical hazards in platooning scenarios. Since the system may continue operating based on invalid data, the driver's ability to intervene is extremely limited. Consequently, hazards classified at ASIL D require the implementation of the most stringent safety measures, including subsystem redundancy, message authentication mechanisms, and plausibility checks to ensure acceptable risk levels.

5 Results and discussion

Using the aforementioned methods and approaches, the risks associated with the autonomous truck platoon are identified and evaluated using the ASIL scale. Table 1 summarizes these hazards for the key subsystems of the vehicles. The analysis covers communication between vehicles, braking components, powertrain, HMI, and the control system of the vehicle. These subsystems are highly connected, and their interaction is relevant to maintaining safe operation of the vehicle.

For each hazard, possible causes were analysed. These can be later used for subsequent development activities, such as safety mechanism specification, redundancy concepts, or monitoring concepts. This approach - linking hazards with possible causes, brings clear relation between identification and implementation of safety features.

A comparison between analysed hazards indicates that the most critical risks are directly leading to unpredictable vehicle or platoon behaviour. This includes erroneous communication, total loss of braking effect, unintended braking, unavailability of the control system, and false negative control reaction. All these hazards are evaluated as ASIL D, with high severity and limited controllability by the driver.

Generally, braking related hazards represent a significant safety concern, as both hazards may quickly change vehicle dynamics, which leads to rear end collisions in the case of vehicle platoons. Similarly, the powertrain related hazards may lead to changes in vehicle dynamics, however, differing from the braking, these changes are more gradual, making more time for the driver to react.

Hazards connected with the vehicle control system and HMI play an important role, as well. Unavailability of the control system or incorrect control decisions may lead to delayed or missing responses to critical situations. In highly automated driving modes, where the driver is only supervising the system, the ability to intervene could be reduced. The HMI-related failures may further delay driver awareness, increasing the overall risk during the fault conditions.

In contrast, hazards that lead to predictable failure are generally less critical. Complete loss of communication could be used as an example; despite its high exposure, it allows reliable fault detection and allows the human driver to take over the system.

Analysis shows that in terms of operational safety, a complete loss of communication is less critical than the communication with errors. In the cases when the communication is unavailable, the system can quickly and reliably detect the fault, alert the driver, and initiate the safe state. All the steps in this process are predictable, and residual risk mainly depends on the driver's skills. In contrast, the communication errors, may lead to false or inconsistent data transition, while the system operates as data are being valid. This may lead to unexpected convoy manoeuvres, with low opportunity for the driver to react.

6 Conclusion

In this paper is presented a functional safety assessment for vehicle-to-vehicle communication for truck platooning using the HARA methodology as defined in ISO 26262 ed. 2. The key hazards, connected to communication between vehicles, braking components, powertrain, HMI, and the global control system of the vehicle were identified, evaluated, and ASIL was assigned for them. The assessment shows how functional safety principles can be applied to cooperative driving scenarios of heavy vehicles with small inter-vehicle distances.

The results show that the highest safety requirements apply to hazards involving erroneous or corrupted communication between vehicles, total loss of braking effect, unintended braking, unavailability of the control system, and false negative control reaction. These may lead to unpredictable behaviour and cause severe accidents and were classified at the ASIL D level. Implementation of robust safety measures is required to ensure an acceptable risk level.

On the contrary, the total loss of communication has been evaluated as less safety critical in cases when the reliable malfunction detection and warning are ensured. Even though the total loss of communication can usually be classified as ASIL A, in the case of heavy vehicles traveling in a short distance platoon, it leads to a stricter classification as ASIL B in this paper.

Other subsystems described in the analysis may also independently or together affect the platoon's safety. While those hazards are typically local to individual vehicles, their impact can be bigger in a short distance platoon scenario. The results underline the need to consider the subsystem interactions when designing safety architectures for cooperative automated driving.

For the future work, simulation-based fault injection, experimental validation, and ASIL level comparison analysis can be presented. These will more precisely evaluate direct relations between the communication malfunctions and other safety-related subsystems. These extensions can lead to further development of platooning systems.

Acknowledgment

The authors received no financial support for the research, authorship and/or publication of this article.

Conflicts of interest

The authors declare that they have no known competing financial interests or personal relationships that could have appeared to influence the work reported in this paper.

References

[1] EUROSTAT. Greenhouse gas emissions by economic activity - transport [online] [accessed 2025-05-04]. Available from: https://ec.europa.eu/eurostat/statistics-explained/index.php?title=Greenhouse_gas_emissions_by_economic_activity

[2] EUROSTAT. Road accident fatalities - statistics by type of vehicle [online] [accessed 2025-05-04]. Available from: https://ec.europa.eu/eurostat/statistics-explained/index.php?title=Road_accident_fatalities_-_statistics_by_type_of_vehicle

[3] SAE International. Taxonomy and definitions for terms related to driving automation systems for on-road motor vehicles. Technical Report J3016_2021 [online] [accessed 2025-05-04]. Available from: https://www.sae.org/standards/content/j3016_202104

[4] MICHAUD, R., LEPAGE, P., FRENETTE, P., LETOURNEAU, D., GAUBERT, N. Coordinated manoeuvring of automated vehicles in platoons. *IEEE Transactions on Intelligent Transportation Systems* [online]. 2006, **7**(4), p. 437-447. ISSN 1524-9050, eISSSN 1558-0016. Available from: https://doi.org/10.1109/TITS.2006.883939

[5] LAMMERT, M. P., DURAN, A., DIEZ, J., BURTON, K., NICHOLSON, A. Effect of platooning on fuel consumption of class 8 vehicles over a range of speeds, following distances, and mass. *SAE International Journal of Commercial Vehicles* [online]. 2014, **7**(2), p. 626-639. ISSN 1946-391X, eISSN 1946-3928. Available from: https://doi.org/10.4271/2014-01-2438

[6] Volvo Group. Trucks on a European tour for platooning [online] [accessed 2025-05-04]. Available from: https://www.volvogroup.com/en/news-and-media/news/2016/mar/news-151 620.html

[7] MILANES, V., SHLADOVER, S. E., SPRING, J., NOWAKOWSKI, C., KAWAZOE, H., NAKAMURA, M. Cooperative adaptive cruise control in real traffic situations. *IEEE Transactions on Intelligent Transportation Systems* [online]. 2014, **15**(1), p. 296-305. ISSN 1524-9050, eISSN 1558-0016. Available from: https://doi.org/10.1109/TITS.2013.2278494

[8] CHOWDURY, H., JUWONO, R., ZAID, M., ISLAM, R., LOGANATHAN, B., ALAM F. An experimental study on the effect of various deflectors used for light trucks in the Indian subcontinent. *Energy Procedia* [online]. 2019, **160**, p. 34-39. ISSN 1876-6102. Available from: https://doi.org/10.1016/j.egypro.2019.02.115

[9] BARHOUMI, O., FARHANI, G., RAHMAN, T., ZAKI, M. H., TAHAR, S., ARAJI, F. Fuel consumption in platoons: a literature review. *arXiv* [online]. 2025, arXiv:2508.10891. eISSN 2331-8422. Available from: https://doi.org/10.48550/arXiv.2508.10891

[10] European Truck Platooning Challenge 2016. Brochure. The Hague: Government of the Netherlands, 2016 [online] [accessed 2025-05-04]. Available from: https://www.government.nl/binaries/government/documenten/leaflets/2015/10/06/leaflet-european-truck-platooning-challenge-2016/brochure-european-truck-platooning-challenge-2016.pdf.

[11] SCHMEITZ, A. Truck platooning projects, programs and cooperation groups. H2020 Project Ensemble, Deliverable D6.14. 2022.

[12] ZHANG, L., CHEN, F., MA, X., PAN, X. Fuel economy in truck platooning: a literature overview and directions for future research. *Journal of Advanced Transportation* [online]. 2020, **2020**, 2604012. eISSN 2042-3195. Available from: https://doi.org/10.1155/2020/2604012

[13] HABIBOVIC, A., ANDERSSON, J., MALMSTAIN LUNGREN, V., STAF, H. Replacing side view mirrors in trucks with integrated digital systems: prototype evaluation and potential fuel savings. Project Dreams. 2017.

[14] HAKAK, S., GADEKALLU, T. R., MADDIKUNTA, P. K. R., PRIYA, S., PARIMALA, M., DE ALWIS, C., LIYANAGE, M. Autonomous vehicles in 5G and beyond: a survey. *Vehicular Communications* [online]. 2022, **39**, 100551. eISSN 2214-210X. Available from: https://doi.org/10.1016/j.vehcom.2022.100551

[15] KOUSARIDIS, A., SCHIMPE, A., EULER, S., VILAJOSANA, X., FALLGREN, M., LANDI, G., MOSCATELLI, F., BARMPOUNAKIS, S., VÁZQUEZ-GALLEGO, F., SEDAR, R., SILVA, R., DIZAMBOURG, L., WENDT, S., MUEHLEISEN, M., ECKERT, K., HARRI, J., ALONSO-ZARATE, J. 5G cross-border operation for connected and automated mobility. *Future Internet* [online]. 2020, **12**(1), 5. eISSN 1999-5903. Available from: https://doi.org/10.3390/fi12010005

[16] International Organization for Standardization. Road vehicles - functional safety - ISO 26262, 2. ed. Geneva: ISO, 2018. ISBN 978-92-67-10667-2.

INTEGRATING RESILIENCE INDICATORS INTO VIRTUAL OPERATIONS SUPPORT TEAM FOR ROAD CRITICAL INFRASTRUCTURE IN CRISIS MANAGEMENT

Ondřej Ryška*, Patricie Gamonová

VSB - TUO, Faculty of Safety Engineering, Department of Civil Protection, Ostrava-Vyskovice, Czech Republic

*E-mail of corresponding author: ondrej.ryska@vsb.cz

Ondrej Ryska 0009-0009-6565-499X

Resume

Increasing disaster frequency intensifies the need for rapid, location-specific information in crisis management. A Virtual Operations Support Team (VOST) can enhance situational awareness by verifying open-source data, but these outputs are rarely transformed into resilience indicators. In this paper is presented a framework that maps verified VOST outputs and metadata to indicators for road critical infrastructure resilience and links them to the crisis decision cycle. A preliminary test on media data (1 Aug-31 Dec 2024; n = 2,045) confirmed a stable baseline and clear peaks usable for management-defined thresholds and trigger actions. The framework also outlines governance, supplier interfaces, and GIS-based operationalization of Exposure, Condition, Accessibility, and Consequence.

Article info

Received 19 February 2026
Accepted 27 March 2026
Online 24 April 2026

Keywords:

scenario modelling
VOST
road infrastructure
resilience
indicators

Available online: https://doi.org/10.26552/com.C.2026.029

ISSN 1335-4205 (print version)
ISSN 2585-7878 (online version)

1 Introduction

According to the World Disasters Report, approximately 631 disasters occur on average each year [1]. The increasing frequency and severity of these events raise demands for rapid, accurate, and spatially specific information for crisis management stakeholders. In situations where the effective management of emergencies is constrained by personnel and capacity limitations, the involvement of digital volunteers can synergistically support crisis management activities. Digital volunteers collaborate online and can improve decision-making by collecting, evaluating, analysing, and verifying crisis-related information from Twitter, Facebook, or YouTube [2]. At the same time, social media and the rise of volunteer and technical communities (V&TC) have changed approaches to handling spatial data in crisis analysis. In response, a new form of organised effort for collaborative information collection and community management has been introduced. It is referred to as Virtual Operations Support Teams (VOST). This concept creates a framework for the systematic linkage of formal crisis management bodies with digital volunteers. However, its implementation has so far remained limited to only a few cases [2].

The VOST-verified data used in crisis management include metadata from geolocation, infrastructure, health, logistics, humanitarian, and meteorological domains. They include both precise quantitative information, such as GPS coordinates, numbers of people, capacities, and status and volume indicators, and qualitative descriptions and multimedia records, such as text messages, photographs, and satellite imagery. The data are dynamic and temporally variable. They are produced both as structured records and as unstructured information streams from the online environment. A key feature is the varying level of verification and reliability. This ranges from official reports by crisis management authorities to unverified content and potential misinformation from social media, which require systematic verification. Once processed and verified, these data and metadata can provide crisis management with a multidimensional real-time picture of the situation and support early threat identification, decision-making, and measures to increase the resilience of critical infrastructure [3]. A major limitation, however,

remains the response time of such information, as current approaches often do not enable the sufficiently rapid identification of the origin of a disruption, the monitoring of its development, and the validation of its local or cascading impacts in real time.

The VOST has the potential to strengthen the information support available to decision-making bodies and to enable more effective coordination among crisis management stakeholders. Its integration into operational management processes can benefit crisis communication and resilience mapping. Although the benefits of VOST have already been demonstrated abroad, the system is currently implemented in only a limited number of countries and it is not yet in place in the Czech Republic. Even where it has been introduced, the use of the monitored data remains limited. These data are often used only to verify information that is generally already known, and the collected data are not systematically used to indicate disruptions in service functionality, network accessibility, or resilience [4].

Despite these benefits, there is still no methodologically integrated framework that would connect, in real time, the identification of deviations in the road network functioning, their independent verification from open sources, and their translation into indicators applicable to crisis management. Current approaches usually focus either on the verification of individual pieces of information or on resilience indicator systems, but without their systematic integration in the environment of road critical infrastructure. At the same time, under the conditions of the Czech Republic, there is no operationally embedded procedure that would elaborate this linkage in organisational and methodological terms.

Indicators are a widely used tool for the timely detection of potential disruptions to the resilience of critical elements and for the continuous assessment of the current situation as well as the actual state of the environment. Monitoring the values of selected indicators over time enables the anticipation of future developments and the timely adjustment of implemented measures.

In the context of such indicators, using data for resilience mapping represents a key extension of disaster prevention. Network metrics can be translated into measurable indicators of infrastructure topology and operation, and they help to identify critical links, nodes, and corridors within the system [5]. Management can use these outputs to prioritise interventions, plan redundancy, and support operational traffic management. These metrics can also be applied to the assessment of communication processes and data flows, for example by monitoring the network availability, density, and latency, or by identifying key nodes within the information system.

Building on the above relationships, the methodological dimension of the paper focuses on approaches applicable to disruption indication and resilience mapping based on data verified through VOST [6]. Particular emphasis is placed on methods that enable verified outputs to be translated into comparable indicators applicable within the road infrastructure environment. Examples include travel time reliability analysis and the Planning Time Index (PTI), geoinformation-based approaches to identifying critical sections of the transport network, methods for determining hydrologically sensitive road sections prone to flash flooding, and the assessment of technical condition through the Pavement Condition Index (PCI).

The need for new assessment approaches follows from the fact that the resilience of road critical infrastructure is affected by uncertainty, data heterogeneity, and dynamically changing operating conditions. Assessment must therefore integrate multi-source data, reflect the spatio-temporal variability of the observed phenomena [7], and enable identified changes to be translated into indicators applicable to decision-making. This requirement supports the adoption of approaches that link standardised infrastructure assessment with operationally acquired data and create a robust framework for resilience assessment [8].

In this paper is given a response to this gap in three ways. First, the VOST activities are defined in relation to disruption indication and the resilience mapping of road critical infrastructure. Second, a framework is proposed that links verified open-source data and metadata with indicator-based assessment applicable to the operational and tactical levels of crisis management. Third, the possibility is demonstrated for establishing a reference level, identifying deviations, and linking them to threshold values and trigger actions in a time-critical environment.

Based on the relationships outlined above, the paper aim was to define the VOST activities and develop a framework for using the verified data and metadata in resilience mapping within the road infrastructure subsector. Achieving this objective is intended to support the establishment of a data framework applicable to early threat identification, decision support, and the planning of measures aimed at increasing the resilience of critical infrastructure [9].

2 The VOST concept and implementation background

A Virtual Operations Support Team (VOST) is an organised form of volunteer support that strengthens the capacity of crisis management authorities in the online environment. It responds to the growing importance of social media during emergencies by converting spontaneously shared citizen-generated data into outputs applicable to management and decision-making [10]. VOST consists of trained volunteers working remotely who are integrated into formal structures and coordinated by crisis management authorities.

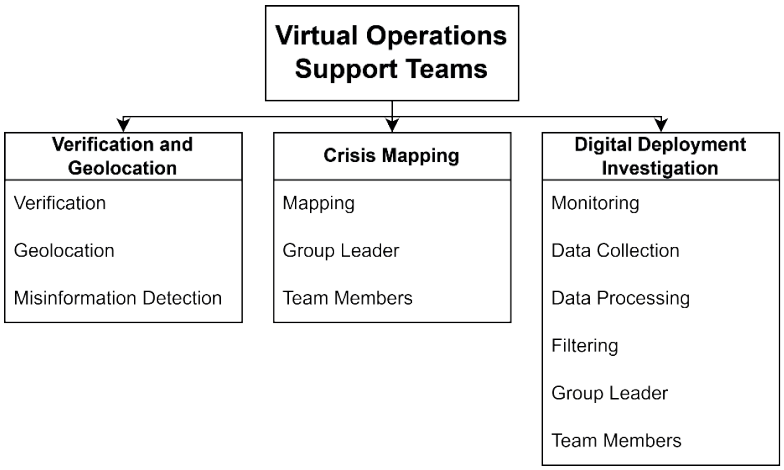

Figure 1 *Main areas of the Virtual Operations Support Team*

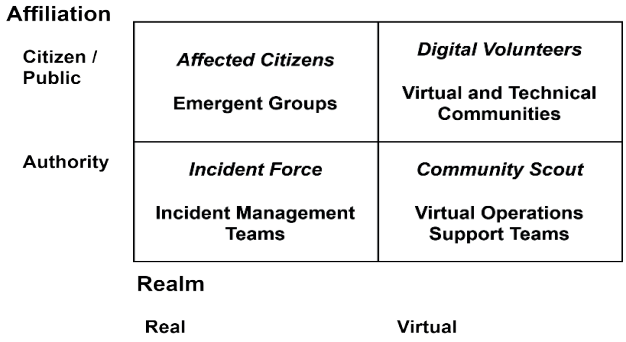

Figure 2 *Typology of actor roles in the real and virtual environment during emergencies*

In practice, however, its systematic implementation within national crisis management structures remains limited because the specific activities, outputs, and implementation steps of VOST have not yet been defined with sufficient clarity.

2.1 Defining the VOST tasks

The VOST tasks can be structured into three consecutive areas that correspond to the core functional domains shown in Figure 1. The first area is verification and geolocation, including authentication of content, identification of misinformation, and determination of the time and location of the report [11]. The second area focuses on crisis mapping, that is, the sorting, spatial organisation, and visualisation of relevant data in the form of aggregated and standardised outputs for operational components of crisis management.

The third area represents the digital deployment investigation, which includes monitoring, systematic data collection, and their basic processing, filtering, and preliminary classification by topic and location [11]. Performing these tasks requires adequate organisational and staffing capacity and the ability of management to flexibly integrate information from informal sources while maintaining requirements for accuracy and reliability [11]. To fully use the potential of digital volunteers, an integrated approach is also necessary, within which the crisis management authorities not only accept these activities but coordinate them, as well.

2.2 Typology of social media actor roles and the position of VOST

The typology of social media actor roles during emergencies provides an appropriate framework for defining the position of VOST within the crisis communication system. An overview of these roles is summarised in Figure 2. The role matrix presented by Fathi et al. [2] offers a differentiated view of behavioural patterns by distinguishing between actors operating in the real and virtual environments and, at the same time, by separating institutional actors, that is, public authorities and organisations, from citizens. This distinction is important for understanding that VOST does not represent an isolated volunteer activity, but rather a specific interface between the formal crisis management structures and the dynamic digital environment.

In this typology, VOST is classified among

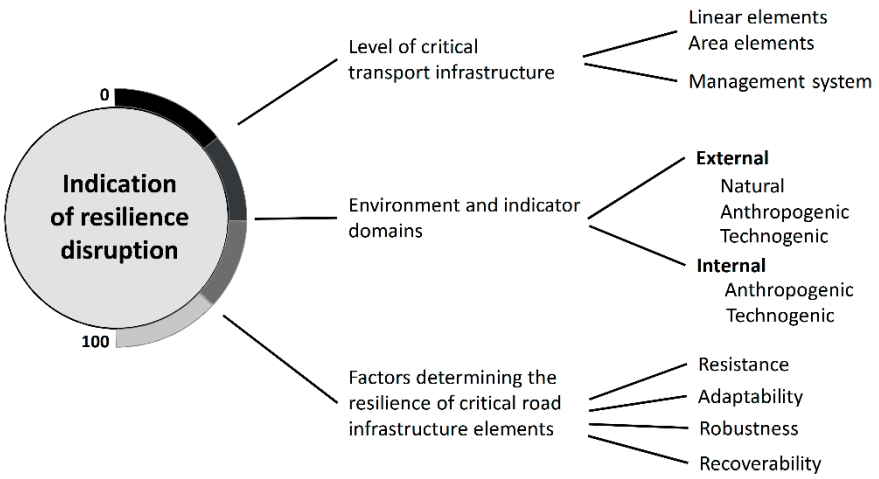

Figure 3 *Framework for indicating disruptions to the resilience of critical infrastructure elements*

institutional organisations operating within public authorities, even though it relies on volunteer capacity and operates predominantly in the virtual environment. As an organisational unit, it cooperates at the inter-institutional level with incident management teams and other components responsible for situation analysis and the operational response to an emergency. VOST therefore does not function merely as a technical intermediary for data handling, but as an operational interface between the official crisis management structure and the dynamic environment of social media.

The literature also highlights efforts by VOST to cooperate with other VOST teams and volunteer and technical communities (V&TC) in joint deployments, typically during large scale or cross-border events. However, the requirements for effective cooperation between the formal humanitarian and crisis response organisations and Volunteered Geographic Information (VGI) communities' place considerable demands on coordination. Challenges arise particularly in the standardisation of data and procedures and in the allocation of accountability [12]. This broadens the standard operational framework of VOST and at the same time indicates the potential of further specialisation of its activities. One such specialisation may be a branch of VOST focused on resilience mapping, which can contribute to strengthening society by supporting prevention, preparedness, adaptability, and recovery, as described by Rehak et al. [13] and Ryska [14].

This development confirms the growing importance of coordinated cooperation between the formal crisis management structures and digital volunteers and is at the same time consistent with the direction of the European regulatory framework, in particular Directive (EU) 2022/2557 of the European Parliament and of the Council [15]. At the same time, the use of data mining and machine learning concepts has accelerated the availability and evaluation of VGI and other data related to disaster response [16]. Even so, it remains difficult to align social media data clearly with users' information needs, because the usefulness of information varies according to their roles and objectives within the disaster response [16]. VOST must therefore not only process data technically, but also continuously adapt its outputs to the changing information needs of crisis management.

2.3 Framework for implementing indicators

The literature describes several metrics and approaches for assessing the resilience of critical infrastructure. Both quantitative and qualitative methods are used, as well as empirical approaches based on data or hypothetical scenarios. However, those methods often face limited availability of information and data [17], subjectivity in the responses provided, dependence on a specific type of infrastructure [18] or on the event scenario, and a limited ability to generalise the results [19].

For these reasons, an indicator-based approach appears to be a suitable direction for implementing a systematic framework for resilience assessment based on a set of measurable indicators. These indicators make it possible to track changes over time, compare different critical infrastructure elements, and support management decision making.

A fundamental prerequisite for the proper functioning of a procedure for indicating disruptions to the resilience of critical infrastructure elements is the clear definition of the framework within which indicators are defined and applied [20]. This framework is illustrated schematically in Figure 3.

The essence of the framework lies in defining the baseline conditions for specifying the key characteristics of indicating disruptions to the resilience of critical infrastructure elements. Splichalova et al. [21] and Patrman et al. [22] distinguish four interrelated levels:

1. Levels of critical infrastructure: individual elements, systems, and networks whose functionality is subject to assessment.
2. Environment and indicator domains: the context in which the infrastructure functions, including the physical, social, and institutional environment, as well as the thematic domains of indicators.
3. Factors determining the resilience of critical infrastructure elements: internal and external factors that influence an element's ability to withstand disruption and restore its functions.
4. Database of resilience disruption indicators: a structured set of indicators, including their definitions, units, data sources, and links to the assessed factors.

Leading indicators reflect conditions and factors that precede a disruption, for example the level of preparedness, maintenance quality, or the degree of dependence on critical suppliers. They allow for management to take preventive action.

Lagging indicators describe impacts that have already occurred and changes in performance over time, for example outage duration, capacity loss, or recovery speed. They are used mainly to assess consequences and the effectiveness of recovery [23].

In this context, the resilience is understood as an overarching concept that links indicators of risk, safety, protection, business continuity, and operational performance [24]. For the purposes of this paper, however, it is operationalised primarily through indicator-based assessment related to road critical infrastructure and to data verified through VOST. This creates a direct conceptual transition between the general resilience framework and the subsequent verification of information flow dynamics for the purposes of the indication framework.

2.4 Verifying the dynamics of the information flow for the indication framework

Resilience mapping of the road critical infrastructure requires a standardised description of deviations from normal conditions and their interpretation in time and space [25]. Indicator systems, including leading and lagging indicators, provide a tool for linking operational observations with the assessment of preparedness, response, and recovery of provided services. For their use in crisis management, the ability to identify a change from a reference level, that is, the baseline, in a timely manner is crucial. It is also necessary to verify its cause so that management can set escalation thresholds and corresponding intervention procedures. Without this link, resilience mapping remains fragmented and limited to partial data sources.

To support the setting of threshold values and escalation rules, the dynamics of the information flow were verified using media data. A preliminary analysis of the sectoral classification of reports led to selection of the transport and logistics sector for the initial construction and validation, with implementation focused on the dominant road transport subsector. Content analysis of media outputs indicates a dominance of transport and logistics topics with 12,522 reports, followed by construction with 7,508 reports, IT and communications with 5,347 reports, sport with 4,529 reports, health with 2,824 reports, culture and education with 1,925 reports, and agriculture with 1,493 reports. With regard to channels, the internet dominates with 68.0 % and 32,281 reports. It is followed by social media with 11.6 % and 5,530 reports, print media with 8.6 % and 4,067 reports, radio with 7.6 % and 3,613 reports, and television with 4.2 % and 1,997 reports.

To verify the temporal variability, the daily number

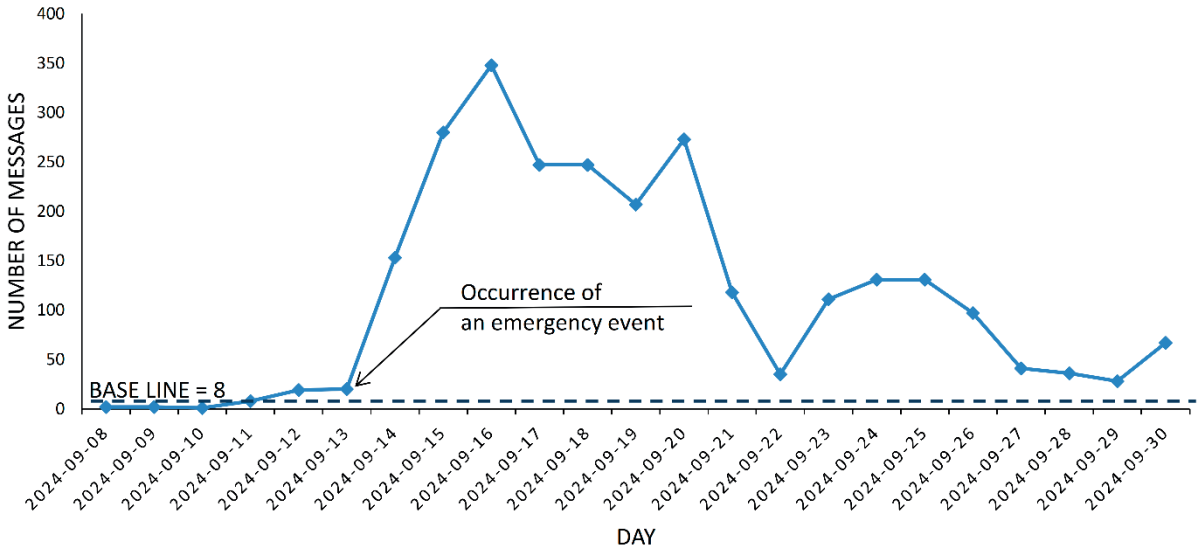

Figure 4 *Daily aggregation of reports for the transport and logistics sector with a focus on the road transport (1 August 2024 to 31 December 2024)*

of published reports was aggregated for the period from 1 August 2024 to 31 December 2024 (n = 2,045, see Figure 4). The time distribution shows a peak during 15 to 19 September 2024, when 729 reports were published, which represents 35.6 % of the total volume. The maximum occurred on 16 September 2024 with 197 reports. It was followed by 15 September with 169 reports and by 17 to 19 September with 111 to 134 reports. Outside the peak period, the volume stabilises at a low level, with approximately 1 to 2 reports per day in August, which represents the baseline. After the peak, a gradual decline predominates.

The identified dynamics can be used to set an indication framework in a time critical environment. The framework uses the baseline as the reference level and escalation thresholds defined by a combination of report volume, geolocation, and event typology. These thresholds and the related trigger actions are set by management with regard to tolerated risk, system capacity, and the required response speed. In this way, the VOST supports not only the verification of individual events, but the continuous trend evaluation and timely escalation of intervention, as well.

3 Synergy between the VOST and indicator systems in crisis management

Synergy between the Virtual Operations Support Team (VOST) and indicator systems in crisis management lies in converting verified VOST outputs from open digital sources into quantitative and qualitative resilience indicators applicable to the assessment of road critical infrastructure resilience. This complements traditional indicators that rely mainly on historical data or expert judgement and strengthens management's ability to respond to dynamic developments. VOST outputs cover a wide range of data types. They include geolocation and geospatial data for locating hotspots and refining map layers, and infrastructure reports that can indicate passability, service availability, and the functionality of nodes within road critical infrastructure. They also include meteorological and environmental data that support early warning, health and humanitarian information that can be used for prioritising resources and capacities, satellite and aerial imagery for damage assessment and verification of visual content, and aggregated mobile data for mobility and exposure indicators [26]. In addition to the content itself, metadata are also an important source for indicators. Examples include reporting frequency, temporal distribution, platform type, linguistic characteristics, and sharing intensity. These attributes describe the crisis dynamics, the level of information noise, and the effectiveness of communication measures. After the filtering and verification, VOST data and metadata can be mapped directly to indicators or used as a supporting layer [11].

3.1 Conceptual model for indicator-based resilience evaluation

To use VOST outputs within indicator systems, it is necessary to map them to indicators that correspond to

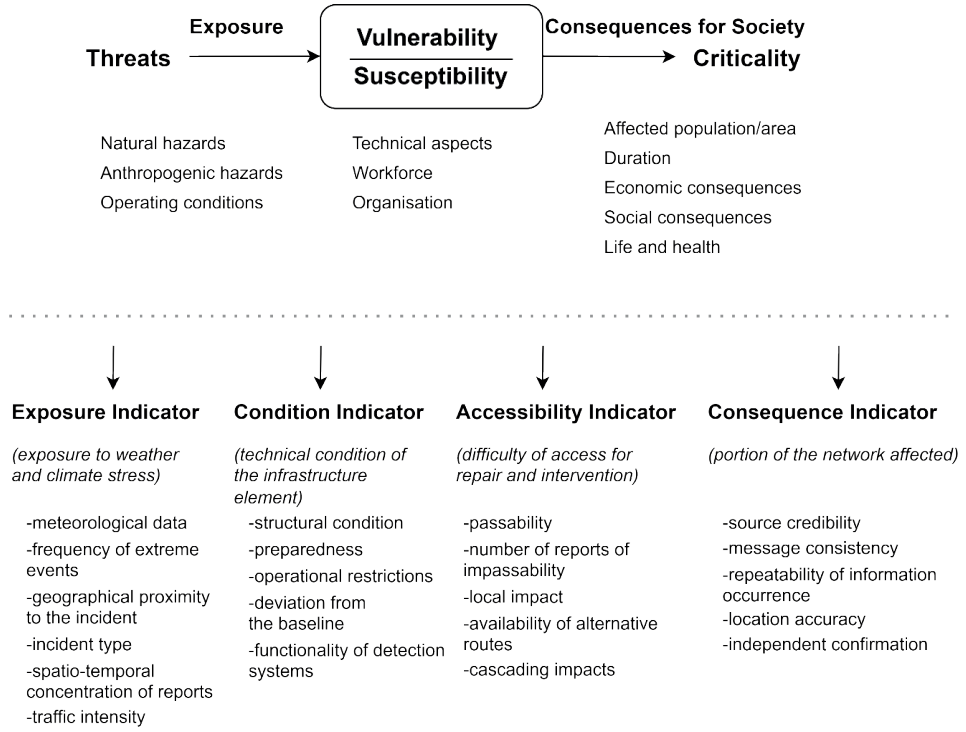

Figure 5 *Resilience indicator model for the road critical infrastructure*

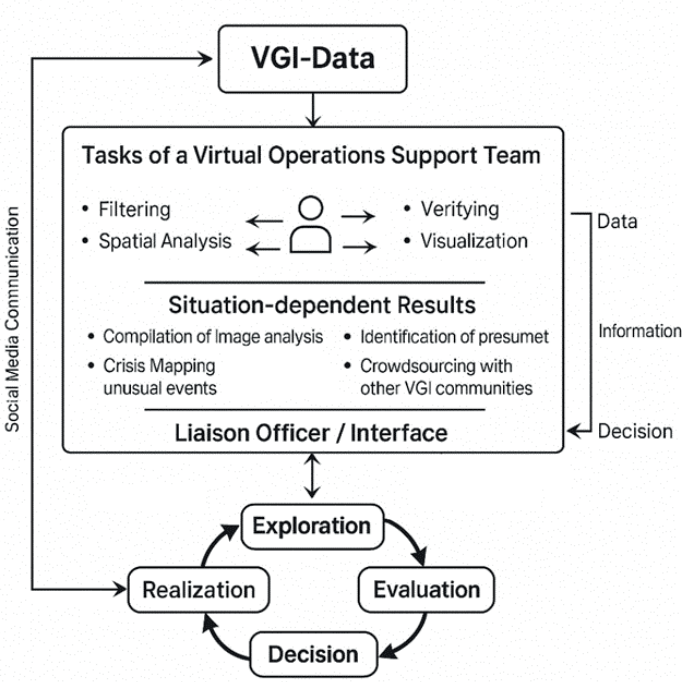

Figure 6 *VOST data flow in crisis management*

the link between Threats, Exposure, Vulnerability and Susceptibility, Consequences for society, and Criticality (Figure 5). In the first part of the chain, threats enter the exposure indicator, which describes the degree to which an infrastructure element is exposed to hazardous phenomena, for example weather and climate related stress. Next, vulnerability and susceptibility are represented primarily by the condition indicator, which captures the technical state of the element, and the accessibility indicator, which reflects the difficulty of access for intervention and repair. Those characteristics are followed by consequence indicators that capture the extent of impacts within the network, for example the size of the affected area or the affected part of the network. Criticality is derived from the combination of network impacts and their significance for society. It provides a basis for prioritising measures and for crisis management decision making within the situational overview.

3.2 Implementing resilience indicators into the crisis management decision cycle

An integrated process connecting incoming VGI data with the crisis management decision cycle is illustrated in Figure 6. The VGI data from social media enter VOST, where filtering, spatial analysis, verification, and visualisation are performed. The outputs take the form of situation dependent products, for example crisis mapping, image-based analyses, and the identification of unusual events. They are then transferred through a liaison officer to the exploration, evaluation, decision, and realisation cycle. In this paper, the framework is extended by converting verified outputs into indicator systems for the resilience of road critical infrastructure in order to provide a comparable basis for operational and tactical management.

At the operational level, indicators enable the setting of threshold values. Exceeding these thresholds initiates predefined trigger actions. Examples include closing of a road segment, rerouting traffic, activating detours, reinforcing Integrated Rescue System units, or changing response priorities in locations with a high concentration of damage reports. Indicators also support continuous updates of situational maps and operational plans based on real time information on passability, weather conditions, impact extent, and population mobility. Decision making also reflects links to supplier entities, in particular equipment availability, response times, backup capacity, and constraints during service restoration.

At the tactical level, indicators and their time series are used to evaluate the effectiveness of the response and to identify the recurring network weaknesses. These are typically lagging indicators of performance loss and recovery, the extent of damage, and recovery time. The outputs make it possible to derive structural vulnerabilities, including dependencies on key nodes and specific suppliers, and to translate them into investment planning, updates of business continuity plans, and the design of standard measures to increase resilience [17].

Threshold values and the definition of trigger actions are set by management with regard to tolerated risk, system capacity, responsibilities, and the legal framework. Some indicators are derived from data

with higher uncertainty, such as crowdsourcing and social media. For this reason, it is appropriate to work with record credibility levels, triangulation rules, and weighting in decision models. Integrated use of VOST and indicator systems therefore supports the management of a specific event and the long term strengthening of the resilience of road critical infrastructure and related services in the supply chain.

To illustrate the practical application of the proposed framework, a model situation can be considered in which a hydrometeorological event causes disruption to the function of a bridge structure or an adjacent section of the road network. The first step is the detection of an anomaly, that is, a deviation from normal conditions, for example a sudden increase in relevant media reports or geolocated records of impassability. In line with the proposed procedure, this triggers the creation of a candidate event record. VOST then initiates the collection and preprocessing of data from the open digital sources, in particular social media, online news reports, map applications, and supplementary meteorological sources. At this stage, the preliminary elimination of information noise is performed, based on basic linguistic analysis of keywords, filtering by location, time, content type, and language, deduplication of records, and basic normalisation of metadata. This step enables the rapid narrowing of the data stream to records with potential relevance for crisis management decision-making. In the second step, the candidate information is verified and enriched. VOST assesses source credibility, message consistency, repeatability of the information, and independent confirmation across multiple channels, adds geolocation, and assigns the record to a specific network element and its operational context.

In the third step, the verified records are translated into indicators. Hydrometeorological loading enters the Exposure indicator, technical condition and operational impairment enter Condition, reachability for intervention and detour options enter Accessibility, and network as well as societal impacts enter Consequence. These indicators are then compared to the reference baseline and with threshold values defined by management. An empirical anchor for this logic was provided by the analysis of media data for the transport and logistics sector for the period from 1 August 2024 to 31 December 2024 (n = 2,045), in which a stable baseline of approximately 1-2 reports per day and a marked peak during 15-19 September 2024 were identified, with a total of 729 reports and a maximum of 197 reports on 16 September 2024. Exceeding the thresholds then activates the corresponding trigger actions, such as traffic restriction, designation of a detour route, prioritisation of technical intervention, or reinforcement of Integrated Rescue System units. The model situation therefore shows that the proposed framework is not merely a conceptual construct, but can be used for early disruption indication, situational overview, and support for operational as well as tactical decision-making.

3.3 Resilience of road critical infrastructure within an indicator framework

In the road transport subsector, resilience should be assessed as a systemic property arising from the interaction of the exposure of infrastructure elements, their vulnerability/susceptibility, the consequences of disruption, and criticality within the network [27]. Within this framework, vulnerability and susceptibility do not represent concepts interchangeable with resilience, but rather its partial analytical dimension expressing the proneness of elements to degradation, loss of functionality, and loss of performance under the action of threats. Lagging indicators capture already manifested impacts and the current loss of system performance, whereas leading indicators indicate conditions preceding disruption and enable its further development to be anticipated [27]. At an aggregated level, indicators therefore serve not only to describe the current vulnerability of the system, but also to assess trends relevant to the evaluation of its resilience [28]. The construction of indicator systems must therefore be based on a coherent theoretical framework and a systematic indicator development process [13]. The road infrastructure should at the same time be modelled as a network of elements and flows in which criticality is determined not only by the technical condition of individual elements, but also by their role within the network, the existence of alternative routes, and links to other transport modes and supply chains [29]. A framework defined in this way provides the basis for indicator selection and for management decisions on monitoring, maintenance, and investment priorities.

For the operational use of the proposed framework, it is also necessary to define how VOST is structurally and procedurally integrated into decision-making in time-critical environments. In performing its tasks, VOST works with heterogeneous VGI data and other open sources, in particular for the purposes of filtering, verification, and interpretative processing of information. In the conditions of the road transport subsector, this procedure should therefore be further extended through the integration of indicator systems that enable verified outputs to be translated into decision-support inputs applicable to monitoring, escalation, and the subsequent evaluation of resilience.

Proposed procedure:

- Definition of target indicators for the road critical infrastructure: Management, in cooperation with infrastructure experts and data analysts, defines a structured set of leading and lagging indicators relevant to individual phases of the resilience cycle and at the same time to the key dimensions of the assessment, in particular exposure, condition, accessibility, consequences, and criticality. Examples include indicators of passability, structural condition,

maintenance preparedness, and the functionality of detection and communication systems, as well as the continuity of provided services.

- Mapping the VOST outputs to indicators: For each indicator, it is necessary to specify which types of data and metadata VOST can provide and what informative value they have for its construction or updating. These may include, in particular, geolocated reports of impassability, metadata on reporting intensity, information extracted from photographs and videos, and supplementary data on weather, event extent, or the humanitarian situation. The mapping must at the same time distinguish whether individual outputs enter indicators of exposure, condition, accessibility, consequences, or criticality, and must take into account their temporal validity, level of verification, and spatial accuracy.
- Integration into the data pipeline: VOST transfers verified data and metadata into a centralised indicator database in which they are normalised, aggregated, and subsequently interpreted for the purposes of the situational overview. The responsible unit, for example the road authority or the crisis staff, ensures the operation of tools for indicator calculation, updating, and visualisation. It is essential that this data pipeline support the continuous transfer of verified outputs into the decision-making process while also enabling their linkage with other relevant data layers.
- Setting roles and responsibilities: The governance framework must clearly define who approves the indicator methodology, who is responsible for VOST operations, who interprets the results, and who makes decisions. It also includes the delineation of interfaces with supplier entities, including ICT, data, and maintenance. A clear allocation of roles and responsibilities is necessary to ensure the consistency of outputs, accountability for their use, and continuity between operational and tactical management.
- Feedback and learning: Results obtained from the use of indicators during the real events must be systematically evaluated and used for the continuous updating of the indicator database, VOST configuration, and institutional relationships with supplier entities. This mechanism closes the adaptation and learning cycle of the proposed framework and at the same time supports its long-term validity and operational applicability.

For indication at the level of the road critical infrastructure subsector, it is appropriate to use a combination of indicators representing exposure, conditions, accessibility, and consequences. This approach captures both leading indicators, meaning early warning signals of deteriorating conditions, and lagging indicators, meaning indications of already manifested failures and their consequences at the level of system performance [30]. Although an analogous categorical structure has also been used in other critical infrastructure sectors [28], in this paper it is adapted specifically to the conditions of road infrastructure and to the informational capacities of VOST.

- Exposure: The exposure indicator expresses the degree to which an element of road critical infrastructure is subjected to natural and anthropogenic threats. It is determined based on the spatial and operational data, in particular on flood-prone areas, slope instability, locations susceptible to icing, traffic intensity, heavy vehicle loading, or incident frequency. The result is a normalised exposure score that can be used as a leading indicator for the early identification of an increased risk of disruption.
- Conditions: The condition indicator expresses the technical and operational state of an element of the road critical infrastructure based on diagnostics, inspection, and maintenance data. In the road infrastructure context, it may be derived, for example, from pavement condition indicators, assessments of bridge structures, or partial indicators of evenness, skid resistance, load-bearing capacity, and material degradation. The result is the translation of these findings into a unified scale that enables comparable evaluation of technical condition across the network and serves as a key input for estimating vulnerability/susceptibility.
- Accessibility: The accessibility indicator expresses the reachability of an element of the road critical infrastructure for intervention, maintenance, and the restoration of its function. It is derived from network topology and response conditions, in particular from road category, the existence of detour routes, constraints on heavy equipment, travel times of maintenance units or Integrated Rescue System components, and the current passability of the affected area. The result is a comparable measure of accessibility that makes it possible to assess how quickly and under what constraints a disrupted element can be addressed.
- Consequence: The consequence indicator expresses the extent and severity of the impacts of failure or functional limitation of an element of the road critical infrastructure on mobility, territorial accessibility, economic activity, and the provision of essential services. It is derived primarily from the position of the element within the network, traffic intensity, the importance of the served area, and links to critical entities such as hospitals, industrial zones, logistics hubs, or Integrated Rescue System components. The result is a comparable measure of consequences that makes it possible to assess the societal and operational significance of the disruption.

An analogous framework can be applied to road infrastructure by using geoinformation technologies. In a GIS environment, Exposure can be derived as a combination of spatial layers representing natural and anthropogenic threats, for example floodplains, slope instability, icing prone locations, heavy vehicle loading, and incident intensity. Condition can be derived from diagnostics and inspections, for example pavement conditions indices such as PCI, assessments of bridge components, and indicators C1 to C4 for evenness, skid resistance, load-bearing capacity, and degradation, converted to a unified scale. Accessibility is derived from network topology and response conditions, including road categories, detour options, constraints on heavy equipment, and travel times of maintenance units or the Integrated Rescue System. Consequence combines the importance of an element within the network, for example its inclusion in backbone corridors and its function within the Trans European Transport Network, transport volumes, and links to critical entities such as hospitals, industrial zones, and logistics hubs. It therefore expresses the network and societal significance of disruption.

Indicators can be derived from operational and maintenance databases, for example congestion frequency, the Planning Time Index, and closure durations, and also from expert assessment of supporting materials such as hazard maps and the strategic importance of a corridor. Subsector management defines threshold values, assessment periodicity, and links to decision-making processes such as maintenance plans, investments, and crisis plans, while taking into account dependencies on supplier entities. From the perspective of resilience assessment, continuity between the leading indicators, including exposure, conditions, and accessibility, and lagging indicators, including capacity loss, congestion extent, recovery time, and incident severity, is essential. Aggregation proceeds vertically from the asset level through corridors and the network, and horizontally into composite indicators for threat scenarios. Weights can be adjusted according to the event type, for example flooding compared to excessive loading, which supports comparability and transparent management decision-making [31].

4 Conclusion

The aim of this paper was to propose a framework that links the activities of a Virtual Operations Support Team (VOST) with indicator systems for the assessment of critical infrastructure resilience and to verify its applicability in the road transport subsector. The paper is based on a literature review of the concepts of VGI, V&TC, and VOST, as well as indicator-based approaches to resilience. It is a response to the need to translate verified information from open digital sources into comparable indicators that can be used directly in crisis management decision-making.

The results show that the VOST provides a systematic source of structured and unstructured data and metadata with a spatiotemporal reference that can support both leading and lagging indicators. Verification of information flow dynamics using media data for the transport and logistics sector confirmed the presence of a stable reference level, that is, the baseline, and distinct peak periods. These findings support the design of threshold values and escalation rules, which are defined by management with regard to tolerated risk and system capacity. The benefit of VOST becomes particularly evident in time critical phases when formal data sources do not provide sufficiently rapid and interpretatively clear information about the nature of the disruption and its impacts on the functioning of elements within the road network and the services they provide.

In the paper is also presented a conceptual model for mapping indicators across the links among threats, exposure, vulnerability/susceptibility, consequences, and criticality and for connecting this model to the procedural framework of VOST and the crisis management decision cycle. For the road transport subsector, the paper describes the operationalisation of the categories of Exposure, Conditions, Accessibility, and Consequence in a GIS environment and their aggregation to the level of assets, routes, corridors, and the network. The framework is complemented by an implementation procedure for integrating indicators into the VOST system, including the delineation of roles, responsibilities, interfaces with supplier entities, and a feedback mechanism. This creates a basis for linking operational event indication with tactical impact evaluation and strategic planning of measures aimed at increasing resilience.

The proposed approach is subject to limitations arising from the nature of open data. Further limitations are related to the elimination of information noise in such data. In the current framework, noise reduction is based primarily on basic linguistic analysis of keywords, filtering by location, time, content type, and language, deduplication of records, and basic normalisation of metadata. This procedure enables basic data preprocessing, but it is not yet fully sufficient for the rapid responsiveness in a time-critical environment. Practical implementation therefore requires the standardisation of verification procedures, more precise linguistic and contextual processing, the establishment of a governance framework, and clarification of the legal and ethical conditions for data handling. Real-world deployment also depends on organisational and staffing capacity, the availability of trained VOST members, data-analytic capability, and the level of trust between institutions and volunteer communities.

Further research should focus on pilot testing of the framework under Czech conditions for selected types of incidents on the road network, validation of threshold values and trigger actions using real events,

and linking VOST outputs with formal data sources of infrastructure operators. It should also focus on refining the mechanisms for eliminating information noise, which in the current framework are based mainly on basic linguistic analysis of keywords and simple filtering. To improve responsiveness, it is necessary to extend this procedure through more advanced linguistic and contextual processing of records and through metrics of record quality and credibility for indicator weighting. These steps would strengthen the usability of the framework for crisis management decision-making and support the long-term increase of the resilience in road critical infrastructure and related services.

Acknowledgements

This research was supported by the VSB - Technical University of Ostrava under projects SP2026/006 and CL03000017.

Conflicts of interest

The authors declare that they have no known competing financial interests or personal relationships that could have appeared to influence the work reported in this paper.

References

[1] *IPCC, 2013. Climate change 2013 - the physical science basis: working group I contribution to the fifth assessment report of the intergovernmental panel on climate change*. STOCKER, T. F., QIN, D., PLATTNER, G.-K., TIGNOR, M., ALLEN, S. K., BOSCHUNG, J., NAUELS, A., XIA, Y., BEX, V., MIDGLEY, P. M. (Eds.). Cambridge: Cambridge University Press, 2013. ISBN 978-1-107-05799-1, p. 1-30.

[2] FATHI, R., THOM, D., KOCH, S., ERTL, T., FIEDRICH, F. VOST: a case study in voluntary digital participation for collaborative emergency management. *Information Processing and Management* [online]. 2020, **57**(4), 102174. ISSN 0306-4573, eISSN 1873-5371. Available from: https://doi.org/10.1016/j.ipm.2019.102174

[3] DEMERTZIS, K., ILIADIS, L. S., TZIRITAS, N., KIKIRAS, P. Anomaly detection via blockchained deep learning smart contracts in industry 4.0. *Neural Computing and Applications* [online]. 2020, **32**(23), p. 17361-17378. ISSN 0941-0643, eISSN 1433-3058. Available from: https://doi.org/10.1007/s00521-020-05189-8

[4] OSEI-KYEI, R., ALMEIDA, L. M., AMPRATWUM, G., TAM, V. Systematic review of critical infrastructure resilience indicators. *Construction Innovation: Information, Process, Management* [online]. 2023, **23**(5), p. 1210-1231. ISSN 1471-4175, eISSN 1477-0857. Available from: https://doi.org/10.1108/CI-03-2021-0047

[5] ALIZADEH, H., SHARIFI, A. Assessing resilience of urban critical infrastructure networks: a case study of Ahvaz, Iran. *Sustainability* [online]. 2020, **12**(9), 3691. eISSN 2071-1050. Available from: https://doi.org/10.3390/su12093691

[6] JOVANOVIC, A., KLIMEK, P., RENN, O., SCHNEIDER, R., OIEN, K., BROWN, J., DIGENNARO, M., LIU, Y., PFAU, V., JELIC, M., ROSEN, T., CAILLARD, B., CHAKRAVARTY, S., CHHANTYAL, P. Assessing resilience of healthcare infrastructure exposed to COVID-19: emerging risks, resilience indicators, interdependencies and international standards. *Environment Systems and Decisions* [online]. 2020, **40**(2), p. 252-286. ISSN 2194-5403, eISSN 2194-5411. Available from: https://doi.org/10.1007/s10669-020-09779-8

[7] JOVANOVIC, A., KLIMEK, P., CHOUDHARY, A., SCHMID, N., LINKOV, I., OIEN, K., VOLLMER, M., SANNE, J., ANDERSSON, S. L., SZEKELY, Z., MOLARIUS, R., KNAPE, T., BARZELAY, U., STANISIC, M., WALTHER, G., LIEBERZ, D. Analysis of existing assessment resilience approaches, indicators and data sources: usability and limitations of existing indicators for assessing, predicting and monitoring critical infrastructure resilience. Research project SmartResilience. Stuttgart, Germany: EU-VRi, 2016. p. 40-41.

[8] KRUPOVA, S., KOMAN, G., SOVIAR, J., HOLUBCIK, M. The role of business models in smart-city waste management: A framework for sustainable decision-making. *Systems* [online]. 2025, **13**(7), 556. eISSN 2079-8954. Available from: https://doi.org/10.3390/systems13070556

[9] JANECKOVA, H., RYSKA, O. Smart city resilience. *Chemical Engineering Transactions* [online]. 2024, **111**, p. 139-144. ISSN 2283-9216, ISBN 979-12-81206-11-3. Available from: https://doi.org/10.3303/CET24111024

[10] LUDWIG, T., REUTER, C., SIEBIGTEROTH, T., PIPEK, V. CrowdMonitor: mobile crowd sensing for assessing physical and digital activities of citizens during emergencies. In: 33rd Annual ACM Conference on Human Factors in Computing Systems CHI '15: proceedings [online]. ACM. 2015. ISBN 978-1-4503-3145-6, p. 4083-4092. Available from: https://doi.org/10.1145/2702123.2702265

[11] REUTER, C., KAUFHOLD, M.-A. Fifteen years of social media in emergencies: a retrospective review and future directions for crisis informatics. *Journal of Contingencies and Crisis Management* [online]. 2018, **26**(1), p. 41-57. ISSN 0966-0879, eISSN 1468-5973. Available from: https://doi.org/10.1111/1468-5973.12196

[12] FIEDRICH, F., FATHI, R. Humanitarian aid and concepts of digital relief. In: *Safety-critical human-computer interaction: interactive technologies and social media in crisis and security management* (in German) [online].

REUTER, CH. (Ed.). 1. ed. Wiesbaden: Springer Vieweg, 2018. ISBN 978-3-658-19523-6, p. 509-528. Available from: https://doi.org/10.1007/978-3-658-19523-6_25

[13] REHAK, D., SPLICHALOVA, A., HROMADA, M., WALKER, N., JANECKOVA, H., RISTVEJ, J. Critical entities resilience failure indication. *Safety Science* [online]. 2024, **170**, 106371. ISSN 0925-7535, eISSN 1879-1042. Available from: https://doi.org/10.1016/j.ssci.2023.106371

[14] RYSKA, O., JANECKOVA, H. Impact of parameters of critical road infrastructure on crisis management [online]. In: *TRANSBALTICA XV: Transportation Science and Technology. TRANSBALTICA 2024. Lecture Notes in Intelligent Transportation and Infrastructure.* PRENTKOVSKIS, O., YATSKIV (JACKIVA), I., SKACKAUSKAS, P., KARPENKO, M., STOSIAK, M. (Eds.). Cham: Springer, 2025. ISBN 978-3-031-85389-0, eISBN 978-3-031-85390-6, p. 579-588. Available from: https://doi.org/10.1007/978-3-031-85390-6_54

[15] REHAK, D., SPLICHALOVA, A., JANECKOVA, H., OULEHLOVA, A., HROMADA, M., KONTOGEORGOS, M., RISTVEJ, J. Critical entities resilience assessment (CERA) to small-scale disasters. *International Journal of Disaster Risk Reduction* [online]. 2024b, **111**, 104748. eISSN 2212-4209. Available from: https://doi.org/10.1016/j.ijdrr.2024.104748

[16] IMRAN, M., CASTILLO, C., DIAZ, F., VIEWEG, S. Processing social media messages in mass emergencies. *ACM Computing Surveys* [online]. 2015, **47**(4), p. 1-38. ISSN 0360-0300, eISSN 1557-7341. Available from: https://doi.org/10.1145/2771588

[17] SVENTEKOVA, E., URBANCOVA, Z., HOLLA, K. Assessment of the vulnerability of selected key elements of rail transport. Slovak case study. *Applied Sciences* [online]. 2021, **11**(13), 6174. eISSN 2076-3417. Available from: https://doi.org/10.3390/app11136174

[18] LOVECEK, T., SVENTEKOVA, E., MARIS, L., REHAK, D. Determining the resilience of transport critical infrastructure element: use case. In: 21 st International Conference Transport Means 2017: proceedings. Vol. 21. 2017. p. 824-828.

[19] YUAN, F., LIU, R., MAO, L., LI, M. Internet of people enabled framework for evaluating performance loss and resilience of urban critical infrastructures. *Safety Science* [online]. 2021, **134**, 105079. ISSN 0925-7535, eISSN 1879-1042. Available from: https://doi.org/10.1016/j.ssci.2020.105079

[20] REHAK, D., SPLICHALOVA, A., JANECKOVA, H., RYSKA, O., OULEHLOVA, A., MICHALCOVA, L., HROMADA, M., KONTOGEORGOS, M., RISTVEJ, J. Critical entities resilience strengthening tools to small-scale disasters. *International Journal of Critical Infrastructure Protection* [online]. 2025, **100**, 766. ISSN 1874-5482, eISSN 2212-2087. Available from: https://doi.org/10.1016/j.ijcip.2025.100766

[21] SPLICHALOVA, A., PATRMAN, D., KOTALOVA, N., HROMADA, M. Managerial decision making in indicating a disruption of critical infrastructure element resilience. *Administrative Sciences* [online]. 2020, **10**(3), 75. eISSN 2076-3387. Available from: https://doi.org/10.3390/admsci10030075

[22] PATRMAN, D., SPLICHALOVA, A., REHAK, D., ONDERKOVA, V. Factors influencing the performance of critical land transport infrastructure elements. *Transportation Research Procedia* [online]. 2019, **40**, p. 1518-1524. ISSN 2352-1457, eISSN 2352-1465. Available from: https://doi.org/10.1016/j.trpro.2019.07.210

[23] KARAKOC, D. B., BARKER, K., ZOBEL, C. W., ALMOGHATHAWI, Y. Social vulnerability and equity perspectives on interdependent infrastructure network component importance. *Sustainable Cities and Society* [online]. 2020, **57**, 102072. ISSN 2210-6707, eISSN 2210-6715. Available from: https://doi.org/10.1016/j.scs.2020.102072

[24] SETOLA, R., LUIJF, E., THEOCHARIDOU, M. Critical infrastructures, protection and resilience [online]. In: *Managing the complexity of critical infrastructures*. *Studies in systems, decision and control*. SETOLA, R., ROSATO, V., KYRIAKIDES, E., ROME, E. (Eds.). Vol. 90. Cham: Springer, 2016. ISBN 978-3-319-51042-2, eISBN 978-3-319-51043-9, p. 1-18. Available from: https://doi.org/10.1007/978-3-319-51043-9_1

[25] OIEN, K., BODSBERG, L., JOVANOVIC, A. S. Resilience assessment of smart critical infrastructures based on indicators. In: *Safety and reliability - safe societies in a changing world* [online]. HAUGEN, S., BARROS, A., GULIJK, C., KONGSVIK, T., VINNEM, J. E. (Eds.). 1. ed. London: CRC Press, 2018. eISBN 9781351174664, p. 1269-1277. Available from: https://doi.org/10.1201/9781351174664

[26] CINGEL, M., DRLICIAK, M., CELKO, J., ZABOVSKA, K. Modal split analysis by best-worst method and multinominal logit model. *Transport Problems / Problemy Transportu* [online]. 2023, **18**(1), p. 55-65. ISSN 1896-0596, eISSN 2300-861X. Available from: https://doi.org/10.20858/tp.2023.18.1.05

[27] FEKETE, A., RHYNER, J. Sustainable digital transformation of disaster risk - integrating new types of digital social vulnerability and interdependencies with critical infrastructure. *Sustainability* [online]. 2020, **12**(22), 9324. eISSN 2071-1050. Available from: https://doi.org/10.3390/su12229324

[28] HOFMANN, M., GJERDE, O., KJOLLE, G. H., GRAMME, E., HERNES, J. G., FOOSNÆS, J. A. Developing indicators for monitoring vulnerability of power lines - case studies. In: 22nd International Conference and Exhibition on Electricity Distribution CIRED 2013: proceedings [online]. IET. 2013. 0577. Available from: https://doi.org/10.1049/cp.2013.0815

[29] REHAK, D., PATRMAN, D., BRABCOVA, V., DVORAK, Z. Identifying critical elements of road infrastructure using cascading impact assessment. *Transport* [online]. 2020, **35**(3), p. 300-314. ISSN 1648-4142, eISSN 1648-3480. Available from: https://doi.org/10.3846/transport.2020.12414

[30] REHAK, D., NOVOTNY, P. Bases for modelling the impacts of the critical infrastructure failure. *Chemical Engineering Transactions* [online]. 2016, **53**, p. 91-96. ISSN 2283-9216, ISBN 979-12-81206-11-3. Available from: https://doi.org/10.3303/CET1653016

[31] SLIVKOVA, S., REHAK, D., NESPOROVA, V., DOPATEROVA, M. Correlation of core areas determining the resilience of critical infrastructure. *Procedia Engineering* [online]. 2017, **192**, p. 812-817. ISSN 1877-7058. Available from: https://doi.org/10.1016/j.proeng.2017.06.140

Dear colleagues,

Journal for sciences in transport Communications - Scientific Letters of the University of Žilina are a wellestablished open-access scientific transport journal aimed primarily at the topics connected with the field of transport. The main transport-related areas covered include Civil engineering, Electrical engineering, Management and informatics, Mechanical engineering, Operation and economics, Safety and security, Travel and tourism studies. Research in the field of education also falls under these categories. The full list of main topics and subtopics is available at: *https://komunikacie.uniza.sk/artkey/inf-990000-0500_Topical-areas.php*

Journal for sciences in transport Communications - Scientific Letters of the University of Žilina is currently indexed, abstracted and accepted by CEEOL, CLOCKSS, COPE (Committee on Publication Ethics), Crossref (DOI), digitálne pramene, DOAJ, EBSCO Host, Electronic Journals Library (EZB), ERIH Plus, Google Scholar, Index Copernicus International Journals Master list, iThenticate, JournalGuide, Jouroscope, Norwegian Register for Scientific Journals Series and Publishers, Portico, ROAD, ScienceGate, SCImago Journal & Country Rank, SciRev, SCOPUS, Ulrich´s, Web of Science database, WorldCat (OCLC).

Journal for sciences in transport Communications - Scientific Letters of the University of Žilina is preserved in CLOCKSS and Portico to guarantee long-term digital preservation and is archived in the national deposit digitalne pramene.

Authors can share their experiences with publishing in our journal on SciRev.

Journal for sciences in transport Communications - Scientific Letters of the University of Žilina has been selected for inclusion in the Web of Science™. Articles published after 2022, beginning with 24(1), are included in the product Emerging Sources Citation Index (ESCI).

I would like to invite authors to submit their papers for consideration. We have an open access **policy under Creative Commons (CC BY) license** and Article Processing Charge (APC) is **400 Euro** (price excluding VAT). The price of one additional page of the submitted article beyond the prescribed scope (8 pages) is **50 Euro** (price excluding VAT). Print edition fee is 100 Euro per one piece (price excluding VAT) including shipping costs. Our journal operates a standard single-anonymous peer-review process, the successful completion of which is a prerequisite for publication of articles.

Our journal is issued four times a year (in January, in April, in July and in October).

I would also like to offer you the opportunity of using already published articles from past issues as source of information for your research and publication activities. All papers are available at our webpage: *http://komunikacie.uniza.sk*, where you can browse through the individual volumes. Our journal offers access to its contents in the open access system on the principles of the license Creative Commons (CC BY 4.0).

For any questions regarding the Journal for sciences in transport Communications - Scientific Letters of the University of Žilina please contact us at: *komunikacie@uniza.sk*.

We look forward to future cooperation.

Sincerely

Gabriel Gašpar
editor-in-chief

KOMUNIKÁCIE
COMMUNICATIONS

VEDECKÉ LISTY ŽILINSKEJ UNIVERZITY
SCIENTIFIC LETTERS OF THE UNIVERSITY OF ZILINA
multidisciplinary journal for sciences in transport

VOLUME 28 Number 2

April 2026

komunikácie
COMMUNICATIONS

VEDECKÉ LISTY ŽILINSKEJ UNIVERZITY
SCIENTIFIC LETTERS OF THE UNIVERSITY OF ZILINA
multidisciplinary journal for sciences in transport

VOLUME 28 Number 2

April 2026

Each paper is reviewed by at least two reviewers.
Individual issues of the journal are available at: http://komunikacie.uniza.sk
The full author quidelines are available at: https://komunikacie.uniza.sk/artkey/inf-990000-0400_Author-guidelines.php
Published quarterly by the University of Žilina via EDIS - Publishing House of the University of Žilina
Multidisciplinary journal for sciences in transport Komunikácie / Communications is currently indexed, abstracted and accepted by CEEOL, CLOCKSS, COPE (Committee on Publication Ethics), Crossref (DOI), digitálne pramene, DOAJ, EBSCO Host, Electronic Journals Library (EZB), ERIH Plus, Google Scholar, Index Copernicus International Journals Master list, iThenticate, JournalGuide, Jouroscope, Norwegian Register for Scientific Journals Series and Publishers, Portico, ROAD, ScienceGate, SCImago Journal & Country Rank, SciRev, SCOPUS, Ulrich´s, Web of Science database, WorldCat (OCLC).

Multidisciplinary journal for sciences in transport Komunikácie - vedecké listy Žilinskej univerzity v Žiline / Communications - Scientific Letters of the University of Žilina has been selected for inclusion in the Web of Science™.

Contact:

Komunikácie - vedecké listy Žilinskej univerzity v Žiline
Communications - Scientific Letters of the University of Žilina
University of Žilina, Univerzitná 8215/1
010 26 Žilina, Slovakia

E-mail: komunikacie@uniza.sk
Web: https://komunikacie.uniza.sk

ISSN (print version): 1335-4205
ISSN (online version): 2585-7878

Registered No. (print version): EV 3672/09
Registered No. (online version): EV 3/22/EPP
Publisher, owner and distribution:
University of Žilina, Univerzitná 8215/1,
010 26 Žilina, Slovakia

Company identification number IČO: 00 397 563
Frequency of publishing: four times a year
Circulation: 30 printed copies per issue
Print edition price: 100 Euro (price without VAT)
Article Processing Charge (APC): 400 Euro (price without VAT)

Publishing has been approved by:
Ministry of Culture, Slovak Republic

UNIVERSITY
OF ŽILINA

In its over 70 years of successful existence, the University of Žilina (UNIZA) has become one of the top universities in Slovakia.

Scientific conferences

organized by University of Žilina

Conference Automotive Safety 2026
Date and venue: 5 - 8 May 2026, Tatranská Lomnica (SK)
Contact: milos.poliak@uniza.sk
Web: https://automotivesafetyconference.com

Conference Unconventional Technologies 2026
Date and venue: 25 - 26 June 2026, Žilina-Budatín (SK)
Contact: jan.moravec@fstroj.uniza.sk

Conference InvEnt 2026
(Invention Enterprises 2026)
Date and venue: 17 - 19 June 2026, Horný Smokovec (SK)
Contact: luboslav.dulina@fstroj.uniza.sk
Web: https://www.priemyselneinzinierstvo.sk/invent2026/

29th International Scientific Conference Crisis Management in Specific Environment
Date and venue: 15 - 16 June 2026, Žilina (SK)
Contact: katarina.buganova@uniza.sk
Web: https://fbi.uniza.sk/stranka/konferencia-rks

Conference OSSConf 2026
Date and venue: 1 - 3 July 2026, Žilina (SK)
Contact: ossconf@fri.uniza.sk;
rudolf.blasko@fri.uniza.sk,
miroslav.kvassay@fri.uniza.sk
Web: https://ossconf.fri.uniza.sk/

UNIVERSITY OF ŽILINA
Science & Research Department

Univerzitná 8215/1,
010 26 Žilina,
Slovakia

Ing. Janka Macurová
tel.: +421 41 513 5143
e-mail: janka.macurova@uniza.sk